Effect of the Extracellular Environment on Astrocyte Phenotype

Zoe Hanna Smith, BSc

Thesis submitted to the University of Nottingham for the degree of Doctor of Philosophy

November 2019



University of Nottingham
UK | CHINA | MALAYSIA

Abstract

Astrocytes are a functionally and morphologically heterogeneous glial subtype essential for the development, function and survival of neurons in the healthy brain. Neuron-glial communication is therefore essential to normal brain function, but the mechanisms regulating signalling and anatomical association between these two cell types are still under investigation. The objective of this project was to develop *in vitro* models, validate the use of 3D culture techniques such as hydrogels and establish their potential for enabling astrocyte and neuron co-culture, and determine the possibility of combining 3D cell culture techniques with compartmentalized microfluidics devices. An additional aim was to discover the feasibility of replacing primary tissue with induced human astrocytes derived from fibroblasts.

2D *in vitro* cell culture environments are known to generate astrocytes with marked morphological differences to *in vivo* cells. 3D *in vitro* culture methods better resemble the *in vivo* microenvironment of astrocytes, therefore I investigated the effect of 3D matrices on cortical astrocyte phenotype and found that in both 2D and 3D environments astrocytes exhibit a highly heterogeneous range of morphological parameters. Astrocytes cultured in 3D hydrogels exhibited morphology that more closely resembled the *in vivo* phenotype compared with cells cultured in 2D. Additionally, considering that astrocytes are highly sensitive to their microenvironment, I have studied the effect of cell culture media on astrocyte phenotype and found that morphology was also highly responsive to the composition of cell culture media, particularly with the presence of serum. Thus the careful selection of cell culture media is crucial to reproduce conditions similar to those *in vivo.*

Neuron-glial communication in *ex vivo* slices of rat cerebellum was investigated by analysing how neuronal stimulation affected both presynaptic vesicle distribution and synaptic coverage by glial processes, as a physiologically relevant model of neuron-glial communication. Next I worked with *in vitro* systems with the potential to offer a similar level of analysis but with increased control of the extracellular environment. Compartmentalized microfluidics devices were used for the study of astrocyte-axon interactions,

and the influence of astrocytes on neuron growth and development. Calcein AM loading determined that it is possible to both culture neurons and astrocytes in compartmentalized microfluidics devices, and within the 3D matrigel matrix, which is a step towards developing a superior *in vitro* model for cellular co-culture. To further improve the translational potential of this model, human induced astrocytes were derived from induced neural progenitor cells and morphological characterisations were conducted in 2D and 3D to determine if they are a suitable for studying human astrocyte complexity.

The ultimate aim of this PhD has been to investigate replacing classical 2D cell culture methods with 3D techniques, and replacing animal tissue with human tissue in order to provide physiologically relevant cell culture models which will facilitate greater understanding of astrocyte and neuron complexity, and their interactions in the brain. These data suggest that 3D hyaluronic acid hydrogels are a suitable culture system to replace 2D culture techniques with the potential to enable more translatable research into astrocyte physiology.

Publications

Dobson KL, Smith ZH, Bellamy TC (2018) Distribution of vesicle pools in cerebellar parallel fibre terminals after depression of ectopic transmission. PLOS ONE 13(7): e0200937. https://doi.org/10.1371/journal.pone.0200937

Acknowledgements

The last three years and seven months I've spent working on this PhD project have been my greatest challenge so far, and this journey would not have been possible without the support of some truly great family and friends. I have had the privilege of undertaking a project that is completely my own, investigating astrocyte phenotype under different *in vitro* conditions, something which has fascinated me.

The person that I am today has been massively influenced by my family, the Smiths. My mum, Lisa, and my dad, Paul, have supported me continually from my first day of school to this very moment and I know will do so throughout the rest of my career. Their help, encouragement and praise related to all subjects at school is what has instilled a love of learning in me, and what has ultimately led me to pursue a doctorate. Without a doubt, I have picked up my driven work ethic from Paul, a trait that I highly value because it is through him that I have learnt that hard work will always pay off, and that if you're going to do something, give it your all. From Lisa I have learnt something of equal value; to not be too hard on yourself. Lisa's belief in me has guided me at times when achieving this PhD felt impossible. I hope that what I have learned in this process can help us all as we continue to grow as a family.

One very special member of my family who I couldn't have done this without is Indie. From my GCSEs all the way until the final stages of writing up my thesis, Indie has always been there for me and is truly the best friend I could have wished for over the last ten years. I am devastated that we recently lost her, she was such a huge part of the Smith family and one of my main motivations to keep going. Every time I visited home she was there for endless cuddles, something that always transformed my mood if I had been finding things hard. Indie has taught me how to enjoy the little things no matter of the struggles besides, and from her I have learned to take nothing for granted.

My fiancé Barnaby deserves a medal for putting up with me over the last few years, and I want to say thank you to him for helping me through this process.

The stresses and pressures of this degree have tested me immensely but Barnaby has always been there to console and support me, and been extremely patient considering how all-consuming the struggle has been at times. Barnaby has also helped me learn not to get upset or worried about things not working as I had hoped and to not give up – something I have seen him do in his own career. I am also thankful for the consistent support from Kate, Terry, Sebastian and Felix, and feel extremely grateful that I can call them my family.

This journey would really not have been possible without my family and I wouldn't be who I am without them. I am also extremely thankful to all of my friends who have been supportive throughout this process, again, I could not have done it without them and I have learned things from them that have shaped me as a person.

Thanks to my supervisory team: Dr Bellamy, Dr Dajas-Bailador and Dr Hathway. I was delighted that they selected me to undertake this project and I am thankful for their help over the years.

"There are no secrets to success. It is the result of preparation, hard work and learning from failure" – Colin Powell.

Contents

Abstract ..... **ii**

Publications ..... **iv**

Acknowledgements ..... **v**

Contents ..... **vii**

Abbreviations ..... **xvi**

Chapter 1. Introduction **1**

1.1 The Brain 1

1.2 Astrocytes 2

1.2.1 Astrocyte Development 3

1.2.2 Astrocyte Subtypes 4

1.2.3 Astrocyte Functions 5

1.2.3.1 Ion and Neurotransmitter Homeostasis 5

1.2.3.2 Nutrient Supply and Metabolic Support 6

1.2.3.3 Synapse Formation, Maintenance and Elimination 7

1.2.3.4 Modulation of Synaptic Transmission 9

1.2.3.4.1 Astrocytes Calcium Signals 9

1.2.3.4.2 The Spatial Range of Astrocyte Calcium Signals 10

1.2.3.4.3 Effects of Calcium on Astrocyte Function 11

1.2.4 Reactive Gliosis 12

1.2.4.1 Damage to the Central Nervous System 12

1.2.4.2 Severity of Reactive Gliosis 12

1.2.4.3 The Glial Scar 13

1.2.4.4 Reactive Astrocytes 14

1.2.4.4.1 Reactive Gliosis Affects Astrocyte Calcium Signalling 16

1.2.5 Human Astrocytes 17

1.3 Neurons 18
1.3.1 Growth and Development 20
1.3.1.1 Polarisation 20
1.3.1.2 Cytoskeleton 21
1.3.2 Synapses and Communication 22
1.3.2.1 Traditional and Ectopic Transmission 23
1.4 *In Vitro* Cell Culture 23
1.4.1 Microfluidics 26
1.4.2 3D Culture Environment 28

1.5 Aims and Objectives 30

Chapter 2. Methods 32

2.1 Ethical Statement 32

2.2 Primary Cells 32
2.2.1 Isolation of Astrocytes 32
2.2.2 2D Cell Culture of Astrocytes 34
2.2.3 Inducing Astrocyte Stellation 34

2.3 Characterisation of Cell Morphology 34
2.3.1 Calcein AM Loading 34
2.3.2 Immunofluorescence for Astrocytes 35
2.3.3 Imaging Live and Fixed Primary Cells 36
2.3.3.1 Confocal Imaging Parameters for Different 2D and 3D Matrices 37
2.3.3.1.1 2D 24-Well Plates 37
2.3.3.1.2 Alvetex 37
2.3.3.1.3 Matrigel and Hyaluronic Acid 37
2.3.3.2 Post Imaging Processing for 3D Z-Stacks 37
2.3.3.2.1 Bead Analysis for 2D Culture Formats 38
2.3.3.2.2 Bead Analysis for 3D Culture Formats 38
2.3.3.2.3 Thresholding 39

Chapter 3. Neuron-Glial Interactions in the Cerebellar Cortex 40

3.1 Introduction 40
3.1.1 The Cerebellum 40
3.1.2 Ectopic Communication with Bergmann Glia 41
3.1.3 Hypothesis and Aims 43

3.2 Methods 45
3.2.1 Cerebellar Slice Preparation and Processing 45
3.2.2 Cerebellar Slice Analysis 46
3.2.3 Statistics 46

3.3 Results 47
3.3.1 Cerebellar Slice Preparation, Processing and Analysis 47
3.3.2 Confirmation of Depression of Ectopic Transmission 49
3.3.3 Synapse Ultrastructure and Vesicle Distribution 50
3.3.4 Vesicle Distribution at the Active Zone 51
3.3.5 Vesicle Distribution at the Glial Facing Membrane 52
3.3.6 Hypothesis Testing 54
3.3.7 Glial Coverage of Synaptic Terminals 55

3.4 Discussion 57
3.4.1 Vesicle Distribution 57
3.4.2 Cerebellum Synaptic Coverage by Bergmann Glial Cell Processes . 59
3.4.3 Conclusion 60

Chapter 4. Effect of Culture Media on Astrocyte Phenotype 61

4.1 Introduction 61
4.1.1 Morphological Assessment of Primary Astrocytes 61
4.1.2 Induction of Stellation 62
4.1.3 Functional Assessment of Primary Astrocytes 62
4.1.4 Co-Culture of Astrocyte and Neurons 63
4.1.5 Influence of Cell Culture Media on Astrocyte Phenotype 64
4.1.6 Aims 65

4.2 Methods 66
4.2.1 Generation of Primary Cortical Astrocytes 66

4.2.2 Morphological Assessment of Primary Astrocytes 66
4.2.3 Induction of Stellation 67
4.2.4 Functional Assessment of Primary Astrocytes 67
4.2.4.1 Calcium Imaging 67
4.2.5 Influence of Media Composition on Astrocyte Morphology 68
4.2.5.1 Assay of Astrocyte stellation 69
4.2.6 Statistics 69

4.3 Results 71
4.3.1 Primary Astrocyte Morphology *in Vitro* 71
4.3.2 Primary Astrocyte Function *in Vitro* 72
4.3.3 The Influence of Cell Culture Media on Astrocyte Phenotype 76
4.3.3.1 Morphological Analysis 76
4.3.3.2 Stellation Analysis 80
4.3.3.3 Functional Analysis 82
4.3.3.3.1 FBS Influence on Astrocyte Function 84

4.4. Discussion 86
4.4.1 2D Culture of Primary Astrocytes 86
4.4.2 Influence of Media Composition on Astrocyte Phenotype 88
4.4.2.1 Morphology 88
4.4.2.2 Function 89
4.4.2.2.1 Dulbecco's Modified Eagles Medium 90
4.4.2.2.2 Serum Supplementation in Media 91
4.4.2.2.3 Media Composition and Astrocyte-Neuron Co-Culture 92
4.4.3 Conclusion 93

Chapter 5. 3D Matrices for Astrocyte Cell Culture 95

5.1 Introduction 95
5.1.1 3D Culture for Primary Astrocytes 95
5.1.1.1 Alvetex 97
5.1.1.2 Matrigel 97
5.1.1.3 Hyaluronic Acid 98
5.1.2 Aims 99

5.2 Methods 100
5.2.1 2D Culture Methods 100
5.2.2 3D Culture Methods 100
5.2.2.1 Alvetex 100
5.2.2.2 Matrigel 100
5.2.2.3 Hyaluronic Acid 101
5.2.3 Viability Assessment 102
5.2.4 Induction of Stellation 102
5.2.5 Morphological Assessment 102
5.2.5.1 Confocal Imaging for 2D Cultured Cells 103
5.2.5.2 Confocal Imaging for 3D Cultured Cells 103
5.2.5.3 Post Imaging Processing 103
5.2.5.4 Morphological Parameters Analysis 104
5.2.6 Statistics 105

5.3 Results 106
5.3.1 3D Matrices for Astrocyte Cell Culture 106
5.3.1.1 Alvetex 106
5.3.1.2 Matrigel 108
5.3.1.3 Hyaluronic Acid 110
5.3.2 Astrocyte Morphology Characterisation in 2D and 3D Cell Culture Environments 111
5.3.2.1 Image Processing for Accurate Morphological Measurements 111
5.3.2.1.1 Z Scale Adjustment 111
5.3.2.1.2 Thresholding 112
5.3.3 Initial Assessment of Astrocyte Morphology in Different 2D and 3D Environments 113
5.3.3.1 Detailed Morphology of Astrocyte Cells Cultured in 2D 115
5.3.3.2 Detailed Morphology of Astrocyte Cells Cultured in 3D Matrigel 118
5.3.3.3 Detailed Morphology of Astrocyte Cells Cultured in 3D Hyaluronic Acid 118
5.3.4 Statistical Analysis of Astrocyte Morphologies in Different *In Vitro* Environments 120

5.3.4.1 Cells Cultured in 2D Compared to Cells Cultured in 3D Matrigel 120
5.3.4.2 Cells Cultured in 2D Compared to Cells Cultured in 3D Hyaluronic Acid 122
5.3.4.3 Cells Cultured in 3D Matrigel Compared to Cells Cultured in 3D Hyaluronic Acid 122
5.3.4.4 Comparing Surface Area to Volume Ratios for all Culture Environments 125
5.3.4.5 Statistical Analysis for Surface Area to Volume Ratios for all Culture Environments 125

5.4 Discussion 128
5.4.1 Astrocyte Morphological Assessment 129
5.4.1.1 Inducing Astrocyte Stellation 131
5.4.1.2 Surface Area to Volume Ratios 133
5.4.1.3 Astrocyte Distribution in Different 2D and 3D Cell Culture Environments 133
5.4.2 3D Matrices for Astrocyte Cell Culture 133
5.4.2.1 Alvetex 133
5.4.2.2 Hydrogels 134
5.4.2.2.1 Matrigel 136
5.4.2.2.2 Hyaluronic Acid 137
5.4.2.2.3 Hydrogels for Brain Cell Growth 138
5.4.3 Conclusion 139

Chapter 6. Exploring New Directions for *In Vitro* Culture Models 140

6.1 Introduction 140
6.1.1 Primary Neurons 140
6.1.2 Microfluidics Chambers 141
6.1.3 Primary Astrocytes and Cell Lines 144
6.1.4 Stem Cells 146
6.1.5 Induced Astrocytes 148
6.1.6 Aims 150

6.2 Methods 151
6.2.1 Generation of Primary Neurons 151
6.2.2 2D and 3D Cell Culture of Neurons 151
6.2.3 Immunofluorescence for Neurons 152
6.2.4 Imaging for Neurons in 2D and 3D 153
6.2.5 Microfluidics Chambers 153
6.2.6 Induced Neural Progenitor Cells 155
6.2.6.1 Conversion and Maintenance of Induced Neural Progenitor Cells 155
6.2.6.2 Maintenance of Induced Neural Progenitor Cells 156
6.2.6.3 Induced Astrocyte Generation from Induced Neural Progenitor Cells 157
6.2.7 Induced Astrocytes 157
6.2.7.1 Calcein AM Loading 157
6.2.7.2 Immunofluorescence 157
6.2.7.3 Inducing Stellation 157
6.2.7.4 Imaging 158
6.2.7.5 Analysis 158
6.2.8 Statistics 158

6.3 Results 160
6.3.1 Primary Neuron Development *In Vitro* 160
6.3.1.1 Axon Length Analysis 161
6.3.2 Astrocyte and Neuron Co-Culture 162
6.3.3 Microfluidics Chambers for the Study of Astrocyte-Neuron Interactions 165
6.3.4 3D Matrices for Neuron Cell Culture 168
6.3.5 Induced Astrocytes 169
6.3.5.1 Morphology 169
6.3.5.2 Culture in 2D and 3D Environments 171
6.3.5.3 Detailed Morphology of iAstrocyte Cells Cultured in 2D and 3D 171
6.3.5.4 Statistical Analysis of iAstrocyte Morphologies in Different *In Vitro* Environments 175

6.3.5.5 Comparison of Primary Rat and Human iAstrocyte Morphology 177

6.4 Discussion 180
6.4.1 2D Culture of Primary Neurons 180
6.4.2 3D Culture of Primary Neurons 180
6.4.3 Astrocyte and Neuron Co-Culture 181
6.4.4 Microfluidics Chambers 182
6.4.4.1 Designing Devices for Cellular Compartmentalization in 3D 183
6.4.5 Induced Astrocytes 185
6.4.6 Conclusion 187

Chapter 7. Discussion 188

7.1 Aims and Objectives 188

7.2 Primary Astrocyte Phenotype *in Vitro* 189

7.3 Effect of Cell Culture Media on Astrocyte Phenotype 191
7.3.1 Cell Culture Media Composition 193

7.4 Effect of 3D Culture Environment on Astrocyte Phenotype 194
7.4.1 3D Matrices for Primary Cell Culture 196
7.4.1.1 The Brain Extracellular Environment 197
7.4.1.2 Composite Gels 198
7.4.1.3 Peptide Gels 199
7.4.1.4 Polysaccharide Gels 200
7.4.1.5 Summary 200

7.5 Primary Neuron Development *in Vitro* 201
7.5.1 2D Culture 201
7.5.2 3D Culture 201

7.6 Astrocyte-Neuron Interactions 202
7.6.1 Ectopic Transmission in the Cerebellar Cortex 202
7.6.2 Compartmentalized Microfluidics Devices 203

7.7 Induced Astrocytes 203

7.8 Conclusion 204

References 205

Appendix 231

Methods 231

Hyaluronic Acid Hydrogels (Section 5.2.2.3) 231

Overview 231

Storage 231

Preparation 231

Confocal Imaging Parameters for Different 2D and 3D Matrices (Section 2.3.3.1) 232

Post Imaging Processing for 3D Z-Stacks (Section 2.3.3.2) 235

Abbreviations

aCSF	Artificial Cerebrospinal Fluid
AM	Astrocyte Medium
AMPA	α-amino-3-hydroxy-5-methyl-4-isoxazolepropionic
APOE	Apolipoprotein E
ATP	Adenosine Triphosphate
AUC	Area Under The Curve
bFGF	Basic Fibroblast Growth Factor
BG	Bergmann Glia
BMP	Bone Morphogenetic Protein
BSA	Bovine Serum Albumin
Calcein AM	Calcein Acetoxymethyl Ester
cAMP	Cyclic AMP
CEC	Cellulose Exopolysaccharide
CNS	Central Nervous System
CNTF	Ciliary Neurotrophic Factor
CTRL	Control
DAG	Diacylglycerol
DIV	Days *in Vitro*
DMEM	Dulbecco's Modified Eagles Medium
EAAT	Excitatory Amino Acid Transporter
ECM	Extracellular Matrix
EGF	Epidermal Growth Factor
EHS	Engelbreth-Holm-Swarm
ER	Endoplasmic Reticulum

ESCs	Extrasynaptic Currents
FBS	Fetal Bovine Serum
FGF	Fibroblast Growth Factor
FSK	Forskolin
GFAP	Glial Fibrillary Acidic Protein
GLAST	Glutamate Aspartate Transporter
GLT1	Glutamate Transporter 1
GPCR	G Protein Coupled Receptor
HA	Hyaluronic Acid
hiPSCs	Human Induced Pluripotent Stem Cells
iAstrocyte	Induced Astrocyte
IGF	Insulin-like Growth Factor
iNPC	Induced Neural Progenitor Cell
JIP-1	JNK Interacting Protein 1
LPS	Lipopolysaccharide
NA	Numerical Aperture
NB+G	Neurobasal supplemented with Glutamax
NGF	Nerve Growth Factor
NM	Neurobasal Medium
NO	Nitric Oxide
PBS	Phosphate Buffered Saline
PFA	Paraformaldehyde
PGE	Prostaglandin E
PIP2	Phosphatidylinositol 4,5-bisphosphate
PIP3	Phosphatidylinositol 3,4,5-trisphosphate
PLC	Phospholipase C
PLL	Poly-L-Lysine Hydrobromide

RGCs	Retinal Ganglion Cells
ROI	Region of Interest
SAPHs	Self-assembling Peptide Hydrogels
SCI	Spinal Cord Injury
Shh	Sonic Hedgehog
TGF-β	Transforming Growth Factor β
TRPA1	Transient Receptor Potential A1

Chapter 1. Introduction

1.1 The Brain

The brain is a complex organ which is composed of a number of different cell types which work together in order to process information and control the body (Figure 1). Two major cell classes account for the majority of cells in the brain: neurons and glia. Neurons are key for information processing; they transmit action potentials along a specialized axon which form synapses with the dendrites of other neurons allowing quick and efficient transfer of signals between cells.

Glial cells, part of the 80 billion non-neuronal cells in the brain, are electrically inactive cells which exist in the central nervous system (CNS) and support neurons in the healthy brain (Khakh and Sofroniew, 2015). Glia can be further subdivided into astrocytes, microglia and oligodendrocytes, all of which have distinct roles (Zuchero and Barres, 2015). Astrocytes are widely regarded as support cells for neurons, ensuring that they function effectively, but they also have active roles in synapse modulation (Kettenmann and Verkhratsky, 2008; Allen, 2014). Microglia are recognized as the resident immune cells of the brain, acting as the first line of defence from injury and infection (Colonna and Butovsky, 2017). Oligodendrocytes produce the myelin sheath required for the insulation of axons to ensure fast transduction of electrical signals (Barateiro, Brites and Fernandes, 2016).

Throughout the CNS, neurons and glia are in close association with one another which is crucial for physiological brain function. In the 1990s the organisation of the presynaptic membrane, postsynaptic density and surrounding glial processes in the form of the tripartite synapse was suggested (Araque *et al.*, 1999). This functional unit and its arrangement facilitates glial responses to local synaptic activity, and has implicated astrocytes in information processing in the brain (Perea, Navarrete and Arague, 2009; Panatier and Robitaille, 2016).

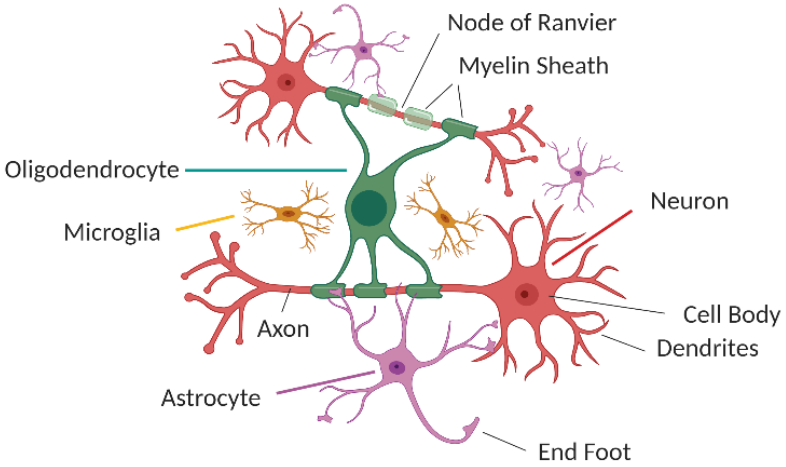


Figure 1. At the cellular level, neurons and glia orchestrate brain function. Typical motor neurons (red) are shown myelinated by oligodendrocyte cells (green). Many astrocytes (purple) make connections with neurons at synapses or gaps in the myelin sheath (Nodes of Ranvier). There are numerous microglia (orange) in the brain which act as the first line of defence following injury. Created with BioRender. https://biorender.com/

1.2 Astrocytes

Neuroglia were first described as a connective material existing between neural elements by Rudolf Virchow in 1856. Contrary to the notion that the neuroglia was a connective tissue without individual cell types, Michael von Lenhossek coined the term ‘astrocyte’ in 1893 after his discovery of star shaped cells in the CNS. Just one year later in 1894, Carl Ludwig Schleich introduced the idea that neuron-glial interactions were important in brain function and that glia regulated neuronal communications, which contradicted the idea that glia were merely support cells to neurons. To this day, the physiological roles of astrocytes are not fully defined, but it is now accepted that glia have active roles in brain function.

Astrocytes represent a population of complex and functionally diverse cells. Astrocytes exhibit many roles which are fundamental for normal neuronal function such as: suppling essential nutrients and metabolic precursors to neurons, removing and recycling neurotransmitters from the synaptic cleft,

and maintaining a balanced extracellular environment (specifically the ion composition of the cerebrospinal fluid) (Khakh and Sofroniew, 2015). Astrocytes are equipped with a wide array of neurotransmitter and hormone receptors that enable them to detect and respond to activity in the neural network (Porter and McCarthy, 1997). Astrocytes respond to neurotransmitters via calcium signalling which is critical for physiological function (Perea and Araque, 2005; Kettenmann and Verkhratsky, 2008). In recent years the active roles of astrocytes have been increasingly acknowledged following the discovery of their influence in the modulation of synaptic transmission and information processing in neural circuits (Sofroniew and Vinters, 2010). Astrocytes can release gliotransmitters which are capable of regulating neuron excitability following calcium signalling (Newman, 2003). Gliotransmitters are important for cell-cell communication among neurons and glia and commonly released gliotransmitters include ATP and glutamate.

1.2.1 Astrocyte Development

As mammalian embryos develop, radial glia derived from the neuroepithelium form and become the primary neural stem cells that generate neurons and glial cells throughout the brain. Neuroepithelial cells and radial glia are spatiotemporally patterned by cell-extrinsic positional signals including dorsal bone morphogenetic protein (BMP) and ventral Sonic hedgehog (Shh) (Bayraktar *et al.*, 2015). Other transcription factors further refine this patterning to generate distinct sub types of neurons and glia. In the cortex, neurogenesis starts with the specification of deeper projection neurons at E11-E13 in mouse and following this the generation of superficial projection neurons occurs at E14-E16 (Bayraktar *et al.*, 2015). At the E16 stage gliogenesis occurs (astrocytes are present at E16 in mice), however the vast majority of astrocytes are produced during postnatal development (Bayraktar *et al.*, 2015), which is also when they begin to show a mature and quiescent phenotype.

Glial cells of the cerebral cortex are derived from the postnatal sub ventricular zone (SVZ) which contains a region of glial and neuronal progenitors (Bayraktar *et al.*, 2015). Neurons migrate anteriorly to the olfactory bulb first

and differentiate into granular and perigomerular interneurons (Bayraktar *et al.*, 2015). Next the glial progenitors migrate dorsally and generate both astrocytes and oligodendrocytes in the grey and white matter (Tabata, 2015). Astrocyte maturation is still not completely understood and it is increasingly acknowledged that cell development and marker expression varies throughout regions of the CNS.

1.2.2 Astrocyte Subtypes

Astrocytes represent a highly heterogeneous population of glial cells with respect to their differences in morphology and have traditionally been divided into two main subtypes: protoplasmic or fibrous.

Protoplasmic astrocytes exhibit several stem branches that give rise to many finely branching processes and exist within the grey matter of the CNS (Sofroniew and Vinters, 2010). A single protoplasmic astrocyte within the human brain has the capacity to interact with two million neuronal synapses (Pekny and Pekna, 2019). Fibrous astrocytes commonly show many long fibre-like processes and reside within the white matter of the CNS (Sofroniew and Vinters, 2010).

Astrocytes express glial fibrillary acidic protein (GFAP) which is an intermediate filament protein that forms part of the astrocyte cytoskeleton and is commonly used as a marker for astrocytes (Sofroniew and Vinters, 2010). However, note that GFAP expression is not restricted to astrocytes: radial neural stem cells express GFAP as they mature and can remain in the adult brain, or alternatively develop into astrocytes (Choi and Lapham, 1978; Levitt and Rakic, 1980).

There are caveats to working with GFAP as the solely relied upon marker for astrocytes. For example, GFAP expression in astrocytes exhibits regional and local variability which is known to be present in development (Lee *et al.*, 2006). GFAP expression variance demonstrates that astrocyte subpopulations exhibit functional diversity in different regions of the cerebral cortex (Ståhlberg *et al.*, 2011; Schitine *et al.*, 2015). Astrocytes also express up to 10 different isoforms of GFAP which increase the complexity of the

astrocyte cytoskeleton and likely relates to subtype specific functions (Middeldorp and Hol, 2011). Generally, it is now widely accepted that the expression of cytoskeletal and cytoplasmic markers for astrocyte identification varies considerably amongst cortical regions (Schitine *et al.*, 2015). In addition to this, it is known that GFAP expression increases following various type of lesions or stress in the CNS (Brenner, 2014). Thus when astrocytes adopt a reactive phenotype in response to injury, GFAP expression levels are a useful marker of astrocyte activation as part of the rearrangement of the intermediate filament system (Hol and Pekny, 2015).

Other frequently used markers for the identification of astrocytes include: S100β, vimentin, glutamate aspartate transporter (GLAST) and glutamate transporter 1 (GLT1) (Roybon *et al.*, 2014). S100β is a calcium binding peptide involved in the regulation of energy metabolism which is localized in both the cytoplasm and nucleus (Dyck, Van Eldik and Cynader, 1993; Fanò *et al.*, 1995; Rothermundt *et al.*, 2003). Vimentin is an intermediate filament of the cytoskeleton expressed by astrocytes (Schnitzer, Franke and Schachner, 1981). GLAST and GLT1, glutamate transporters, are in high abundance in astrocytes due to their key role in the clearance of extracellular glutamate (Souza *et al.*, 2013).

1.2.3 Astrocyte Functions

1.2.3.1 Ion and Neurotransmitter Homeostasis

Neuronal activity leads to an increase in potassium ion concentration in the extracellular space; since potassium is important in modulating neuronal activity, astrocytes work to maintain potassium ion levels at their resting concentration. There are thought to be two mechanisms which astrocytes use to remove extracellular potassium ions: spatial buffering and the Na+/K+-ATP pump (Bellot-Saez *et al.*, 2017). The spatial buffering mechanism is a passive process where potassium ions are taken up at sites of higher concentration and then redistributed within the astrocyte and released at sites where the concentration is lower (Bellot-Saez *et al.*, 2017).

In addition to removing excess potassium ions from the extracellular space, astrocytes also remove excess glutamate which is released during neuronal signalling. Glutamate is the major excitatory neurotransmitter in the brain of vertebrates but when it accumulates in the extracellular space it causes excitotoxicity (Lau and Tymianski, 2010). Astrocytes uptake a high proportion of the total glutamate that is released by neurons (the remaining is taken up by other neurons) using excitatory amino acid transporters (EAATs). It is thought that since astrocytes are arranged in networks linked together by gap junctions they can rapidly dissipate potassium ions and glutamate in order to control their potentially detrimental accumulation (Sofroniew and Vinters, 2010).

1.2.3.2 Nutrient Supply and Metabolic Support

Astrocytes are critical for providing essential nutrients to neurons, for example, they supply neurons with glutamine to assist in the maintenance of glutamatergic transmission (Laake *et al.*, 1995) and for mitochondrial metabolism (Fendt and Verstreken, 2017). Glutamate removed from the extracellular space by astrocytes is enzymatically converted into glutamine using glutamine synthetase (Trabelsi *et al.*, 2017). Glutamine is taken up by neurons (Rose, Verkhratsky and Parpura, 2013) and is an inactive precursor for both glutamate and GABA neurotransmitters. This supply of glutamine to neurons is essential because they do not have the capacity to generate glutamate through other routes (Verkhratsky *et al.*, 2014).

In addition to providing metabolic support, astrocytes are important for the energetic support of neurons. Astrocytes convert glucose into lactate in order to provide an energy substrate to neurons (Kimelberg, 2010). Astrocytes are also the principal storage sites of glycogen granules throughout the CNS with high concentrations of these stores in regions of high synaptic density (Brown and Ransom, 2007). The astrocyte glycogen stores are used to sustain neuronal activity during periods of high activity and hypoglycaemia (Brown and Ransom, 2007). During hypoglycaemia, glycogen is broken down to lactate which is then available for neurons to utilise as an energy substrate (Brown and Ransom, 2007).

Disruptions to the supply of glucose in the brain, via low glucose metabolism or failure, has been associated with early events that take place in the progress of neurodegenerative disease, including alterations to the expression of nutrient transporters and metabolic enzymes (La Joie *et al.*, 2012). Such changes occur in Alzheimer's disease, where glucose hypometabolism takes please following glycolytic breakdown, resulting in hyperphosphorylation of tau and interfering with synaptic transmission and leading to cognitive impairment (Gong *et al.*, 2006; Afridi *et al.*, 2020).

1.2.3.3 Synapse Formation, Maintenance and Elimination

Astrocytes can produce a number of growth factors and related molecules which may act individually or in combination to regulate the proliferation, differentiation and survival of neurons. Such factors include mitogenic and trophic factors such as basic fibroblast growth factor (bFGF), epidermal growth factor (EGF), insulin and nerve growth factor (NGF) (Bramanti *et al.*, 2007). For example, astrocytes secrete NGF in the developing brain which acts as a trophic factor for cholinergic neurons (Hatanaka and Tsukui, 1986; Johnston *et al.*, 1987). Secreted or contact-mediated signals in the extracellular space may direct the formation and maintenance of synapses, implicating astrocytes in the regulation of synaptogenesis and synaptic maturation (Clarke and Barres, 2013).

Synapse formation, maturation and elimination are essential to neural circuit development which is key for functional information processing in the brain. Refinement of neural circuits takes place in three stages: firstly, synapses form between axons and dendrites, secondly, silent synapses undergo maturation to become active synapses and finally, excess synapses are removed (Clarke and Barres, 2013). Whilst the neuron-derived molecules that drive this process are well known, the reliance of neurons on astrocytes to direct synapse refinement is still being discovered.

In 1997, Pfrieger and Barres discovered the importance of glial cells in the formation and function of synapses. They observed that in glia free cultures, retinal ganglion cells (RGCs) form synapses with normal ultrastructure but

display little spontaneous synaptic activity, as well as high failure rates in evoked synaptic transmission (Pfrieger and Barres, 1997). They also found that in co-cultures with neurons and glial cells, the frequency and amplitude of spontaneous post synaptic currents were potentiated by 70-fold and 5-fold respectively, and there were fewer transmission failures (Pfrieger and Barres, 1997).

In vitro studies illustrate that astrocytes determine the number of synapses that form, are critical for post synaptic function and are necessary for synaptic stability and maintenance (Ullian, Christopherson and Barres, 2004). Apolipoprotein E (APOE) with bound cholesterol was the first astrocyte-secreted molecule to be identified that enhanced presynaptic differentiation in cultured RGCs by increasing the release probability of individual synapses (Mauch *et al.*, 2001). Specifically, APOE was found to promote presynaptic terminal and dendritic differentiation, and promote ongoing synapse development (Goritz, Mauch and Pfrieger, 2005).

Immature astrocytes have been found to release thrombospondins, large extracellular matrix proteins, capable of promoting CNS synaptogenesis *in vitro* and *in vivo* via formation of structurally normal excitatory synapses (Christopherson *et al.*, 2005; Kucukdereli *et al.*, 2011; Blanco-Suárez, Caldwell and Allen, 2017). Other important astrocyte-derived factors include hevin and SPARC which are members of the matricellular SPARC family (Blanco-Suárez, Caldwell and Allen, 2017). Unlike thrombospondins, which are primarily expressed in the developing brain, hevin and SPARC are expressed in the adult brain and also aid the generation of excitatory synapses. Hevin regulates synapse number and increases synapse size, which is itself regulated by SPARC which antagonizes the synaptogenic function of hevin (Kucukdereli *et al.*, 2011).

Taken together, astrocyte-neuron interactions via astrocyte-secreted molecules, in the extracellular space, are crucial for developing physiological functions of neurons in the brain. Neurotransmitters released from neurons, which bind to cell surface receptors on astrocytes, are another important

mode of astrocyte-neuron communication which is essential in the modulation of synaptic transmission.

1.2.3.4 Modulation of Synaptic Transmission

Neural networks have to be flexible in order to be able to respond to an ever-changing external environment. Similarly, experience must be able to influence, refine and reorganize spatio-temporal patterns of network activity. Neurotransmitters and hormones released by neurons can evoke intracellular calcium elevation in astrocytes (Agulhon *et al.*, 2008). Following rises in intracellular calcium concentration in astrocytes, those within close proximity of synapses can release molecules with the capacity to control subsequent modification to the structure and strength of neuronal synapses (Blanco-Suárez, Caldwell and Allen, 2017).

1.2.3.4.1 Astrocytes Calcium Signals

Astrocyte calcium signalling, in response to electrical stimulation of neurons, was first demonstrated in the hippocampus in the 1990s (Dani, Chernjavsky and Smith, 1992). Since then, the mechanisms by which intracellular calcium concentrations increase in astrocytes have been described.

Activation of astrocyte G protein coupled receptors (GPCRs), via neurotransmitters released from synapses, can activate a wide array of intracellular signalling cascades (Huang and Thathiah, 2015). Astrocytes have numerous Gq-coupled GPCRs (e.g. mGluR5) which trigger the IP3 signalling cascade (Guerra-Gomes *et al.*, 2018). When Gq GPCRs are activated, phospholipase C (PLC) hydrolyses phosphatidylinositol 4,5-bisphosphate (PIP2) to generate diacylglycerol (DAG) and inositol 1,4,5- trisphosphate (IP3). This results in IP3 receptor activation and subsequent calcium release from the endoplasmic reticulum (ER) and internal stores (Agulhon *et al.*, 2008).

Calcium waves resulting from neuronal signalling represent a form of intercellular communication between astrocytes in the neural network and are an important part of information processing in the CNS. Of note, astrocytes also show transient intracellular calcium rises that are independent of activity

at the synapse during development, as well as calcium fluctuations due to transient receptor potential A1 (TRPA1) channel activity that contributes to resting calcium levels (Volterra, Liaudet and Savtchouk, 2014).

1.2.3.4.2 The Spatial Range of Astrocyte Calcium Signals

Increases in intracellular calcium concentration may be restricted to local glial processes or alternatively may extend globally across a network of many astrocytes (Matsui, 2005). The way in which local signals are transduced into global signals and the roles for the different signal types are still not well understood (Croft *et al.*, 2015). Calcium waves can propagate from the astrocyte soma to the processes and from astrocyte to astrocyte, and may do so via gap junctions or alternatively increases in ATP in the extracellular matrix (ECM) (Nedegaard, 1994; Newman, 2001).

The rise in intracellular calcium in astrocytes, following the release of neurotransmitters at synapses, was mainly studied in the soma for many years, yet recent work shows that calcium transients also occur in astrocytes processes (Rungta *et al.*, 2016). Experimental work that knocked out the type 2 IP3 receptor found that, whilst the number of intracellular calcium transients was greatly reduced in the soma, there were limited effects on neuronal excitability or synaptic plasticity (Fiacco *et al.*, 2007; Petravicz, Fiacco and McCarthy, 2008; Agulhon, Fiacco and McCarthy, 2010). Additionally, evidence now shows that calcium level changes in astrocyte processes occur more often than those in the soma (Kanemaru *et al.*, 2014).

Barrett *et al*., (2018) recently characterised spatio-temporal calcium dynamics for astrocyte micro domains to evaluate their relationship with nearby neuronal dendrites and somata. They observed that a sub-population of astrocyte calcium signals have similar temporal dynamics to neurons, and signals occur in end feet and fine processes up to 120 ms after neuronal events (Barrett *et al.*, 2018). Such quick responses of astrocytes suggest that they are fundamental in synaptic modulation which can be achieved by the release of gliotransmitters (Barrett *et al.*, 2018).

1.2.3.4.3 Effects of Calcium on Astrocyte Function

Intracellular calcium elevation in astrocytes, resulting from neural network activity, regulates astrocyte homeostatic roles used to maintain healthy neurons. One example includes energy supply in the CNS: following intracellular calcium elevation in astrocytes, more glucose transporters can be inserted into the cell membrane facilitating glucose uptake from the blood supply when synapses are stimulated (Loaiza, Porras and Barros, 2003).

Calcium signalling in astrocytes facilitates the release of gliotransmitters, such as ATP or D-Serine, which modulate neurons, other glial cells or vascular cells (Guerra-Gomes *et al.*, 2018). Gliotransmitters stimulate or inhibit synaptic transmission and either cause LTP or LTD (Volterra, Liaudet and Savtchouk, 2014). For example, ATP can cause pre and postsynaptic inhibition of excitatory synaptic transmission (Tautenhahn *et al.*, 2012).

Astrocyte calcium signalling is crucial in development: studies with hippocampal astrocytes from a transgenic mouse line show that astrocytes have the capability of undergoing changes to their patterns of activity throughout development (Nakayama *et al.*, 2016). For example, day 30 postnatal astrocytes had increased numbers of subcellular calcium events and an increased proportion of somatic calcium events in comparison with day 7 postnatal astrocytes (Nakayama *et al.*, 2016). Furthermore, evidence has begun to emerge to suggest that calcium signalling in the adult brain occurs in a distinct manner from that which takes place during development.

Aberrant astrocyte calcium signals play a role in neurodegenerative diseases such as Alzheimer's. In such instances calcium signalling hyperactivity results in abnormal calcium oscillations such as long range calcium waves with pathological effects. *In vitro* and *in vivo* evidence have verified the link between amyloid β (Aβ) accumulation and disruption to calcium ion homeostasis within the cell cytoplasm: Aβ induces the formation of more cation selective pores in the membrane that facilitate calcium diffusion into the cell (Hermes, Eichhoff and Garaschuk, 2010; Tong *et al.*, 2018). Following this, increases in the intracellular calcium concentration can lead to

phosphorylation of tau via calcium linked kinases (Hermes, Eichhoff and Garaschuk, 2010; Tong *et al.*, 2018).

1.2.4 Reactive Gliosis

1.2.4.1 Damage to the Central Nervous System

Acute and chronic damage to the CNS evokes reactive gliosis, a three stage process orchestrated by astrocytes with mechanisms which overlap but are distinct from one another. The first phase is inflammation and cell death, followed by proliferation in the second phase (Gadea, Schinelli and Gallo, 2008) and the final phase is tissue remodelling (Burda and Sofroniew, 2014). The second phase involves the local migration of cells that aid tissue repair and replacement, including scar forming astrocytes and their progenitor cells (Faulkner *et al.*, 2004). CNS responses to damage therefore involve multiple neural and non-neural cell types that interact over time in an effort to maintain homeostasis, protect viable cells, clear debris and preserve function.

Acute focal insults include traumatic injury and ischemic stroke, whereas chronic focal insults include infection with abscess formation, tumours and autoimmune lesions. Physical and molecular disturbances experienced with traumatic brain injury strongly influence astrocyte gene expression, morphology, and secretory and proliferative capacities which influence the response to injury (Burda, Bernstein and Sofroniew, 2016).

1.2.4.2 Severity of Reactive Gliosis

Mild reactive gliosis usually results from non-penetrative traumas such as bacterial or viral infections and commonly involves the up regulation of GFAP and vimentin, and hypertrophy of astrocyte cell bodies and processes (Sofroniew and Vinters, 2010). Moderate astrogliosis can also be achieved *in vitro* with lipopolysaccharide (LPS) treatment (Sofroniew, 2009). In healthy brain tissue the branched processes of individual astrocytes do not overlap and occupy their own domains - at mild levels of trauma to the CNS, despite the hypertrophy of astrocyte cell bodies and processes, there is preservation of these non-overlapping astrocyte domains (Sofroniew and Vinters, 2010). Such mild trauma doesn’t result in astrocyte proliferation or scar formation

which means that if the original insult is resolved, there is the potential for astrocytes to return to their original morphology and regain normal physiological function.

Severe brain damage results following penetrative trauma, invasive infections or autoimmune inflammation. Severe brain insults result in: upregulation of GFAP, astrocyte cell body and process hypertrophy, and astrocyte proliferation that results in a significant change to the astrocyte network (Sofroniew and Vinters, 2010). Astrocyte processes also extend considerably beyond the previous domains of individual astrocytes resulting in substantial overlapping which is due in part to the proliferation of new astrocytes and increased numbers of astrocytes at the lesion site (Pekny and Pekna, 2019). Severe brain trauma also induces the formation of a glial scar which is a physical barrier which forms along borders of severe tissue damage. Often such mechanisms result in long lasting reorganisations of the tissue architecture (Sofroniew and Vinters, 2010).

1.2.4.3 The Glial Scar

The glial scar is a physical barrier formed by astrocytes following insults to the CNS in order to prevent the spread of damage and protect viable cells. The formation of a glial scar has long been thought to hinder functional recovery in the CNS following injury because axons are unable to regenerate beyond this physical barrier. Understanding the mechanisms underlying the lack of axon regeneration across lesions is critical for improving therapies for CNS repair following traumatic injury. The mechanisms that may lead to axon regeneration failure include: reduced intrinsic growth capacity of mature CNS neurons, absence of external growth stimulating factors, and the presence of external inhibitory factors associated with astrocytic scars. Chronic astrocytic scars are considered to continually prevent axon regrowth even after the inflammation has been resolved.

The extracellular matrix that surrounds the glial scar contains chondroitin and keratin sulphate which are proteoglycans released by reactive astrocytes that inhibit axon regrowth (Silver and Miller, 2004). Severed axons can achieve

some sprouting in this extracellular matrix but this does not equate to full functional recovery (Silver and Miller, 2004). It was assumed that removing the proteoglycan inhibition created by the astrocyte scar would subsequently lead to spontaneous axon regeneration. However, Anderson *et al.,* (2016) used three genetically targeted loss-of-function manipulations in adult mice and showed that preventing scar formation, attenuating scar-forming astrocytes or ablating chronic astrocytic scars did not result in spontaneous regrowth of transected corticospinal, sensory or serotonergic axons through severe spinal cord injury (SCI) lesions (Anderson *et al.*, 2016). Also, it was found that that scar forming astrocytes can upregulate growth supportive chondroitin sulphate proteoglycans 4 and 5 as well as expressing multiple axon growth supportive molecules including laminins (Anderson *et al.*, 2016).

It is clear therefore that astrogliosis and glial scar formation can improve outcome following injury via: wound closure, neuronal protection, blood-brain-barrier repair, and restriction of CNS inflammation. Preventing the spread of pathology to surrounding healthy tissue is critical in containing CNS damage and thus is an extremely valuable role of reactive astrocytes.

1.2.4.4 Reactive Astrocytes

Damage to the brain stimulates astrocytes to undergo a phenotypic switch which is characterised by: hypertrophy, a change in morphology, migration to the site of damage, down regulation of genes involved in normal physiological functioning of the cell and up regulation of genes involved in the immune response (Silver and Miller, 2004). Research into reactive gliosis suggests that this is not an all-or-none phenomenon but a continuum of cellular, molecular and functional changes (Sofroniew and Vinters, 2010). These changes occur in a context-dependent manner dependent on the original insult, and whilst some of the changes are reversible, such as gene expression, there can be non-reversible changes such as scar formation and rearrangement to tissue structure (Sofroniew and Vinters, 2010).

Reactive astrocytes undergo changes to gene expression as part of the inflammatory response to trauma (Khakh and Sofroniew, 2015). The

phenotype of reactive astrocytes has been found to depend upon the initial injury, although there appears to be core genes which are upregulated in multiple injury models (Zamanian *et al.*, 2012). Alteration to reactive astrocyte function subsequently impacts surrounding neurons (Sofroniew and Vinters, 2010).

Transcriptome profile analysis of astrocytes shows that following exposure to LPS, *in vivo* or *in vitro*, the astrocyte transcriptome profile becomes pro-inflammatory and potentially cytotoxic (Liddelow *et al.*, 2017). Reactive astrocytes can produce a number of pro-inflammatory molecules such as: chemokines, cytokines, growth factors and even small molecules such as prostaglandin E (PGE) and nitric oxide (NO) (Lieberman *et al.*, 1989). Reactive gliosis can lead to a change in the receptor expression at the astrocyte surface, including an increase in toll-like receptors, which allow the release of pro-inflammatory chemokines and cytokines including TNFα and IL-6 (Kimelberg, 2010).

On the other hand, reactive astrocytes can respond to various types of intercellular signalling molecules by releasing molecules with anti-inflammatory functions, for example, releasing TGFβ in response to IL-10 (Sofroniew and Vinters, 2010). Additionally it seems that activated astrocytes can protect neuronal cells in a multitude of different ways including uptake of potentially excitotoxic glutamate (Rothstein *et al.*, 1996) and protection from oxidative stress (Shih *et al.*, 2003).

Reactive astrocytes can be considered as detrimental to neuronal survival and function following functional changes post traumatic insults in the CNS. Genes involved in the normal physiological functions of astrocytes are down-regulated following trauma, and gene expression profiles are altered leading to different astrocyte phenotypes. Induction of neuroinflammation via LPS treatment, or ischaemia via cerebral artery occlusion in mice, resulted in two different types of reactive astrocytes that were termed A1 and A2 based on gene expression (Zamanian *et al.*, 2012). A1 astrocytes upregulated complement cascade genes which can be destructive to synapses, thus it was postulated that these may have negative impacts on neuronal survival,

whereas A2 astrocytes facilitated the upregulation of neurotrophic factors suggesting that they may have positive effects (Liddelow *et al.*, 2017).

The A1 subtype of reactive astrocyte were subsequently investigated in more detail and it was shown that they lose their ability to promote neuron outgrowth and synaptogenesis (Liddelow *et al.*, 2017). Liddelow *et al.,* (2017) investigated the ability of A1 astrocytes to induce the formation of functional synapses *in vitro* via the purification of RGCs with quiescent or A1 astrocytes and quantified synapse number. RGCs cultured with A1 astrocytes had 50% less synapses compared to those cultured with quiescent astrocytes (Liddelow *et al.*, 2017). This suggested that A1 astrocytes are either unable to maintain these synapses or actively disassemble them (Liddelow *et al.*, 2017). Additionally, A1 astrocytes can cause the death of neurons and mature differentiated oligodendrocytes because they gain a neurotoxic function (Liddelow *et al.*, 2017).

In summary, astrocytes clearly demonstrate plasticity and are sensitive to environmental changes. Astrocyte heterogeneity of morphology, gene expression and function has been observed and it is important to fully elucidate resultant changes to astrocytes following reactivity in order to determine their roles in CNS pathology.

1.2.4.4.1 Reactive Gliosis Affects Astrocyte Calcium Signalling

Experimental evidence suggests that the release of ATP and inflammatory mediators, such as TNFα, by microglia is necessary for astrocyte activation following injury in the CNS (Liu, Tang and Feng, 2011). Subsequently, astrocytes release gliotransmitters following intracellular calcium elevation which may contribute to excitotoxicity, synaptic damage and neurodegeneration (Pascual *et al.*, 2012).

Astrocyte calcium signals can change acutely or chronically in response to traumatic brain insults: reactive astrocytes exhibit aberrant calcium signals which may have altered amplitudes, frequencies and durations (Shigetomi *et al.*, 2019). In addition to this it has been observed that reactive astrocyte calcium signals, and the differences between them and quiescent cells, differ

dependent on brain region and the models used to replicate naturally occurring CNS insults (Shigetomi *et al.*, 2019). Considering that altered calcium signalling by reactive astrocytes will influence gliotransmitters release following neuronal excitability, synaptic signalling and its modulation will also be significantly affected, therefore it will be important to discover more about alterations to the mechanisms of calcium signalling in reactive astrocytes.

1.2.5 Human Astrocytes

The physiology and pathology of astrocytes has been discovered for the most part using a mixture of *in vivo*, *ex vivo* and *in vitro* culture techniques with primary rodent tissue. Whilst an abundance of astrocyte functional characteristics have been determined using animal models, such findings need to be verified using human astrocytes to establish if human astrocytes have an analogous function. Evidence so far suggests that human astrocytes can conduct more complex information processing than their rodent counterparts (Oberheim *et al.*, 2006). Discovering human-specific astrocytic properties is integral for developing translational research.

It has been discovered that human protoplasmic astrocytes are larger in diameter by a factor of 2.6, have up to 10 times more GFAP positive primary processes, propagate calcium waves 4 times faster and are more functionally complex than primary rodent protoplasmic astrocytes (Oberheim *et al.*, 2010). With a larger diameter and greater numbers of processes, human protoplasmic astrocytes can occupy a 16.5 fold greater volume compared to mouse astrocytes (Vasile, Dossi and Rouach, 2017). Consequently, human protoplasmic astrocytes may have domains that cover up to 2 million synapses versus 120,000 synapses in mice as a result of their dramatically increased volume (Oberheim *et al.*, 2010).

Human protoplasmic astrocytes have been described as highly symmetrical whereas rodent astrocytes may be polyhedral with a cell body centrally located or can be polarised with processes orientated in one direction (Oberheim *et al.*, 2006). Whilst rodent astrocytes have cell bodies between 30-60 µm and 3-4 primary astrocyte processes which branch distally, human

astrocytes have smaller cell bodies (~10 µm) with up to 40 GFAP positive processes which span over 100-200 µm (Oberheim *et al.*, 2006). Such numerous processes extend radially in all directions from the cell body (in a symmetrical manner) which leads to a dramatic increase in human astrocyte volume compared to rodent astrocytes (Oberheim *et al.*, 2006).

This evolution of protoplasmic astrocytes in humans is not the only observed difference: interlaminar astrocytes, which were first described in the 1890s, are primate-specific cells which extend long and unbranched processes throughout the layers of the cortex and terminate in layers three and four (Foa, 1893; Colombo and Reisin, 2004). These interlaminar astroglial processes from layers one and two develop slightly differently to other types of astrocytes, they do not originate from radial glia but develop postnatally in the cerebral cortex (Vasile, Dossi and Rouach, 2017).

Transcriptomic analysis, following astrocyte purification via immunopanning, has revealed a correlation with genes that are highly expressed in rodents including GFAP (Vasile, Dossi and Rouach, 2017). Only 30% of the genes found in human astrocytes were also found in rodent astrocytes, thus it has been postulated that glial transcripts represent the biggest differences in gene expression between humans and rodents (Vasile, Dossi and Rouach, 2017). It seems likely that there will be many more significant morphological and functional differences between rodent and human astrocytes and more research is necessary to fully uncover them.

1.3 Neurons

The neuron was first described by Santiago Ramón y Cajal and Camillo Golgi back in the 1880s. It was at this time that Cajal and Charles Sherrington proposed the neuron doctrine which stated that the neuron is the structural and functional unit of the CNS. However, not long after the discovery of the individual neuron, it became apparent that focusing on the neuron as a single unit to elucidate nervous system function did not accurately represent the combined function of networks of neurons. Today, the development of new optical and electrophysiological techniques, such as multi-neuronal recording

methods, illustrate that ensembles of neurons form the units that lead to functional states (Yuste, 2015). Studying the way in which neurons work together will further our understanding of how functional states generate behaviour and cognition.

Over 80 billion electrically active neurons, which innervate the entire body, are typically classified according to their function and morphology. Sensory neurons respond to stimuli, motor neurons control muscle contractions to initiate movement, and interneurons connect neurons to other neurons within the same region of the CNS. There are a variety of types of neuron throughout the central and peripheral nervous systems which are categorized according to their size, shape and location. For example, Purkinje cells are large multipolar GABAergic neurons that exist in the cerebellum and the cortex is largely occupied by a different type of multipolar neuron known as the pyramidal neuron (Elson, 2007).

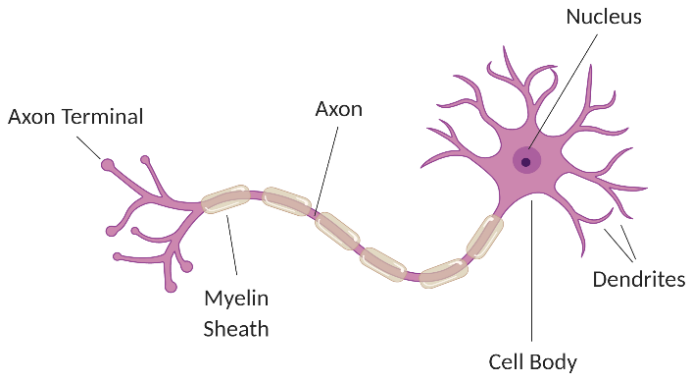


Figure 2. Neurons in the CNS are highly adapted for function. An example of a motor neuron is shown with a cell body within which the nucleus resides. Dendrites and a polarised axon extend from the cell body. Axons are covered with a myelin sheath via oligodendrocytes in the CNS. Created with BioRender. https://biorender.com/

Neurons are highly specialised for the transmission of action potentials. They are comprised of a cell body, dendrites and an axon which may be myelinated by oligodendrocytes in the CNS (shown in Figure 2) (Zipursky SL, 2000). Dendrites extend outwards from the cell body, which contains the nucleus, differing in size and shape depending on neuron type (Zipursky SL, 2000). The axon also extends from the cell body but further than any of the individual

dendrites (Zipursky SL, 2000). The cell body and dendrites are capable of receiving synaptic inputs from their local environment and the axon transmits this information to other neurons. Voltage gradients exist across the membrane of neurons, and changes to the membrane potential allow the passage of action potentials along the axon (Zipursky SL, 2000).

1.3.1 Growth and Development

1.3.1.1 Polarisation

Neuron connectivity and physiological brain function relies on the polarisation of axons and dendrites (Barnes and Polleux, 2009). Asymmetric activation of intracellular signalling pathways and extracellular cues are critical for neuronal polarisation, which is itself integral for unidirectional signal flow from dendrites to the soma and axons to pass information between cells in the CNS (Yoshimura, Arimura and Kaibuchi, 2006).

Primary cortical neurons are transformed from a non-polarised state, into structures with an axon and a number of dendrites, within the first five days of culture *in vitro* (Dotti, Sullivan and Banker, 1988). Initially neurons have a number of short processes extending from the cell body but after two days axons can be identified (Dotti, Sullivan and Banker, 1988). As axons grow and develop, they require the formation of membrane and cytoplasm (Goldberg, 2003), and may exhibit branching by the formation of collaterals (Dotti, Sullivan and Banker, 1988). At the tip of the axon is the growth cone which is specialised for elongation and is critical for generating the forward tension of the elongating axon (Goldberg, 2003).

The cellular and molecular mechanisms that underpin the establishment of axon-dendrite polarity have been discovered by *in vivo* and *in vitro* work on rodent cortical and hippocampal neurons (Barnes and Polleux, 2009). JNK interacting protein-1 (JIP-1), a kinase which has been shown to localise to neurites and is highly expressed in neurons, is a critical regulator of axon formation (Dajas-Bailador *et al.*, 2014). Prior to the polarisation of primary cortical neurons, JIP-1 localises to a single neurite, and post axonal specification, it builds up in the developing axon (Dajas-Bailador, Jones and

Whitmarsh, 2008). Thus, JIP-1 is required for normal axonal development and is commonly used as a marker to identify the neuronal growth cone in culture.

Other kinases involved in axon specification include phosphatidylinositol 3-kinase (PI3K), a lipid kinase, which increases sites enriched for phosphatidylinositol (3,4,5)-triphosphate (PIP3) in the membrane (Barnes and Polleux, 2009). PIP3 has been shown to accumulate within individual neurites extending out from the cell bodies of neurons (Ménager *et al.*, 2004). PI3K phosphorylates Akt, activating it, which in turn phosphorylates and deactivates glycogen synthase kinase-3β (GSK-3β), which is otherwise constitutively active (Jiang *et al.*, 2005). The decreased activity of GSK-3β is necessary for neuronal polarisation (Jiang *et al.*, 2005).

At the tip of a polarised axon, the axon growth cone navigates through the ECM according to molecular cues. The tip of the axon is extremely sensitive to chemical gradients which are necessary to accurately guide the axon to its final and desired location. Two molecules which have an integral role in this process are Netrin-1 and Shootin1 (Baba *et al.*, 2018). Small netrin-1 gradients are sufficient to dramatically influence phosphorylation of shootin1a which binds with L-CAM and acts as a mechanism to attach neurons to their surroundings (Baba *et al.*, 2018). In addition to this, the semaphorin family of proteins also direct axon guidance, such as Sem3A which acts as a repulsive cue when bound with neuropilin-1 and plexin at the surface of growth cones (Nakamura, Kalb and Strittmatter, 2000).

1.3.1.2 Cytoskeleton

Axon function is heavily reliant upon a cytoskeleton composed of intermediate filaments and microfilaments for structural support, as well as microtubules for intracellular transport (Moloney, de Winter and Verhaagen, 2014). Although microtubules provide most of the long distance transport, transport along actin filaments is also important including at axon growth cones and end point areas (Luo, 2002). Furthermore, neurons are commonly identified using cytoskeletal markers such as acetylated tubulin and β-III tubulin in immunofluorescence techniques.

1.3.2 Synapses and Communication

Neurons communicate with one another across synapses which are composed of a presynaptic terminal, a synaptic cleft and a postsynaptic spine (Figure 3). Axons propagate action potentials along their length which stimulate the release of neurotransmitter from vesicles that fuse with the presynaptic membrane.

Synaptic vesicles are clustered at the active zone in the presynaptic terminal which is abundant with voltage gated calcium channels. These allow calcium influx which is responsible for the activity dependent fusion of vesicles to the active zone and subsequent neurotransmitter release (Connors and Long, 2004). Diffusion of neurotransmitter across the synaptic cleft activates receptors on the postsynaptic membrane (Figure 3) (Rutecki, 1992).

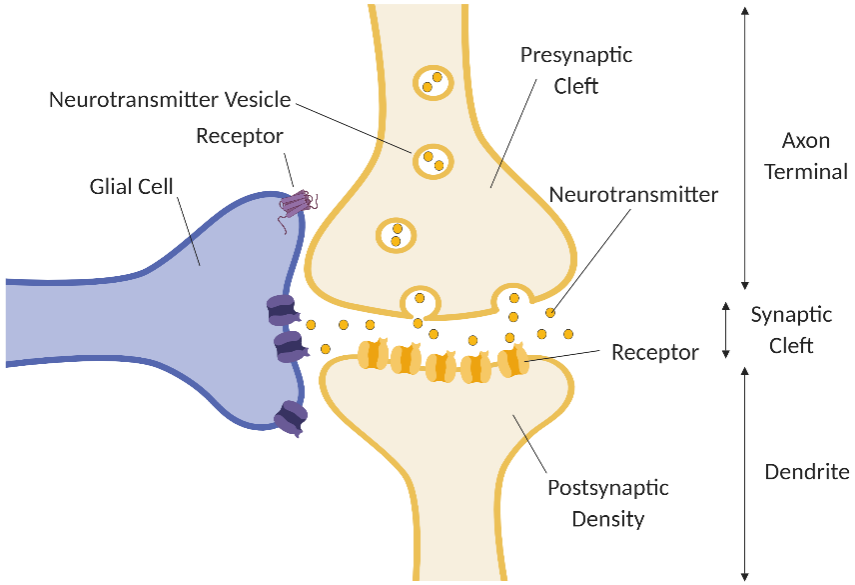


Figure 3. Neurons transmit electrical signals via neurotransmitter release at specialised junctions known as synapses. Presynaptic vesicles containing neurotransmitter (yellow filled circles) are stimulated to bind to the active zone on the presynaptic cleft. Neurotransmitter is released into the synaptic cleft where it diffuses and binds to receptors on the post synaptic density. Glial cells, most notably astrocytes, surround synapses and can remove neurotransmitter from the synaptic cleft. Created with BioRender. https://biorender.com/

1.3.2.1 Traditional and Ectopic Transmission

The traditional model of synaptic transmission between neurons involves the release of synaptic vesicles from the active zone which diffuse across the synaptic cleft to interact with receptors on the post synaptic membrane as discussed (see section 1.3.2). However, in recent years research indicates that neurons can release synaptic vesicles at sites distinct from the active zone, termed 'ectopic' sites. In this case, neurotransmitters are released directly into the extracellular space (Matsui, 2005). While the full significance of this mechanism is still unknown, it is generally thought to promote the interaction of glial cells with neurons since neurotransmitters can activate receptors on astrocytes that ensheathe the synapses.

Ectopic communication has been well investigated in the molecular layer of the cerebellar cortex where Purkinje neurons and Bergmann glia (BG) reside in close proximity. Here, glutamate activates calcium permeable AMPA receptors on BG cells that enclose Purkinje cell synapses (Matsui and Jahr, 2006; Balakrishnan and Bellamy, 2009; Fendler *et al.*, 2012). Resulting BG calcium transients have been found to regulate the uptake of potassium ions, suggesting their role in Purkinje cell membrane potential maintenance (F. Wang *et al.*, 2012). Evidence is also compelling that ectopic release directs glial processes to glutamate release sites in order to inhibit excitotoxicity to Purkinje neurons via neurotransmitter clearance (Balakrishnan *et al.*, 2011). Additionally, in recent years it has been confirmed that BG are essential for synaptic organisation in the Purkinje cell layer (Miyazaki *et al.*, 2017).

Further research into this alternative mechanism of communication is necessary to understand the location of ectopic release sites which were hypothesised to exist in parallel fibre presynaptic terminals close to the plasma membrane that lies opposite Bergmann glial membranes (Matsui and Jahr, 2006).

1.4 *In Vitro* Cell Culture

For decades now, *in vitro* culture of primary astrocyte cells has been used to study the physiological and pathological states of astrocyte cells. Key

discoveries about their roles in metabolism and neurotransmission have been uncovered, however, there are key differences between the cells and signalling molecules that astrocytes are exposed to *in vivo* compared to *in vitro*.

Astrocytes *in vivo* are surrounded by a specialised ECM containing proteoglycans, hyaluronic acid, laminins and tenascins (Novak and Kaye, 2000). This ECM facilitates cell-cell and cell-ECM interactions which are vital in processes such as proliferation, differentiation and gene expression (Watson *et al.*, 2017). Astrocytes cultured *in vitro* lack the interactions of other cell types, and the molecules they secrete, and are exposed to cell culture media compositions and coating substrates that don't replicate the *in vivo* environment. For example, fibronectin and collagen, often used for coating 2D substrates, are not present in the brain (Yamaguchi, 2000). Consequently, using *in vitro* primary cell culture as a model experimental system has limitations and may be reaching the limits of physiological relevance.

Primary rat astrocytes can be grown as monolayers on the surface of cell culture flasks; such 2D cell culture techniques have also been found to induce astrocyte reactivity (East *et al.*, 2010). In addition to this, the surface coating of 2D culture ware influences astrocyte morphology; this was shown with human fetal-derived astrocytes cultured on matrigel, fibronectin, collagen IV and collagen I (Levy *et al.*, 2014). Therefore, the tendency of 2D culture to generate reactive astrocytes and the inability to recreate the molecular complexity found in the *in vivo* environment calls into question the validity of experimental findings *in vitro*. Whilst the lack of a dynamic microenvironment is clearly a disadvantage to understanding some elements of cell physiology, it means that when astrocytes are co-cultured with another cell type, their interactions can be carefully assessed. Seeding cortical embryonic or neonatal neurons on top of a layer of astrocytes is relatively common practice for astrocyte and neuron co-culture.

Primary murine or rodent cell culture protocols for astrocytes can vary greatly, a somewhat confounding factor in understanding the translational relevance of experimental findings, considering that gene and receptor expression in

astrocytes is dramatically influenced by the environment (Lange *et al.*, 2012). Additionally, astrocyte maturation is crucial for the expression of key receptors in rodents, such as EAAT1, which occurs during the late stages of embryogenesis and into the early stages of postnatal development (Rusnakova *et al.*, 2013). However primary astrocytes are extracted from the brain at different embryonic and neonatal time points and will subsequently be exposed to different coating substrates and media compositions to encourage maturation depending on the research group.

Since embryonic or neonatal rodent tissue is commonly used to generate primary cultures of astrocytes at a point at which gliogenesis is incomplete, factors such as fetal bovine serum (FBS) are added to the culture medium to encourage astrocyte maturation so that cells will divide until they become confluent. However, the full impact FBS may have on gene expression is unknown, especially considering that FBS exhibits significant batch to batch variation (Fang *et al.*, 2017). Astrocyte cultures can also be supplemented with the cell permeable analogue dibutyryl cyclic AMP (dbcAMP) after 14 DIV which induces striking morphological changes and rearrangement to the cytoskeleton (Fedoroff *et al.*, 1987), and upregulates the expression of glutamine synthetase and GLT-1 which are important in astrocyte differentiation (Hertz, Peng and Lai, 1998).

In vitro methods offer the opportunity to investigate phenotypic features of a single cell type under carefully controlled experimental conditions, but whilst this is advantageous in some respects, it removes the understanding of the important interplay of other cell types in cell-specific mechanisms. Both astrocytes and microglia have important homeostatic and reactive functions in the CNS, but activation of microglia precedes reactive astrogliosis following injury and is necessary for astrocyte activation (Kirkley *et al.*, 2017; Liddelow *et al.*, 2017). Furthermore, in such examples, understanding of the mechanisms of astrocyte reactivity in single pure cultures *in vitro* may not recapitulate the *in vivo* mechanisms.

1.4.1 Microfluidics

Traditionally, neuroscience research has been conducted *in vivo* using experimental animals, but the environment is overwhelmingly complex and it is challenging to pick out specific variables in disease pathology (East *et al.*, 2010). The brain has a huge range of cell types such as neurons, astrocytes, microglia, oligodendrocytes and even invading macrophages following injury. In this complex environment, where all the different cell types are releasing different factors at different time points and in response to different cues, it is a huge challenge to try and work out the underlying mechanisms of processes such as neurodegeneration.

Microfluidics refers to a set of technologies used to manipulate small fluid volumes which enable culture, analysis and experimentation on cells in micro scale volumes (Halldorsson *et al.*, 2015). Thus, it is possible to study small numbers of cells or even single cells with high temporal and/or spatial resolution (Badiola-Mateos *et al.*, 2018). Such up and coming technologies provide sophisticated *in vitro* models for the study of the CNS.

Microfluidics technologies can offer a number of advantages compared to macroscopic cell culture (large culture ware). Firstly, the flexibility of design in microfluidic devices means that devices can be tailored to the requirements of individual cell types and cellular co-cultures (Yeo *et al.*, 2011). Microfluidics devices also have the capacity to mimic a cell's natural microenvironment with greater accuracy than macroscopic culture via continuous perfusion culture or creating chemical gradients (which is difficult to achieve in large culture ware) (Halldorsson *et al.*, 2015). Since only micro scale volumes are required, both the consumptions of reagents and cells is minimised and dramatically reduced compared to macroscopic culture.

There are still challenges to working with microfluidics devices; whilst macroscopic techniques present an established culture material with well characterised influences on cell behaviour, new polydimethylsiloxane (PDMS) devices may detrimentally affect cell viability (Millet *et al.*, 2007). In addition to this, currently there are not many standard culture protocols for specific cell

types in microfluidic devices. Whilst the possibility of personalised device design for tailored studies is an attractive feature of microfluidics techniques, changes to device material, surface coating and cell density all influence experimental outcome (Halldorsson *et al.*, 2015). Furthermore, more experimental research is necessary to determine optimised protocols for neuron culture and development for example, in order to routinely adopt such techniques (Millet *et al.*, 2007; Millet and Gillette, 2012).

Compartmentalised microfluidics devices offer the potential to anatomically isolate domains of cell types to study cellular mechanisms in different locations. Additionally, compartmentalized devices offer the potential for cellular co-culture and the detailed study of their interactions. Considering that astrocyte-neuron communication is an integral element to physiological brain function, *in vitro* devices such as compartmentalised microfluidic systems can be used to isolate neuronal somata and axons and enable the addition of astrocytes to parallel compartments to infer more about the communication between the two cell types (see Figure 4). It will be possible to fully elucidate diffusible molecules released by astrocytes that result in axon growth as well as synaptogenesis and maturation. In addition to this cell-cell interactions at the astrocyte-axon interface may be measured in the channel seeded with astrocytes.

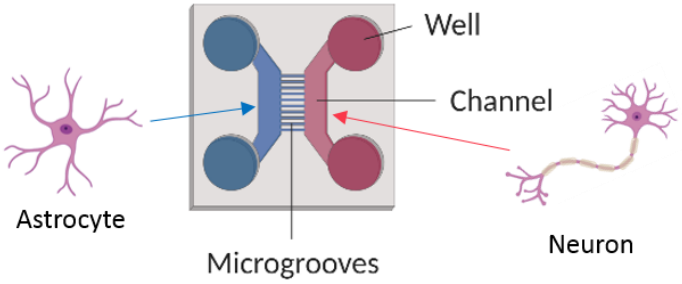


Figure 4. Compartmentalised microfluidics devices allow detailed investigations into cell-cell interactions. In the device shown, neurons could be seeded into the wells on the right hand side (red) and subsequently axons will extend from the right hand channel (red), across the microgrooves and into the left hand channel (blue). Astrocytes could be seeded into the wells on the left hand side (blue) of the chamber but their processes will be too big to extend across the microgrooves. Cartoon created with BioRender. https://biorender.com/

1.4.2 3D Culture Environment

2D *in vitro* techniques have been instrumental in developing understanding of primary astrocyte physiology and pathology: however murine and rodent cells develop flat and rounded morphologies unlike *in vivo,* and are unable to form characteristic cell-cell and cell-matrix interactions in this monoloayer environment. In conjunction with this, primary astrocytes may express higher levels of cytoskeletal elements GFAP and vimentin, and undergo cytoskeletal rearrangements in response to the culture environment. 3D culture environments, which offer the possibility of developing physiologically relevant *in vitro* systems, offer the capacity to capture the complexity of the brain microenvironment reproducing cell-cell and cell-matrix interactions (Vickerman *et al.*, 2008). Research suggests that mammalian cell types more closely resemble cells *in vivo* when cultured in 3D environments (Wong *et al.*, 2008). There are currently lots of commercially available options for culturing astrocytes in 3D, including hydrogels and physiologically inert scaffolds.

In addition to new 3D substrates and relevant protocols for primary cell culture, there has been the development of 2.5D cultures where cells can be seeded onto a layer of a hydrogel (and are not encapsulated). 2D culture allows cell types to form focal adhesions with a coated substrate, whilst 2.5D culture with hydrogels enables cells to form adhesions more realistic of the *in vivo* microenvironment for the investigation of cell migration *in vitro* (Pebworth, Cismas and Asuri, 2014). 2.5D culture has promoted studies considering the geometry of the environment and, for example, has established the impact of the extracellular environment on fibroblast activation in hydrogels (Smithmyer, Cassel and Kloxin, 2019).

Engineered scaffolds can be used to maintain astrocytes in a non-reactive state, such as Alvetex®, a 3D polystyrene porous scaffold (Ugbode, Hirst and Rattray, 2016). Alvetex enables cells to maintain their *in vivo* morphology, behaviour and responsiveness within an *in vitro* model system. Additionally, no cell is more than 100 microns from a nutrient source allowing easy exchange of nutrients, gases and waste products via passive diffusion across

short distances. Cells are also freely able to interact with neighbouring cells in 3D.

Despite being advertised as a 3D culture system, the alvetex polystyrene scaffold could be considered as a 2.5D substrate since it is common that primary cells seeded into this matrix from the top do not migrate through the 200 micron depth. In addition to this, the alvetex material has a high tensile strength (35 – 55 mPa) which is greater than that of the brain extracellular matrix which is more malleable. Therefore, this polystyrene scaffold may influence process extension and the cytoskeletal arrangement of astrocytes.

Natural or synthetically made hydrogels are networks of polymers or proteins which provide a 3D culture system for glial cells (Watson *et al.*, 2017). Astrocytes cultured in hydrogel matrices exhibit greater ramification, and smaller and more spherical volumetric shapes when compared to those in 2D which are flat and tend to have few projections (Watson *et al.*, 2017). 3D hydrogels provide a form of cell culture with dimensions identical to *in vivo* and thus the hope is that such systems should reveal more accurate morphological information about primary astrocytes since the astrocyte cytoplasm and processes have the opportunity to extend in all axes. One caveat includes the density of the matrix (related to the molecular weight used in preparations) which may interfere in process extension.

One commercially available hydrogel that is extensively used, especially in cancer cell studies, is Matrigel®. Matrigel Basement Membrane Matrix Growth Factor Reduced is a solubilized basement membrane preparation extracted from the Engelbreth-Holm-Swarm (EHS) mouse sarcoma. This tumour is rich in ECM proteins and growth factors such as: laminin, collagen IV, entactin and heparan sulphate proteoglycans. Whilst proven to induce neurite outgrowth, this matrix is not highly representative of the brain extracellular matrix which is primarily composed of hyaluronic acid, as well as proteoglycans and laminin (Novak and Kaye, 2000). Another hydrogel which can be synthesised commercially and allows the encapsulation of cells is hyaluronic acid. Hyaluronic acid is a naturally occurring component of the brain and such gels are therefore an attractive option for 3D *in vitro* culture models. Furthermore

hydrogel composition should influence the choice of which hydrogel to use for specific cell types.

A study by Placone *et al.,* (2015) showed that combining various hydrogels to mimic aspects of the brain microenvironment allowed human astrocytes to develop physiological morphology and remain quiescent. The authors used an optimized matrix of collagen, hyaluronic acid and matrigel, and discovered that human astrocytes exhibited numerous processes and low levels of GFAP expression (Placone *et al.*, 2015). The careful formulation of physiologically relevant hydrogels for 3D *in vitro* cell culture will be invaluable for bridging the gap between simple 2D models and whole animal models.

Hydrogels and inert scaffolds offer crucial advances in the field of neural tissue engineering, where grafts and scaffolds are implanted into the brain or spinal cord with the purpose of encouraging nerve regeneration and repairing damage. When injury is incurred in the CNS, a lack of regeneration of brain tissue follows due to the lack of availability of structural support which would host cells resulting from neurogenesis (Modo, 2019). Inert scaffolds thus provide the opportunity for transplantation to induce the invasion and proliferation of relevant cell types responsive to injury (Modo, 2019). At the same time, biodegradable and biocompatible scaffolds and grafts for implantation may also benefit patients with Alzheimer's or Parkinson's disease by stimulating new neuronal growth where cells have been lost (Dehqan Niri *et al.*, 2019).

1.5 Aims and Objectives

The National Centre for the Replacement, Refinement and Reduction of Animals in Research (NC3Rs) is the UK's national organisation for the 3Rs which is dedicated to providing a framework for performing more humane animal research. NC3Rs collaborate with research scientists and organisations from across the life sciences sector both nationally and internationally to reduce, refine and replace the use of animals in research and testing. The 3Rs impacts are diverse, ranging from policy and regulation changes to embracing new technologies and approaches for various research

avenues. NC3Rs have funded this research project which has been dedicated to developing new technologies in order to reduce the use of animals used in scientific research. The hope is that developing more physiologically relevant *in vitro* models will reduce the need for *in vivo* and *ex vivo* experiments using transgenic animals.

The primary objective of this PhD project was to further understanding of the influence of 3D culture systems on physiological astrocyte function. Additionally, a key aim was to assess the influence of the cell culture environment on astrocyte phenotype, with a specific focus on the effects of cell culture media composition on astrocyte calcium signalling.

A key objective, alongside the main aims, has been to develop 3D culture methods to generate viable cells in 3D matrices that permit the study of quiescent and reactive cell state. Specifically, the aim was to categorize the morphological parameters of primary neonatal cortical astrocytes which develop following *in vitro* culture methods. I hypothesised that primary astrocytes cultured in 3D hydrogels *in vitro* would develop a morphological profile similar to *in vivo* cells. I believed that this work would illustrate that closely mimicking *in vivo* conditions in cell culture techniques will generate more translational findings.

Chapter 2. Methods

2.1 Ethical Statement

All experiments were performed according to policies on the care and use of laboratory animals of British Home Office and European Community laws. The University of Nottingham Animal Welfare and Ethical Review Body approved the experiments. All efforts were made to minimize animal suffering and reduce the number of animals used.

Primary rat cells were obtained in accordance with guidelines set out in the code of practice for humane killing under Schedule 1 of the UK Home Office Animals Scientific Procedures Act (1986).

2.2 Primary Cells

2.2.1 Isolation of Astrocytes

Unless otherwise stated, primary cortical P2 neonatal astrocytes were derived from Wistar rats (Charles River Laboratories, Oxford) and used for experimental investigations. Initial experimentation involved the use of E18 embryonic astrocytes which have an increased growth rate and proliferative capacity compared to neonatal cells, however, personal communication with a colleague in the Bellamy lab revealed the difficulty of inducing reactive gliosis with primary cortical E18 embryonic astrocytes. Since an aim of this PhD has been to evaluate the impact of induced reactive gliosis on astrocyte morphology, P2 neonatal tissue has been used.

Primary cortical astrocyte cultures were generated under sterile conditions according to a protocol obtained through personal communication with Tomas Bellamy. Schedule one killing method using carbon dioxide exposure was used to sacrifice female adults. Neonatal pups were sacrificed by cervical dislocation and decapitation.

Incisions were made along the skull midline and laterally to ease the removal of the intact brain, and forceps were used to separate the cortices and remove

the meningeal membranes. Cortices were placed into a falcon tube containing 5 ml of astrocyte medium: DMEM with 10% FBS (10500064, Gibco, UK), 45.5 units/ml penicillin (P0781, Sigma-Aldrich, Poole, UK), 0.05 mg/ml streptomycin (P0781, Sigma-Aldrich) and 50 mg/ml L-proline (P5607, Sigma-Aldrich). Next 15 µg/ml papain solution (LK003178, Worthington Biochemical Corporation, New Jersey, US) was added to the dissected tissue which was incubated at 37ºC and 5% CO_2 for 40 minutes.

All following steps were carried out at room temperature. 500µl of 20 mg/ml DNAse solution (A3778.0100, VWR, Bedfordshire, UK) was added and the tissue was triturated to dissociate the cells following the incubation step. Tissue was centrifuged at 212 g for 6 minutes, the supernatant was removed and 2 ml of astrocyte medium and 20 mg/ml DNAse was added to the pellet. Tissue was triturated for 20 cycles and centrifuged at 182 g for 3 minutes. Supernatant was collected in a new falcon tube and 10 ml of astrocyte medium was added to the cell pellet which was triturated for another 20 cycles. Tissue was centrifuged again at 182 g for 3 minutes. The removal of supernatant, trituration and centrifugation at 182 g was repeated once more. Collected supernatant was centrifuged finally for 6 minutes at 212 g. The supernatant was removed, 10 ml of astrocyte medium was added to the cell pellet, which was resuspended, and the cell suspension was passed through a 100 µm cut-off cell strainer (352360, Falcon Scientific, Northumberland, UK). 1 ml of the cell suspension was then distributed into T75 flasks (83.3911.002, Sarstedt, Leicestershire, UK) containing approximately 5 $x10^5$ cells which were then topped up with 20 ml of astrocyte-specific media. Astrocytes seeded into T75 flasks were kept in a 37ºC and 5% CO_2 incubator until use. Astrocyte medium was replaced every 3-4 days until 14 *days in vitro* (DIV) when primary cortical astrocytes were ready for experimental use.

Astrocytes grown in T75 flasks were split after 14 DIV. Under sterile conditions and at room temperature, the media was aspirated from the flasks which were then washed with Dulbecco's Phosphate Buffered Saline (PBS) (D8537, Sigma-Aldrich). PBS was removed and 2 ml of trypsin-EDTA (T3924, Sigma-Aldrich, final concentration = 0. mg/ml trypsin, and 0.2 mg/ml EDTA)

was added to dissociate the cells from the surface of the flask when incubated at 37ºC and 5% CO_2 for 5 minutes. Flasks were tapped to aid cell detachment and then viewed under the microscope: if cells were rounded and floating, trypsin treatment was sufficient. 8 ml of astrocyte medium was then added to each flask before it was transferred to a falcon tube which was centrifuged at 212 g for 6 minutes. Supernatant was poured off the cell pellet which was resuspended in 5 ml of astrocyte-specific media. The cell density of the suspension was calculated using a haemocytometer and cells were then seeded onto coverslips or plates at 2.5 $x10^4$ cells per ml, or into 3D matrices at 1.25 $x10^4$ cells per ml.

2.2.2 2D Cell Culture of Astrocytes

For experiments requiring 2D substrates, either 22 mm glass coverslips (12333138, Fisher Scientific) or 24-well glass-bottomed cell culture plates (662892, Greiner Bio-One, Gloucestershire, UK) were used. Coverslips or plates were coated with 400 µL of sterile 0.1 mg/ml poly-l-lysine hydrobromide (PLL) (P1524, Sigma-Aldrich) for 30 minutes and then washed with 1 ml of PBS twice. PLL was necessary for cells to attach to the coverslips or plates they were seeded onto.

2.2.3 Inducing Astrocyte Stellation

Forskolin (FSK) treatment (an adenylate cyclase activator) was used to induce astrocytes to develop a stellate morphology. Astrocytes in both 2D and 3D culture formats were treated with 10 µM FSK (0.4% in DMSO vehicle) (93049, Sigma-Aldrich) which was added directly to the bathing medium for 3 hours at 37ºC and 5% CO_2. FSK was removed by washing with either 1 ml of astrocyte medium or imaging buffer (see section 2.3.1).

2.3 Characterisation of Cell Morphology

2.3.1 Calcein AM Loading

Live cell labelling was extensively used to determine both the health and morphology of astrocyte cells. In 2D and 3D formats, astrocytes were left for

24-48 hours after seeding onto coverslips/plates or into gels before they were loaded with calcein AM (C3100MP, Invitrogen).

4 µL of 1 µM Calcein AM in Pluronic F-127 (P3000MP, Invitrogen) was added directly to the bathing medium for cells for 30 minutes at 37°C and 5% CO_2. Astrocyte medium containing calcein AM was removed and replaced with either 2 ml or 400 µL (depending on cell culture plate size) of a HEPES buffered saline solution necessary to keep cells alive during imaging. The complete imaging buffer recipe is as follows: 135 mM NaCl, 3 mM KCl, 10 mM HEPES, 15 mM Glucose, 1 mM $MgSO_4$ and 2 mM $CaCl_2$ in deionised water with pH 7.4 using NaOH. For hydrogels, there was a small adjustment to the imaging buffer recipe: 1 mM $MgSO_4$ was substituted for 1 mM $MgCl_2$.

2.3.2 Immunofluorescence for Astrocytes

To investigate astrocyte morphology in 2D formats, or in the alvetex scaffold, cells were fixed with either 1 ml or 400 µL of 4% paraformaldehyde (PFA) respectively. Fixing was carried out for 10 minutes at room temperature and followed by 3 washes with either 400 µL/ 1ml of PBS. 400 µL/ 1ml of 0.1% Triton X-100 (T8787, Sigma-Aldrich) in PBS was added to cells for 10 minutes at room temperature and then there was a further 3 washes with PBS. Non-specific binding sites were blocked with 400 µL/ 1ml of 0.5% bovine serum albumin (BSA) (4215015, VWR) in PBS for 1 hour at room temperature.

Antibodies were prepared in 0.5% BSA. Glial fibrillary acidic protein (GFAP) was used at 1:1000 dilution (ab7260, rabbit, polyclonal, Abcam, Cambridge, UK). A solution of DAPI was used at 1:300 dilution (D9542, Sigma-Aldrich). Additionally S100β was used at 1:100 (ab52642, rabbit, monoclonal, Abcam). ‘Neuron-specific’ primary antibodies were also used to label astrocytes: β-III tubulin at 1:300 (ab18207, rabbit, polyclonal, Abcam) and acetylated tubulin at 1:300 (T7451, mouse, monoclonal, Sigma-Aldrich).

Preparations were incubated with 300 µL or 100 µL of primary antibodies for 22 mm coverslips or 24-well plate preparations respectively, at 4°C overnight. Next secondary antibody incubations (same volumes apply) were carried out in 0.5% BSA for 45 minutes at room temperature. Secondary antibodies used

include: Alexa Fluor® 568 goat anti-mouse IgG (A11004, Invitrogen) and Alexa Fluor® 488 goat anti-rabbit IgG (A1008, Invitrogen). Coverslips were mounted onto slides using 50 µL of Vectashield® with DAPI (H-1500, Vector Laboratories Inc, Peterborough, UK) and allowed to dry in the dark for 2 hours before being stored in the dark at 4ºC.

2.3.3 Imaging Live and Fixed Primary Cells

Investigations into astrocyte morphology and neuron survival, growth and development primarily used imaging with a Nikon Eclipse Ti-E, an Olympus IX70 and a Zeiss 710 confocal microscope.

The Nikon Eclipse Ti-E and Olympus IX70 microscopes were used for both live-cell and fixed-cell labelling with astrocytes and neurons prepared in 2D, generating single plane images. The Zeiss confocal microscope was set up to collect z-stacks of astrocytes and neurons cultured on 24-well glass-bottomed plates, in the alvetex scaffold, in 3 mg/ml matrigel or in 5 mg/ml hyaluronic acid.

Images were acquired with micromanager software and the 10x magnification lens on the Nikon-Eclipse Ti-E and Olympus IX70. The software was set so that coverslips had a 100 ms exposure time to an LED source (470 nm peak, 10-20% intensity; Cool LED pE2). Binning was selected as 1x1 for optimal resolution with 16-bit images. ND4 and ND8 neutral density filters could be used to modify the intensity of all wavelengths but were not selected as default when imaging with the Nikon-Eclipse Ti-E.

Images acquired with the Nikon-Eclipse Ti-E or Olympus IX70 were analysed using Image J (Rasband, W.S., ImageJ, U. S. National Institutes of Health, Bethesda, Maryland, USA, https://imagej.nih.gov/ij/, 1997-2019). If necessary, images were blinded using the Blinding Image J macro (written by Tiago Ferreira, 2009). Data was input into Graph Pad Prism Version 7.01 for Windows (GraphPad Software, La Jolla California USA, www.graphpad.com) for statistical analysis.

2.3.3.1 Confocal Imaging Parameters for Different 2D and 3D Matrices

2.3.3.1.1 2D 24-Well Plates

A 40x water objective with a numerical aperture (NA) of 1.20, and a z stack interval of 0.48 µm, was used when imaging astrocytes seeded onto glass-bottomed 24-well plates. Cells were imaged for approximately 6 minutes depending on the overall depth of the astrocytes lying flat on the glass surface of the plates. Samples were exposed to lasers at 2% intensity (488 nm peak). Additional imaging parameters are described fully in the appendix (see page 240).

2.3.3.1.2 Alvetex

An apochromat 10x water objective with a NA of 0.45 was used to try and match the refractive index of alvetex discs immersed in PBS and low magnification was necessary to image deeper into the scaffold. Samples were exposed to lasers at 2 - 10% intensity (405 or 488 nm peak). Full imaging parameters can be found in the appendix (see page 241).

2.3.3.1.3 Matrigel and Hyaluronic Acid

Cells in 3D gels were imaged with a 10x water objective with an NA of 0.45 and stack interval of 1.6 µm. This stack interval ensured we had an appropriate level of sampling when imaging 3D hydrogels. Cells were imaged up to approximately 12 minutes depending on the overall depth of the cells in the matrix. Full imaging parameters can be found in the appendix (see page 242).

2.3.3.2 Post Imaging Processing for 3D Z-Stacks

Four micron fluorescent beads (T7283, Invitrogen) were added into 2D or 3D preparations to determine the impact of stretching in the z-axis when imaging on the confocal. Beads were fluorescent when exposed to 470 nm light and were therefore visible in preparations of cells that had been loaded with

calcein AM. In 2D formats beads were mixed with cells in a 1:1000 dilution, whereas with 3D gels, beads were mixed with cells at a 1:100 dilution.

Post confocal imaging, the lengths of beads were measured in X, Y and Z using Zen software. The rectangle tool was then used to draw a box around the desired bead which was cut and saved as a new file. Then the z position slider was used to mark the 3D distance from one end of the bead to the other for length assessment.

2.3.3.2.1 Bead Analysis for 2D Culture Formats

For cells cultured on 24-well glass-bottomed plates, nine 4 micron beads were analysed to determine the extent of spherical aberration in the Z axis (see appendix, page 242). The mean calculated length in the Z axis for the nine beads was 7.73 µm. This was divided by the actual length of the beads (4 µm) to give a factor of 1.93. The original z-stack interval of 0.476 µm was divided by this calculated factor (1.93) to give a new z-stack interval that needed to be manually applied in Zen software for each image (0.247 µm). At this point, the appearance of beads in the orthogonal view were checked to make sure they appeared spherical and bead lengths in X, Y and Z were measured to check they were close to 4 microns (see appendix, page 242).

2.3.3.2.2 Bead Analysis for 3D Culture Formats

A total of 21 beads were analysed for their lengths in X, Y and Z when encapsulated within 3D matrigel. This was because cells were imaged over a great depth in the matrix, thus the extent of stretching is likely to differ at different depths, so a more representative mean was required. For beads in 3D matrigel, the average length in Z was 23.2 µm which when divided by 4 µm gives a factor of 5.79. The z-stack interval was 1.6 µm so dividing this by 5.79 gives an applied z-scale of 0.276 µm. Beads looked spherical after adjusting the z-scale (see appendix, page 243 for X, Y and Z length measurements post z scale adjustment).

This established protocol was also carried out for beads encapsulated in 5 mg/ml hyaluronic acid. A total of 17 beads were measured and were found to have an average length of 30 µm. Thus, the extent of stretching in the z plane

is equal to 30 divided by 4, so 7.5. This factor was used to deduce a new z-stack interval value of 0.213 µm (1.6 / 7.5). Again each bead was checked to confirm a spherical shape and bead lengths in X, Y and Z were measured manually post Z scale adjustment (see appendix, page 244).

2.3.3.2.3 Thresholding

Once confocal images for 2D and 3D culture formats had had their Z scale adjusted in Zen software, following analysis and calculations with 4 micron fluorescent beads, Volocity software was used to analyse key parameters of astrocyte morphology. In Volocity, freehand or box regions of interest (ROI) were drawn around a single cell of interest for the analysis of cell volume, surface area, shape factor and longest axis. Such parameters were determined automatically in the software based on fluorescence intensity.

The thresholding applied to images determined the number of pixels detected per ROI in each image analysed. At 0% auto thresholding, astrocytic process extremities and regions of the cell soma were not necessarily detected for quiescent or forskolin treated cells cultured in the various 2D or 3D cell culture formats. In order for thresholding to reflect what we detect to be part of a cell by eye, we trialled different auto thresholding values in the different culture formats. Visible differences were seen at 0, -25, -50 and -75% auto thresholding: the -75% auto thresholding value was selected since it was the best for discriminating astrocyte processes from the background.

Once -75% auto thresholding had been applied to images, measurements for volume, surface area, shape factor and longest axis were copied from Volocity software into Graph Pad Prism for statistical analysis. To determine if there were any significant changes to morphological parameters for astrocytes following forskolin treatment in different 2D and 3D culture conditions, a Kruskal-Wallis One Way ANOVA test with Dunn’s correction for multiple comparisons was used (0.05 significance level).

Chapter 3. Neuron-Glial Interactions in the Cerebellar Cortex

3.1 Introduction

3.1.1 The Cerebellum

The cerebellum is a region in the cerebral cortex of the brain associated with many functions, primarily motor coordination and the fine control of movement, as well as sensory and cognitive functions. Recent findings also show the cerebellum's active role in implicit learning in humans (Zhao *et al.*, 2016).

Neuronal and glial cells interact with one another in the cerebellum as part of normal neurophysiology (Figure 1). In addition to the three main classes of glial cell in the cerebellum (astrocytes, microglia and oligodendrocytes) there is another major glial class known as the radial glia. Radial glia are bipolar cells with elongated processes extending out from a cell body which develop from neural progenitor cells and transform into stellate astrocytes (Campbell and Götz, 2002). The cerebellum contains some semi-radial glia (or unipolar glia) known as Bergmann glial cells which have their cell bodies in the Purkinje layer and processes that extend into the molecular layer terminating with bulbous end feet at the pial surface similar to other types of astrocytes (Figure 1) (Buffo and Rossi, 2013). Bergmann glial cells have been found to surround a single Purkinje neuron, and their elongated processes encompass Purkinje cell dendrites in the molecular layer of the cerebellar cortex. Besides their role in the early development of the cerebellum, Bergmann glia are also required for the pruning or addition of synapses (Bellamy, 2006; Miyazaki *et al.*, 2017).

The cerebellum is a highly folded layer of the cortex which can be subdivided into three layers: at the bottom lies the thick granular layer which contains lots of granule neurons, on top of this lies the Purkinje layer containing the cell bodies of the Purkinje neurons and Bergmann glial cells, and the top

molecular layer contains the dendritic trees of Purkinje cells as well as the unmyelinated parallel fibres that run at right angles originating from granule cells (Figure 1) (Saab and Willis, 2003). Parallel fibres are glutamergic and can excite a whole row of Purkinje cells orientated perpendicular to them (Saab and Willis, 2003). The cerebellum accounts for 10% of the brain's volume but contains up to 80% of all the neurons in the brain (Herculano-Houzel, 2010).

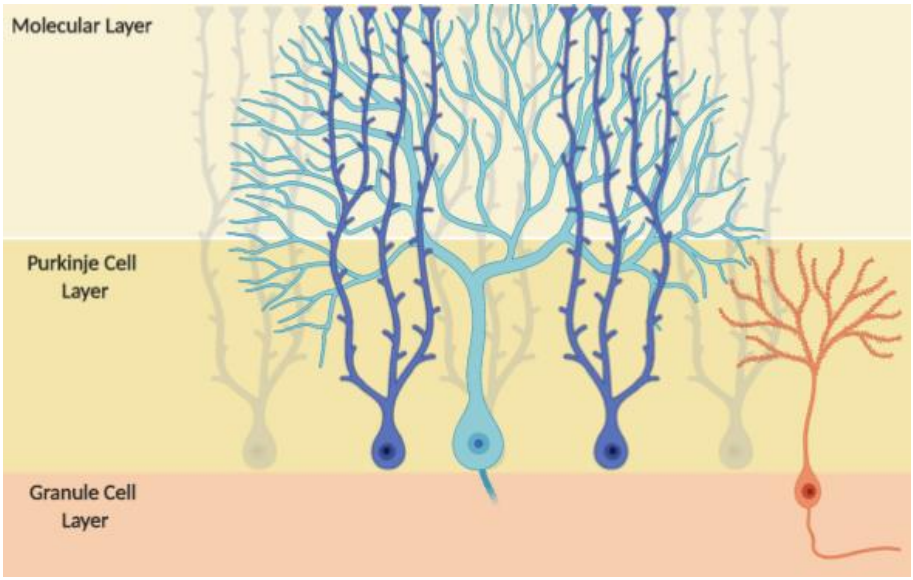


Figure 1. A schematic representation of the organisation of neurons and glial cells in the cerebellar cortex. Numerous granule cell axons (orange cell extending an axon from the granule cell layer) interact with Purkinje cell dendrites (light blue dendritic trees). Bergmann glial cells (dark blue cells originating in the Purkinje cell layer) make contact with these synapses in order to carry out normal physiological function. Image created with Biorender. https://biorender.com/

3.1.2 Ectopic Communication with Bergmann Glia

The pre-synaptic terminals of neurons are equipped with vesicles containing excitatory or inhibitory neurotransmitters which are released from the active zone following calcium elevation within the terminal (Südhof, 2012). This traditional mechanism of synaptic transmission, where neurotransmitter is released at the active zone, has been studied for many years. In recent years, an additional transmission mechanism has emerged, known as 'ectopic'

transmission, where vesicles containing neurotransmitter are released at sites distinct from the active zone into the extracellular space (Matsui and Jahr, 2006).

Evidence for ectopic release first came from freeze fracture studies of the neuromuscular junction (Matsui and Jahr, 2006). The phenomena was found in diverse brain regions and a good example of this process has been shown in the cerebellar cortex: glutamate released from ectopic sites activates calcium permeable α-amino-3-hydroxy-5-methyl-4-isoxazolepropionic (AMPA) receptors on Bergmann glial cells that enclose Purkinje cell synapses (Balakrishnan *et al.*, 2011). Bergmann glia express transcripts for GluA1 and GluA4, and lower levels of GluA2, which accounts for their AMPAR subunit composition and results in a high level of calcium permeability (Ceprian and Fulton, 2019). AMPARs are likely to have an important role in neuron-glial communication since alteration (via genetic deletion) in young mice or inactivation in old mice results in a retraction of glial processes from neuronal synapses and has detrimental effects on motor coordination (Fendler *et al.*, 2012).

Ectopic synaptic transmission is thought to promote the interaction of glial cells with neurons both physically and functionally. Following climbing fibre activation, the excitation of Bergmann glial cells and Purkinje cells is not equal: the two cell types monitor neurotransmitter release from separate sites (Matsui and Jahr, 2003). Additionally, spill over of neurotransmitter from the active zone is not sufficient to activate low affinity AMPARs on Bergmann glial cells since such receptors rely on nearby release (Matsui and Jahr, 2003). Further investigation into this form of synaptic transmission is necessary, since it provides an example of a dedicated route for neuron-glial transmission, rather than a simple activation of glial receptors by transmitter spill over from the synapse.

Ectopic transmission, as a form of neuron-glial communication, may be a mechanism to promote BG cells to carry out their homeostatic roles. Evidence suggests that ectopic release directs glial processes to glutamate release sites in order to prevent excitotoxicity to Purkinje neurons and thus ensure

Bergmann glia carry out neurotransmitter clearance (Balakrishnan *et al.*, 2011). Additionally, BG cytosolic calcium transients have been reported to regulate the uptake of potassium ions which means they are important in maintaining Purkinje cell membrane potential and therefore activity (F. Wang *et al.*, 2012).

Ectopic transmission may also be integral to the induction and maintenance of synaptic plasticity (Balakrishnan and Bellamy, 2009). Our lab found that the strength of ectopic release is dependent on the frequency at which neurons are stimulated meaning that neuron-glial communication strength will alter over time (Bellamy and Ogden, 2006). It is known that ectopic transmission from neurons to glia exhibits long term depression during repetitive stimulation at frequencies in the 0.1-1 Hz range due to the inability to recycle vesicles to ectopic sites (Bellamy and Ogden, 2006; Balakrishnan *et al.*, 2011). Thus, a key determinant of ectopic transmission strength is the average neuronal firing rate, since synaptic transmission depresses ectopic transmission (Bellamy and Ogden, 2005, 2006). This observation highlights the importance of investigating the relationship between stimulation frequency and the strength of ectopic transmission in order to fully elucidate this form of neuron-glial transmission.

3.1.3 Hypothesis and Aims

Previously Matsui and Jahr (2006) demonstrated the presence of vesicles in presynaptic parallel fibre terminals close to the plasma membrane that originated opposite Bergmann glial membranes - this was hypothesised to be the ectopic vesicle pool. In this study, I intended to resolve the location of ectopic release sites, and determine how the distribution of vesicles in the various compartments of cerebellar granule neurons varied before and after treatments that theoretically deplete ectopic pools. I have compared synapses stimulated in the 0.1-1Hz range in order to test the prediction that the depression of ectopic transmission is associated with a loss of vesicles positioned at sites opposite extra synaptic glial processes.

It has been suggested that dynamic changes in glial structure are linked to the strength of ectopic transmission, thus I have investigated how dynamically morphological changes occur in response to changes in synaptic transmission, in order to understand if the mechanism of ectopic transmission may control the morphology of Bergmann glia. Therefore I examined if depression of ectopic transmission is associated with a change in the coverage of synapses by glial processes. This study has acted as a benchmark for future *in vitro* studies by beginning the investigation of neuron-glial interactions using a physiologically-relevant preparation.

3.2 Methods

3.2.1 Cerebellar Slice Preparation and Processing

Dr Katharine Dobson generated hundreds of electron micrographs of cerebellar slices stimulated at different frequencies to investigate the effects of synaptic activity on neuron-glial interactions. The methods used here are described in detail by Dobson, Smith and Bellamy (2018).

In brief, transverse cerebellar slices (300 µm) were prepared from 16-20 day old Wistar rats of either sex. Animals were humanely killed by cervical dislocation, decapitated, and the cerebellum rapidly excised and sliced using a vibrating microtome (Leica VT1000S). During slicing, tissue was kept in a chilled sucrose-based artificial cerebrospinal fluid (aCSF) (see Dobson, Smith and Bellamy (2018) for buffer composition). Slices were allowed to recover at 32°C for one hour, followed by 30 minutes at room temperature in a different composition of aCSF (see Dobson, Smith and Bellamy (2018) for buffer composition).

Once a suitable glial cell was identified and the stimulating electrode was in position, a bright field image (4x) was captured to enable slice realignment later on. Cells were patched with the whole-cell recording configuration and loaded for 10 minutes to ensure good infiltration with dye. Each of the three stimulation protocols (no stimulation, 0.033 Hz and 1 Hz) had a duration of 10 minutes and was assigned to cells randomly. Following recording, slices were fixed using a microwave (700W, 8 seconds) in a fixative solution containing 6% PFA and 2% glutaraldehyde prepared in PBS. Subsequent steps for slice preparation post fixation were carried out according to Dobson, Smith and Bellamy (2018).

Ultrathin samples were imaged by transmission electron microscopy (FEI Tecnai 12 Biotwin TEM, 120kV, magnification up to 43,000X). Ten high-power images of synapses located within the arborisation of the loaded Bergmann glial cell were captured for each ultrathin section for analysis. Images obtained were analysed blind to the stimulation paradigm employed for each sample.

Dr Tomas Bellamy provided technical support with stimulation methods and analysis for the measurement of extra synaptic currents (ESCs) for Bergmann glia (BG).

3.2.2 Cerebellar Slice Analysis

The ultrastructural features of EM images were analysed in Image J. The freehand line tool was used to trace around the presynaptic terminal, the post synaptic density and any extra synaptic glial membranes that were present and adjacent to the terminal. The point tool was used to pinpoint the position of every single vesicle (marked in the centre) in the presynaptic terminal. Coordinates of all of the aforementioned anatomical features were exported into Matlab where a custom-written plugin was used for further analysis (see Dobson, Smith and Bellamy, (2018)).

The custom-written plugin, written and provided by Dr Tomas Bellamy, compartmentalized the terminal membrane into the active zone and glial-facing membrane regions by demarcating those sections directly facing the postsynaptic density and extra synaptic glial processes, respectively. For all vesicles, the shortest distance (measured as the Euclidean distance) to the nearest active zone or glial-facing membrane region was determined.

3.2.3 Statistics

Graph Pad Prism was used for statistical analysis (Windows Version 7.01). Contingency tests (Fisher's exact test) were used to determine if there was a significant difference in the number of vesicles within <50 nm of the active zone and glial facing membrane in the terminals stimulated at 0.033 Hz and 1 Hz. A Kruskal-Wallis ANOVA test with Dunn's correction for multiple comparisons was used to compare anatomical parameters between stimulation conditions. Aggregate data are the mean ± the standard error of the mean (S.E.M) of multiple cells as indicated in figure legends.

3.3 Results

3.3.1 Cerebellar Slice Preparation, Processing and Analysis

This investigation aimed to understand changes to synapse ultrastructure before and after a stimulation protocol that would deplete vesicles from sites of ectopic transmission. To do this, a stimulating electrode was placed into the molecular layer on the surface of a sagittal cerebellar slice and a recording electrode was established following the identification of a BG cell (Figure 2A). Paired pulse stimulation of the molecular layer was conducted for 10 minutes at 0.033 Hz or 1 Hz with a high stimulation intensity (100 µA) after which slices were fixed.

Electron-dense labelling of BG cells by DAB conversion enabled the observation of dark processes when imaged using electron microscopy (Figure 2B & 2C). In this way, it was possible to identify regions of the slices that had been stimulated. In these areas, pre synaptic terminals with numerous vesicles at the active zone, as well as extra synaptic glial processes were identified (Figure 2D). Identified regions were subsequently analysed manually after contrast adjustment with images taken at 43,000x magnification (Figure 2E).

Detailed image analysis was carried out as follows (see section 3.2 for full details): the presynaptic terminal was traced, the active zone was identified and the centre of vesicles were marked (Figure 2F). Next extra synaptic glial processes surrounding the presynaptic terminal were traced (Figure 2F). A colour coded map of the presynaptic terminal, the active zone and the facing glial membranes was generated using Matlab (Figure 2G). In the case of each vesicle, the Euclidean distance (straight line between two points) from its centre to the nearest point on the active zone or glial facing membrane was then calculated (Figure 2G).

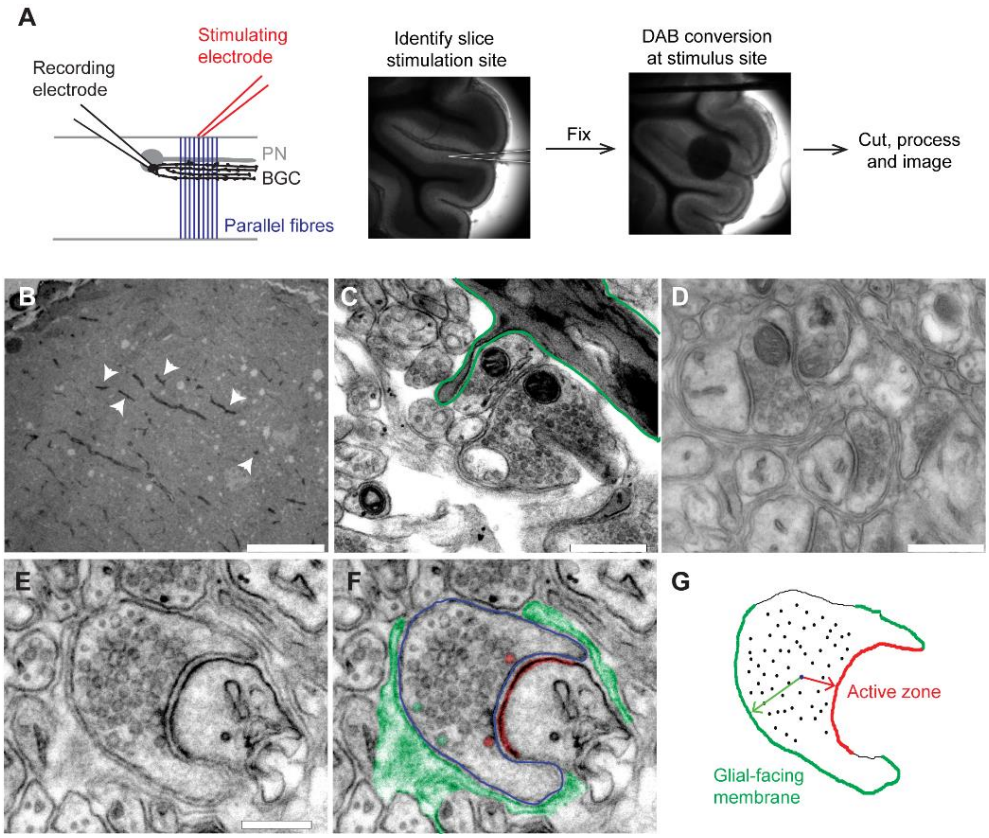


Figure 2. Analysis of vesicle distribution and glial coverage in presynaptic terminals of parallel fibre synapses in the cerebellar cortex. A) Schematic representation of the molecular layer isolated in sagittal cerebellar slices where a stimulating electrode was placed on top to activate parallel fibres and whole cell patch clamp technique was used to record from a BG cell. B) Electron dense fibres in the molecular layer highlights the stimulation and recording sites (arrows). Scale bar = 25 µm. C) Electron dense deposits also highlight the location of Bergmann fibres (green line). Scale bar = 500 nm. D) Individual pre synaptic terminals were identified manually via the presence of vesicles and mitochondria. Scale bar = 500 nm. E) Individual terminals were used to assess vesicle distribution after contrast adjustment for visualisation. Scale bar = 150 nm. F) The presynaptic terminal (blue line), post synaptic density (red line), extra synaptic glial processes (green fill) and vesicles (red and green circles) were drawn manually. G) Export of coordinates allowed reconstruction of the terminal in Matlab and for every vesicle (black dots) the shortest distance to the nearest glial facing membrane (green) and active zone (red) was calculated. Figure previously published in PlosOne.

Each cerebellar slice within a stimulation condition group was derived from a singular P16-20 Wistar neonate of either sex. Four animals were used to generate four cerebellar slices which acted as the control group (not

stimulated), five animals generated five cerebllar slices for slices stimulated at 0.033 Hz, and seven animals generated seven cerebellar slices stimulated at 1 Hz.

A total of 295 synapses were analysed from six slices stimulated at 0.033 Hz, 287 synapses analysed from seven slices stimulated at 1 Hz, and 167 synapses analysed from four slices that were not simulated. All of the analysed synapses from multiple slices for each stimulation condition were analysed to generate Figures 4-6 and Tables 1 & 2. In all figures, n number represents multiple biological replicates of analysed synapses from up to seven slices generated from a total of seven animals.

3.3.2 Confirmation of Depression of Ectopic Transmission

To determine whether the applied stimulation protocol successfully changed the strength of ectopic transmission, the extra synaptic currents (ESCs) generated by the activation of AMPA receptors and glutamate transporters in the BG were measured (Figure 3). Stimulation at 0.033 Hz for 10 minutes resulted in cells retaining 82% of the initial ESC amplitude ($p > 0.2$, single sample *t* test) (Figure 3A & B). In contrast to this, 1 Hz stimulation depressed the ESC to 25% of the initial amplitude (Figure 3A & B). In both cases data is an aggregate of 9 cells which were recorded for each frequency (Figure 3A & B). These results are in-keeping with previous findings (Balakrishnan and Bellamy, 2009; Balakrishnan *et al.*, 2011).

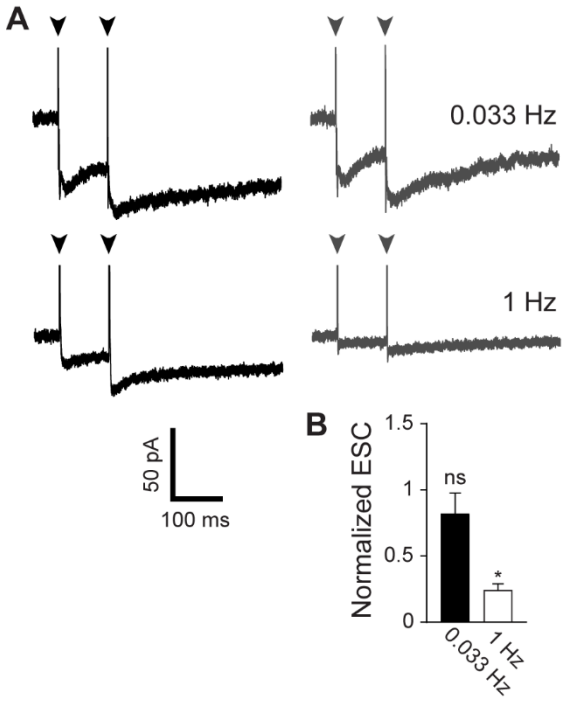


Figure 3. Depression of ectopic transmission. A) Extra synaptic currents (ESCs) were recorded from Bergmann glia (BG) after paired pulse stimulation (shown by arrows, 100 ms interval). Black traces represent the average of the first three stimuli at 0.033 Hz (top traces) or 1 Hz (bottom traces). Grey traces show the average of the final three stimuli after ten minutes of continuous stimuli at either 0.033 Hz or 1 Hz. Stimulus artefacts have been truncated for trace clarity. B) Aggregate data for the amplitude of ESCs after stimulation at 0.033 Hz (black bar) or 1 Hz (white bar) for 10 minutes and normalized to the amplitude of the first ESC. N = 9 cells for each frequency. P < 0.001, single sample *t* test. Experiments were performed by Dr Katharine Dobson. Figure previously published in PlosOne.

3.3.3 Synapse Ultrastructure and Vesicle Distribution

When different protocols of paired pulse stimulation (no stimulation, 0.033 Hz and 1 Hz) were applied to sagittal cerebellar slices over a period of 10 minutes, there were no statistically significant changes to the general anatomical features observed at presynaptic terminals of parallel fibres (Figure 4A). There were no differences in the number of vesicles per terminal, the length of the presynaptic terminal perimeter or the length of the active zone (Figure 4B). In addition, the presence of vesicles located in close

proximity to the presynaptic membrane opposite the glia sheath (the putative ectopic pool) was observed in all cases – control, 0.033 Hz and 1 Hz stimulation (Figure 4A).

3.3.4 Vesicle Distribution at the Active Zone

To interpret vesicle distribution data the approximate vesicle diameter from the slice population was measured. This was calculated as 52.5 ± 1.39 nm (n = 12 vesicles, 4 from each stimulation condition picked at random) which is consistent with findings in the literature (Xu-Friedman, Harris and Regehr, 2001). With this in mind vesicles within 50 nm or less from the active zone have been considered to be part of the releasable pool.

For synapses that have not been stimulated, vesicle distribution at the active zone appeared to display bimodal peaks, one at less than 50 nm from the active zone and one at 100 nm from the active zone (Figure 5A). The bimodal vesicle peak distribution was also seen at 0.033 Hz and 1 Hz stimulation conditions, but an extra peak at 117 nm was observed at 1Hz (Figure 5A). In both stimulated conditions, we observed that the peak location varied by less than the width of a bin implying that it is unlikely that the relative abundance of the different vesicle pools has changed following stimulation (Figure 5A).

To consider the vesicle pools in more detail, a kernel-fitting method was used to establish a probability density function for the distribution (Table 1). This showed that the probability density at the first two peaks was closely similar for the two stimulation frequencies and thus further supports the notion that vesicle pool location had remained unaffected.

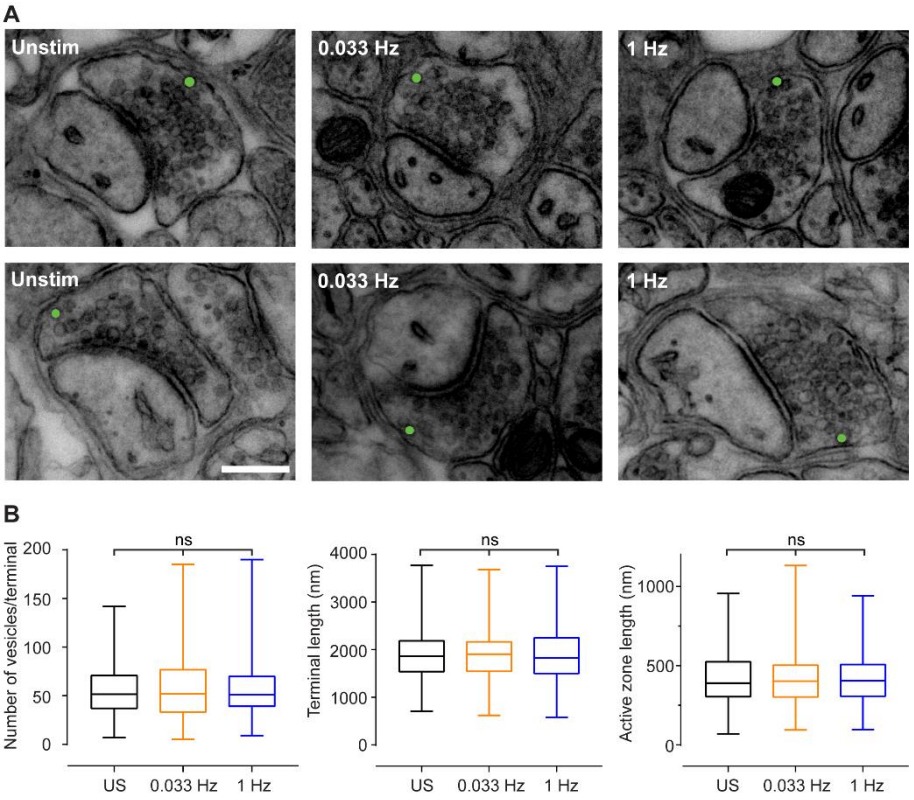


Figure 4. Effect of stimulation on synapse ultrastructure, including the presence of ectopic vesicles. A) Representative electron micrographs of synapses from each stimulation condition (no stimulation, 0.033 Hz and 1 Hz) with putative ectopic vesicles labelled (green fill). Scale bar = 500 nm. B) Box and whisker (min to max) plots of the number of vesicles per terminal (left panel), terminal length (middle panel), and active zone length (right panel) for unstimulated (US, black), 0.033 Hz stimulated (orange) and 1 Hz stimulated (blue) slices. ns $p > 0.05$, Kruskal-Wallis ANOVA test with Dunn's correction for multiple comparisons. N = 295 synapses analysed at 0.033 Hz, 287 synapses at 1 Hz and 167 synapses that were not simulated (control). Figure previously published in PlosOne.

3.3.5 Vesicle Distribution at the Glial Facing Membrane

For vesicles associated with the glial facing membrane a single peak was observed, for a single population with a skewed Gaussian distribution (Figure 5B). Vesicles were observed within 50 nm of the glial-facing membrane, but there was a clear peak at <50 nm, in contrast to the active zone data.

Stimulation at 0.033 Hz and 1 Hz resulted in no alterations in vesicle distribution relative to extra synaptic glial processes.

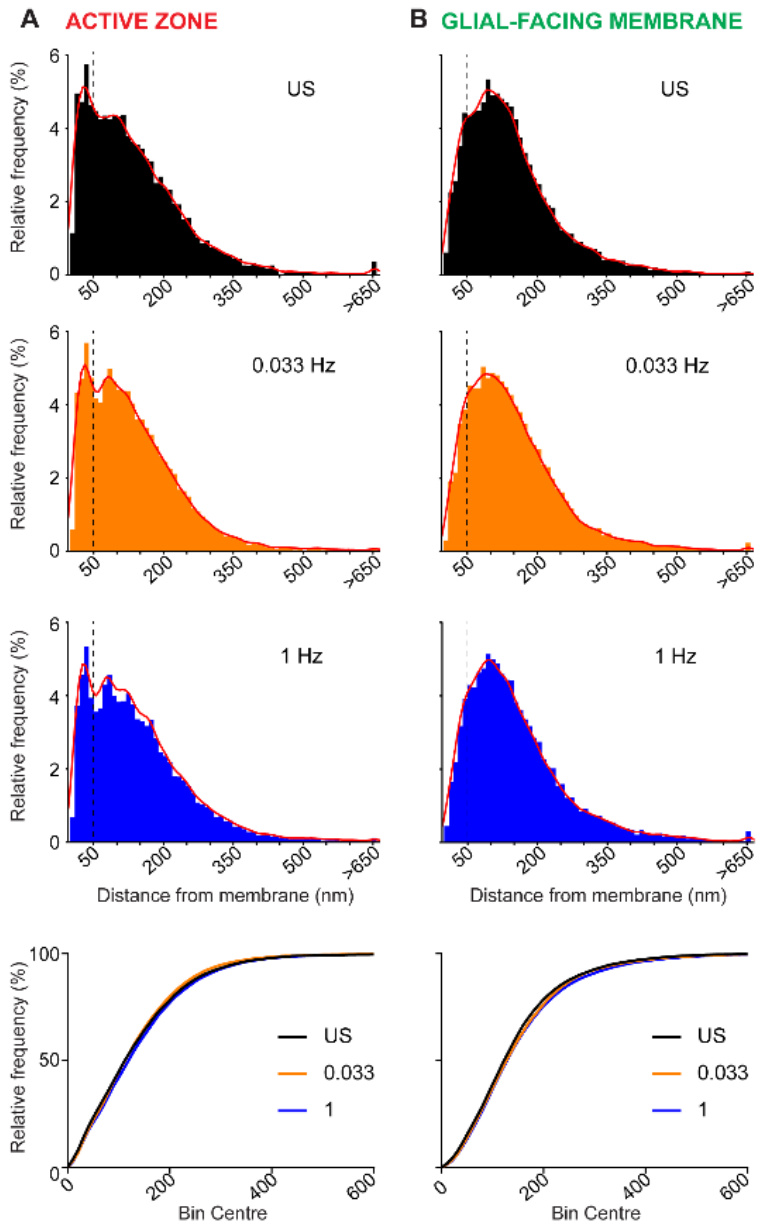


Figure 5. Vesicle distribution at the active zone and glial facing membrane. A) Histogram of the percentage of vesicles relative to distance from the active zone (nm) in unstimulated (black, upper panel), 0.033 Hz stimulated (orange, middle panel) and 1 Hz stimulated (blue, bottom panel) slices. The dashed grey line represents the separation of the bimodal population at 50 nm. Cumulative frequency plots of vesicles for the three conditions are provided in the final panel. B) Histograms and cumulative frequency distributions of vesicles relative to the glial facing membrane (panels same as for A). N = 295 synapses analysed at 0.033 Hz, 287 synapses at 1 Hz and 167 synapses that were not simulated (control). Figure previously published in PlosOne.

	Active Zone			Glial Facing Membrane
	1st Peak nm (%)	2nd Peak nm (%)	3rd Peak nm (%)	1st Peak nm (%)
US	32 (7.2)	97 (6.2)	-	97 (7.2)
0.033 Hz	36 (7.2)	87 (6.8)	-	95 (7.0)
1 Hz	31 (6.8)	81 (6.4)	117 (5.9)	95 (7.1)

Table 1. Kernel distribution analysis of vesicle pools at the active zone and glial facing membrane. Peak identification for frequency histograms was determined via Matlab. Curve fitting was achieved via a kernel-distribution function with a band width determined using Silverman's rule. Peak locations are highlighted in nm and the associated probability as a percentage determined from the probability density function values are shown.

3.3.6 Hypothesis Testing

To directly test whether vesicles associated with the glial-facing membrane are the ectopic pool, and that a 1 Hz stimulation protocol depletes that pool, the number of vesicles within 50 nm of the active zone or glial-facing membrane within a terminal were quantified (Table 2).

The analysis shows a statistically significant decrease in the fraction of total vesicles that were within 50 nm of the active zone following 1Hz stimulation ($p = 0.192$). In contrast, the abundance of vesicles at the glial-facing membrane for terminals stimulated at either 0.033 Hz or 1 Hz did not show a statistically significant decrease ($p = 0.113$). In the instance of the unstimulated slices, there is a greater proportion of vesicles within 50 nm of the active zone and the glial facing membrane at both stimulation frequencies.

	Fraction <50 nm from the Active Zone	Fraction <50 nm from the Glial Facing Membrane
US	0.213 (2019/9472)	0.135 (1278/9472)
0.033 Hz	0.200 (3479/17380)	0.117 (2033/17380)
1 Hz	0.192* (3107/16212)	0.113^{ns} (1836/16212)

Table 2. Contingency table of vesicle distances from the parallel fibre presynaptic membrane. Data are expressed as the number of vesicles less than 50 nm from the membrane divided by the total number. Data were analysed using a two-sided Fisher's exact test to compare vesicle distribution between 0.033 Hz and 1 Hz stimulation. ns p = 0.2890, p = 0.0493.

3.3.7 Glial Coverage of Synaptic Terminals

In order to establish the dynamics of neuron-glial interaction, and potentially rapid changes to glial coverage of parallel fibres depending on the neuronal firing rate, the fraction of the presynaptic terminal that was covered by glial membrane, and the distance between the presynaptic terminal and the adjacent glial membrane (at the midpoint of their apposition) was quantified.

Results show that the fractional coverage of the presynaptic terminal is unaffected by a 0.033 Hz or 1 Hz stimulation, but the mean distance at the midpoint was significantly increased for a 1 Hz stimulation ($p = 0.0232$) (Figure 6B & C). The observed increase in the mean is small, but there is a clear distribution shift from shorter to increased distances within the 1 Hz population (Figure 6C). Unstimulated slices had a mean distance from the midpoint of 5.32 ± 0.14 nm. When the mean distance was significantly increased at 1 Hz it went from 6.01 ± 0.15 nm at 0.033 Hz to 6.26 ± 0.10 nm at 1 Hz. Thus, whilst the increase in mean and median at the 1 Hz stimulation frequency is small, the values have shifted from shorter to greater distances in this population.

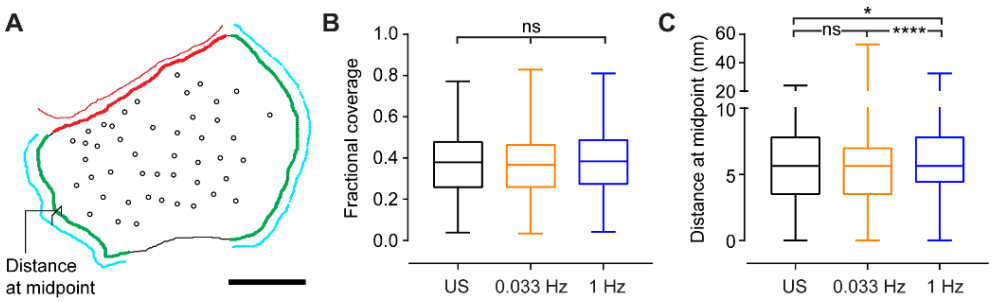


Figure 6. Glial process coverage of parallel fibre presynaptic terminals in sagittal cerebellar slices. A) Example of a terminal reconstruction from an original EM image showing the aforementioned ultrastructural features and the calculated distance at the midpoint. Labels as for Figure 1 - blue lines represent synaptic encompassing glial processes. Scale bar = 100 nm. B) Box and whisker (min to max) plot of fractional coverage of the terminal by the glial membrane (length of green highlights/terminal perimeter). C) Box and whisker plot of distance between the glial process and glial facing membrane (blue line and green highlight) at the midpoint along the glial facing membrane length. Synapses typically have 2 or 3 glial facing regions per terminal. For unstimulated slices, n = 431 glial membranes from 166 terminals, for 0.033 Hz stimulation n = 806 glial membranes from 295 terminals, and for 1 Hz stimulation n = 801 glial membranes from 287 terminals. Statistical comparisons: ns $p > 0.05$, $p = 0.0232$, $p < 0.0001$ Kruskal-Wallis ANOVA test with Dunn's correction for multiple comparisons. Figure previously published in PlosOne.

3.4 Discussion

Ectopic release mechanisms, where neurotransmitter is released from locations independently of the active zone, have been described at numerous classes of synapse. This includes the study of cerebellar parallel fibre inputs to the Purkinje neurons of the cerebellar cortex. To study this phenomenon paired pulse stimulation at 0.033 Hz or 1 Hz for 10 minutes in sagittal cerebellar slices has been used. The two main aims were to discover more about vesicle distribution and the location of ectopic pools, as well as to establish the synaptic coverage by glial processes and changes to this following neurotransmission.

3.4.1 Vesicle Distribution

Under control conditions, at the active zone, there was a peak in the percentage of vesicles between 30-40 nm consistent with the presence of a readily releasable pool (Figure 5, Table 1). When terminals were stimulated, there were no changes to the total numbers of vesicles, but at 1 Hz there was a redistribution into a second smaller peak at 100 nm and even a third peak at 117 nm (Figure 5, Table 1). Vesicles at 50 nm or less from the active zone are thought to correspond to the readily-releasable vesicle pool, so it is likely that the second peak at 100 nm represents the reserve pool. This minor change in vesicle location likely results from vesicle turnover during increased neurotransmission.

Under control conditions at the glial facing membrane, there was a single broad peak at 100 nm (Figure 5, Table 1). Following stimulation, there were no alterations to the vesicle pool relative to the glial facing membrane sites which directly contradicts the hypothesis that the number of vesicles within 50 nm of the glial facing membrane would decrease due to the depletion of this putative ectopic pool.

There are a few possible explanations for this result. Firstly, there are some experimental limitations to be taken into account. It is possible that there may have been the misidentification of stimulated synapses, for example, some synapses that are lying within the arborisation of the glial cells may not

actually have been stimulated to release ectopic vesicles (thus they will have been inappropriately included in the 1 Hz population). This is improbable since the stimulation intensity applied to slices is sufficient to recruit a large number of parallel fibres (Bellamy and Ogden, 2005) when repetitively stimulating for 10 minutes to ensure no detectible ectopic transmission remained, and care was taken to ensure that annotated synapses were at the heart of the stimulated zone.

It is possible to estimate the volume of the neuropil stimulated under these experimental conditions from another study using rat visual cortex slices which prepared data in a similar way (Nowak and Bullier, 1996). By taking the median value for excitation thresholds for axons in the study by Nowak and Bullier (1996), at the stimulation intensity in this study, parallel fibre axons within a radius of 60 μm of the electrode would be activated with 100% probability, and, axons up to 108 μm away would have a 50% probability of activation. Furthermore, it is estimated that axons within an area of 200 μm diameter around the stimulation site would be engaged (taking into account this stimulation protocol). Given these observations, the likelihood of synapses capable of ectopic transmission evading such widespread and long-lasting stimulation seems low.

Secondly, the lack of change to vesicle distribution at stimulated synapses could result because depression of ectopic transmission may not rely on the literal depletion of vesicles from the assigned vesicle pool. It has been suggested that ectopic transmission is a consequence of a failure to recycle vesicles to the ectopic pool (Balakrishnan *et al.*, 2011), but instead it could be the failure to refill vesicles with neurotransmitter or even the inability to initiate vesicle docking, priming or fusion. This is plausible because all of these alternative mechanisms would lead to a loss of neurotransmitter release from ectopic sites but without the removal of vesicles from the hypothesised pool.

Another explanation for the minimal changes in vesicle distribution found in this study could be explained by the general misidentification of ectopic release sites. Matsui and Jahr (2006) previously suggested that vesicles were docked at sites juxtaposing glial membranes, however that has not been

confirmed in this study and I would speculate that the vesicles exist elsewhere within the cell. On the other hand, ectopic release may not occur at every terminal within the region of stimulation or alternatively the ectopic pool may have a low release probability. If release probability of the ectopic pool was low, then ectopic release mechanisms may not be detected amongst the great number of non-releasing terminals. Ultimately, these findings indicate asynchrony between anatomical and functional data previously discovered, and the true location of ectopic sites requires further investigation.

3.4.2 Cerebellum Synaptic Coverage by Bergmann Glial Cell Processes

This study has found that following a 1 Hz stimulation of parallel fibres, Bergmann glial processes withdraw from the presynaptic terminal – this result is consistent with previous reports (Iino *et al.*, 2001). Furthermore, this indicates that depressing neuron-glial transmission within a 10 minute timescale (as was the stimulation period) was sufficient to detect the first morphological rearrangements to Bergmann glia in that same time-frame. Such a mechanism seems plausible considering that in the brain stem it was found that extra synaptic glial processes are dynamic and morphological changes can occur within minutes based on alterations to the original transmission strength (Hirrlinger, Hülsmann and Kirchhoff, 2004). Thus, this suggests that neuron-glial interactions and synaptic connectivity may be remodelled following LTP or LTD and potentially have resultant effects on motor coordination via changes to Purkinje cell synaptic function (Ceprian and Fulton, 2019).

AMPAR on glial processes in the cerebellum are known to regulate excitatory synapses: calcium influx has been linked to the regulation of glutamergic synapses on Purkinje cell dendrites via electrophysiological recording data (Iino *et al.*, 2001). These mechanisms may be specific to brain region considering that the subunit composition of astrocyte AMPAR alters in different regions and leads to variability in permeability to calcium (Ceprian and Fulton, 2019). For example, in the cortex GluA2 is a highly expressed

AMPAR subunit compared to GluA1 and 4 (Mölders *et al.*, 2018). Therefore, stimulation of AMPARs fails to induce calcium influx into cortical astrocytes, or if it does, shows only small AMPA-mediated currents (Ceprian and Fulton, 2019). Studies have even shown the deletion of AMPARs and the subsequent retraction of glial processes (Saab *et al.*, 2012). Working towards elucidating ectopic transmission is important to further understanding about this specific form of transmission for neuron-glial interactions and its role in synapse modulation.

3.4.3 Conclusion

The physiological roles of ectopic transmission still remain poorly understood, thus the purpose of this study was to try and combine understanding of this directed transmission to the glial facing membrane with observed changes to the distribution of vesicles within the terminal and alterations to synaptic coverage. The stimulation protocol that depresses ectopic transmission had no major influence on the number of vesicles within the terminals, or the spatial distribution of the vesicles relative to the glial facing membrane. However, the relative abundance of vesicles in close proximity to the active zone was marginally reduced at 1 Hz stimulation and there was also a statistically-significant increase in the distance between glial membrane and the presynaptic terminal. Therefore this suggests that there is a withdrawal of glial membranes from synapses following stimulation, which is detectable in ultrastructural anatomy within minutes, but further investigation is required to elucidate how this happens.

Chapter 4. Effect of Culture Media on Astrocyte Phenotype

4.1 Introduction

For decades, primary rodent astrocytes have been extracted from the brain and cultured on 2D surfaces, such as flasks or plates coated with substrates, to study an isolated cell population. The physiological and pathological states, as well as the many roles of astrocytes, have been discovered and extensively investigated using this method of *in vitro* culture.

4.1.1 Morphological Assessment of Primary Astrocytes

Glial fibrillary acidic protein (GFAP) is expressed by astrocytes in the CNS and can act as a marker of the astrocyte cytoskeleton (Gomes, Paulin and Neto, 1999). GFAP labelling is often used to validate the purity of *in vitro* astrocyte cultures generated from *in vivo* cells. GFAP is upregulated when astrocytes become reactive and therefore it is often used as a marker of astrocyte reactivity (Bignami and Dahl, 1974). Whilst GFAP is a commonly used astrocyte label, it comes with the drawbacks that not all astrocytes express GFAP (Pekny and Nilsson, 2005). For this reason, it would be logical for the field to gravitate towards working with other astrocyte-specific markers, such as glutamine synthetase, for the distinction of pure astrocyte cultures in the future. Additionally, ALDH1 is selectively expressed in cortical astrocytes *in vivo* and labels both GFAP-positive and GFAP-negative astrocytes and could be a good alternative marker (Rowitch and Kriegstein, 2010). ALDH1 has been proven as a reliable marker in astrocyte differentiation (Alexandra Adam *et al.*, 2012). Whilst ALDH1 would also be an ideal marker for primary astrocyte cultures, it is also expressed in postnatal neural stem cells (Chandrasekaran *et al.*, 2016).

S100β is a calcium-binding peptide (Donato, 1999) mainly produced by astrocytes and often used as a primary astrocyte label. S100β can be utilised

as a marker of astroglial activation since it is important in CNS recovery following injury (Souza *et al.*, 2013). Calcein acetoxymethylester (calcein AM) is a cell-permanent non-fluorescent compound which is converted by intracellular esterases into calcein, an anionic fluorescent form (Uggeri *et al.*, 2000). Calcein AM is used as a marker of cell viability and depicts the cytoplasmic morphology of cell types (Uggeri *et al.*, 2000).

To determine the morphology of primary neonatal (P2) rat cortical astrocytes in 2D *in vitro* cultures, calcein AM loading followed by live imaging has been used, or alternatively astrocyte cells have been fixed and labelled with either GFAP or S100β.

4.1.2 Induction of Stellation

Forskolin is a pharmalogical agent that can be used to raise levels of cyclic AMP (cAMP) for studies of cell physiology. Forskolin induces a stellate morphological profile of astrocytes via the activation of adenylyl cyclase which catalyses the synthesis of cAMP from ATP (Goldman and Abramson, 1990). cAMP is an important second messenger molecule necessary for extracellular responses which can act through protein kinase A (Beavo and Brunton, 2002). Primary astrocytes have been treated with forskolin to assess resultant changes to astrocyte morphology and function.

4.1.3 Functional Assessment of Primary Astrocytes

Astrocytes express G protein-coupled receptors (GPCRs) on their surface which allows them to respond to events in the neural network and vasculature (Agulhon *et al.*, 2008). Activation of GPCRs, from neurotransmitters released at neuronal synapses, results in rises in intracellular calcium concentration, which may be limited to glial processes or spread across a network of many astrocytes, and implicates astrocytes in active information processing in the brain (Matsui, 2005; Croft *et al.*, 2015).

Astrocytes express receptors for adenosine triphosphate (ATP) and glutamate (primary excitatory amino acid in the brain) (Meldrum, 2018). Numerous reports from studies conducted *in vivo*, in culture or in brain slices, have

deduced that astrocytic cytosolic calcium increases can be evoked by ATP and glutamate (Cornell-bell *et al.*, 1990), and cause astrocytes to release ATP, glutamate and GABA (Oliveira *et al.*, 2015; Bazargani and Attwell, 2016). This study has used two agonists for these receptors, ATP and glutamate, to investigate how the culture environment influences receptor expression in astrocytes.

4.1.4 Co-Culture of Astrocyte and Neurons

Astrocytes have vital roles in neuron growth and survival in the CNS but it can be challenging to study these interactions *in vitro*. A sophisticated model for the study of astrocyte and neuron communication *in vitro* is compartmentalized microfluidics devices: these separate cell types into compartments, but a microgroove barrier permits the growth and migration of cellular processes from one compartment to another (section 1.4.1, Figure 4, page 27). Compartmentalization of neuronal segments (axon and cell body) in such devices allows detailed investigations at the axon interface, something which has been limited with traditional *in vitro* culture methods (D. Jadhav, Wei and Shi, 2015).

A goal of this study was to co-culture astrocytes and neurons in compartmentalized Xona Microfluidics devices and subsequently determine the effect of astrocytes on axon growth and development. It was important to carefully select culture media since axons would grow on top of a monolayer of astrocytes once they had crossed the microgrooves. Since astrocytes are an extremely plastic cell type, and the intention was to culture them in neuronal media in future co-culture experimentation, it was necessary to investigate the influence of different cell culture media on astrocyte phenotype. Astrocyte morphology and responses to neurotransmitters for astrocyte medium, neuronal medium and neurobasal medium (NB) supplemented with glutamax (L-glutamine substitute) have been compared in this study.

4.1.5 Influence of Cell Culture Media on Astrocyte Phenotype

A caveat of studying primary astrocyte cells *in vitro*, rather than using *in vivo* techniques, arises from astrocyte heterogeneity in experimental results. The observable heterogeneity of astrocyte phenotype results from: variety in culture protocols, differing media compositions, different coatings for coverslips, and the length of time over which astrocytes are cultured *in vitro* (Lange *et al.*, 2012). Data gathered under such wide-ranging experimental conditions is not commonly reported or acknowledged, therefore there is not a comprehensive understanding of the impact of the cell culture environment on astrocyte phenotype.

Young postnatal rodents are commonly used to generate *in vitro* astrocyte populations meaning that tissue is collected at a stage at which gliogenesis will be incomplete (Bayraktar *et al.*, 2015). Immature astrocytes are subsequently grown and divide on 2D surfaces until they are prevented from doing so via contact inhibition (Lange *et al.*, 2012). To encourage the development of mature astrocytes, it is common practice to supplement media with fetal bovine serum (FBS), however the influence this serum has on the gene expression of developing primary astrocytes is unknown. Additionally there is dramatic batch variation for FBS (resulting from its production) and it contains proteins that can't cross the blood brain barrier (BBB), thus, it is not something that astrocytes would be exposed to *in vivo* (Fang *et al.*, 2017).

Dulbecco's Modified Eagles Medium (DMEM) supplemented with FBS is a common choice for primary astrocyte cell culture and has been used in this study. To determine whether the presence of serum in media influences astrocyte phenotype, astrocytes have been cultured with astrocyte medium (see section 2.2.1 for composition) or DMEM with no supplements. Additionally, stellation has been induced via forskolin treatment to evaluate whether the presence of serum in media changes reactive astrocyte responses.

4.1.6 Aims

Considering that astrocytes are heterogeneous and highly responsive to their environment, I aimed to investigate the impact of cell culture media in the 2D *in vitro* microenvironment on primary rat neonatal (P2) cortical astrocyte phenotype. Additionally, I hoped to determine the influence of forskolin treatment on astrocyte phenotype under standard *in vitro* conditions and in combination with changes to cell culture media composition.

I hypothesised that primary astrocytes cultured with standard astrocyte media and treated with forskolin would have a reduced percentage of cells responding to the addition of calcium-linked receptor agonists ATP and glutamate. I also expected that culturing astrocytes with media compositions optimised for neural cell culture would reduce the overall percentage of cells responding to the addition of ATP and glutamate.

4.2 Methods

Some of the methods referred to in this chapter have been described in greater detail - see Chapter 2 for full details of experimental procedures.

4.2.1 Generation of Primary Cortical Astrocytes

Rat primary neonatal (P2) cortical astrocytes were generated via the removal of cortices from neonate brains which were subsequently prepared using papain enzymatic digestion and mechanical dissociation. Astrocytes were seeded into T75 flasks and incubated at 37°C and 5% CO_2 with astrocyte medium which was changed every 3-4 days. Astrocytes were grown for 14 DIV in flasks for maturation purposes prior to experimental use.

Astrocytes were split using trypsin-EDTA for removal from flasks to generate a cell suspension. Astrocytes were seeded onto 0.1 mg/ml poly-l-lysine (PLL) coated 22 mm coverslips in 6-well plates at normal density (2.5 $x10^4$ cells per ml). Plates were kept in the incubator (37 °C and 5% CO_2) for a minimum of 2 DIV prior to live imaging for morphological or functional assays, or fixing for immunofluorescence techniques. Plates were not used after 7 DIV.

4.2.2 Morphological Assessment of Primary Astrocytes

Astrocytes were fixed with 4% paraformaldehyde (PFA) and treated according to the immunofluorescence protocol previously described (see section 2.3.2). GFAP and S100β were used to distinguish differences between control and forskolin (FSK) treated astrocyte morphology.

Calcein AM, a live cell label, has also been used for the assessment of control and forskolin treated astrocyte morphology. Astrocytes were loaded with 1 µM calcein AM for 30 minutes before media was removed and replaced with an imaging buffer (see section 2.3.1 for buffer composition).

4.2.3 Induction of Stellation

Astrocytes were induced to become stellate via 10 µM forskolin (FSK) treatment for three hours. Astrocytes were washed with an imaging buffer (see section 2.3.1 for buffer composition) to remove forskolin before cells were either imaged live or fixed and labelled.

4.2.4 Functional Assessment of Primary Astrocytes

4.2.4.1 Calcium Imaging

Calcium imaging has been used extensively to understand astrocyte function *in vitro*. The following protocol was adapted from James *et al.*, (2011).

22 mm coverslips with adhered astrocytes were transferred to 35 mm petri dishes containing 2 ml of imaging buffer (see section 2.3.1 for buffer composition). Coverslips were incubated with 1 µM fluo-5 AF (F14222, Invitrogen) in 20% pluronic for 30 minutes in the dark at room temperature (30 µL of fluo-5 dissolved by swirling in 3 ml of imaging buffer). Next the coverslips were moved to a petri dish containing 2 ml of imaging buffer only and left in the dark at room temperature for another 30 minutes to allow de-esterification of the AM group. Prior to imaging, grease was used to secure coverslips into a small chamber that allowed complete imaging buffer to be kept in contact with the coverslip while the cells were imaged. The chambers were mounted on the stage of a Brunel SP981 inverted fluorescent microscope and the vacuum pump was placed appropriately to allow bath solution exchange in preparation for the addition of agonist.

Live fluorescence microscopy was carried out using micromanager software: coverslips were exposed to an LED source (470 nm peak) for 100 ms and 1 frame was imaged per second with the experiment running for 20 minutes (1,200 frames total). Calcium-linked receptor agonists (10 µL of ATP or glutamate in 10 ml of imaging buffer) were added after 120 seconds via manual displacement of the bath solution. Control and forskolin treated astrocytes which had been incubated with different media compositions for up to 14 DIV were also subjected to ATP or glutamate addition.

Image J software (Rasband, W.S., ImageJ, U. S. National Institutes of Health, Bethesda, Maryland, USA, https://imagej.nih.gov/ij/, 1997-2018.), with the Time Series Analyser V3 plugin (https://imagej.nih.gov/ij/plugins/time-series.html), was used to analyse calcium imaging data. Each astrocyte was identified with an ROI and then time course data were analysed using MatLab R2015a software with a calcium GUI plugin necessary to analyse fluorescence intensity. The calcium GUI script was written by Dr Wayne Croft in the Bellamy lab (University of Nottingham) for the purpose of calcium imaging analysis. The percentage of cells responding, the maximum fold change and area under curve (AUC) data were calculated. Graph Pad Prism (Windows Version 7.01) was used for statistical analysis; descriptive statistics as well as Fisher's exact test were used to determine differences in the percentage of cells responding in a given class.

4.2.5 Influence of Media Composition on Astrocyte Morphology

The impact of cell culture media on astrocyte morphology has been determined via both 2D and 3D imaging techniques for astrocytes cultured in astrocyte medium (AM), neuronal medium (NM) or neurobasal supplemented with glutamax (NB+G). The compositions of each culture media are as follows: 1) astrocyte medium is composed of Dulbecco's Modified Eagle's Medium (DMEM) with 10% FBS, 0.5% penicillin/streptomycin and 0.2% L-proline, 2) neuronal medium is composed of chemically defined Neurobasal Medium (NB) with 2% B27 and 1% glutamax, and 3) neurobasal supplemented with glutamax is simply NB with 1% glutamax.

Astrocytes were split from flasks using the standard procedure and seeded onto PLL coated coverslips at normal density (2.5×10^4 cells per ml). Coverslips were incubated with the relevant media and imaged live following 1 µM calcein AM loading on the Olympus IX70 or Zeiss 710 confocal to assess morphology at 2, 5, 7, 9, 12 and 14 DIV.

For detailed astrocyte morphology analysis, astrocytes were imaged on the confocal. Z-stacks were firstly altered: the z-stack interval was changed from

0.476 µm to 0.247 µm in each image (see section 2.3.3.2.1). Next the 3D reconstructions were analysed in Volocity where the freehand tool was used to draw an ROI around individual cells. Parameter measurements including volume, surface area, shape factor and longest axis were collated for all culture media treatments at 7 and 14 DIV.

4.2.5.1 Assay of Astrocyte stellation

To quantitatively assess astrocyte stellation, cells were treated with 1 µM calcein AM for 30 minutes and imaged with the Olympus IX70. Images were blinded using the Image J Blinding Macro for manual stellation analysis. Blinded images were analysed according to the following criteria: cells were defined as stellate when they had two or more obvious fibrous processes projecting from a smaller cell soma, and an elongated or star shaped appearance. Cells were classed as protoplasmic if they had no obvious processes, or a single process, and a vellate or polygonal appearance.

The numbers of stellate and protoplasmic cells were counted and recorded using ImageJ. The percentage of stellate cells was calculated for each coverslip for each treatment condition at each time point and statistical analysis was carried out with Graph Pad Prism (Windows Version 7.01).

4.2.6 Statistics

To investigate quiescent astrocyte phenotype, descriptive statistics as well as Fisher's exact test were used to determine differences in the percentage of cells responding in a given class in calcium imaging experiments.

To assess the impact of culture media treatment on astrocyte morphology a Kruskal-Wallis test (one-way ANOVA) with Dunn’s correction for multiple comparisons was conducted (0.05 significance level). Additionally, two-way ANOVAs with Tukey’s correction were used to determine significant differences in the percentage of astrocyte stellation for different media treatments and across the time course.

A Kruskal-Wallis test with Dunn’s correction for multiple comparisons was also used to determine the changes to astrocyte function via calcium signalling

following culture with different media treatments. Mann-Whitney t tests were used to discover the influence of culturing astrocytes in Dulbecco's Modified Eagles Medium (DMEM).

4.3 Results

4.3.1 Primary Astrocyte Morphology *in Vitro*

Astrocytes are known to exhibit flat and protoplasmic morphology when cultured on 2D substrates *in vitro*. To validate the morphology of cortical astrocytes on coated coverslips in tissue culture plates, live and fixed cell labelling techniques have been used. Both calcein AM loading, and GFAP and S100β labelling, have revealed the heterogeneous morphology of astrocytes, as well as their tendency to form a monolayer in culture (Figure 1). Astrocytes in 2D culture normally exhibit a sheet-like or polygonal appearance and exhibit few defined process extensions from the cell body (Figure 1).

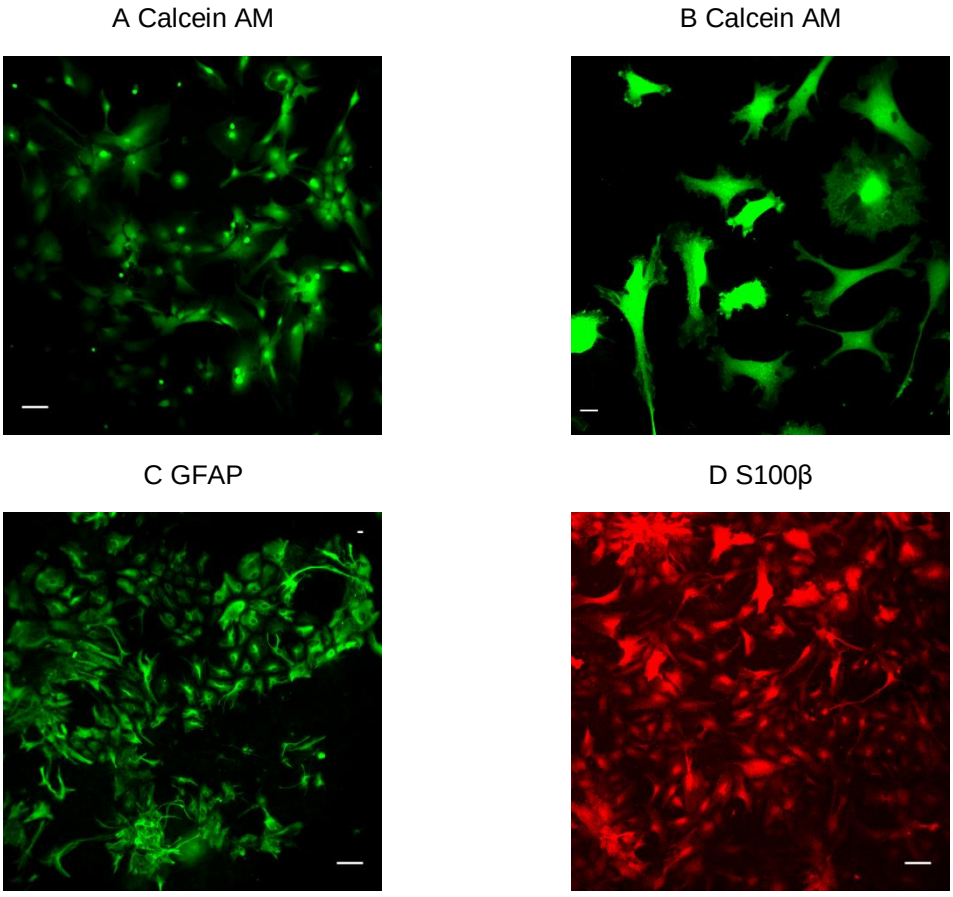


Figure 1. Cortical astrocytes exhibit heterogeneous morphologies on 2D coverslips. Astrocytes cultured on 0.1 mg/ml PLL coated coverslips and cultured with astrocyte medium were loaded with 1 µM calcein AM directly into the bathing media (A & B), or fixed and labelled with GFAP primary antibody (C), or S100β primary antibody (D). Representative images shown from N = 20 coverslips per marker, generated from a minimum of three astrocyte preparations in each case. Scale bar = 100 µM in A, C & D, scale bar = 20 µm in B.

Primary astrocytes treated with forskolin (FSK) undergo a dramatic change to their morphology: a dramatic reorganisation of the cytoskeleton occurs, forming cells with a smaller soma which lots of fibrous processes project from (Figure 2). This gives the cells a ‘spikey’ or stellate appearance. FSK treated astrocytes are distinct from control cells and demonstrate the capability of astrocytes to respond to external stimuli with dramatic morphological changes within 3 hours (Figure 2).

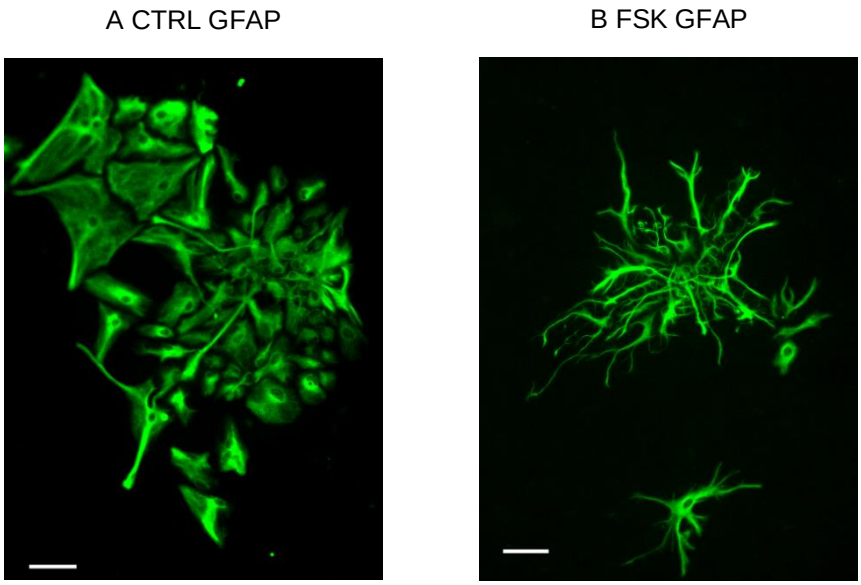


Figure 2. Cortical astrocytes treated with forskolin (FSK) undergo significant morphological changes. Control (A) or FSK treated (B) astrocytes cultured on 0.1 mg/ml PLL coated coverslips were cultured with astrocyte medium and fixed and labelled with GFAP primary antibody. Representative images shown from N = 20 coverslips, generated from a minimum of three astrocyte preparations. Scale bars = 100 µM.

4.3.2 Primary Astrocyte Function *in Vitro*

Astrocyte cells are highly responsive to external stimuli but are also extremely heterogeneous - not all cells respond in the same way to identical stimuli. Calcium elevation in astrocytes serves as a useful indication of cell activity, thus we have carried out calcium imaging to investigate astrocyte function.

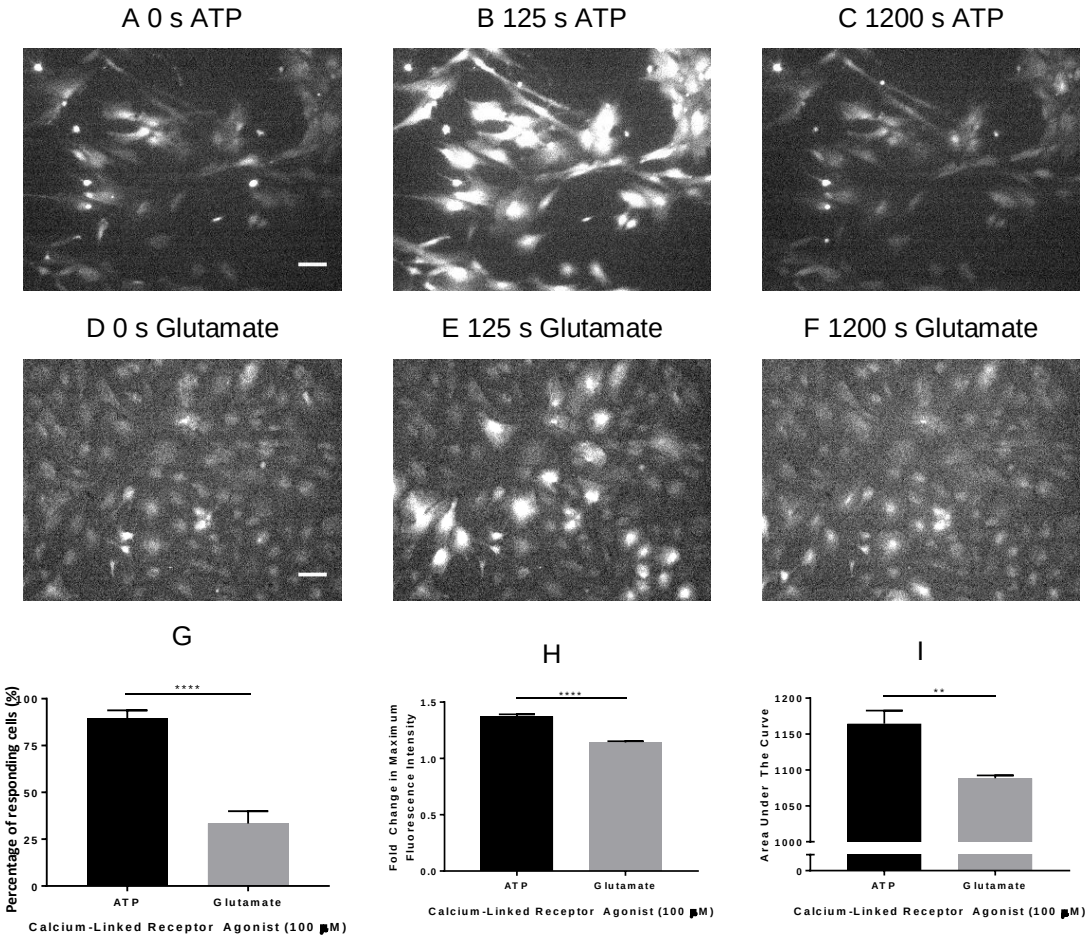


Figure 3. Cortical astrocytes undergo changes to intracellular calcium concentration following the addition of ATP or glutamate. Astrocytes cultured on 0.1 mg/ml PLL coated coverslips and cultured with astrocyte medium were treated with 1 µM fluo-5 for 30 minutes at room temperature in imaging buffer before live cell imaging. Either 100 µm ATP (A-C) or glutamate (D-F) was added after 2 minutes and imaging was conducted over 20 minutes. Representative intracellular calcium responses are shown for ATP and glutamate at 0 s (A & D), 125 s (B & E) and 1200s (C & F). Cortical astrocytes exhibit different responses to the addition of agonists ATP (black bars) and glutamate (grey bars) as quantified in G-I: Percentage of responding cells (G), fold change in maximum fluorescence intensity (H) and Area Under the Curve (without baseline subtraction) (I). Mean ± SEM shown. Mann-Whitney t test to compare ranks. N = 16 coverslips for ATP and N = 20 coverslips for glutamate, both generated from a minimum of three astrocyte preparations. Scale bars = 100 µm.

Astrocytes were loaded with 1 µM fluo-5F for 30 minutes before live cell imaging for 20 minutes where agonists such as ATP and glutamate were added after 2 minutes to determine the functional responses of astrocytes to

neurotransmitters *in vitro* (Figure 3). ATP and glutamate were selected because they are known to elicit cell responses within a population.

Minimal spontaneous calcium activity was initially observed before the addition of agonist (Figure 3A & D). In the first 120 seconds used to calculate the baseline activity of cells, there were few calcium spikes or waves observed, and therefore little change to fluorescence intensity after loading with fluo-5 (Figure 3A & D, Figure 4). Post ATP agonist addition, significant increases in fluorescence emission were observed in nearly all cells, consistent with robust calcium responses (Figure 3B & E). Such changes to fluorescence intensity occurred over approximately 30 seconds post agonist addition and were subsequently dissipated (Figure 3C & F). Glutamate agonist addition elicited up to a 50% response of cells within a field of view (Figure 3E).

An average of 89.8% of cells responded to ATP agonist addition (cells counted from 16 coverslips), whereas in contrast to this, the average percentage of cells responding to glutamate agonist addition was significantly lower at 33.5%, ($p < 0.0001$, cells counted from 20 coverslips) (Figure 3G). For cells that responded to agonist addition, there was a significantly greater fold change in maximum fluorescence intensity and the area under the curve (without baseline subtraction) for ATP treated cells compared to glutamate treated cells ($p < 0.0001$ and $p = 0.0011$ respectively) (Figure 3H & I).

Individual traces for six cells treated with ATP or glutamate illustrate the heterogeneity of astrocyte responses when exposed to the same external stimuli (Figure 4). The first five traces for ATP and glutamate represent the changes in intracellular calcium activity for individual cells responding to agonists over the time course of an experiment (Figure 4). The bottom traces for ATP and glutamate show cells which have not responded to agonist addition (Figure 4).

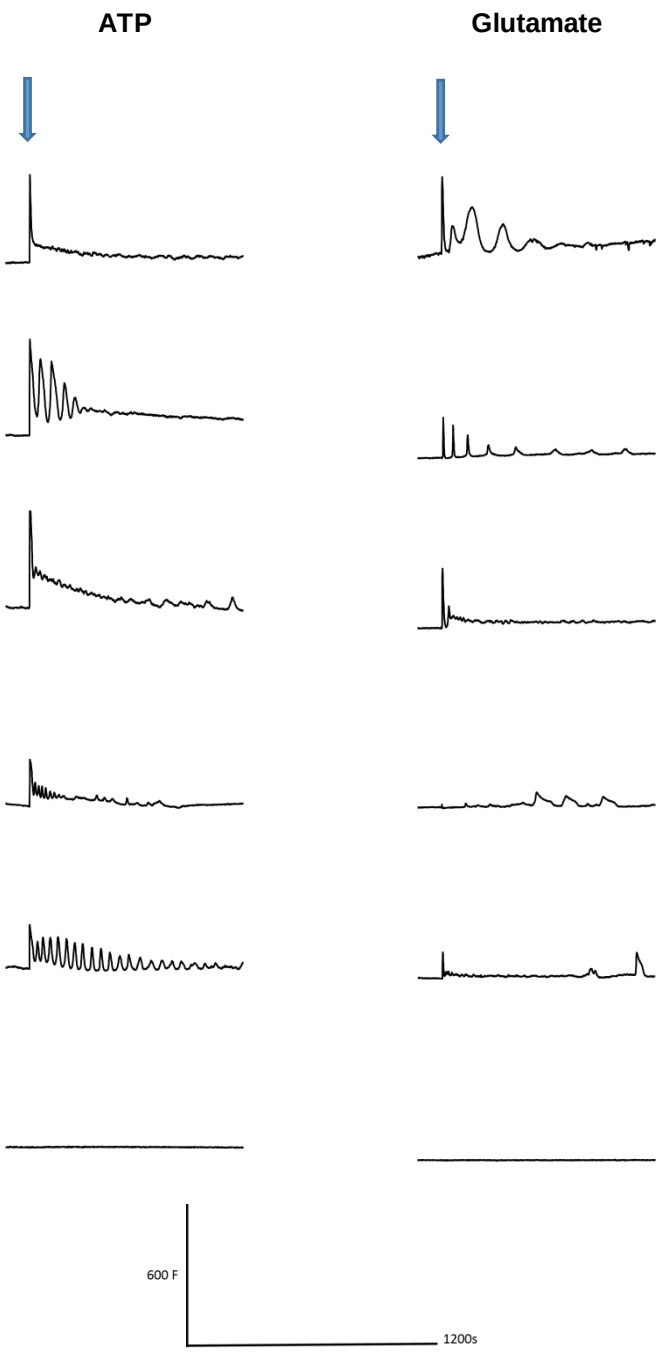


Figure 4. Cortical astrocytes exhibit heterogeneous responses to the addition of ATP and glutamate agonists. Traces of fluo-5 fluorescence intensity for individual astrocytes when treated with 100 µm ATP (left) or glutamate (right). Blue arrows represent the point of agonist addition. Traces selected at random from a total of N = 16 coverslips for ATP and N = 20 coverslips for glutamate, from a minimum of three astrocyte preparations. Scale shown in bottom panel.

4.3.3 The Influence of Cell Culture Media on Astrocyte Phenotype

4.3.3.1 Morphological Analysis

Astrocytes cells are highly responsive to their microenvironment, thus the composition of culture media is likely to play a significant role in determining their morphology. Astrocytes cultured in different media compositions for up to 7 or 14 DIV showed distinct morphologies (Figure 5).

At 7 and 14 DIV astrocytes cultured with astrocyte medium (AM) embodied a typically flat and protoplasmic morphology often found *in vitro* (Figure 5A & D). Astrocytes cultured with neuronal medium (NM) had clearly defined processes and exhibited morphological similarities to astrocytes treated with forskolin, suggesting that cells may have become reactive (Figure 5B & E). By eye, it seemed that induced astrocyte stellation, resulting from NM treatment, affected more than 50% percent of cells per field of view where cells had two or more obvious processes (Figure 5B & E). For astrocytes cultured with neurobasal supplemented with glutamax (NB+G), some cells developed a stellate morphology but this appeared to be proportionally less than for cells cultured with neuronal medium at around 15% (Figures 5C & F).

Further qualitative analysis of morphological differences between astrocytes in different culture media was confirmed by confocal imaging (Figure 6). Astrocytes cultured in AM had a protoplasmic appearance (Figure 6A & D) whereas astrocytes cultured in NM had highly defined processes extending out from the cell body (Figure 6B & E). Astrocytes cultured with NB+G had an intermediate morphology between the other two conditions (Figure 6C). By 14 DIV astrocyte cell counts in NB+G media were typically low and I did not find many cells to image in my preparations.

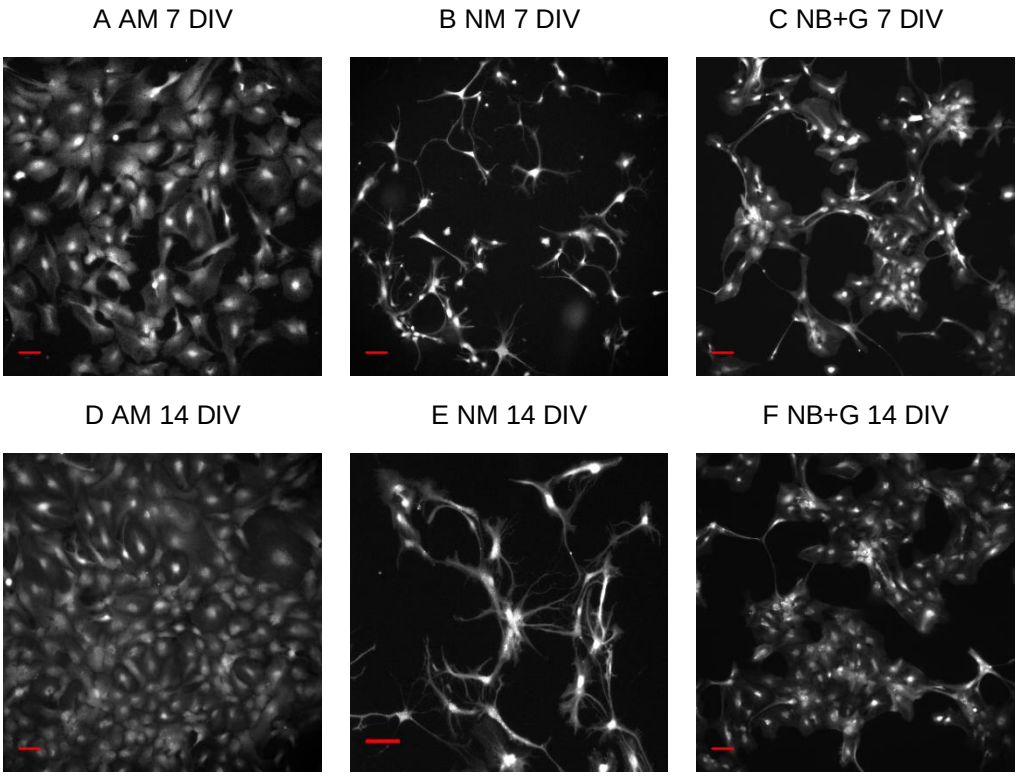


Figure 5. Cortical astrocytes developed strikingly different morphologies when cultured with different media. Astrocytes were cultured with astrocyte medium (AM) (A & D), neuronal medium (NM) (B & E) or neurobasal with glutamax (NB+G) (C & F) for either 7 DIV (A-C) or 14 DIV (D-F). Cells were loaded with 1 µm calcein AM for 30 minutes before live cell imaging. Representative images shown where N = 4 cells for AM at 7 DIV and 5 at 14 DIV, N = 10 cells for NM at 7 DIV and 14 at 14 DIV, and N = 7 cells for NB+G at 7 DIV and 3 at 14 DIV, from a minimum of three astrocyte preparations. Scale bars = 100 µm.

Quantitative analysis was conducted to define the morphological differences for astrocytes cultured with the three different media treatments (AM, NM or NB+G). In a preliminary analysis, it has been possible to measure astrocyte volume, surface area, shape factor and longest axis using Volocity software (Figure 7). Volume and surface area measurements have been calculated based on pixel intensity detected using the -75% auto threshold function. Shape factor is the numerical representation of how similar the 3D shape is to a perfect sphere: the 3D measurement is based on the ratio of the surface area of a sphere (with the same volume as the object) to the surface area of

the object (see section 5.2.5.4, page 105 for the relevant formula). The shape factor is close to 1 for a perfect sphere and will be closer to zero for irregular shapes. Longest axis measurements are based on surface area calculations.

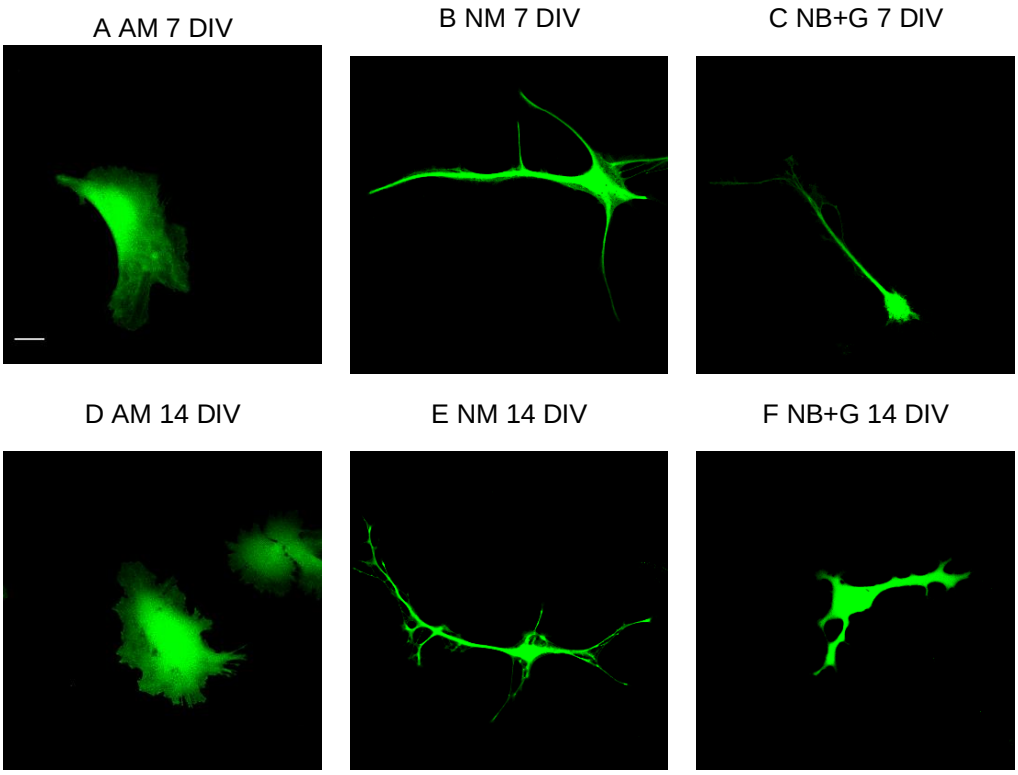


Figure 6. Cortical astrocytes developed strikingly different morphologies when cultured with different media. Astrocytes were cultured with either astrocyte medium (AM) (A & D), neuronal medium (NM) (B & E) or neurobasal with glutamax (NB+G) (C & F) for 7 (A-C) or 14 DIV (D-F). Cells were loaded with 1 µM calcein AM for 30 minutes. Representative images shown where N = 4 cells for AM at 7 DIV and 5 at 14 DIV, N = 10 cells for NM at 7 DIV and 14 at 14 DIV, and N = 7 cells for NB+G at 7 DIV and 3 at 14 DIV, from a minimum of three astrocyte preparations. Scale bar = 20 µm in A.

At 14 DIV, astrocytes cultured with AM had a significantly greater volume than cells equivalently cultured to 7 DIV ($p = 0.0448$, Figure 7A). For astrocytes cultured with NB+G, the mean longest axis was significantly decreased after 14 DIV compared to 7 DIV ($p = 0.0134$, Figure 7D). At 7 DIV, astrocytes cultured with NB+G had a significantly smaller volume and surface area compared to astrocytes cultured with NM ($p = 0.0050$ for volume, $p = 0.0067$ for surface area, Figure 7A & B). Similarly, at 14 DIV, astrocytes cultured with

NB+G had significantly smaller volumes and surface areas than cells cultured with either AM or NM ($p = 0.0022$ for AM volume, $p = 0.0004$ for AM surface area, $p = 0.0050$ for NM volume, and $p = 0.0019$ for NM surface area, Figure 7A & B). At both 7 and 14 DIV, shape factor was significantly increased for astrocytes cultured with NB+G compared to cells cultured with the other two media treatments ($p = 0.0221$ AM vs NB+G at 7 DIV, $p = 0.0038$ NM vs NB+G at 7 DIV, $p = 0.0001$ AM vs NB+G at 14 DIV and $p < 0.0001$ NM vs NB+G at 14 DIV, Figure 7C).

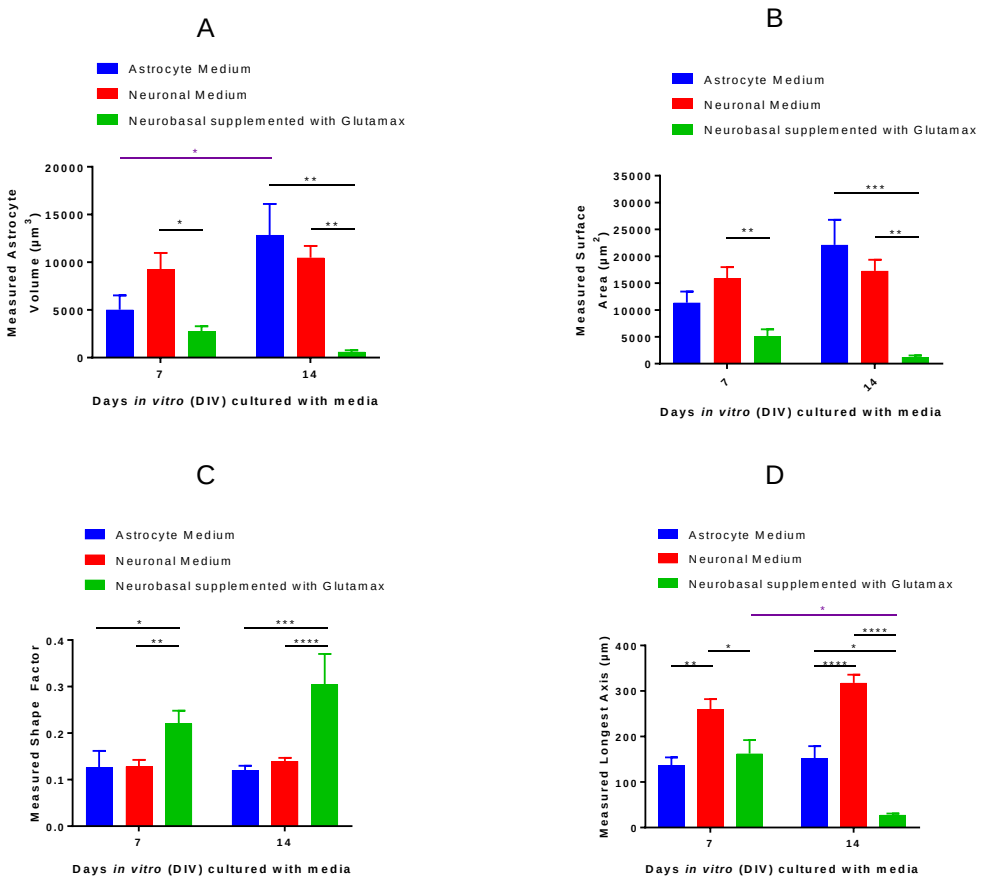


Figure 7. Quantitative assessment of cortical astrocyte parameters when cultured with different media. Astrocytes were cultured for either 7 or 14 DIV in either astrocyte medium (blue), neuronal medium (red) or neurobasal with glutamax (green). Parameters shown: Volume (μm^3) (A), Surface Area (μm^2) (B), Shape Factor (C) and Longest Axis (μm) (D). Mean ± SEM shown. N = 4 cells for AM at 7 DIV and 5 at 14 DIV, N = 10 cells for NM at 7 DIV and 14 at 14 DIV, and N = 7 cells for NB+G at 7 DIV and 3 at 14 DIV. Ordinary Two way ANOVA with Tukey's test for multiple comparisons to compare the effect of media treatments within a time point. Ordinary Two way ANOVA with Sidak's test for multiple comparisons to compare media treatments from 7 to 14 DIV.

Mean longest axis was significantly higher for astrocytes cultured with NM at 7 and 14 DIV compared to the other two media treatments ($p = 0.0070$ AM vs NM at 7 DIV, $p = 0.0108$ NM vs NB+G at 7 DIV, otherwise $p < 0.0001$, Figure 7D). Longest axis measurements for astrocytes cultured in NB+G were also significantly reduced compared to cells cultured with AM ($p = 0.0316$, Figure 7D).

4.3.3.2 Stellation Analysis

To assess the impact of different cell culture media on astrocyte stellation, 1 µM calcein AM loading was conducted for 30 minutes at 2, 5, 7, 9, 12 and 14 DIV. A blinded stellation assay was carried out on images acquired at the stated time points. Data was analysed from up to 8 coverslips for each condition and time point, from 4 different astrocyte preparations. Stellate cells were defined according to the criteria described in the methods (see section 4.2.5.1).

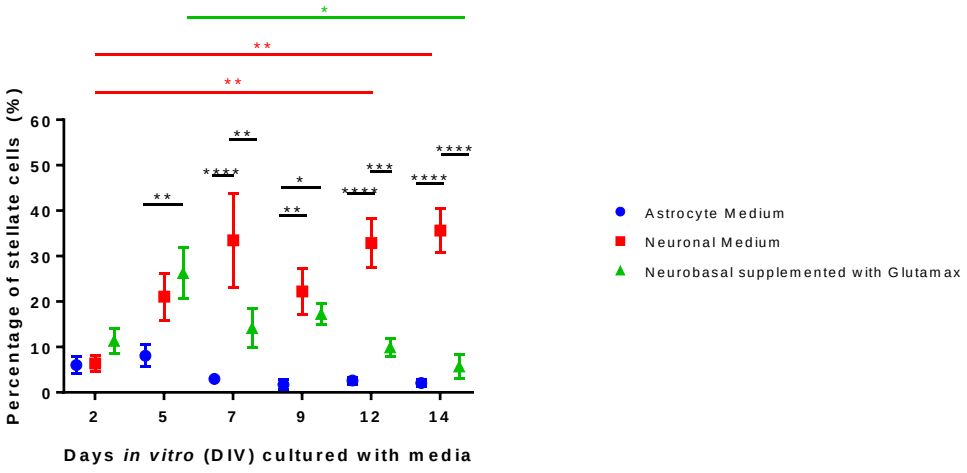


Figure 8. Different media compositions resulted in differing percentages of stellate cortical astrocytes in culture. Astrocytes were cultured in astrocyte medium (blue), neuronal medium (red) or neurobasal with glutamax (green). Mean ± SEM shown. Data was analysed from up to 8 coverslips for each condition and time point, from 4 different astrocyte preparations. Stellate cells were defined as having two or more obvious fibrous processes projecting from a smaller cell soma, and an elongated or star shaped appearance. Protoplasmic cells were counted if they had no obvious processes, or a single process, and a polygonal appearance.

There was no statistically significant change in the percentage of stellate cells over the time course for cells cultured with AM (Figure 8). In contrast to this, the percentage of stellate cells for astrocytes cultured with NM was significantly increased from 6.4% at 2 DIV to 32.9% at 12 DIV ($p = 0.0085$) and 35.6% at 14 DIV ($p = 0.0022$) (Figure 8).The maximum percentage of stellate cells measured was found for astrocytes cultured with NM until 14 DIV (Figure 8). There was also a significant decrease in the percentage of stellate cells for astrocytes cultured with NB+G from 26.3% at 5 DIV to 5.7% at 14 DIV which may result from reduced cell viability ($p = 0.0232$) (Figure 8). From 7 DIV, the percentage of stellate cells for astrocytes cultured with NM was significantly higher compared with the other two media treatments ($p = 0.0031$ NM vs NB+G at 7 DIV, $p < 0.0001$ AM vs NG+G at 7 DIV, $p = 0.0037$ AM vs NM at 9 DIV, $p < 0.0001$ 1at 2 & 14 DIV, Figure 8).

To investigate whether differences in the percentage of stellate cells across the time course may have resulted from variation in the number of cells counted at each time point with each media treatment, cell counts per coverslip were calculated across the time course (N = 8 coverslips per condition and DIV, Figure 9). For both NM and NB+G treatments, there was a significant decrease in the number of cells counted at 2 DIV compared with 14 DIV ($p = 0.0326$ for NM, $p = 0.0251$ for NB+G, Figure 9B & C). Whilst the number of cells counted steadily declined across the time course for astrocytes cultured with NM or NB+G, cell numbers remained reasonably constant for astrocytes cultured with AM (Figure 9A). This is most likely a result of the fact that NM and NB+G media treatments are not optimal for astrocyte survival.

The decrease in the number of cells counted per coverslip for NM and NB+G media treatments across the time course may result from astrocytes dying due to an insufficient cell culture media composition (total of 8 coverslips for each condition and time point). Calcein AM is a marker of cell viability and thus shows only live cells, but it must be considered that rounded cells are potentially apoptotic and not healthy. To confirm cell death in the future, the protease family responsible for the caspase cascade and the initiation of

apoptosis could be labelled via immunofluorescence techniques (McIlwain, Berger and Mak, 2015).

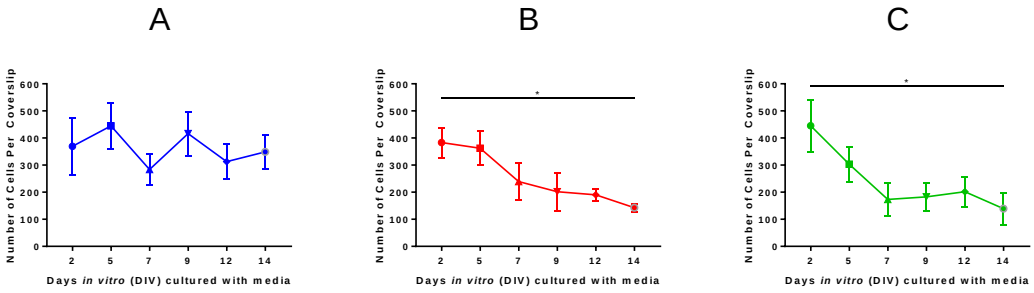


Figure 9. Line graphs for mean astrocyte cell counts per coverslip (including protoplasmic and stellate cells) for three different media treatments from 2-14 DIV. A) Astrocyte Medium B) Neuronal Medium and C) Neurobasal supplemented with Glutamax. Mean ± SEM shown. Data analysed from up to 8 coverslips for each condition and time point, from 4 astrocyte preparations. Ordinary One Way ANOVA with Tukey's test for multiple comparisons.

4.3.3.3 Functional Analysis

To discover if culturing astrocytes with different media compositions influenced their function, calcium imaging was carried out to quantify the percentage of responding astrocytes to agonists ATP and glutamate. Additionally, the effect of forskolin on cell function was assessed when astrocytes were cultured with the different media compositions (AM, NM or NB+G). Data was analysed from up to 8 coverslips from a minimum of three different astrocyte preparations for each treatment condition at each time point for both agonists.

Whilst FSK treatment significantly reduced the percentage of astrocytes that exhibited a calcium response to ATP addition when cultured with AM ($p = 0.0043$), in contrast, there was a significant increase in the percentage of cells responding to ATP following FSK treatment when cultured with NB+G ($p < 0.0001$) (Figure 10). Control astrocytes cultured with either NM or NB+G had a significantly reduced percentage of responding cells to ATP compared to cells cultured with AM ($p < 0.0001$) (Figure 10).

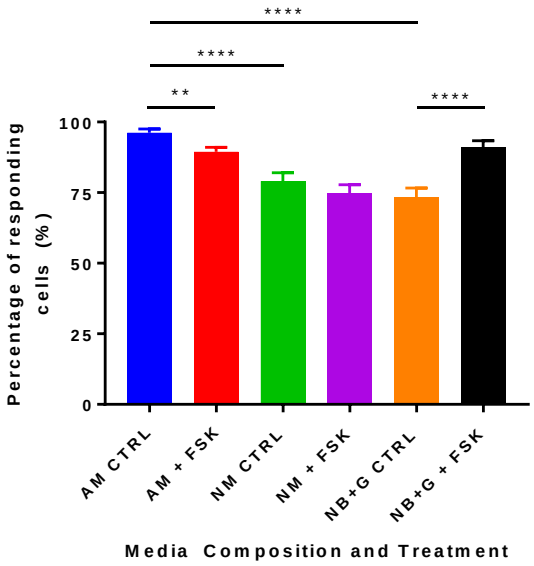


Figure 10. Assessment of media composition and FSK influence on astrocyte responses to ATP agonist addition. Astrocytes were cultured with either astrocyte medium (AM), neuronal medium (NM) or neurobasal supplemented with glutamax (NB+G) for 7 DIV. Coverslips were treated with 10 µM forskolin for 3 hours to induce stellation (AM + FSK, NM + FSK or NB+G + FSK). All coverslips were loaded with 10 µM fluo-5 for 30 minutes before imaging. Numbers of coverslips analysed: AM CTRL = 7, AM + FSK = 5, NM CTRL = 8, NM + FSK = 7, NB+G CTRL = 8 and NB+G + FSK = 7. Mean ± SEM shown. Mann Whitney for comparison of CTRL astrocytes to FSK treated astrocytes cultured for each of the three media compositions. Kruskal-Wallis ANOVA test with Dunn's correction for multiple comparisons to compare CTRL astrocytes cultured with the three media compositions.

Forskolin treatment significantly decreased the percentage of astrocytes responding to glutamate when cultured with either of the three media conditions ($p < 0.0001$) (Figure 11). The percentage of astrocytes responding to glutamate when cultured with NB+G significantly decreased over 50% ($p < 0.0001$, Figure 11). Control astrocytes cultured with NM or NB+G had a significantly increased percentage of responding cells to glutamate agonist addition in comparison to control cells cultured with AM ($p = 0.0018$ for NM, $p < 0.0001$ for NB+G) (Figure 11).

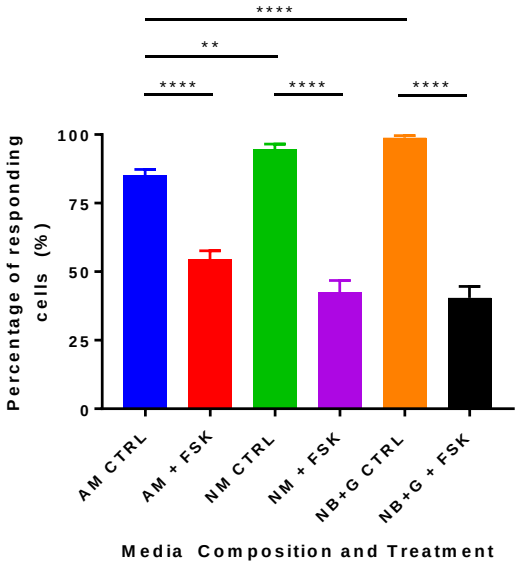


Figure 11. Assessment of media composition and FSK influence on astrocyte responses to glutamate agonist addition. Astrocytes were cultured with astrocyte medium (AM), neuronal medium (NM) or neurobasal supplemented with glutamax (NB+G) for 7 DIV. Coverslips were treated with 10 µM forskolin for 3 hours to induce stellation (AM + FSK, NM + FSK or NB+G + FSK). All coverslips were loaded with 10 µM fluo-5 for 30 minutes before imaging. Number of coverslips analysed: AM CTRL = 8, AM + FSK = 7, NM CTRL = 8, NM + FSK = 6, NB+G CTRL = 8 and NB+G + FSK = 6. Mean ± SEM shown. Mann Whitney for comparison of CTRL astrocytes to FSK treated astrocytes cultured for each of the three media compositions. Kruskal-Wallis ANOVA test with Dunn's correction for multiple comparisons to compare CTRL astrocytes cultured with the three media compositions.

4.3.3.3.1 FBS Influence on Astrocyte Function

To discover more about the influence of astrocyte cell culture media on the *in vitro* phenotype of primary astrocytes, specifically the influence of FBS on astrocyte receptor expression, control or forskolin treated cells cultured with DMEM were assessed for their responses to ATP or glutamate agonist addition and compared to cells treated with AM. Data was analysed from 6 coverslips for each condition from a minimum of two astrocyte preparations.

Culturing astrocytes with DMEM had no significant effect on the percentage of responding cells to ATP compared with cells cultured with AM (Figure 12A). Similarly, culturing astrocytes with DMEM had no impact on the percentage of

responding cells to glutamate in comparison to cells cultured with AM (Figure 12B).

Whilst forskolin treatment significantly reduced the percentage of astrocytes responding to ATP and glutamate for cells cultured with AM ($p = 0.0107$ for ATP, $p < 0.0001$ for glutamate), there were no significantly altered responses to the two agonists for cells cultured in DMEM (Figure 12). Astrocytes cultured with DMEM and treated with FSK had a significantly greater percentage of cells responding to ATP and glutamate agonist addition compared to control cells ($p = 0.0004$ for ATP, $p < 0.0001$ for glutamate) (Figure 12B).

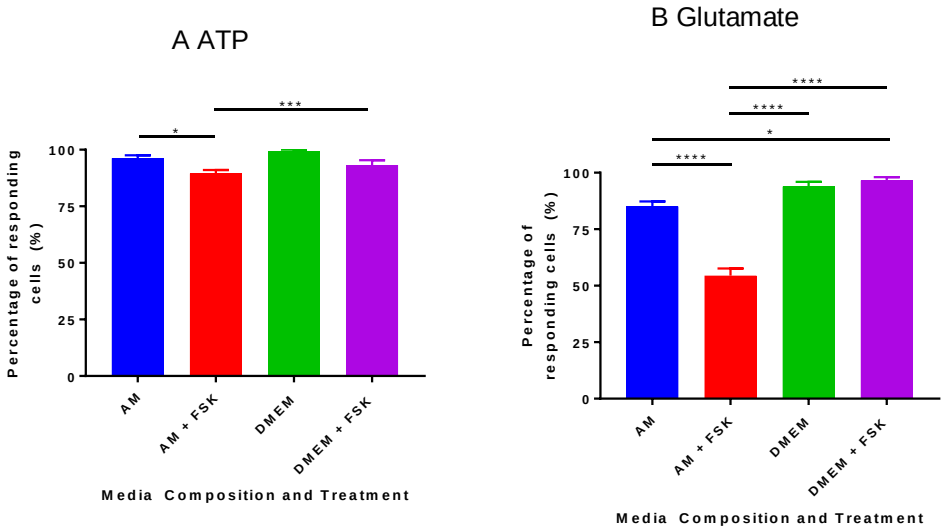


Figure 12. Assessment of the influence of FBS on cortical astrocyte responses to ATP or glutamate agonist addition. Percentage of responding astrocytes to ATP (A) or glutamate (B) addition for cells cultured in either astrocyte medium (AM) or Dulbecco's Modified Eagles Medium (DMEM) for 7 DIV. Coverslips were treated with 10 µM forskolin for 3 hours to induce stellation (AM + FSK or DMEM + FSK). Coverslips were loaded with 10 µM fluo-5 for 30 minutes before imaging. Mean ± SEM shown. N = 6 coverslips analysed for each treatment from a minimum of two astrocyte preparations. Kruskal-Wallis ANOVA test with Dunn's correction for multiple comparisons.

4.4. Discussion

4.4.1 2D Culture of Primary Astrocytes

Primary astrocytes have long been cultured with 2D methods *in vitro* as an alternative way to studying cells *in vivo*. Astrocytes are a highly plastic cell type which adapt their phenotype in response to external stimuli, thus it is conceivable that laboratory practices may account for some of their observed phenotypic differences. One variable of *in vitro* culture is media composition which is specialised according to the brain region cells have been extracted from.

The aim of this chapter was to generate primary neonatal (P2) cortical astrocytes to study their phenotype and how this changes in response to different compositions of culture media. Additionally, this study assessed whether the induction of stellation would alter astrocyte phenotype in response to different compositions of culture media.

Primary astrocytes cultured with astrocyte medium (see section 2.2.1 for cell culture media composition) were GFAP and S100β positive, and exhibited heterogeneous morphology which is characteristic of cortical astrocytes (Figure 1) (Hu *et al.*, 2016). Morphological heterogeneity of astrocytes was discovered back in the 1990s when neonatal spinal cord cultures revealed five types of astrocyte (Miller and Szigeti, 1991). In the following years, the phenotypic diversity of *in vitro* spinal cord astrocytes was well classified revealing a total of nine distinguishable morphologies (Black, Sontheimer and Waxman, 1993). Furthermore, astrocytes of various morphologies can be derived from a particular CNS region, as has been found with cortical astrocytes generated in this study.

Forskolin is known to increase cellular cAMP levels and alter morphology in neonatal forebrain astrocytes which are transformed from polygonal cells to those which are process bearing via re-arrangements to the cytoskeleton (Goldman and Abramson, 1990; Won and Oh, 2000). Significant rearrangements to neonate astrocyte morphology, via a significant decrease in the cross-section area and an increase in the cell perimeter, have also

previously been found following FSK treatment (Vardjan, Kreft and Zorec, 2014). This study found striking morphological changes and cytoskeletal reorganisation with primary astrocytes following 10 µM FSK treatment for 3 hours which confirms that it is possible to induce stellation with FSK (Figure 2).

Astrocytes exhibit spontaneous and ligand-evoked intracellular calcium concentration increases, a form of astrocyte excitability. Primary astrocytes cultured with astrocyte medium had a high percentage of responding cells to key neurotransmitters ATP and glutamate (Figure 3). These findings are in-keeping with the literature which has previously verified glutamate as a mechanism for the increase in astrocytic calcium (Wang *et al.*, 2006), and that cortical astrocytes demonstrate calcium wave propagation in response to extracellular ATP (Guthrie *et al.*, 1999). Similar findings have been verified *in vivo* where protoplasmic astrocytes of the cerebral cortex have been found to exhibit spontaneous and sensory-evoked calcium transients using anesthetized rats (Hirase *et al.*, 2004).

Primary astrocytes induced to undergo stellation demonstrated striking morphological differences compared to control cells (Figure 2), therefore I aimed to investigate changes to astrocyte receptor expression and responses to neurotransmitter following FSK treatment. The percentage of FSK treated astrocytes responding to ATP and glutamate was significantly reduced compared to control cells (Figures 10 & 11). This suggests that FSK treatment effects astrocyte cell surface receptor expression.

With all of the data shown here it must be taken into consideration that astrocytes are a heterogeneous cell type (Zhang and Barres, 2010; Lin *et al.*, 2017). Cellular responses to neurotransmitters can vary across coverslips and between different experimental preparations, and will account for the observed phenotypic variation with astrocytes generated and cultured with the same protocol. Astrocyte heterogeneity is important when comparing experimental findings to those in the literature since culture conditions will significantly affect gene and receptor expression (Miller, Romano and Cotman, 1995; Cahoy *et al.*, 2008) and thus influence data interpretation. The

brain region astrocytes are extracted from is also important since astrocytes show extensive functional and morphological diversity originating from different brain regions (Lange *et al.*, 2012).

4.4.2 Influence of Media Composition on Astrocyte Phenotype

4.4.2.1 Morphology

Astrocytes respond to changes in their external environment with alterations to their phenotype. Striking differences in the morphology of astrocytes cultured with either astrocyte medium (AM), neuronal medium (NM) or neurobasal supplemented with glutamax (NB+G) have been found (Figures 5 & 6). Astrocytes cultured with NM embodied a characteristically stellate morphology (Figures 5 & 6) and evoked the greatest percentage of stellation for astrocytes cultured for up to 14 DIV (Figure 8).

Quantitative analysis revealed that astrocytes cultured with NB+G had significantly smaller volumes, surface areas and longest axes, but conversely had a significantly greater shape factor compared to astrocytes cultured with the other two media treatments (Figure 7). This suggests that when astrocytes were exposed to NB+G, they were smaller, occupied smaller domains, and were more rounded than astrocytes cultured with AM. Additionally the number of cells counted per coverslip steadily declined over the time course, and was significantly reduced from 448 at 2 DIV to 139 14 DIV (Figure 9C), suggesting that this media composition is not sufficient for astrocyte survival or development *in vitro*. Similar to this, the number of cells counted per coverslip for astrocytes cultured with NM also significantly decreased from 383 at 2 DIV to 143 at 14 DIV (Figure 9B), also implying that this media doesn't support astrocyte growth. The significant impact of culture media composition on cell survival, development and morphology emphasizes how crucial media selection is for the culture of primary astrocytes.

4.4.2.2 Function

We also assessed changes to astrocyte responses to agonists ATP and glutamate for cells cultured with the three different media compositions (Figures 10 & 11). The percentage of responding astrocytes to ATP was significantly decreased when control cells were cultured with either NM or NB+G (Figure 10) indicating that these media compositions are incapable of allowing primary astrocytes to develop physiological phenotype. Yet, in contrast to this, there is a significantly increased percentage of responding cells to glutamate when control cells are exposed to NM or NB+G when compared with AM (Figure 11).

For astrocytes cultured with any of the three media treatments (AM, NM or NB+G) the percentage of cells responding to glutamate addition following forskolin treatment was significantly decreased compared to control counterparts (Figure 11). Unlike this, astrocytes cultured with NB+G and treated with FSK had a significantly increased percentage of responding cells to ATP addition (Figure 10). These data indicate that cell-surface receptor expression has changed over the course of 3 hour forskolin treatment and suggest that different media treatments influence purinergic receptor expression in astrocytes. Additionally, these data imply that forskolin treatment interferes with glutamate agonist binding, either through changed receptor expression at the cell surface, or effects on ligand binding at the cell surface. To determine the mechanism of action, astrocytes could be labelled for glutamate-specific receptors and analysed for changes prior to and post forskolin treatment.

A study at the end of the 1980s showed that in cultured cortical astrocytes, voltage-dependent L-type calcium channels were induced following exposure to substances such as forskolin which are known to increase intracellular cAMP concentration (Barres, Chun and Corey, 1989). It was discovered that forskolin could induce such currents when astrocytes had been treated with serum for a minimum of 2 days, but the L-type calcium currents weren't present in control cultures (Barres, Chun and Corey, 1989). Additionally the research revealed that different batches of sera resulted in differential types of

calcium currents; some batches induced T-type calcium currents similar to those found in the control cultures (Barres, Chun and Corey, 1989). This suggested that the rise in intracellular cAMP prompted the insertion of channels into the membrane from submembrane stores, or even the modification of silent channels already present in the membrane.

In 2003, Velasco *et al*., (2003) identified that serum-containing medium and serum-free medium (NB + B27) resulted in different cortical neuron responses following treatment with glutamate for 15 minutes. Therefore considering that neuronal cells exhibit different sensitives to glutamate-mediated toxicity depending on their culture medium (Velasco *et al.*, 2003), it is possible that glutamate receptor expression may also vary in astrocyte cells cultured in different media compositions. In connection with this, it has been shown that classic neuronal basal medium, as well as the presence of serum, interfere with action potential generation and synaptic communication (Bardy *et al.*, 2015). Bardy *et al.*, (2015) also discovered that adjusting the concentrations of the amino acids and inorganic salts not only supported neuronal survival and activity, but improved the percentage of neurons that were synaptically active for human tissue samples as well as rodent. Again, considering the sensitivity of astrocytes to their external microenvironment, it is likely that the concentrations of amino acids and inorganic salts in culture media will influence gene expression.

Furthermore, I have found that astrocyte responses to agonists ATP and glutamate differ significantly depending on the media which they are cultured with. This highlights that media composition *in vitro* significantly influences astrocyte phenotype and must be taken into account when trying to co-culture astrocytes with other cell types.

4.4.2.2.1 Dulbecco's Modified Eagles Medium

Dulbecco's Modified Eagles Medium (DMEM) is used for the growth and development of embryonic or neonatal rodent primary cells, and is usually supplemented with serum. I have determined the functional responses of astrocytes when cultured in DMEM alone to understand phenotypic alterations

in primary astrocytes as a result of components in the cell culture media (Figure 12).

Culturing primary astrocytes with DMEM only media had no effect on the percentage of responding astrocytes to ATP and glutamate when compared with AM (Figure 12). However, there was a significant increase in the percentage of responding cells to ATP when FSK treated astrocytes were cultured with DMEM compared with AM (Figure 12A). We suggest that proteins in FBS may interfere with cell-surface receptor activity: FBS is a nutritional support for live cells which contains proteins such as BSA which bind fatty acids and peptides (Spector, John and Fletcher, 1969), thus there may be non-specific binding with astrocyte receptors.

These data suggest that primary astrocyte function develops similarly with astrocytes cultured with or without FBS serum supplemented in DMEM. DMEM could be supplemented with other carefully selected components which both expose primary astrocytes to molecules found in the *in vivo* brain microenvironment and allow them to develop physiological phenotype in an attempt to derive a standardised minimal essential media for cortical astrocytes.

4.4.2.2.2 Serum Supplementation in Media

Primary astrocytes are usually cultured with media supplements such as FBS to provide growth factors and thus promote cell survival and proliferation (Prah *et al.*, 2019). FBS is also used to induce astrocyte maturation, since cells generated from neonatal tissue are extracted from the brain at a developmental stage when gliogenesis is incomplete (Lange *et al.*, 2012). Additionally, astrocytes *in vivo* are not exposed to serum and therefore it is not a physiologically relevant addition to cell culture media.

Since FBS is unclassified, with lots of batch variability (Van Der Valk *et al.*, 2004), supplementation of cell culture media with FBS is known to introduce variables into research protocols which result in phenotypic differences for cell cultures (Even, Sandusky and Barnard, 2006; van der Valk *et al.*, 2010). In this PhD project I have used a maximum of two different batches of FBS

serum; the data in this chapter represents media supplementation with the same batch, thus differences in individual cell responses will result from natural astrocyte heterogeneity rather than subtle changes in the FBS composition. It is imperative to derive a culture media formulation that can be standardised between laboratories for future studies with astrocytes extracted and cultured in different brain regions in order to increase data reproducibility.

It is possible to culture primary astrocytes with serum free media: astrocytes develop gene expression profiles which closely resemble *in vivo* astrocytes, and more so than astrocytes cultured with media containing FBS (Foo *et al.*, 2011). A study by Prah *et al.,* (2019) used a combination of serum free astrocyte base medium supplemented with fibroblast growth factor 2 (FGF2) and epidermal growth factor 2 (EGF2) to successfully culture primary neonatal cerebellar cortex astrocytes which developed higher process bearing morphology than astrocytes cultured in DMEM with 10% FBS.

A strategic approach to developing a defined and reproducible cell culture media for primary astrocytes is needed: culture medium influences gene expression profile, culture purity and homeostatic mechanisms and cellular responses (Codeluppi *et al.*, 2011). Using defined media specific to the astrocyte cell type increases the expression levels of astrocyte specific proteins in rat spinal cord astrocytes when compared with medium supplemented with three different types of sera (Codeluppi *et al.*, 2011). In conclusion, since it is accepted that astroglial conditioned medium influences the development and maturation of astrocytes (Bramanti *et al.*, 2007), as well as culture purity (Codeluppi *et al.*, 2011), it will be important to refine media compositions which enable primary astrocytes to develop a similar phenotype to *in vivo* cells in the future.

4.4.2.2.3 Media Composition and Astrocyte-Neuron Co-Culture

Investigations into the effects of media compositions, which support neuron growth and survival, on astrocytes were prompted by the goal to co-culture both cell types in compartmentalized microfluidic devices. These data show that neuronal medium and neurobasal supplemented with glutamax significantly impact astrocyte morphology (Figures 5 - 8), function (Figures 10

& 11) and survival (Figure 9). This means that choosing to culture astrocytes with neuronal media, for the promotion of axon growth in microfluidics devices, will affect astrocyte phenotype, which will in turn affect neuronal function.

Astrocytes exposed to neuronal medium developed stellate morphologies (Figures 5 & 6) which is typical of reactive cells, indicating that cells are in a stressed state. NM media treatment for primary astrocytes resulted in significantly decreased percentages of cells responding to ATP (Figure 10), thus there may be resultant changes to astrocyte receptor expression and subsequently their capacity to modulate neurons. Thus, data interpretation of results from co-culture experimentation using compartmentalised microfluidics devices may falsely represent the influence of quiescent astrocytes on axon growth depending on the culture media used.

In summary, co-culturing the two cell types, without careful consideration of the media composition, will generate data that ultimately reflects the influence of cell culture media rather than cell-cell interactions. For successful co-culture in the future, physiologically relevant media compositions reflecting the microenvironment of both cell types will be crucial for translatable findings.

4.4.3 Conclusion

It is well known that astrocytes are highly responsive to their microenvironment and these results show that the composition of cell culture media had significant effects on primary astrocyte morphology and function *in vitro*. Specifically, neuronal medium resulted in a significant increase in the percentage of stellate astrocytes in culture from 7 DIV until the end of the time course in comparison to the other media treatments analysed (astrocyte medium and neurobasal supplemented with glutamax). Primary astrocytes cultured with neuronal medium also had significantly reduced percentages of cells responding to ATP. These findings highlight potential difficulties for the co-culture of astrocytes and neurons in compartmentalised microfluidics devices. Serum addition to DMEM for primary astrocytes had no effect on the percentage of astrocytes responding to ATP which suggests that cells can

develop physiological function with this minimal medium. Furthermore, these results support the notion that astrocytes are sensitive to culture conditions and confirm that careful selection of cell culture media *in vitro* is crucial to reproduce conditions similar to those *in vivo*.

Chapter 5. 3D Matrices for Astrocyte Cell Culture

5.1 Introduction

5.1.1 3D Culture for Primary Astrocytes

Astrocytes are a heterogeneous population of glial cells known to embody a range of morphologies depending on their location within the brain and their function. Assessments of astrocyte physiology have traditionally characterised morphology and function in 2D formats, such as on coated coverslips in tissue culture plates. However, 2D cell culture models are limited in their ability to recapitulate the *in vivo* brain microenvironment. Culturing astrocytes in 2D results in decreased morphological complexity compared to that frequently observed with astrocytes *in vivo* (Pekny and Pekna, 2019). *In vitro* formats also induce the formation of astrocyte monolayers which lead to an artificial astrocyte reactivity (East *et al.*, 2010). Since 3D cell culture models represent a more physiologically meaningful model, providing an environment in which cell-cell and cell-matrix interactions can be studied, this study has investigated astrocyte morphology in three different cell matrices.

The brain ECM is unique in its composition and composed largely of hyaluronic acid (HA), proteoglycans, laminins and tenascins (Krishnaswamy *et al.*, 2019). The brain microenvironment is critical to function, influencing neuronal development and synaptic signalling, as well as disease progression in neurodegeneration and trauma (Krishnaswamy *et al.*, 2019). Developing *in vitro* models which can replicate the molecular complexity of the microenvironment astrocytes are exposed to, coupled with the 3D factor, will benefit the understanding of physiological astrocyte phenotype.

Primary cell culture practices *in vitro* vary substantially between research groups, where for the same cell type different 2D surface coatings are used. Coupled with this, it is known that cell culture geometry affects the behaviours of most cell types (Smithmyer, Cassel and Kloxin, 2019). One study with

human fetal derived astrocytes showed that there was a significant impact of surface coating on cell morphology: uncoated glass, fibronectin, collagen I, collagen IV and matrigel were used for comparisons (Levy *et al.*, 2014). Matrigel is a soluble basement membrane preparation which can be used for coating and seeding cells on top of, or can be used to encapsulate cells. This research revealed that matrigel surface coating had the most significant influence on cell morphology (Levy *et al.*, 2014). Such techniques, where hydrogels can be used to coat 2D surfaces are regarded as 2.5D culture which facilitates greater cell spreading and migration, as well as more polarisation (Smithmyer, Cassel and Kloxin, 2019). Using biomimetic hydrogels formed by photo polymerisation and seeding cells at their interface, showed that cell morphology was similar with 2D and 2.5D techniques, but still significantly different from 3D techniques (Smithmyer, Cassel and Kloxin, 2019). Taken together this suggests that 3D cell culture involving the encapsulation of cell types may be integral to *in vitro* astroglial research in the future.

There are a number of options for culturing astrocytes in 3D, including hydrogels and physiologically inert scaffolds. Engineered scaffolds can be used to maintain astrocytes in a non-reactive state, such as Alvetex® (Ugbode, Hirst and Rattray, 2016). Natural or synthetically made hydrogels are networks of polymers or proteins which provide a 3D culture system. Hydrogels are porous and thus allow the entry of most proteins and nutrients, and the diffusion of metabolites and waste products out (Ahmed, 2015). Natural polymers capable of forming hydrogels include agarose, collagen, hyaluronan and alginate. Many synthetic hydrogels are formed from acrylamide-based polymers, such as polyethylene (glycol) and diacrylate (PEGDA).

To investigate primary cortical astrocyte morphology *in vitro*, three 3D matrices for cell culture were selected: Alvetex ®, Matrigel ® and Hyaluronic Acid (HA). Hydrogel composition for the 3D culture of astrocytes was hypothesised to significantly influence astrocyte phenotype. Hyaluronic acid was selected since it contains an important component of the brain ECM, and

matrigel was tested since it is a popular hydrogel for 3D cell culture. This study additionally investigated cell culture with alvetex which provides a 3D scaffold for cell attachment (Figure 1).

5.1.1.1 Alvetex

Alvetex®, a 3D polystyrene porous scaffold (Figure 1), enables the 3D culture of dissociated mammalian cells which develop *in vivo* morphology, behaviour and responsiveness. Each disc of alvetex is 200 microns in diameter with pore sizes of 36-40 microns. As such, no cell is more than 100 microns from the nutrient source allowing easy exchange of nutrients, gases and waste products via passive diffusion across short distances. Cells are also freely able to interact with neighbouring cells in 3D.

Primary murine postnatal (P4) cortical astrocytes grown on the 3D polystyrene scaffold have been show to develop a mature morphology and a protoplasmic phenotype (Ugbode, Hirst and Rattray, 2016). Therefore, in this study I seeded the alvetex scaffold with primary rat neonatal (P2) cortical astrocytes to identify features of astrocyte morphology when cell are cultured in 3D *in vitro* environments.

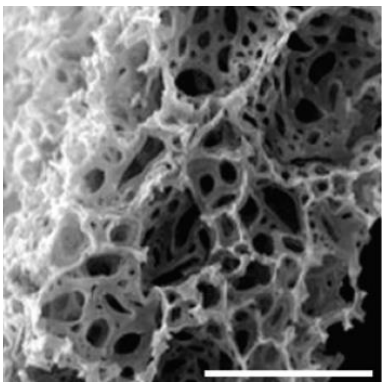


Figure 1. Scanning electron micrograph of Alvetex® scaffold in transverse section. Scale bar = 100 µm. Image taken from Reprocell.com.

5.1.1.2 Matrigel

Matrigel® is a gelatinous protein mix, rich in extracellular matrix (ECM) proteins, derived from the Engelbreth-Holm-Swarm (EHS) Mouse Sarcoma. The major components of matrigel include: laminin (60%), collagen IV (30%),

and heparin sulphate proteoglycans and entactin (8%). The remaining 2% of the gel is made up of growth factors such as: transforming growth factor β (TGF-β), epidermal growth factor (EGF), insulin-like growth factor (IGF), fibroblast growth factor (FGF) and other naturally occurring growth factors. The preparation of matrigel results in batch variation which alters the properties of the gel (Hughes, Postovit and Lajoie, 2010). To address this, as far as possible, this study has used the same batch of matrigel (Lot Number 7317015, Product 354230, Corning Life Sciences, Buckinghamshire, UK).

Matrigel is known for its capacity to support the growth of neural cell types, including neurons (LaPlaca *et al.*, 2010), and composite gel formulations with matrigel have supported the development of quiescent human astrocytes (Placone *et al.*, 2015). This study has investigated whether primary astrocytes cultured in this growth factor rich hydrogel develop *in vivo* morphology.

5.1.1.3 Hyaluronic Acid

Hyaluronic acid (HA) is a naturally occurring component of the brain ECM and can be used as a 3D matrix for cell culture via the formation of a hydrogel. Hyaluronic acid from Hystem® kits is made by a proprietary bacterial-fermentation process using bacillus subtilis, or Novozymes (GS311, Esi-Bio, California, US).

HA formation requires crosslinking which occurs when Extralink®-Lite (polyethylene glycol diacrylate) is added to Glycosil® (thiol-modified hyaluronan). Extralink®-Lite is derived from petroleum and inorganic sources and contains no animal source materials. Hystem Kits (Esi-Bio) result in a viscoelastic matrix of variable rigidity that can support the expansion of cells when they are encapsulated within the matrix. HyStem hydrogels are customizable; ECM proteins can be mixed into the hydrogel and incorporated non-covalently before gelation. HA hydrogels were chosen for primary astrocyte culture since they provide an important component of the *in vivo* microenvironment and can be tailored to mimic the brain region under investigation.

5.1.2 Aims

One key aim of this PhD project was to use 3D culture techniques with primary neonatal (P2) cortical astrocytes to mimic a more physiological extracellular environment. In this chapter three 3D culture materials have been compared: alvetex, matrigel and hyaluronic acid. The viability and morphology of astrocytes within these different environments was assessed. The addition of forskolin (a compound that activates adenylyl cyclase and increases cAMP concentration) and how it influenced morphology in the 3D matrices was also investigated, to determine whether the induction of cell stellation in 3D environments differs from 2D environments.

5.2 Methods

5.2.1 2D Culture Methods

Primary neonatal (P2) cortical astrocytes were seeded onto PLL-coated glass-bottomed 24-well plates to investigate cell morphology when cultured on flat surfaces. Astrocytes were detached from flasks after 14 DIV using trypsin-EDTA to generate a cell suspension. Plates were coated with 0.1 mg/ml PLL for 45 minutes prior to cell seeding. Astrocytes were seeded at low density (1.25×10^4 cells per ml) and plates were kept in a 37°C and 5% CO_2 incubator for a minimum of 2 DIV before experimental use. See Section 2.2.2, page 34.

5.2.2 3D Culture Methods

5.2.2.1 Alvetex

Engineered scaffolds and hydrogels were used as 3D cell culture matrices to investigate the influence of astrocyte microenvironment on phenotype. Alvetex® scaffold 24-well plates (AVP006, ReproCELL Europe Ltd, Glasgow, UK) were prepared by fully submerging the alvetex disc in 500 µL of 70% ethanol to render the scaffold hydrophilic. Alvetex discs were subsequently washed three times with 500 µL of sterile water before incubating with 400 µL of 1.5 µg/ml PLL for 24 hours to help cells adhere to the scaffold. Next alvetex discs were washed with 500 µL of PBS and incubated with 500 µL of astrocyte medium (see section 2.2.2.2) for 2 hours at 37ºC and 5% CO_2 before seeding cells. Alvetex discs were seeded with 2.5×10^4 cells per ml and incubated at 37°C and 5% CO_2 for five days before cells were fixed using 400 µL of 4% paraformaldehyde (PFA).

5.2.2.2 Matrigel

Matrigel® Basement Membrane Matrix Growth Factor Reduced (354230, Lot Number 7317015, Corning Life Sciences, Buckinghamshire, UK) was kept on ice at all times and all culture ware and media were pre-cooled before they came into contact with the gel. Matrigel was thawed by submerging the vial in ice in a 4°C fridge overnight. Once thawed, the vial was swirled to ensure that material was evenly dispersed and aliquoted into appropriate 145 µL aliquots

(volume necessary for 1x 3mg/ml gel) using a pre-cooled pipette, to prevent multiple freeze-thaw cycles with the gel.

Matrigel was mixed with cells and astrocyte medium to ensure homogeneity, and placed in an incubator at 37°C and 5% CO_2 for 30 minutes. Different batches of matrigel were supplied at differing concentrations, but usually had a concentration of approximately 8 mg/ml which was diluted using astrocyte medium for experimental preparations. For 3 mg/ml final concentration, 142.5 µL of matrigel and 237.5 µL of combined cell suspension and astrocyte medium were mixed together. Once gels were set, 400 µL of culture medium was added to the top of the gel to maintain viable cells. After a minimum of 2 DIV gels with encapsulated astrocytes were used for experimental procedures; gels were kept in a 37ºC and 5% CO_2 incubator until use.

5.2.2.3 Hyaluronic Acid

The preparation of Hyaluronic Acid from Hystem® Kits (GS311, Esi-Bio, California, US) required preparation of the individual components before mixing. Glycosil® (Esi-Bio - GS311) was mixed with de-gassed (DG) water (Esi-Bio - GS311) and placed horizontally on a rocker for 30 minutes to allow the lyophilized solid to dissolve. DG water was added to Extralink-lite® (Esi-Bio – GS311) and inverted several times to dissolve. See appendix for manufacturer's instructions (page 232).

To form the hydrogel, Glycosil was combined with Extralink-lite at a ratio of 4:1. As cells were to be encapsulated in the gel, they were added to the mixture of Glycosil and Extralink-lite and the solution was allowed to react for 10 minutes before mixing again by pipette to ensure even distribution of cells. Mixing Glycosil and Extralink-lite in the 4:1 ratio generates a 10 mg/ml concentration hyaluronic acid hydrogel. To form 5 mg/ml hydrogels, 38 µL of Extralink-lite was added to 152 µL Glycosil and 190 µL total of cell suspension and astrocyte medium. Gelation can occur within 30 minutes at room temperature, since the hydrogel forms via cross-linking between Glycosil and Extralink-lite, but 24-well plates with formed gels were placed in a 37ºC and 5% CO_2 incubator for 30 minutes to protect cell viability.

Once gels had formed after 30 minutes via the cross-linking of components, 400 µl of astrocyte culture medium was added to the top of the gel. Astrocytes encapsulated in HA gels were incubated at 37°C and 5% CO_2 for a minimum of 2 DIV before experimental use.

5.2.3 Viability Assessment

Primary astrocytes were loaded with 1 µM calcein AM for 30 minutes, which was added directly to the culture medium, at 37°C and 5% CO_2. Culture medium containing calcein AM was removed and replaced with an imaging buffer (see section 2.3.1 for buffer composition) after which preparations were imaged for the assessment of cell survival at different concentrations of hydrogels.

Images were manually blinded to the gel concentration by other researchers in the laboratory. Cell counts were carried out according to the following criteria: alive astrocytes were recognised by a multitude of fusiform, polygonal, and star-shaped morphologies, whereas dead cells exhibited circular morphologies. Percentages of alive cells were calculated and guided final working concentrations for hydrogels.

5.2.4 Induction of Stellation

Astrocytes were induced to become stellate via treatment with 10 µM forskolin (FSK) for three hours. To remove forskolin, cells were washed with either astrocyte medium or imaging buffer (see section 2.3.1 for buffer composition). Forskolin is an adenylyl cyclase activator which causes astrocytes to develop a stellate morphology.

5.2.5 Morphological Assessment

Calcein AM is a fluorescent dye used for short-term loading of the cell cytoplasm. Astrocytes were incubated with 1µM calcein AM (with final concentration 0.2% pluronic and 1% DMSO vehicle) for 30 minutes at 37°C and 5% CO_2. Calcein AM was removed and cells were sustained in an imaging solution (see section 2.3.1 for buffer composition) for live cell

imaging. For immunofluorescence labelling, cells were fixed with 4% PFA and treated according to the standard protocol for astrocytes (see section 2.3.2).

5.2.5.1 Confocal Imaging for 2D Cultured Cells

To assess astrocyte morphology in detail, a protocol with an inverted confocal fluorescence microscope (Zeiss 710) was optimised to investigate cells seeded onto 0.1 mg/ml PLL-coated glass-bottomed 24-well plates (see section 2.3.3.1.1). Different objectives were tested to match the sample and objective refractive indexes as much as possible to prevent spherical aberration: the 40x water objective with a 1.2 numerical aperture (NA) provided an optimum refractive index match between samples and the objective. A z-stack interval of 0.476 µm was used and the 488 nm laser (2%) was used to visualise calcein-loaded astrocytes.

5.2.5.2 Confocal Imaging for 3D Cultured Cells

Two protocols were optimised with the Zeiss 710 to image astrocytes in the alvetex scaffold, or matrigel and hyaluronic acid hydrogels (see section 2.3.3.1.2 and section 2.3.3.1.3). The apochromat 10x water objective with a numerical aperture of 0.45 was used to match the refractive index of alvetex discs immersed in PBS. A z-stack interval of 6.98 µm was selected and the 405 and 488 nm lasers were used to visualise DAPI and GFAP labelling respectively (2 & 10% intensity).

The 10x water objective was also used for imaging hydrogels - the refractive index of the objective closely matched that of matrigel. A z-stack interval of 1.6 µm was used, and again the 488 nm laser (2%) was used to detect calcein-loaded astrocytes. The imaging protocol was optimized for the detection of cell processes: cell bodies were saturated in comparison to processes in order to visualize the entirety of a cell's morphology.

5.2.5.3 Post Imaging Processing

To discover the extent of spherical aberration in all culture formats imaged on the confocal, fluorescent 4 micron beads (T7283 (lot number 766546), Invitrogen) were mixed with the cell suspension and seeded into the relevant

culture format. Beads were added at a 1:1000 dilution for 2D formats and a 1:100 dilution in 3D formats.

In order to establish an applied z scale, beads cultured in 2D formats or 3D hydrogels were only selected for analysis when the whole bead was captured in the z-stack. Beads were cropped, saved as a new image for analysis and the bead lengths in X, Y and Z were manually measured in Zen software. The mean length of the beads in Z was divided by the actual length of the bead in Z to derive a stretching factor. The original z-scale was then divided by this stretching factor to derive a new z-scale which was applied and saved as a new image. Bead lengths in X, Y and Z were measured again and values in the Z dimension gave a value close to 4 microns (Table 1) and beads looked spherical (see section 5.3.2.1.1). See appendix for full details, from page 236.

Cell Culture Environment	Length in X (µm)	Length in Y (µm)	Length in Z (µm)
2D	4.45	4.45	4.67
3D Matrigel	4.78	4.86	5.15
3D Hyaluronic Acid	4.64	4.54	4.24

Table 1. Mean bead lengths in X, Y and Z post z-scale alteration for beads cultured in all culture environments (2D, 3D matrigel and 3D HA). Means shown. N = 9 beads analysed for 2D, N = 21 beads analysed for 3D matrigel and N = 17 beads analysed for 3D HA.

5.2.5.4 Morphological Parameters Analysis

To measure astrocyte morphological parameters from 3D reconstructions, including volume, surface area, shape factor and longest axis, Volocity software was used. Analysis was conducted on images with the relevant applied z-scale as calculated following 4 micron bead analysis.

Box ROI were drawn around single cells of interest and minus 75% thresholding was applied manually. The thresholding value was chosen following a subjective assessment; values were identified which accurately associated all necessary pixels with a cell for the full reconstruction of cell shape in 3D (see section 5.3.2.1.2). The assessment was conducted with

images selected at random for control and forskolin treated cells cultured on 2D plates or within 3D matrigel.

Volocity software describes shape factor as the numerical representation of how similar the 3D shape is to a perfect sphere. The 3D measurement is based on the ratio of the surface area of a sphere (with the same volume as the object) to the surface area of the object (formula shown in Table 2). Shape factor is close to 1 for a perfect sphere and will be closer to zero for irregular shapes.

$$3D\ Shape\ Factor = \frac{\pi^{\frac{1}{3}}(6V_O)^{\frac{2}{3}}}{A_O}$$

Table 2. Formula for the calculation of 3D Shape Factor in Volocity Software.
A = Area and V = Volume.

Additionally, surface area to volume ratios were calculated for all cells cultured in the different matrices by dividing measured surface areas by volumes.

5.2.6 Statistics

To investigate whether there were any significant changes to morphological parameters for astrocytes following forskolin treatment under different 2D and 3D culture conditions, a Kruskal-Wallis One Way ANOVA test with Dunn's correction for multiple comparisons was used (0.05 significance level). Outliers in data sets were determined using Grubb's test (also known as the extreme studentized deviate) and excluded from the analysis appropriately (0.05 significance level). Additionally a Kruskal-Wallis One Way ANOVA test with Dunn's correction for multiple comparisons (0.05 significance level) was used to discover significant differences between calculated surface area to volume ratios for astrocytes cultured in the different *in vitro* formats.

5.3 Results

5.3.1 3D Matrices for Astrocyte Cell Culture

5.3.1.1 Alvetex

Cells were seeded onto Alvetex scaffold 24-well plates to determine neonatal primary rat astrocyte morphology but subsequent image analysis proved challenging. Calcein AM loading is a simple and economic way to assess astrocyte morphology since it accumulates in the cytoplasm of viable cells after de-esterification, giving a fluorescence signal throughout the cytoplasmic contents of the cell. However, calcein AM loading for astrocytes in alvetex was challenging since hydrophobic dyes such as calcein AM bind strongly to the scaffold, and in addition to this, the scaffold auto-fluoresces (Figure 2A).

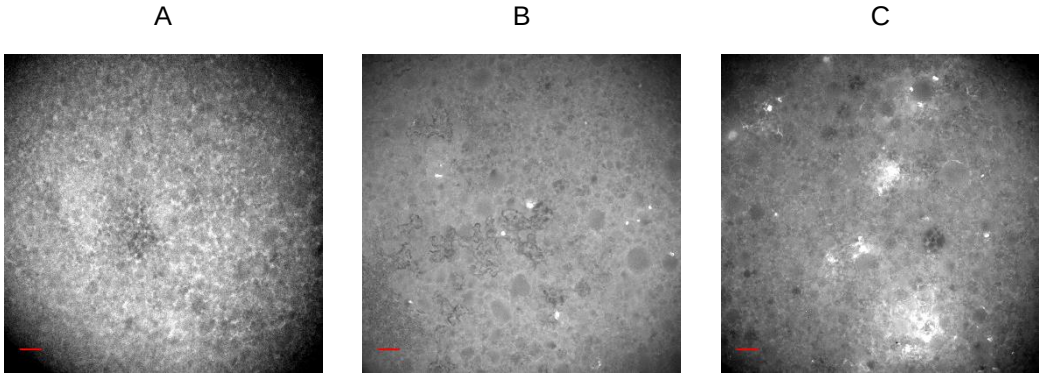


Figure 2. Assessment of cortical astrocyte morphology in the alvetex scaffold. A) Visualisation of the porous scaffold and the auto-fluorescence prior to seeding cells and 1 µM calcein AM loading. B & C) The alvetex scaffold was seeded with cells and treated with 1 µM calcein AM for 30 minutes. Spots of high intensity fluorescence may represent astrocyte cells. B) Cell density = 2.5 x 10^4 cells per ml. C) Cell Density = 1.25 x 10^4 cells per ml. Representative images shown from a minimum of two astrocyte preparations. Scale bars = 100 µm.

With standard protocols it has not been possible to accurately detect individual cells using calcein AM loading in the 3D alvetex scaffold (Figure 2B & C). Although cells could be identified, background fluorescence and scattering was too extensive to reliably assess morphology (Figure 2).

Immunofluorescence techniques allowed the visualisation of astrocytes in the 3D alvetex scaffold (Figure 3). Staining of the scaffold with GFAP primary antibody and DAPI meant that it was difficult to distinguish individual cells from the background fluorescence (Figure 3A & B).

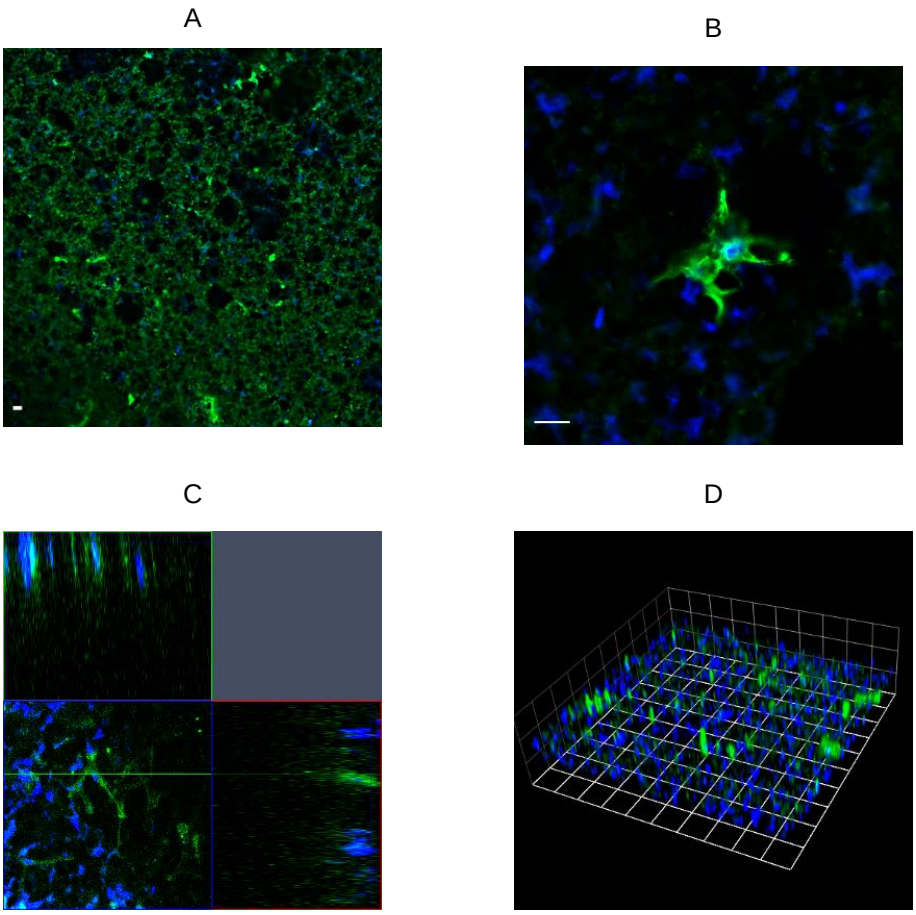


Figure 3. Assessment of cortical astrocyte morphology in the alvetex scaffold following DAPI and GFAP labelling. Astrocytes were seeded into 1.5 µg/ml PLL coated alvetex scaffold at normal cell density (2.5 x 10^4 cells per ml) and cultured with astrocyte medium for 5 DIV before fixing. Cells were labelled with GFAP (green) and DAPI (blue) primary antibodies. A & B) Extended focus view of astrocytes within the scaffold where (A) shows the field of view and (B) shows an individual cell. C) Orthographical projection of GFAP and DAPI labelling intensity and location within the scaffold. D) 3D reconstruction of GFAP and DAPI signals in the scaffold (Z scale = 6.98 µm). Representative images shown from a minimum of three astrocyte preparations. Scale bars = 20 µm in A & B.

Cells did not migrate well from where they had been seeded onto the top of the scaffold and only occupied the top third of the scaffold (Figure 3C).

Confocal imaging resolution was poor for acquired z-stacks due to spherical aberration which meant it was not possible to investigate cell parameters such as volume and surface area as originally intended (Figure 3D).

Despite optimising the cell density seeded into the polystyrene scaffold and trying different confocal configurations, we were unable to improve image resolution beyond that shown in Figure 3. Due to these limitations, experiments with alvetex scaffolds were not continued, as they were not suitable for detailed morphological analysis of whole cell volumes.

5.3.1.2 Matrigel

Matrigel is rich in growth factors and ECM proteins which facilitate the growth of cells either on top of the gel or within the gel. The working concentration of matrigel is application dependent, but the lowest concentration that a gel will form at is 3 mg/ml. Initial experimentation with matrigel thus involved testing cell viability at different concentrations. Matrigel is supplied at 8 mg/ml and so we tried a range of concentrations: 3, 5, 6, 7 and 8 mg/ml. Once gels had been set with cells in and topped up with astrocyte medium, they were left for 2 DIV so that cells could acclimatise to the matrix. Bright field imaging and calcein AM loading were used to identify the influence of the hydrogel on astrocyte health and shape; cells displayed heterogeneous morphologies (Figure 4).

Cells seeded into low concentrations of matrigel (3 or 5 mg/ml) displayed heterogeneous morphology (Figure 4D & E). Gels at higher concentrations (6-8 mg/ml) resulted in lots of debris and rounded cells suggesting that cells in the matrix were not healthy (Figure 4F - H).

Epifluorescent images of astrocytes loaded with 1 µM calcein AM were used to determine the percentage of healthy astrocytes at different concentrations of matrigel. Images were blinded to the gel concentration and a manual cell count was carried out with the following criteria: healthy astrocytes were categorised by a multitude of fusiform, polygonal and star-shaped morphologies, whereas rounded cells were counted as unhealthy cells. At

lower concentrations of matrigel, astrocytes appeared to be healthier which prompted the use of 3mg/ml matrigel in following experimentation (Figure 4I).

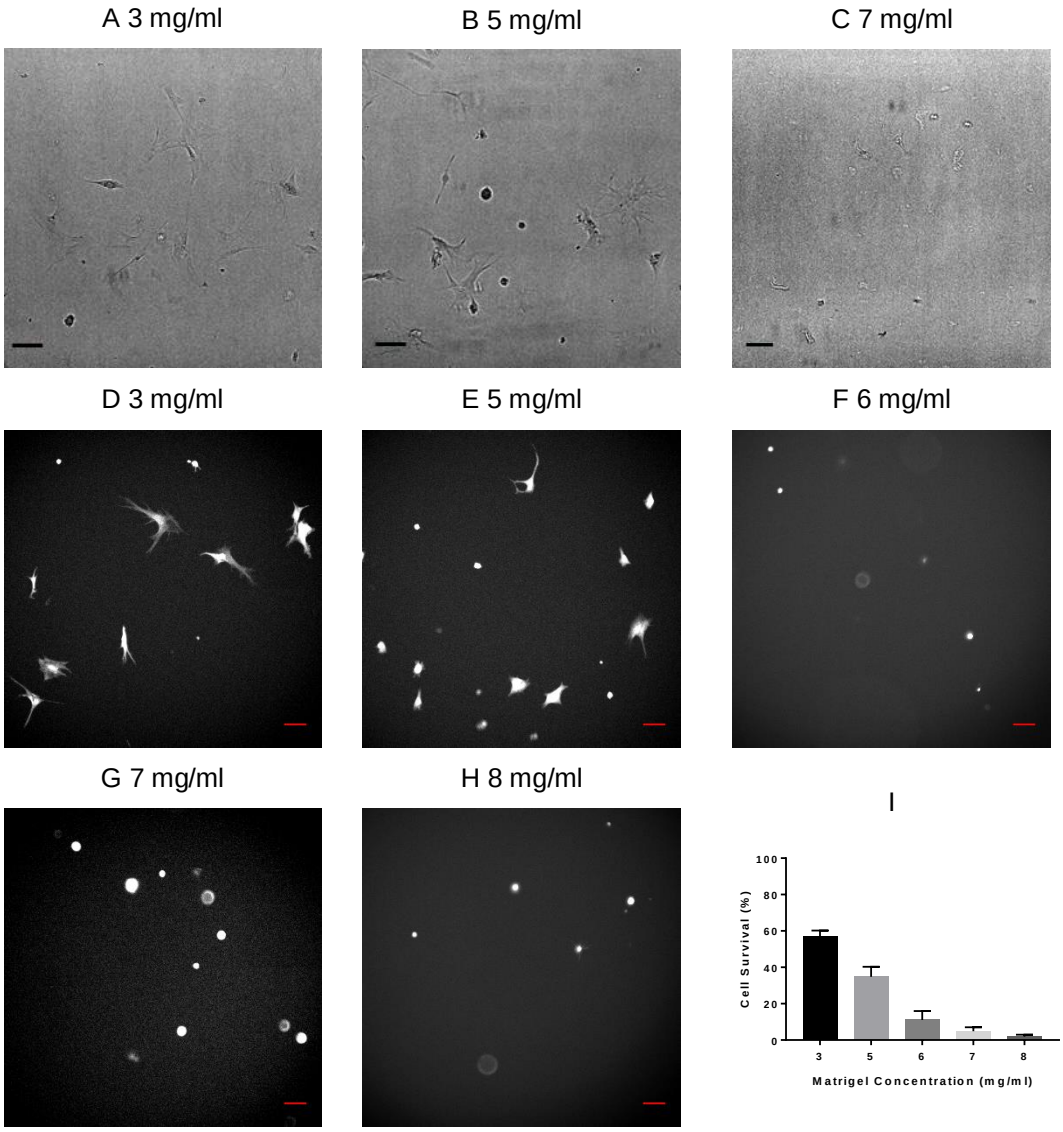


Figure 4. Assessment of cortical astrocyte morphology and viability when cultured in 3-8 mg/ml matrigel. Primary astrocytes were seeded at 1.25 x 10^4 cells per ml into the hydrogel and cultured with astrocyte medium once gels had formed. Cells were visualised using either bright field imaging (A-C) or loaded with 1µM calcein AM in the culture medium for 30 minutes prior to live imaging (D-H) from 2 DIV. The percentage of healthy cortical astrocytes cultured in 3-8 mg/ml matrigel was calculated (I). Mean ± SEM shown. Representative images shown from a minimum of three technical replicates (three hydrogel preparations from one astrocyte preparation). Scale bars = 100 µm.

5.3.1.3 Hyaluronic Acid

Mixing glycosil and extralink for the production of HA gels at the recommended 4:1 ratio gives a final gel concentration of 10 mg/ml (GS311, ESI-BIO). Astrocyte viability, when encapsulated within HA gels, was assessed for a range of concentrations (3, 5, 6 and 7 mg/ml) to determine the best working concentration for optimum cell viability. Cell density was kept consistent with previous matrigel investigations (1.25 x 10^4 cells per ml).

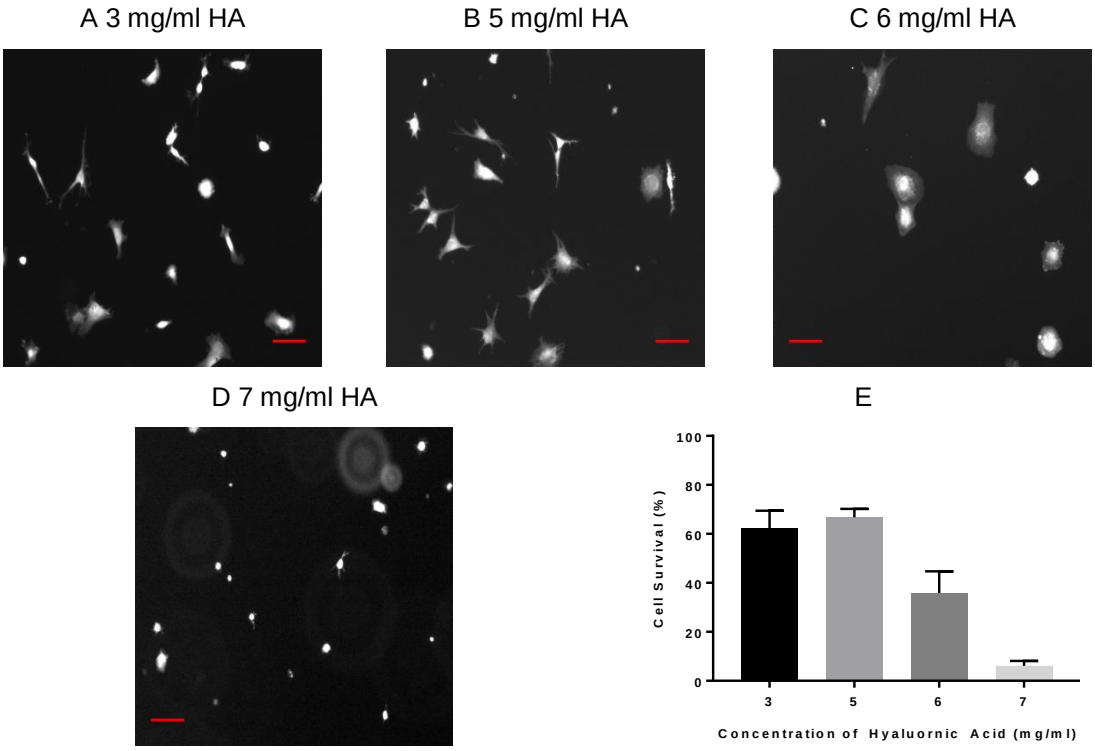


Figure 5. Assessment of cortical astrocyte health and percentage of healthy cortical astrocytes cultured in 3-7 mg/ml hyaluronic acid (HA). Primary astrocytes were seeded into HA gels at 1.25 x10^4 cells per ml and cultured with astrocyte medium once gels had formed. After a minimum of 2 DIV astrocytes were treated with 1 µM calcein AM for 30 minutes prior to the acquisition of images which were used for a healthy or unhealthy cell count. Mean ± SEM shown. Representative images shown from a minimum of three technical replicates (three gel preparations from one astrocyte preparation). In all cases, approximately equal numbers of total cells were analysed for each gel concentration: 358 for 3 mg/ml, 390 for 5 mg/ml, 338 for 6 mg/ml and 295 for 7 mg/ml. Scale bars = 100 µm.

From 3-6 mg/ml HA gel concentration, astrocytes displayed polygonal and multiple process bearing morphologies (Figure 5A - C). In contrast, at 7 mg/ml cells were round with little to no process extension, and there was the presence of debris, implying that cells were not healthy (Figure 5D). Astrocyte

health appeared to decrease at HA gel densities greater than 5 mg/ml (Figure 5E). Therefore, experimental work with HA gels was conducted at 5 mg/ml concentration since gels reliably formed, there were no issues with depolymerisation, and astrocytes had the highest percentage of cell survival (Figure 5E).

5.3.2 Astrocyte Morphology Characterisation in 2D and 3D Cell Culture Environments

Primary neonatal (P2) cortical astrocytes were prepared as stated previously and seeded either onto glass-bottomed 24-well plates in 2D culture methods, or into 3 mg/ml matrigel or 5 mg/ml hyaluronic acid for 3D culture techniques. Cells were loaded with the live cell label calcein AM and imaged after 30 minutes on an inverted epifluorescent confocal (Zeiss 710). 3D reconstructions were generated and analysed using Volocity software which used pixel intensity to measure parameters related to cell morphology including: volume, surface area, shape factor and longest axis. Surface area to volume ratios were calculated to deduce further quantitative differences between cells cultured in different conditions and exposed to pharmalogical agents.

5.3.2.1 Image Processing for Accurate Morphological Measurements

5.3.2.1.1 Z Scale Adjustment

Spherical aberration was observed in 3D reconstructions of images despite matching the refractive indexes of objectives and samples. Samples were seeded with four micron beads to aid post imaging processing for the correction of spherical aberration. Lengths of fluorescent beads were measured in Zen software to calculate a mean stretching factor in Z which was used to deduce an applied Z-scale factor to a new copy of the image. All images of cells cultured in 2D and 3D formats had their Z scale altered following visual validations that this scale resulted in spherical beads (Figure 6). Spherical aberration is an unavoidable limitation of 3D imaging but use of

4 micron fluorescent beads to calculate post imaging processing factors allowed me to be confident that morphological parameters measured by Volocity software are close to the true values.

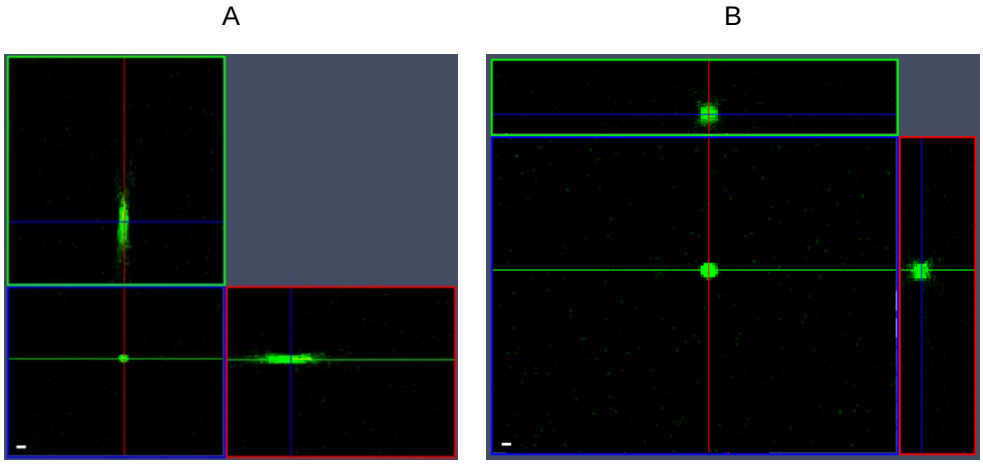


Figure 6. Applied Z-scales resulted in spherical four micron beads. Four micron fluorescent beads were mixed with cells in 3D matrigel for post imaging processing preparations. Beads were mixed with cells at a 1:100 dilution. Preparations were loaded with 1 µM calcein AM for 30 minutes prior to confocal imaging and analysed using Volocity software. A) Orthographical view of a single bead with original Z scale 1.6 µm and spherical aberration. B) Orthographical view of the same single bead with new 0.276 µm Z scale showing a more spherical bead and reduced spherical aberration. Representative image shown from a total of 21 beads analysed. Scale bars = 4 µm.

5.3.2.1.2 Thresholding

Thresholding tests were conducted with both 2D and 3D cultured cells in order to work towards a uniform thresholding value that could be applied to images post imaging processing for the accurate reconstruction of cell shape. Alterations to the threshold percentage measured in volocity had clear influences on the number of pixels that were counted as part of a cell within a box ROI (Figure 7). A threshold value of -75% was selected for volocity analysis since it was the best value for discriminating astrocyte processes from the background (Figure 7D & H). Analysis was conducted on eight quiescent cells and seven reactive cells selected at random from within the 2D data set.

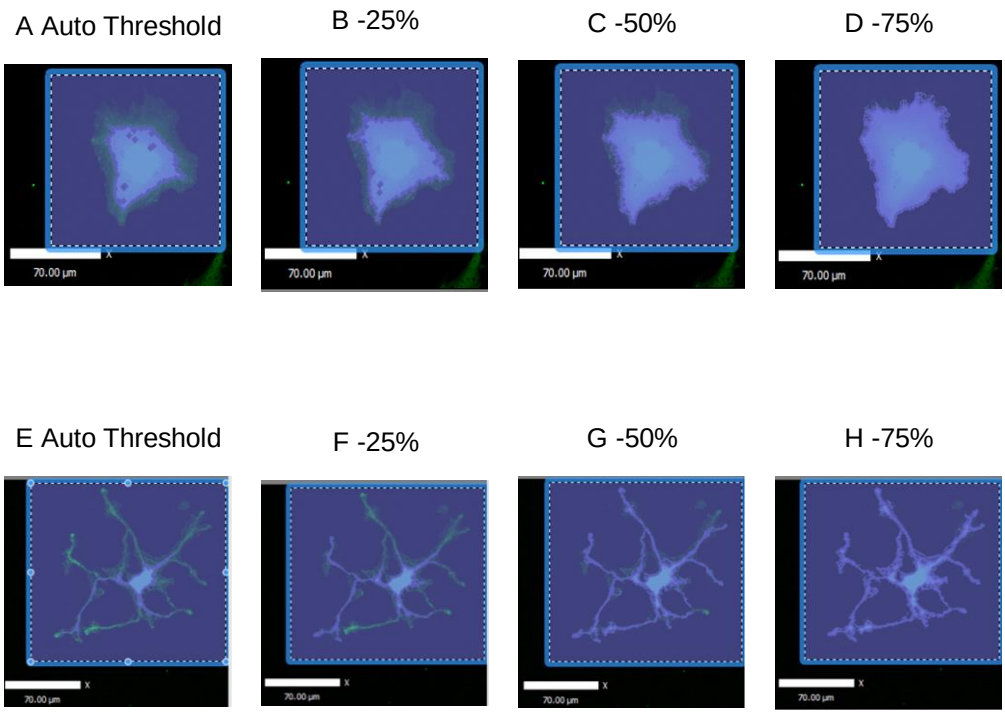


Figure 7. Threshold method selection for cortical astrocytes. Astrocytes were cultured on 0.1 mg/ml PLL coated glass-bottomed 24-well plates and different thresholding selections for a quiescent (A-D) and reactive (E-G) cell are shown. Cells were loaded with 1 µM calcein AM for 30 minutes prior to imaging. Volocity was used for threshold adjustment. Pixels that have been picked up by the software are represented by the blue of the box ROI, whereas those that have been missed appear green due to the calcein AM label. N = 8 for untreated cells, N = 7 for cells treated with forskolin. Scale bars = 70 µM.

5.3.3 Initial Assessment of Astrocyte Morphology in Different 2D and 3D Environments

Primary neonatal (P2) cortical astrocytes exhibited a highly heterogeneous range of morphological parameters when cultured in different 2D and 3D environments (Figure 8). *In vivo* rodent astrocytes have been shown to consist of a soma with up to 10 major branches from which thousands of branchlets emerge and create an overall stellate appearance for cells in contrast to the generally fusiform and polygonal geometries typically expressed by *in vitro* astrocytes (Gottfried *et al.*, 2003; Khakh and Sofroniew, 2015). This study has

confirmed the flat and protoplasmic morphology of 2D *in vitro* astrocytes cultured on coated coverslips in tissue culture plates (Figure 8A & B). Additionally, this study has found *in vitro* astrocytes cultured in 3D hydrogels with numerous primary branches from the cell soma, with secondary branchlets, exhibiting overall stellate appearances, therefore demonstrating characteristic *in vivo* morphological features (Figure 8E, F, J & K).

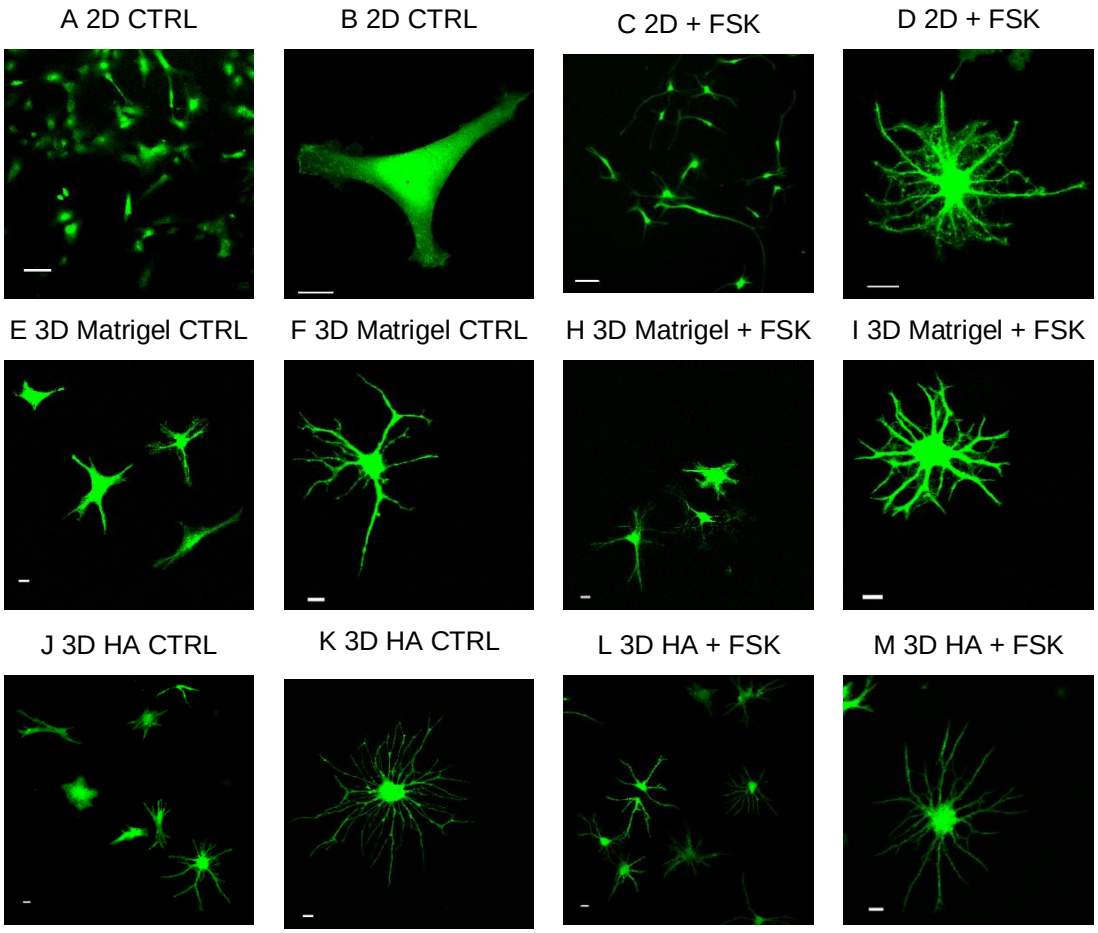


Figure 8. Assessment of control (CTRL) and forskolin (FSK) treated cortical astrocyte morphology in different 2D and 3D environments. Astrocytes were cultured on 2D PLL coated coverslips (A-D), in 3 mg/ml matrigel (E-H) or in 5 mg/ml hyaluronic acid (HA) (I-M) and cultured with astrocyte medium for a minimum of 2 DIV before experimental use. 2D and 3D formats were loaded with 1 µM calcein AM for 30 minutes directly into the culture medium prior to confocal imaging. Cells treated with 10 µM forskolin (+ FSK) for 3 hours prior to 1 µM calcein AM loading to induce stellation and are shown in panels: C, D, G, H, L & M. Representative images are shown for fields of view (A, C, E, H, J & L) and single cells (B, D, F, I, K & M), where N = 135 for 2D CTRL preparations, N = 135 for 2D + FSK preparations, N = 164 for 3D matrigel preparations, N = 141 for 3D matrigel + FSK preparations, N = 269 for 3D HA preparations and N = 208 for 3D HA + FSK preparations. Representative images are shown where from a minimum of three astrocyte preparations. Scale bars = 20 µm (B & D-L) or 100 µm (A & C).

The addition of 10 µM FSK induces dramatic morphological changes to individual astrocytes cultured in 2D formats and they develop stellate morphologies (Figure 8C & D). FSK treatment to astrocytes cultured in 3 mg/ml matrigel or 5 mg/ml hyaluronic acid did not induce any striking morphological changes (Figure 8H, I, L & M).

5.3.3.1 Detailed Morphology of Astrocyte Cells Cultured in 2D

Morphology data was analysed from 135 control and 135 FSK treated cells. All cells were generated from a minimum of three separate astrocyte preparations where the average litter size was between 8-14 pups at P2. Primary astrocytes cultured in 2D were flat and protoplasmic (Figure 8A & B) but developed stellate morphologies when treated with FSK (Figure 8C & D). Astrocytes cultured in 2D were quantitatively assessed for volume, surface area, shape factor and longest axis and treated with FSK to determine if the treatment had a significant effect on cell morphology (Figure 9).

Control and FSK treated astrocytes cultured in 2D showed unimodal peaks and skewed right distributions for cell volume, surface area and longest axis, but the range was greater for FSK treated cells (Figure 9A – D, G & H). Astrocyte shape factor distribution was similar for control and FSK treated cells with unimodal peaks (Figure 9E & F). The small changes to the distribution of morphological parameters for cells subjected to FSK treatment suggested that it was influencing cell morphology, thus statistical analysis was conducted to discover if there were significant changes to cell parameters (see section 5.3.4).

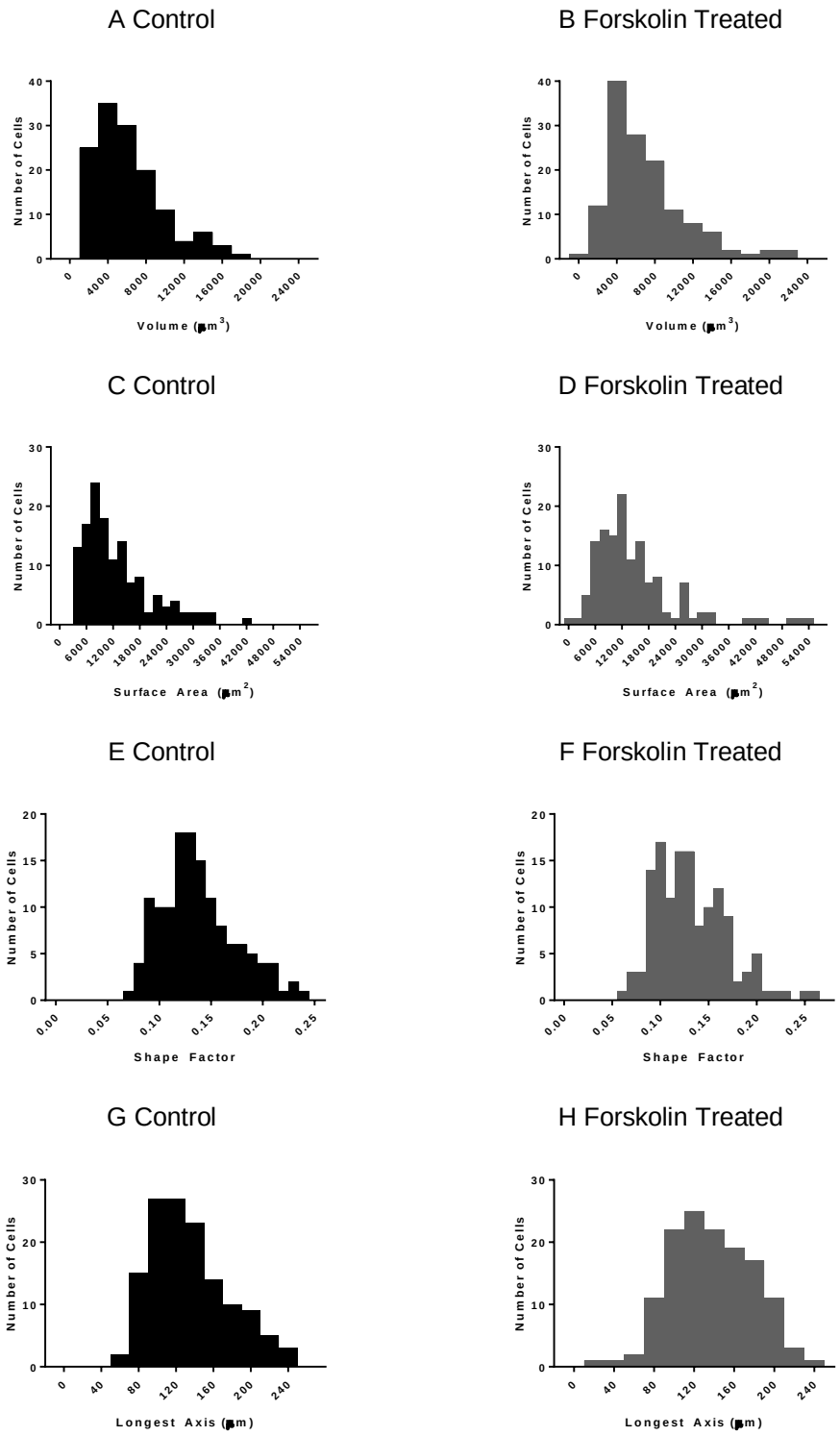


Figure 9. Frequency distribution histograms for control astrocytes (left panels) and forskolin treated astrocytes (right panels) cultured in 2D. Astrocytes were cultured on 0.1 mg/ml PLL coated glass-bottomed 24-well plates with astrocyte medium for 2 DIV. Cells were treated with 10 µM forskolin (+ FSK) for 3 hours to induce stellation. Parameters shown: Volume (μm^3) (A & B), Surface Area (μm^2) (C & D), Shape Factor (E & F) and Longest Axis (µm) (G & H). N = 135 for control cells, N = 135 for forskolin treated cells.

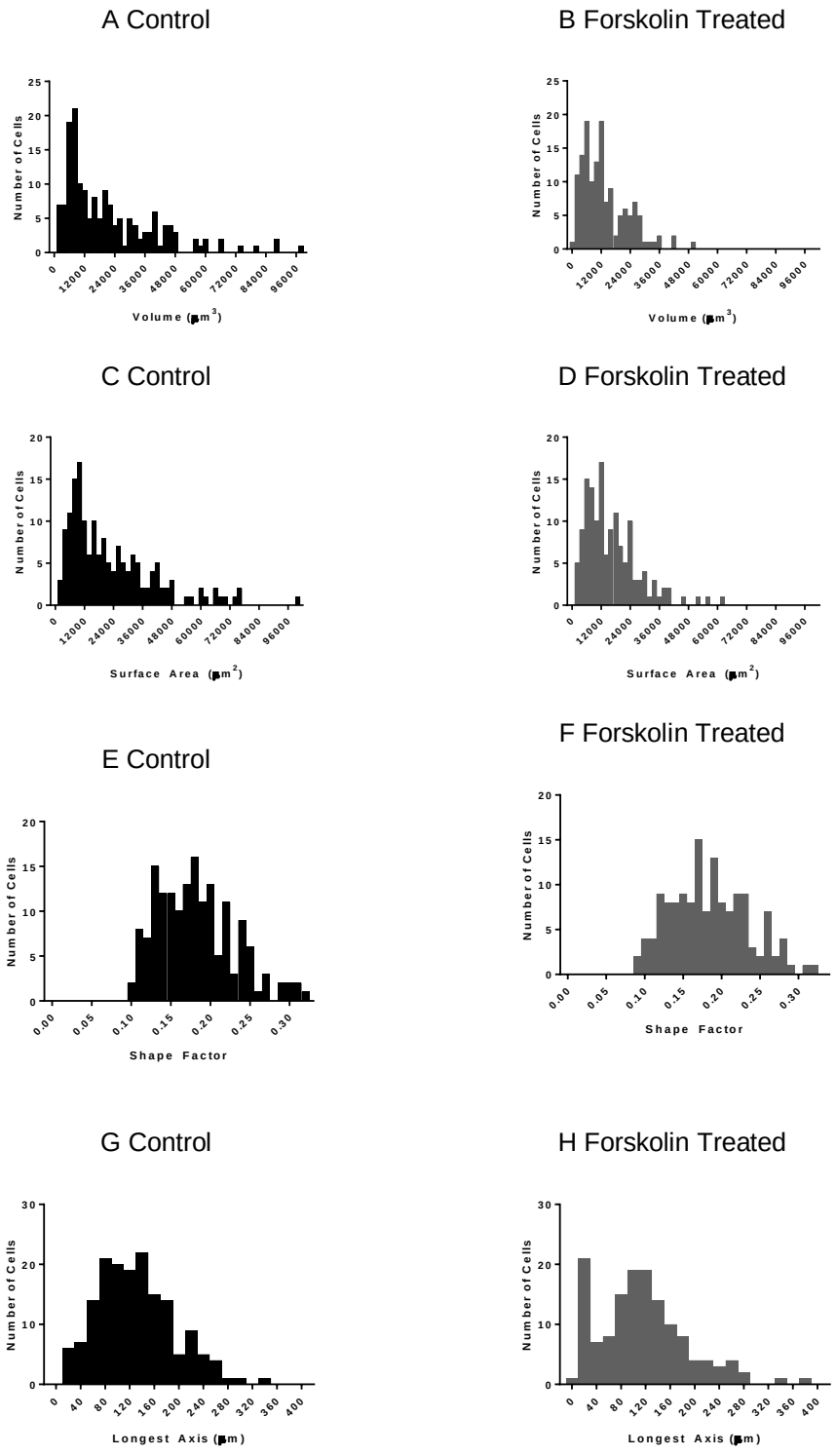


Figure 10. Frequency distribution histograms for control astrocytes (left panels) and forskolin treated astrocytes (right panels) cultured in 3 mg/ml matrigel. Astrocytes were cultured on 0.1 mg/ml PLL coated glass-bottomed 24-well plates with astrocyte medium for 2 DIV. Cells were treated with 10 µM forskolin (+ FSK) for 3 hours to induce stellation. Parameters shown: Volume (µm^3) (A & B), Surface Area (µm^2) (C & D), Shape Factor (E & F) and Longest Axis (µm) (G & H). N = 164 for control cells, N = 141 for forskolin treated cells.

5.3.3.2 Detailed Morphology of Astrocyte Cells Cultured in 3D Matrigel

Data for astrocytes cultured in 3 mg/ml matrigel was analysed from 164 control cells and 141 FSK treated cells. Volume and surface area distributions were unimodal with right skewed distributions, where control cells had a greater range (Figure 10A – D), in direct contrast to the distribution in 2D. Similar to 2D cells, control and FSK treated astrocytes cultured in 3D matrigel had a unimodal distribution for shape factor across a similar range, but the shape factor values were greater for cells in 3D matrigel (Figure 10E & F). Longest axis distribution was unimodal for control cells cultured in matrigel, but bimodal for FSK treated cells with peaks at 20 and 110 µm (Figure 10J & K). To determine if there were significant changes to cell parameters statistical analysis was conducted (see section 5.3.4).

5.3.3.3 Detailed Morphology of Astrocyte Cells Cultured in 3D Hyaluronic Acid

Data for astrocytes cultured in 5 mg/ml HA was analysed from 269 control cells and 208 FSK treated cells. Control and FSK treated cell volume, surface area and longest axis distributions displayed unimodal peaks which were right shifted (Figure 11A – D, G & H). The range of volume and surface area distributions was much greater compared to astrocytes cultured in 2D, but close to cells cultured in 3D matrigel (Figure 11A – D). Both control and FSK treated astrocytes had unimodal distributions for shape factor, but this was greater for FSK treated cells (Figure 11E & F).

In summary, for astrocytes cultured in all three conditions (2D, 3D matrigel and 3D HA), changes to cell measurement parameters following FSK treatment needed to be confirmed statistically by non-parametric tests.

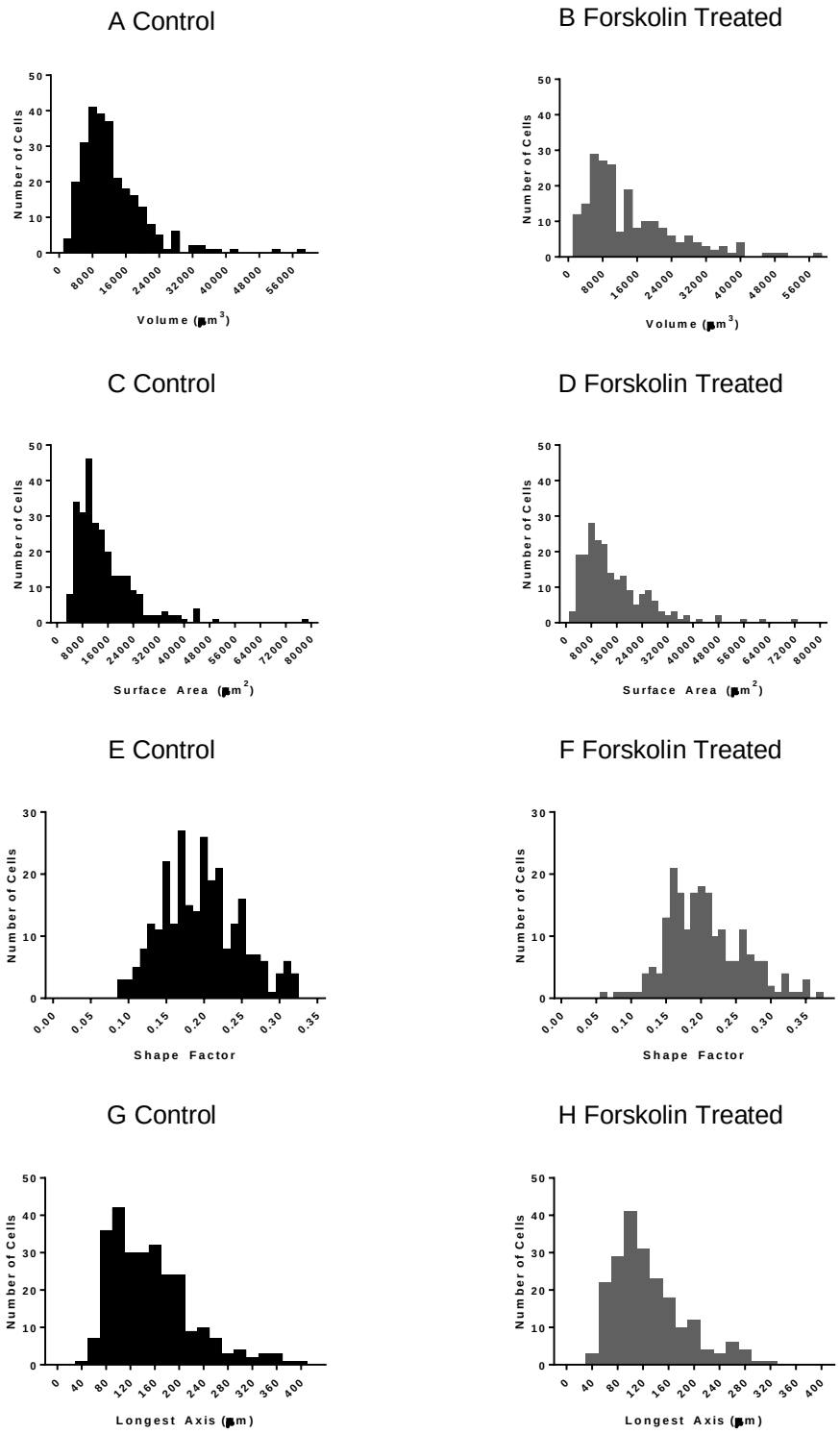


Figure 11. Frequency distribution histograms for control astrocytes (left panels) and forskolin treated astrocytes (right panels) cultured in 5 mg/ml hyaluronic acid (HA). Astrocytes were cultured on 0.1 mg/ml PLL coated glass-bottomed 24-well plates with astrocyte medium for 2 DIV. Cells were treated with 10 µM forskolin (+ FSK) for 3 hours to induce stellation. Parameters shown: Volume (μm^3) (A & B), Surface Area (μm^2) (C & D), Shape Factor (E & F) and Longest Axis (µm) (G & H). N = 269 for control cells, N = 208 for forskolin treated cells.

5.3.4 Statistical Analysis of Astrocyte Morphologies in Different *In Vitro* Environments

5.3.4.1 Cells Cultured in 2D Compared to Cells Cultured in 3D Matrigel

Normality tests (D'Agostino-Pearson) were used to confirm that data were not normally distributed. The only two conditions to pass the D'Agostino-Pearson test were longest axis data for FSK treated cells in 2D and shape factor data for FSK treated cells in 3D matrigel. The non-parametric Kruskal-Wallis ANOVA test with Dunn's correction for multiple comparisons was therefore used to test for differences between parameters of the different data sets (Figures 12-14).

Whilst FSK treatment had no significant effect on volume or surface area measurements for astrocytes cultured in 2D plates, it significantly reduced the mean volume and surface area of astrocytes cultured in matrigel ($p = 0.0075$ and $p = 0.0291$ respectively) (Figure 12A-D). FSK treatment for astrocytes in either 2D or 3D matrigel had no significant effect on shape factor or longest axis (Figure 12E - H).

Both control and FSK treated astrocytes cultured in matrigel had significantly increased mean volumes and shape factors in comparison to astrocytes grown on 2D substrates ($p = <0.0001$) (Figure 12A, B, E & F). Also, control astrocytes in matrigel had significantly increased mean surface areas compared to control and FSK treated astrocytes in 2D ($p = <0.0001$ 2D vs 3D Matrigel and $p = 0.0034$ 2D FSK vs 3D Matrigel) (Figure 12B). FSK treated astrocytes in 3D matrigel had a significantly decreased mean longest axis when compared to cells cultured in 2D ($p = 0.0115$ 2D vs 3D Matrigel + FSK, and $p = 0.0003$ 2D + FSK vs 3D Matrigel + FSK) (Figure 12G).

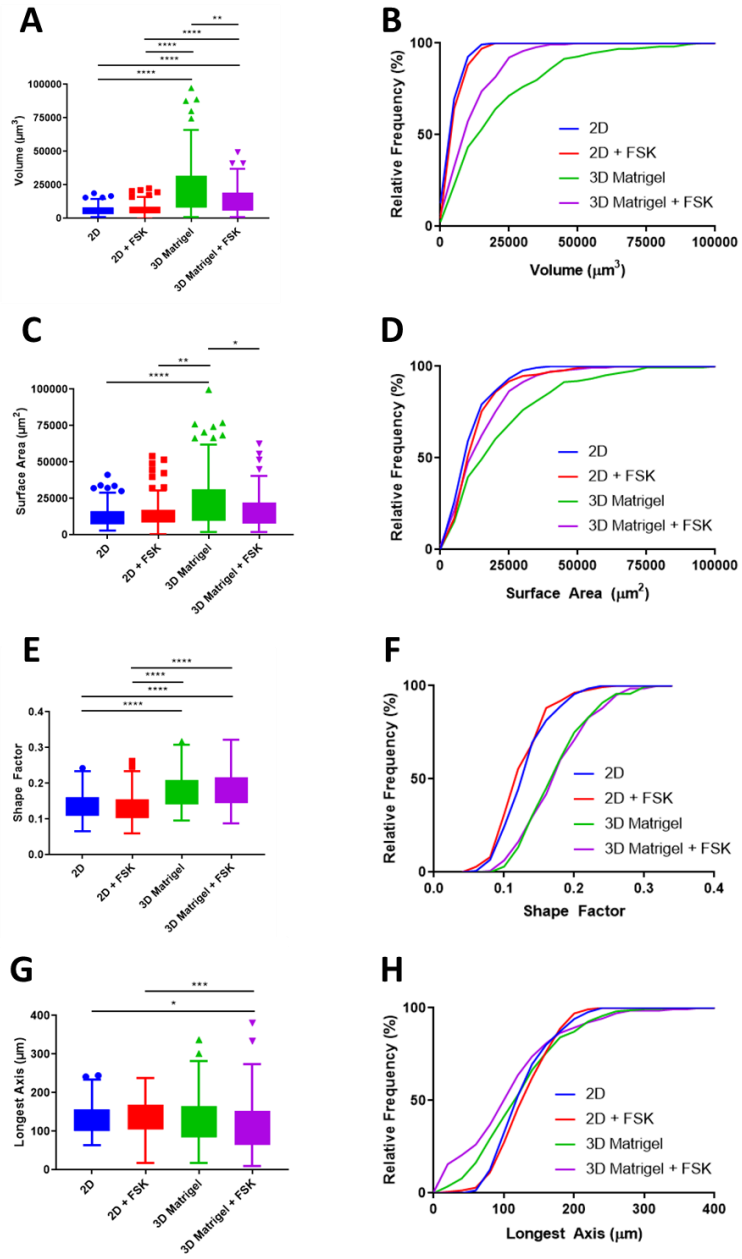


Figure 12. Box and whisker (tukey) plots and cumulative frequency plots for control and forskolin (FSK) treated cortical astrocyte morphological parameter comparisons. Astrocytes were cultured on 0.1 mg/ml PLL coated glass-bottomed 24-well plates (2D or 2D + FSK), or within 3 mg/ml matrigel (3D Matrigel or 3D Matrigel + FSK), with astrocyte medium for 2 DIV. Cells were treated with 10 µM forskolin (+ FSK) for 3 hours to induce stellation. Parameters shown: Volume (µm^3) (A & B), Surface Area (µm^2) (C & D), Shape Factor (E & F) and Longest Axis (µm) (G & H). N = 135 cells for 2D, N = 135 cells for 2D + FSK, N = 164 cells for 3D Matrigel and N = 141 cells for 3D Matrigel + FSK. Kruskal-Wallis ANOVA test with Dunn's correction for multiple comparisons: ns $p > 0.05$, ****$p = <0.0001$.

5.3.4.2 Cells Cultured in 2D Compared to Cells Cultured in 3D Hyaluronic Acid

FSK addition to astrocytes cultured in 5 mg/ml HA resulted in a significant decrease in mean longest axis measurements compared to control cells ($p = <0.0001$), but had no effect on volume, surface area or shape factor measurements (Figure 13). Both control and FSK treated astrocytes cultured in 3D HA had significantly increased mean cell volumes and shape factors compared to cells cultured in 2D ($p = <0.0001$) (Figure 13A, B, E & F). However, there were no significant differences between astrocytes cultured in 2D or 3D HA for surface area or longest axis measurements (Figure 13C, D, G & H).

5.3.4.3 Cells Cultured in 3D Matrigel Compared to Cells Cultured in 3D Hyaluronic Acid

Control astrocytes cultured in matrigel had a significantly increased mean volume and surface area compared to control or FSK treated astrocytes in 3D HA ($p = 0.0020$ 3D Matrigel vs 3D HA + FSK for volume, $p = 0.0001$ 3D Matrigel vs 3D HA for surface area and $p = 0.0002$ 3D Matrigel vs 3D HA + FSK) (Figure 14A – D). In contrast, control astrocytes in matrigel had a significantly decreased shape factor compared to control or FSK treated astrocytes in 3D HA ($p = 0.0113$ 3D Matrigel vs 3D HA and $p = 0.0005$ 3D Matrigel vs 3D HA + FSK) (Figure 14E & F). Also there was a significant mean increase in longest axis measurements for control astrocytes cultured in HA compared to control astrocytes cultured in matrigel ($p = 0.0047$) (Figure 14G & H).

In summary, it is clear that the environment which quiescent astrocytes are exposed to influences cell volume, surface area, shape factor and longest axis. Additionally, FSK treatment can cause significant changes to astrocyte morphology when cells are cultured in 3D matrices.

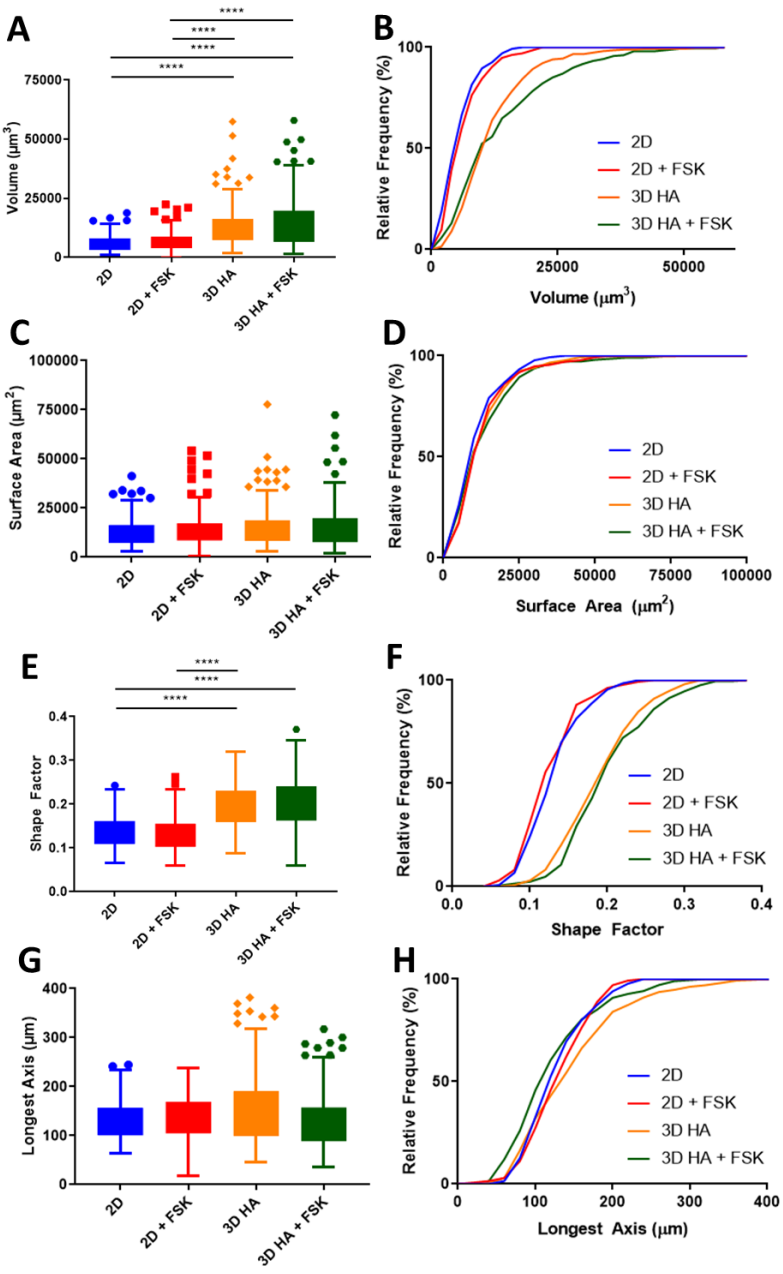


Figure 13. Box and whisker (tukey) plots and cumulative frequency plots for control and forskolin (FSK) treated cortical astrocyte morphological parameter comparisons. Astrocytes were cultured on either 0.1 mg/ml PLL coated glass-bottomed 24-well plates (2D or 2D + FSK), or within 5 mg/ml hyaluronic acid (3D HA or 3D HA +FSK) with astrocyte medium for 2 DIV. Cells were treated with 10 µM forskolin (+ FSK) for 3 hours to induce stellation. Parameters shown: Volume (µm^3) (A & B), Surface Area (µm^2) (C & D), Shape Factor (E & F) and Longest Axis (µm) (G & H). N = 135 cells for 2D, N = 135 cells for 2D + FSK, N = 269 cells for 3D HA and N = 208 cells for 3D HA + FSK. Kruskal-Wallis ANOVA test with Dunn's correction for multiple comparisons: ns $p > 0.05$, ****$p = < 0.0001$.

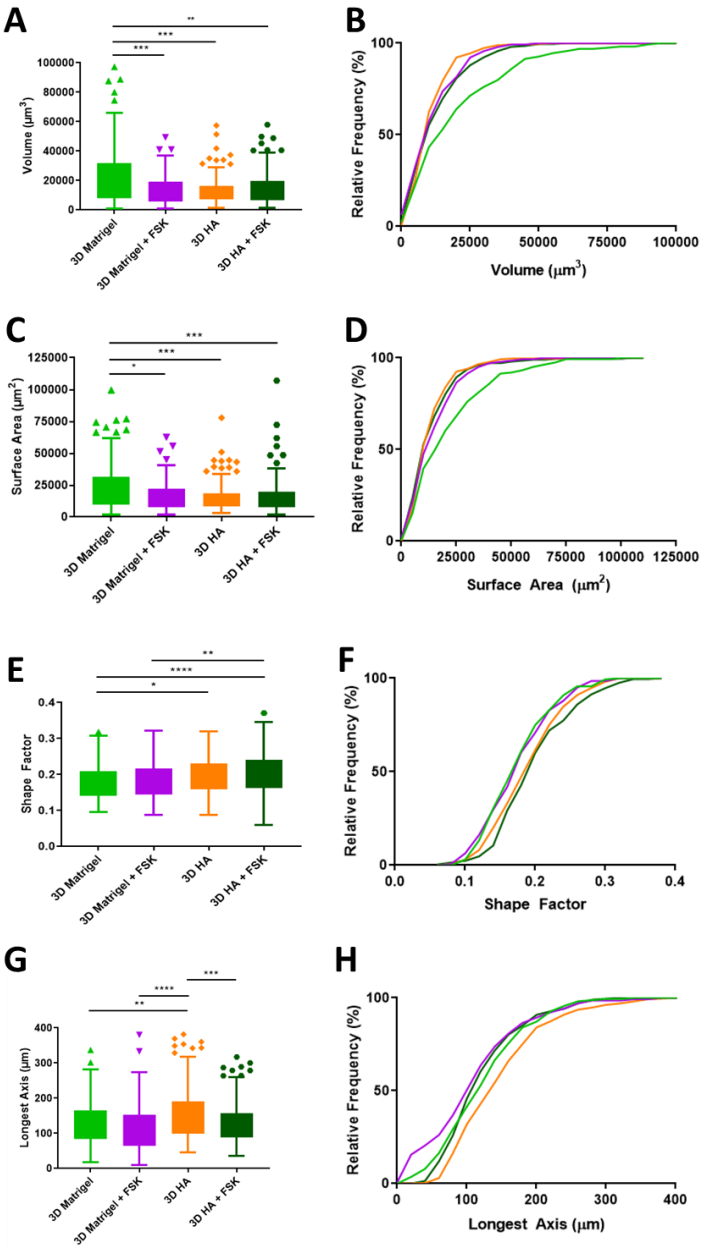


Figure 14. Box and whisker (tukey) plots and cumulative frequency plots for control and forskolin (FSK) treated cortical astrocyte morphological parameter comparisons. Astrocytes were cultured within either 3 mg/ml matrigel (3D Matrigel or 3D Matrigel + FSK) or 5 mg/ml hyaluronic acid (3D HA or 3D HA + FSK) with astrocyte medium for 2 DIV. Cells were treated with 10 µM forskolin (+ FSK) for 3 hours to induce stellation. Parameters shown: Volume (µm^3) (A & B), Surface Area (µm^2) (C & D), Shape Factor (E & F) and Longest Axis (µm) (G & H). N = 164 cells for 3D Matrigel, N = 141 cells for 3D Matrigel + FSK, N = 269 cells for 3D HA and N = 208 cells for 3D HA + FSK. Kruskal-Wallis ANOVA test with Dunn's correction for multiple comparisons: ns $p > 0.05$, ****$p = <0.0001$.

5.3.4.4 Comparing Surface Area to Volume Ratios for all Culture Environments

Surface area to volume ratios were calculated on an individual cell-cell basis, and then a mean was calculated in order to indicate the distribution of this factor across cell datasets.

The surface area to volume ratio for both control and FSK treated astrocytes for all culture environments exhibited unimodal peaks (Figure 15). For astrocytes cultured in matrigel, FSK treated cells had a right shifted peak compared to their control counterparts (Figure 15C & D). The overall distribution for cells cultured in 2D is dramatically right shifted compared to astrocytes cultured in 3D hydrogels (Figure 15) since astrocytes cultured in 2D had greater surface area to volume ratios. To discover if the distributions were significantly different from one another, more non-parametric statistical tests were conducted (only surface area to volume ratio for FSK treated astrocytes cultured in matrigel passed D'Agostino-Pearson normality tests).

5.3.4.5 Statistical Analysis for Surface Area to Volume Ratios for all Culture Environments

The mean surface area to volume ratio was significantly increased for control and FSK treated astrocytes cultured on 2D plates compared to control and FSK treated cells cultured in hydrogels ($p = <0.0001$) (Figure 16).

FSK resulted in a significant increase in the mean surface area to volume ratio for astrocytes cultured in matrigel ($p = 0.0007$), but not cells cultured in 2D or in HA (Figure 16). Additionally, FSK treated astrocytes cultured in matrigel had a significantly greater mean surface area to volume ratio than either control or FSK treated astrocytes in HA ($p = 0.0136$ 3D Matrigel + FSK vs 3D HA and $p = 0.0001$ 3D Matrigel + FSK vs 3D HA + FSK (Figure 16).

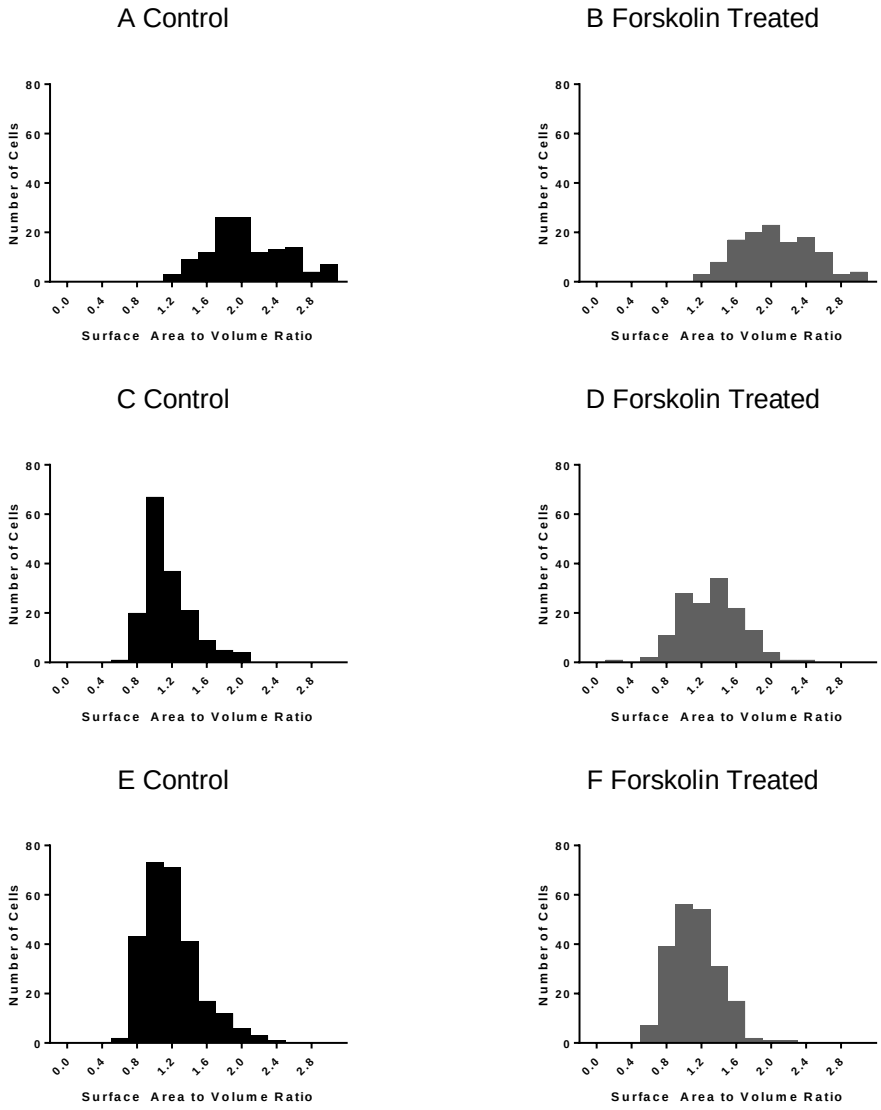


Figure 15. Frequency distribution histograms for the comparison of surface area to volume ratios for cortical astrocytes cultured in 2D and 3D environments. Astrocytes were cultured on 2D plates (A & B), in 3 mg/ml matrigel (C & D) or 5 mg/ml hyaluronic acid (HA) (E & F) with astrocyte medium for 2 DIV. Cells were treated with 10 µM forskolin (+ FSK) for 3 hours to induce stellation. Control astrocytes are shown in left panels and forskolin treated astrocytes are shown in right panels. N = 135 for control cells in 2D, N = 135 for forskolin treated cells in 2D, N = 164 for control cells in 3D matrigel, N = 141 for forskolin treated cells in 3D matrigel, N = 269 for control cells in 3D HA and N = 208 for forskolin treated cells in 3D HA.

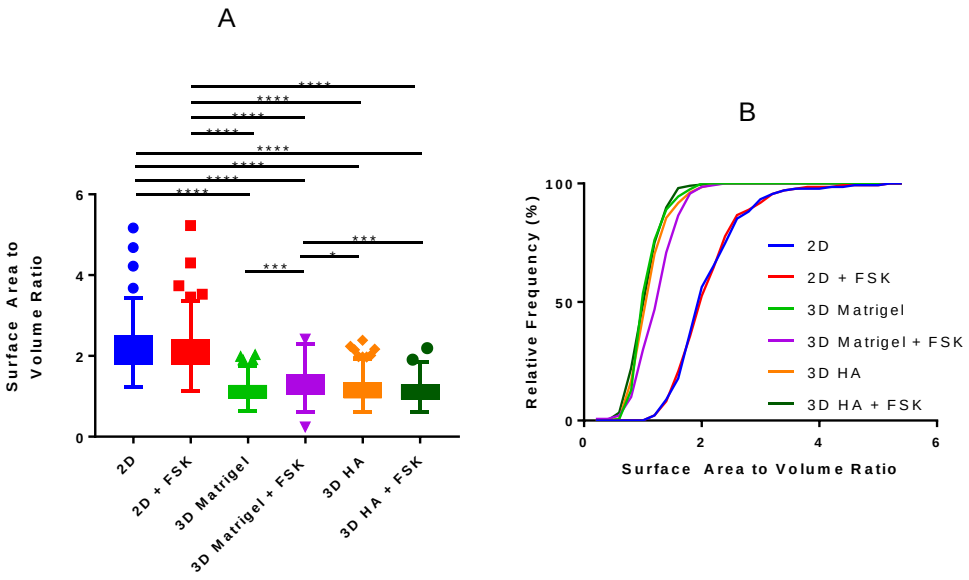


Figure 16. Box and whisker (tukey) plot and cumulative frequency plot for surface area to volume ratios for cortical astrocytes cultured in 2D and 3D environments. Astrocytes were cultured on either 0.1 mg/ml PLL coated glass-bottomed 24-well plates (2D or 2D + FSK), in 3 mg/ml matrigel (3D Matrigel or 3D Matrigel + FSK) or in 5 mg/ml HA (3D HA or 3D HA + FSK). Cells were treated with 10 µM forskolin (+ FSK) for 3 hours to induce stellation. N = 135 for 2D, N = 135 for 2D + FSK, N = 164 for 3D Matrigel, N = 141 for 3D Matrigel + FSK, N = 269 for 3D HA and N = 208 for 3D HA + FSK. Kruskal-Wallis ANOVA test with Dunn's correction for multiple comparisons: ns $p > 0.05$, ****$p = <0.0001$.

5.4 Discussion

Astrocytes are a morphologically and functionally diverse population of cells which exhibit significant phenotypic plasticity *in vivo* and *in vitro* (Khakh and Sofroniew, 2015). *In vitro* study of primary astrocytes commonly involves the culture of cells on flat 2D surfaces, therefore, unsurprisingly, astrocytes do not exhibit the stellate appearance of astrocytes found *in vivo* when cultured *in vitro*. It is well acknowledged that *in vitro* culture techniques are limiting the comprehensive understanding of astrocyte phenotype, physiology and pathology, thus the current hope is that 3D systems can improve the field's understanding of astrocytes and their roles in the central nervous system and inflammation, with the aim to deduce potential strategies to encourage functional regeneration after trauma (Maclean *et al.*, 2016).

Since there is a need to work with astrocytes in more physiologically relevant environments in order to generate meaningful phenotypic data, developing 3D culture techniques to mimic the brain microenvironment will be invaluable for understanding how *in vitro* culture conditions influence astrocyte phenotype. Hydrogels are commonly used as 3D cell culture matrices, and I have compared how matrigel (a protein mix extracted from a mouse sarcoma), and hyaluronic acid (which is naturally abundant in the brain) gels influence the morphological heterogeneity of primary neonatal (P2) cortical astrocytes (Figures 12 - 14). Comparison with classical 2D culture methods shows how substantially the *in vitro* environment affects astrocyte phenotype (Figures 8 & 12 - 14).

Astrocytes cultured in 3D hydrogels extended branches, with numerous branchlets, from a cell soma resembling the process bearing appearance of cells *in vivo* (Figure 8) (Khakh and Sofroniew, 2015). This study has measured astrocyte volume, surface area, shape factor and longest axis using the live cell label calcein AM. Calcein AM is a good marker for highlighting the stellate appearance of astrocytes which are derived from a multitude of cellular processes with varying diameters (Pekny and Pekna, 2019). It was not possible to fix cells in matrigel at the selected working concentration and therefore it has not been possible to label astrocytes with

GFAP. GFAP is a marker of astrocyte morphology and reactivity, but only visualises the astrocyte intermediate filament system representing approximately 15% of the cell's total volume (Bushong *et al.*, 2018), and therefore ultimately can't recapitulate whole cell morphology.

5.4.1 Astrocyte Morphological Assessment

Miller & Rothstein (2016) recently reported that murine astroglia can span across 100 µm or 23,000 μm^3, and other reports have stated the volume of a single astrocyte to be 24,465 μm^3 (Halassa *et al.*, 2007). Astrocytes within the CA1 stratum radiatum of the hippocampus were reported to occupy a volume of 66,000 μm^3, up to 3 times larger compared to other findings, representing the regional variety in astrocyte morphology *in vivo* (Agulhon *et al.*, 2008). In our preparations, control astrocytes in 3 mg/ml matrigel had a mean volume of 22,029 μm^3 which is similar to the aforementioned findings. In contrast to this, control astrocytes in 5 mg/ml HA had a significantly smaller mean volume of 12,685 μm^3.

Control and FSK treated astrocytes cultured in either 3 mg/ml matrigel or 5 mg/ml HA had significantly increased mean cell volumes compared to astrocytes cultured in 2D (Figures 12 & 13, A & B). In addition to this, control astrocytes cultured in matrigel had a significantly increased mean cell volume compared to control astrocytes in 3D HA (Figure 14A & B). Considering that control astrocytes cultured in matrigel developed a mean volume *in vitro* similar to astrocytes *in vivo*, our data suggest that hydrogels allow astrocytes to develop a more physiological phenotype in comparison to traditional 2D cell culture techniques. Specifically, matrigel enables astrocyte growth *in vitro* to a volume similar to cells *in vivo*.

The mean surface area of control astrocytes cultured in matrigel was 23,044 μm^2 which was significantly greater compared to control astrocytes cultured in HA with a value of 14,669 μm^2 (Figure 14B). The mean surface area of control astrocytes in matrigel was also significantly increased compared to control cells cultured on 2D plates which had a mean value of 12,756 μm^2 (Figure 13B). In terms of longest axis, the mean longest axis for control astrocytes

was greater in HA than in matrigel (Figure 14G). One theory to explain the differences in these morphological parameters is that different densities of the hydrogels used for culture will affect their mass and arrangement (Bryant *et al.*, 2004). When the molecular weight of a polymer is increased, so too is the density which influences the viscosity of the material due to increased connections in the matrix (Stansbury, 2013). A higher density of HA compared to matrigel used for 3D culture may have inhibited astrocyte process extension into the surrounding matrix (Puschmann *et al.*, 2013).

Shape factor measurements are difficult to interpret as stand-alone values but aid quantitative comparisons of cells cultured in different 2D and 3D environments. The closer shape factor is to 1, the closer the object is to being a perfect circle when cultured in 3D environments. There were significant increases in shape factor for control and FSK treated astrocytes cultured in 3D hydrogels compared to cells in 2D (Figures 12 & 13, E & F). I suggest that astrocytes cultured in 3D gels are able to develop a more defined and circular soma from which astrocytic processes extend, compared to astrocytes cultured in 2D which are largely flat and protoplasmic (Figure 8).

One could hypothesise that the difference in composition of the hydrogels may be the cause for observed morphological differences between astrocytes cultured in matrigel or HA. Matrigel contains a variety of growth factors that boost cell growth via growth-promoting signals (Kleinman and Martin, 2005), whereas the hyaluronic acid gels only contain a repeating unit of glucoronate and N-acetyl-D-glucosamine (Caliari and Burdick, 2016). Therefore, whilst hyaluronic acid is a robust and easy to use hydrogel for primary cell culture, customizing the gel by adding growth factors and other molecules relevant to the brain microenvironment could generate a realistic *in vitro* cell culture model for astrocyte studies. Whilst matrigel generates astrocytes with volumes which are close to physiological values *in vitro*, the hydrogel is extremely variable and still remains largely unclassified with respect to its matrix composition (Hughes, Postovit and Lajoie, 2010). Additionally, some of matrigel's components, such as laminin and collagen, do not accurately reflect the brain microenvironment.

To progress understanding of the influence of the dimensional culture environment on astrocyte morphology, a more refined approach to the data analysis is required. At large, astrocyte morphology definitions and measurements are not uniform in the field, thus a repeatable and objective method of analysis for cell geometry is needed. I suggest some semi-objective measures such as the number of processes extending from the cell soma, and the number of branching processes with recorded number of branches.

5.4.1.1 Inducing Astrocyte Stellation

One aim of this study was to deduce specific morphological parameter changes to primary neonatal (P2) cortical astrocytes following forskolin treatment because it is known that reactive astrocytes undergo changes to gene expression and subsequently show distinct morphological and functional features (Pekny and Pekna, 2019). The dramatic physical rearrangements that take place during astroglial reactivity require careful quantification to further our understanding of the influence of astrocyte activity on changes in the CNS. In order to do this, this study has analysed changes to cell volume, surface area, shape factor and longest axis following FSK treatment.

FSK treated astrocytes cultured in matrigel had a significant decrease in their mean volumes and surface areas, and FSK treated astrocytes cultured in HA gels had a significant decrease to their mean longest axis (Figures 12A & C, 15G). Considering that the mean volume and surface area for HA cultured cells was not significantly changed following FSK treatment (Figure 14A & C), this suggests that astrocytes in HA retain their overall volume and surface area but there is a rearrangement to the cell architecture where cell domains shrink with FSK treatment. To test this hypothesis further, a form of continuous imaging during FSK treatment would allow the observation of any cytoplasmic rearrangements.

FSK treatment had no significant effect on any of the parameters measured for astrocytes cultured in 2D (Figures 12 & 13). This contrasts reports by Vardjan *et al.,* (2014) that state that 50 µM forskolin treatment caused a significant 65.7% reduction in cell shape factor (calculated in the same way as

this study) after 30 minutes to one hour of treatment. In this study, it has been possible to identify stellate cells in 2D (Figure 8), but this has not been detected using the morphological parameters described here after 3 hours of 10 µM forskolin treatment. This could be in part due to the lower concentration of FSK used in this study. Moreover, this apparent contradiction may result from the observed heterogeneity within a population – unless all of the cells that are treated with FSK develop a stellate morphology, geometric measurements will be confounded by cells which have undergone no changes to their morphology.

Forskolin causes cAMP levels to rise in cells by activating adenylyl cyclase, a mechanism normally evoked in response to injury for the regulation of cytokine and inflammatory factor release (Zhou, Ikegaya and Koyama, 2019). FSK has not been confirmed to result in astrocyte reactivity, therefore we have ultimately measured geometric changes in astrocytes in response to rising cAMP levels, a factor which may account for the lack of influence of FSK on 2D astrocyte morphologies. However, forskolin significantly increased mean astrocyte volume and surface area in 3 mg/ml matrigel, and mean longest axis measurements in 5 mg/ml HA, which means that in both cases FSK related changes to astrocyte morphology for cells encapsulated within hydrogel matrices are detectable.

One aspect for consideration is whether primary cortical astrocytes are already stellate when cultured in 3D hydrogel matrices – thus such changes with measured parameters would not be as readily detectable compared to traditional 2D methods. Astrocytes cultured in hydrogels consistently adopted a process bearing morphology (Figure 8), so perhaps detecting cytoskeletal and cytoplasmic rearrangements for cells in 3D, which already have a number of processes extending out from the cell body, is more difficult compared to polygonal fusiform cells that form monolayers on 2D coverslips. To determine whether the hydrogel matrix may be interfering with the process of stellation, cAMP levels could be measured as this would provide a quantitative measure of cell activity. Forskolin increases the formation of cAMP in astrocytes, therefore there would be a rise in cAMP following forskolin addition.

5.4.1.2 Surface Area to Volume Ratios

This study has found that the mean surface area to volume ratio for control and FSK treated astrocytes cultured in 2D was significantly greater when compared to control and FSK treated astrocytes cultured in hydrogels (Figure 16). Thus these results suggest that astrocytes in 2D have larger surface areas compared to their volumes which suggests that they are flat. Additionally, 2D astrocytes have significantly higher and more variable values for surface area to volume ratios compared to 3D cells, which demonstrates the differences in cell morphology when culturing in the different environments.

5.4.1.3 Astrocyte Distribution in Different 2D and 3D Cell Culture Environments

With respect to astrocyte physiology and phenotype, the density of cells in 2D and 3D experimental preparations has been chosen to allow for the visualisation and characterisation of individual cells. Individual astrocyte morphology is thus reflective of cells which are relatively spread out and potentially have little communication with other astrocytes, an element which is not an accurate reflection on the *in vivo* arrangement. Therefore this study more accurately shows the way in which cells are influenced by matrigel or hyaluronic acid. This is due to the fact that cells are not exposed to the complex milieu of signalling that takes place with the numerous interactions of cells.

5.4.2 3D Matrices for Astrocyte Cell Culture

5.4.2.1 Alvetex

Alvetex has not enabled assessment of astrocyte morphology when the cells are cultured in an environment which allows them to adopt physiological morphology and replicates cell-cell interactions and cell-matrix interactions. Spherical aberration generated when imaging the engineered scaffold on the confocal inhibited meaningful analysis. Experimental use of alvetex was therefore discontinued, especially considering that it may be considered as a

2.5D matrix where cells are seeded on top of the polystyrene scaffold and didn't definitely penetrate through the entire 200 micron depth of the scaffold (Figure 3).

Matrices with similarities to alvetex have been shown to generate astrocytes which support neuronal survival: poly-ε-caprolactone scaffolds have been used to culture murine astrocytes until 12DIV (Lau *et al.*, 2014). Poly-ε-caprolactone is a biodegradable polyester which enabled astrocyte survival, proliferation and migration through 3D scaffolds (Lau *et al.*, 2014). Astrocytes also developed stellate 3D morphologies (Lau *et al.*, 2014). One study has revealed the possibility of preparing mixed primary mouse neuron and glial cultures with the alvetex scaffold and the subsequent formation of functional networks: signalling activity was assessed via planar multi-electrode arrays and compared to that recorded in mixed 2D monolayer cultures (Smith *et al.*, 2015).

Despite the accomplishment of growing astrocytes on polyester and polystyrene polymers respectively, and the accomplishment of established neuron-astrocyte networks, my main criticism is that such inert scaffolds only partially replicate the 3D brain microenvironment (and could more accurately be described as 2.5D). Since alvetex only provides a physical substrate for cell growth, this study has focused on the use of hydrogels for 3D cell culture since they expose cells to molecules found *in vivo*. In conclusion, I believe that alvetex isn't a suitable 3D culture method to replace 2D culture techniques and I would suggest the preferential use of hydrogels to formulate a realistic replica of the brain microenvironment.

5.4.2.2 Hydrogels

Various hydrogels have been tested for their ability to preserve functional and morphological *in vivo* complexity of astrocyte cells transferred to *in vitro* systems. Important considerations for *in vitro* culture include mimicking the structural support, signal transduction and differentiation functions of the brain extracellular environment. Hydrogel compositions are therefore really important since a cell's extracellular environment influences cell properties

such as adhesion, proliferation, stiffness and morphology (Puschmann *et al.*, 2013).

Brain tissue poses a relatively unique challenge for brain tissue engineering since it is a soft tissue with a different immune system mechanism in comparison to the rest of the body (Aurand *et al.*, 2012). Due to this, polymer chemistry, polymerisation, degradation and the mechanical properties must be carefully considered in order to make the hydrogels compatible with brain tissue. Recent technological advancements have proven that it is possible to 3D bioprint cells and polymers together with alginate hydrogels (Rastogi and Kandasubramanian, 2019).

Considering that hydrogels must provide structural support that is replicative of a cell's in vivo microenvironment, and this environment influences cell properties in turn, it is important to consider the mechanical properties of hydrogels. Hydrogels have a high water content which means they are less firm comparatively to engineered scaffolds, but they can be tailored appropriately to act as an anatomical and physiological structural support (Martin and Youssef, 2018). Alginate is a naturally occurring hydrogel with well-established tissue engineering applications due to its low toxicity and biodegradability when implanted into a legion site for example (Nisbet *et al.*, 2008). Alginate hydrogels have been shown to resist mechanical deformation when cross-linked with higher molecular weight elements such as divalent and trivalent cations which form an inter-penetrating polymer network (Martin and Youssef, 2018).

One of the key attractions of hyaluronic acid for biomedical applications is its viscoelasticity which means its capability of demonstrating solid-like elastic behaviour and liquid-like viscous behaviour under different circumstances. Hyaluronic acid contains repeating units of a high molecular weight glycosaminoglycan polymer and can be cross-linked with other components in order to modify its properties (Nisbet *et al.*, 2008); this means that solutions of HA can be highly viscous caused by their high molecular weight (Cowman *et al.*, 2015). The mechanical properties of the HA can be altered via changing polymer concentration and cross-linking density to better match the stiffness

of brain tissue since cross-linking influences pore size and structure (Fernandez-Serra *et al.*, 2020). Since hydrogels can be transplanted into patients to encourage cell growth and migration following injury (Modo, 2019), biocompatibility, toxicity and mechanical attributes are all crucial for successful cell proliferation at the site of injury (Dehqan Niri *et al.*, 2019). HA gels have a good biocompatibility for transplantation into the brain, and in addition to this can be easily chemically modified, but they are also prone to rapid degradation and can have weak mechanical stability in some instances (Lee *et al.*, 2018). Tannic acid is a naturally occurring polyphenol which exists in plants and has been proven to enhance the physical properties of HA gels which are cross-linked by polyethylene glycol diglycidyl ether (PEGDE) (Lee *et al.*, 2018).

One of the advantages of 3D culture over 2D in vitro techniques, which generate a tiling of planar astrocytes, is that cells cultured in 3D systems have well-formed cell-cell interactions (Puschmann *et al.*, 2013). Yet, such systems do not come without caveats: cells will be surrounded by a dense hydrogel matrix which can hinder process extension and can compromise the distribution of cells (Puschmann *et al.*, 2013). The hydrogel concentration utilized for *in vitro* studies, and its molecular weight, determine its viscosity which in turn influences mechanical traits and the extent of crosslinking (Rastogi and Kandasubramanian, 2019).

5.4.2.2.1 Matrigel

Despite its popularity in cell culture techniques, commercially available matrigel is not a well-defined matrix and thus generates inconsistency in experimentation with the hydrogel (Hughes, Postovit and Lajoie, 2010). Experimental results involving matrigel in this study have been extremely variable at times and not reproducible from batch to batch. One frequent variant in our experimental results was the process of depolymerisation: lots of time was spent deducing which components of buffers and reagents rendered the gel matrix unstable. This was necessary to determine if it was possible to pursue live cell loading and immunofluorescence techniques with astrocytes and neurons cultured in the gel. In some instances, solution

exchange destabilized the gel, and so it was necessary to work carefully with the gel in order for it to remain intact for imaging purposes. This instability is likely a consequence of using the gel at a low concentration since 3 mg/ml is the lowest concentration at which matrigel can be formed.

Matrigel is a mixture of proteins released from mice bred to develop a tumour; it is rich in ECM proteins and contains laminin, collagen IV, entactin and heparan sulphate proteoglycans. Proteins extracted from this mixture for gel formulation are secreted in the tumour formation process meaning that the mixture is not representative of the physiological brain microenvironment. Thus, I believe that the observed variation in experimental results for astrocytes cultured within the matrigel matrix is reflected in the range of values for astrocyte volume, surface area, shape factor and longest axis when cultured in the gel, particularly for control cells (Figures 12 & 14).

Whilst matrigel is rich in growth factors which support cell growth of a variety of cell types, including neural cells, I would advise the use of alternative hydrogels for 3D astrocyte cell culture which are chemically defined, highly reproducible and more representative of the brain extracellular environment, such as hyaluronic acid.

5.4.2.2.2 Hyaluronic Acid

Hyaluronic acid gels are favourable for 3D cell culture techniques since this molecule is abundant naturally in the brain. Also hyaluronic acid exhibits chemical adaptability which means that it can be modified according to requirement. For example, the addition of functional groups is possible – this will alter cross-linking chemistry and ultimately leads to a customized gel (Caliari and Burdick, 2016). The hyaluronic acid gel used in this study combines elements of synthetic and natural polymers (Caliari and Burdick, 2016).

From an experimental point of view, hyaluronic acid is robust, there is a good degree of cell viability and cells developed a morphology that closely replicates the *in vivo* phenotype. However, there is still a high degree of variation in our data sets for measured astrocyte volume, surface area, shape

factor and longest axis but I am more inclined to believe that this is a result of the heterogeneous nature of astrocytes (whose morphology is highly influenced by the external environment) in contrast to matrigel (Figures 13 & 14).

For added experimental control for an optimised 3D set up for astrocyte cell culture, to facilitate the accurate interpretation of the impacts of media and gel composition on astrocyte phenotype, it would be preferable to customize hyaluronic acid gels with factors relevant to the brain extracellular environment. In my opinion, working with hyaluronic acid gels for cortical astrocyte cell culture *in vitro* is a solid first step on the path to developing a customized 3D gel.

5.4.2.2.3 Hydrogels for Brain Cell Growth

Hydrogel matrices may be used in tissue engineering applications to derive brain tissues for implantation since subsequent regenerative capacity following damage to the CNS is limited. Effective hydrogels in these kinds of applications must have optimal biological and mechanical properties, thus many different kinds of hydrogels have been investigated. One study investigated the culture of PC12 neuronal cells (cell line derived from the rat adrenal medulla) in methacrylated gelatin hydrogels (GelMA) and assessed viability following implantation in mice *in vivo*; this study found that the GelMA didn't result in neurotoxic effects to the animals (Al Rifai *et al.*, 2015).

Hydrogel models will also benefit disease research, including malignant brain tumours for example. One research group carefully derived a brain ECM that closely mimics the brain microenvironment which was based on HA and a stiffness representative of normal or tumourgenic brain tissue (Ananthanarayanan, Kim and Kumar, 2011). This research used short Arg-Gly-Asp (RGD) peptides to encourage cell adhesion, and scanning electron micrographs showed a sheet-like structure with a derived porosity similar to native brain tissue (Ananthanarayanan, Kim and Kumar, 2011). This specific hydrogel composition, with the possibility for tuneable ligand density and stiffness, made it possible to study brain regulation of tumour progression. 3D cell culture using customisable hydrogels, defined serum-free media and

human cells will develop highly translatable *in vitro* models for the future and are currently under investigation: implantation of such models can decrease astrogliosis and lower the immune response to improve functional recovery (Marchini *et al.*, 2019).

5.4.3 Conclusion

Since astrocytes are extremely sensitive to their external environment, cell culture media composition and format should be carefully considered in order to study astrocytes in a physiologically relevant manner. Culturing astrocytes within 3D matrices enables them to develop a morphology that more closely resembles cells *in vivo*. This study has found that 3D hyaluronic acid hydrogels are a suitable culture system to replace 2D culture techniques so that research into astrocyte phenotype is more translatable. The inability to recapitulate the complex structure of astrocytes and maintain their quiescent state *in vitro* prevents further developments in tissue engineering and regenerative medicine, and is the rationale for working towards a superior *in vitro* 3D cell culture model.

Chapter 6. Exploring New Directions for *In Vitro* Culture Models

6.1 Introduction

The significant effect of cell culture media on primary rat astrocyte phenotype and the impact of 2D culture techniques has been shown in Chapter 4. Additionally it has been demonstrated that 3D culture methods for primary rat astrocyte culture *in vitro* result in a more physiological morphology for astrocytes compared to traditional 2D techniques (Chapter 5). A long term goal of this project was to investigate neuron-glial interactions in a superior *in vitro* model to enable comparisons with analyses that can be carried out *ex vivo* (Chapter 3). In this chapter, preliminary data for two technical advances that would have a significant impact on the way in which astrocytes are studied *in vitro* and help to develop a more translationally relevant model for pre-clinical research are presented.

6.1.1 Primary Neurons

In vitro cell culture approaches have enabled the study of neuron growth and development, and have been significant in the discovery of the mechanisms that underpin neuronal polarity. Neurons are a highly polarised cell type which is an important aspect of information processing in the brain (Barnes and Polleux, 2009).

The growth of primary cortical neurons on coated coverslips in tissue culture plates is well classified: neurons with immature neurites are observed by 2 *days in vitro* (DIV), and by 5 DIV it is possible to visualise neurons with a defined axon (Dotti, Sullivan and Banker, 1988). During neuron development, JNK Interacting Protein 1 (JIP-1) localises to neurites within the first 2-3 DIV but then specifically accumulates to a single neurite preceding axon specification at 5 DIV (Dajas-Bailador, Jones and Whitmarsh, 2008). JIP-1 promotes axon growth and is required for normal axon development (Dajas-Bailador, Jones and Whitmarsh, 2008), thus the axon growth gone can be

labelled by highly expressed JIP-1. Neuron-specific markers acetylated tubulin and β-III tubulin are routinely used to track axon growth during development.

6.1.2 Microfluidics Chambers

Microfluidics refers to a branch of technology using small fluid volumes for the manipulation of a cell's environment within an engineered microsystem (Halldorsson *et al.*, 2015). Microfluidic devices offer the potential for complete experimental control, assessing the influence of specific molecules on cell phenotype in a refined manner compared to traditional culture methods (Vickerman *et al.*, 2008). Microfluidics devices also offer experimental features that can't be achieved with regular culture techniques using multi-well plates; for example, microfluidic cell culture can create chemical gradients, an important feature of tissue microenvironments (Bhattacharjee and Folch, 2017).

Many microfluidics devices provide a 2D format for cell culture where devices are adhered onto coated substrates. Compartmentalized microfluidic chambers allow the culture of different cell types, and the growth of cell processes from a chamber on one side, across a series of microgrooves embedded in a physical barrier, to reach another chamber on the other side (Figure 1). With compartmentalised devices it is possible direct the anatomical development of neurons and fluidically isolate the separate anatomical domains of the cell. This is dissimilar to standard culture vessels where neurons form random synaptic connections making it difficult to distinguish axons and dendrites morphologically. Therefore compartmentalized microfluidics devices are sophisticated *in vitro* cell culture devices which facilitate neuronal organisation within the device so that their subcellular domains can be accessed for experimental manipulations and measurements.

Microfluidic devices offer precise spatial and temporal control, and thus facilitate defined microenvironments with the capacity to mimic *in vivo* conditions, and control parameters which are otherwise challenging to manipulate *in vivo* (Taylor and Jeon, 2010). Compartmentalized microfluidic devices enforce axon growth along parallel microgrooves from one channel

which is fluidically isolated from the adjacent channel since cell bodies are too large to migrate through the microgrooves. Additionally, since they are up to 150 µm in length, only axons will reach the adjacent compartment, and not the dendrites. Thus, these devices have enabled sophisticated studies into axonal biology, including neurite formation, outgrowth and regeneration, as well as synapse formation and function (Jeon, 2008).

The isolation of axons via compartmentalized microfluidics chambers has advanced understanding of axon growth; hippocampal axon guidance was found to be netrin-1 gradient dependent (Taylor, Menon and Gupton, 2015; Bhattacharjee and Folch, 2017). Such devices have also helped to characterize translation-independent basal outgrowth using NGF, and stimulated outgrowth which relies on the involvement of local protein synthesis (Hengst *et al.*, 2010). Perfusion microfluidic devices have been used to manipulate the formation of presynaptic and postsynaptic compartments *in vitro*; synapse formation has been directed in parallel rows connecting different neuronal populations for the study of spatial signalling in neuronal domains (Taylor *et al.*, 2010). Taylor *et al.*, (2010) used Fluo-4 to investigate intracellular calcium concentrations at dendrites and somata. Subsequent to the local perfusion of glutamate at somata, there were increases to Arc transcription and transcript localization to the dendrites (Taylor *et al.*, 2010).

Understanding of axonal degeneration induced by the chemotherapeutic drug paclitaxel has been revealed by the use of compartmentalized microfluidic culture devices (Yang *et al.*, 2009). Paclitaxel is commonly used in the treatment of breast cancer but is known to cause toxicity to neurons, resulting in distal axonal degeneration, but it was unclear whether such effects were happening directly on the axon or resulted from toxicity at the cell body. Yang *et al.*, (2009) demonstrated that axons are more susceptible to the toxic effects of paclitaxel, since when this was applied to the axonal side there was clear degeneration of axons, but when paclitaxel was applied to the soma side there was no change in axon length.

Microfluidics devices have also enabled the study of mRNA transcript expression by mature cortical axons which were found to be enriched for

protein translational machinery and cytoskeletal elements (Taylor *et al.*, 2009). Such devices have also permitted the observation that presynaptic, not postsynaptic mRNA is localized to developing rat and hippocampal axons (Taylor *et al.*, 2005).

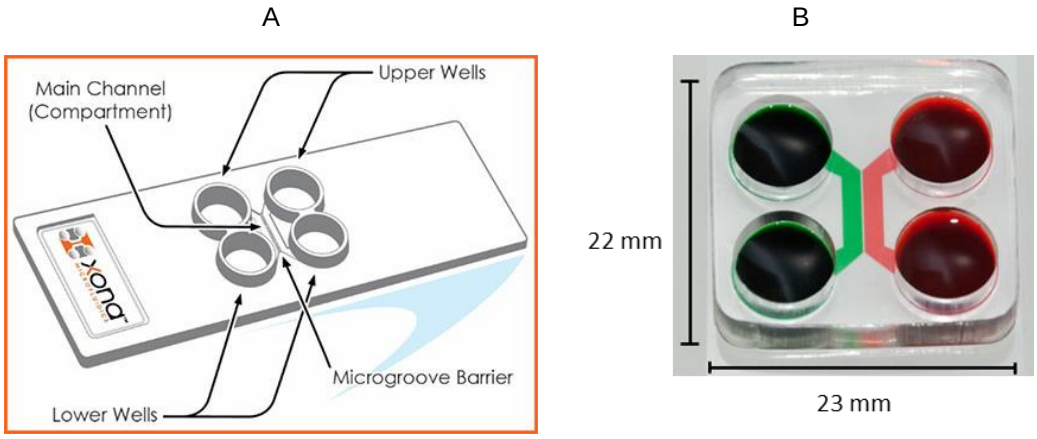


Figure 1. Cartoon representations of compartmentalized microfluidics devices purchased from Xona with 150 µm microgroove barriers between the main channels. A) The devices consist of two wells on each side which are connected to a main channel. The main channels are connected by a microgroove barrier. B) Devices can be adhered onto coated substrates including plastic culture ware. Images from: https://xonamicrofluidics.com/introducing-xonachips https://xonamicrofluidics.com/product/snd150/.

Compartmentalized microfluidics chambers also enable the study of the interaction between neurons and astrocytes by seeding different cell types in separate sides of the device. This means that it is possible to investigate axon growth in the presence and absence of astrocytes. Incorporating a 3D element into microfluidics designs offers the opportunity to understand neuron-glial interactions when both cell types are cultured in a more physiologically relevant manner. Forming hydrogels in microfluidics chambers has previously been successful with matrigel; two macrophage-like cell lines were cultured together separated by a micro slab of hydrogel which allowed the study of intercellular communication (Wong *et al.*, 2008).

I have worked with Xona Microfluidics compartmentalized devices (SND 150) to assess the influence of astrocytes on neuron growth and development. Such chambers were manufactured from PDMS (or occasionally silicone)

measuring 22 mm in length, 23 mm in width and 8 mm in height (Figure 1B). The microgrooves are 8-10 microns in width and 3-5 microns in height. The two parallel compartments are 1.5 mm by approximately 7 mm and are 80-100 microns in height (Figure 1B).

6.1.3 Primary Astrocytes and Cell Lines

Primary rat astrocytes have been used for many years by glial researchers to establish key mechanisms of astrocyte physiology and pathology. Working with primary rat tissue is preferable to using mouse tissue because rats are biologically closer to humans in evolutionary terms and their genome has a structure closer to the human genome (Zhao *et al.*, 2004). Caveats to using rodent tissues include: it is difficult to grow and expand the cells in culture, and rodents don't develop disorders of the CNS that humans do (McComish and Caldwell, 2018).

Immortal cell lines offer the potential to reduce the use of rodents for tissue or as models of specific diseases. Additionally, cell lines are cost effective and act as an unlimited source of a pure population of cells (Kaur and Dufour, 2012). Immortal astrocyte cell lines have been derived from explant cultures of postnatal mouse cerebella (Alliot and Pessac, 1984). Alliot & Pessac (1984) reported spontaneous *in vitro* transformation and the development of three different types of GFAP expressing clones based on morphological characteristics. In the early 1990s, another study reported the derivation of astrocyte cell lines from H-2KbtsA58 transgenic mice that exhibited the same functions *in vitro* as previously reported *in vivo* with respect to glial scar properties (Groves *et al.*, 1993). This H-2KbtsA58 cell line has been shown to generate astrocytes expressing GFAP, Glu1, EAAT1 and NMDA receptors (Langley *et al.*, 2009). Despite this, working towards developing human cell lines is much more preferable for therapeutic discoveries and clinical applications.

Technical challenges have made it difficult to establish immortal human cell lines in culture. Price *et al.,* (1999) demonstrated their creation of an immortal cell line (A735) where cells retained the correct morphology and

developmental features of astrocytes. They used recombinant DNA vectors expressing SV40 T antigen to transfect primary human astrocytes to generate one of the first non-tumour derived immortal glial cell lines (Price, Burke and Mayne, 1999). Yet, primary human astrocytes are of limited availability and thus new techniques, including the generation of neural populations from stem cells, are ideal alternative options.

Malignant astrocytomas develop when there is uncontrolled proliferation of this cell type, most likely as a result of the aberrant expression of positive growth regulators, or the loss of negative regulators (Hartwell and Kastan, 1994). In the 1980s, cell lines derived from human malignant gliomas were characterised and subsequently used for the biological study of gliomas (Rutka *et al.*, 1987). In 1994, astrocytoma C6 cells were used to identify the function of GFAP beyond its known role in cell growth and differentiation (Toda *et al.*, 2002). Toda *et al.*, 2002 transfected rat astrocytoma C6 cell lines with murine GFAP cDNA to investigate the specific effect of GFAP. Transfected astrocytoma cells developed elongated shapes with extended processes rich in GFAP and suppressed cell growth, thus increased GFAP expression has a dramatic influence on astrocyte morphology and may act as a tumour suppressor in astrocytoma (Toda *et al.*, 2002).

Neuroblastoma cell lines have been generated from mouse and rat primary tissue, however they lack the human aspect which may mean that observed results may be species-specific and mechanisms may behave differently in humans. In addition to this, not all neurons derived in this way have stable karyotypes which give rise to potential experimental issues related to studies of cell signalling and gene expression. In 2016 a protocol emerged to obtain homogeneous and viable neuronal cultures from a chromosomally stable human neuroblastoma cell line SH-SY5Y (Shipley, Mangold and Szpara, 2016). Such types of cell line are more appropriate for cellular and molecular analysis and can provide a more translational model of human physiology and pathology (Shipley, Mangold and Szpara, 2016). This SH-SY5Y cell line has been used to investigate how lactate influences cell energy metabolism:

lactate supplementation resulted in increased cell respiration and decreased the glycolysis flux (Lezi and Swerdlow, 2016).

6.1.4 Stem Cells

Human tissue, for neuroscience research, has consistently been in short supply due to the number of ethical and public health issues. The availability of human tissues for the advancement of translational research is crucial and will help direct new methods for personalized medicine. In the last decade protocols to derive human neural stem cells and functional neuronal populations from pluripotent stem cells have emerged. Human induced pluripotent stem cells (hiPSCs) can be derived from adult somatic cells and offer the ability to derive disease and patient specific cell lines. However, whilst such cell lines offer an inviting platform to study numerous CNS disorders, functional characterisations of these cell lines are necessary.

Technological advances in the field of stem cell biology have revealed that it is possible to reprogramme somatic cells into iPSCs using c-Myc, Klf4, Oct4 and Sox2 transcription factors (Polo *et al.*, 2013; Takahashi *et al.*, 2014). Evidence has also emerged to show that cells are distinct in their original, transitional and reprogrammed forms, and it is common to observe iPSC lines which show features consistent with incomplete reprogramming (Ohnuki *et al.*, 2014). Therefore it is possible that iPSCs maintain some of the pluripotency features initially gained in such techniques, thus other procedures have been developed to resolve this and include the use of human endogenous retroviruses (HERVs) which occur naturally and account for 8% of the human genome (Ohnuki *et al.*, 2014). HERV type-H (HERV-H) transcripts are expressed in ESCs and iPSCs at higher levels than differentiated cells, but decrease following successful reprogramming, thus transient hyper activation of HERVs drives somatic cells towards pluripotency and establishes differentiation potential, and thus is an important mechanism in cellular reprogramming methods (Ohnuki *et al.*, 2014).

iPSCs offer greater models for disease study and drug screening compared to animal models and the way they can recapitulate human diseases (Ebert,

Liang and Wu, 2012; Ohnuki *et al.*, 2014; Takahashi *et al.*, 2014). Disease-specific iPSC cell lines were first reported in 2008 (Dimos *et al.*, 2008; Park *et al.*, 2008), and one of the first successful *in vitro* studies investigated spinal muscular atrophy (Ebert, Liang and Wu, 2012). However, iPSCs tend to exhibit greater diversity than ESCs which arises from retained epigenetic memory and potentially new features obtained during the reprogramming protocol (Ohnuki and Takahashi, 2015). Furthermore whilst iPSCs have facilitated the study of numerous neurodevelopmental and neurodegenerative disorders to date (Pen and Jensen, 2017; Linda, Fiuza and Nadif Kasri, 2018), they still require further development *in vitro* to eliminate issues of incomplete differentiation (De Lázaro, Yilmazer and Kostarelos, 2014).

Neurons and oligodendrocytes have been generated from neural progenitor cells with relative simplicity yet it has been more challenging to develop astrocytes. Advances in the past decade are promising: populations of immature astrocytes, greater than 90% positive for GFAP and S100β, have been generated and exhibit key functional properties including glutamate uptake and synaptogenesis, and have gene expression profiles similar to primary astrocytes (Krencik *et al.*, 2011). These cells were also found to become mature after developing connections with blood vessels following transplantation into the mouse brain (Krencik *et al.*, 2011). However, the protocol described by Krencik *et al.,* (2011) requires 6 months of culturing prior to the generation of pure cultures of immature astrocytes.

Shorter culturing protocols have since emerged for the derivation of astrocytes from hiPSCs. For example, Roybon *et al.,* (2013) reported the generation of mature spinal cord astrocytes which expressed GFAP, S100β, vimentin, CX43 and ALDH1 after 80 days in culture. Additionally, functional analysis revealed the cells' capability of glutamate uptake (Roybon *et al.*, 2013). Lundin *et al*., (2018) derived astrocytes after 28 days: hiPSCs were differentiated via exposure to fibroblast growth factor 2 (FGF2) and epidermal growth factor (EGF2), and astrocyte induction was achieved by exposure to FGF2, Heregulin1β, insulin-like growth factor 1 (IGF1) and activin A. Non-overlapping domain profiles developed over differentiation and there was an increase in

astrocyte associated markers (Lundin *et al.*, 2018). The development of reliable differentiation protocols for mature human astrocytes from hiPSCs is important as it offers a new way to study human astrocyte morphology, function and pathology.

Human protoplasmic astrocytes are 2.6 fold larger in diameter, have up to 10 times more primary processes, propagate calcium waves 4 times faster and are more functionally complex than primary rodent astrocytes (Han *et al.*, 2013). Human astrocytes also have a greater number of neuronal interactions compared to animal astrocytes, therefore further investigation into the unique features of human astrocytes is required and could, in principle, be achieved with astrocytes derived from hiPSCs.

6.1.5 Induced Astrocytes

Techniques now exist to convert hiPSCs or human ESCs into neural progenitor cells (NPCs) and then pattern and switch them to glial progenitor cells (GPCs) that eventually differentiate into mature astrocytes (Santos *et al.*, 2017). iPSC derived cortical NPCs are now commercially available and generated from patient dermal fibroblasts.

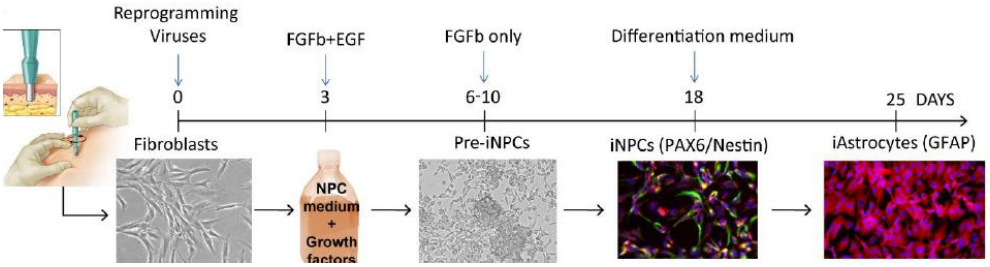


Figure 2. Schematic representation of the method for deriving induced astrocytes from human fibroblasts. Human fibroblasts are obtained from skin biopsies and are directly reprogrammed into induced neural progenitor cells (iNPCs) within 3 weeks. iNPCs are treated with induced astrocyte (iAstrocyte) differentiation medium for 5 days to generate iAstrocytes. Schematic credited to Dr Laura Ferraiuolo (University of Sheffield) and Dr Tomas Bellamy (University of Nottingham).

A common approach to derive astroglial cells requires dissociating NPCs with accutase and seeding a cell suspension onto a coated substrate and incubating with specific media treatment. For example, Jones *et al.*, (2017) differentiated astrocytes from NPCs using a combined coating of poly-l-ornithine and mouse laminin, and incubated with neurobasal supplemented with B27, non-essential amino acids, penicillin/streptomycin, L-glutamine, CNTF, FGF2, BMP2, EGF and insulin. Jones *et al.*, (2017) cultured cells until they reached 80% confluency and passaged the cells up to three times before use. di Domenico *et al.*, (2019) used a similar protocol to derive astrocytes: incubation with accutase was followed by mechanical disaggregation before plating on matrigel coated plates and culture with neurobasal supplemented media for 14 DIV (contained 0.2% B27, 1% non-essential amino acids, 1% penicillin/streptomycin, 1% glutamax, and 10 ng/ml CNTF). These cells were passaged four times before they were considered to be mature and subsequently characterised. Such successes with iPSC derived astrocyte technology have allowed the study of neurodegenerative disorders such as Parkinson's disease (di Domenico *et al.*, 2019) and Alzheimer's disease (Jones *et al.*, 2017).

Meyer *et al*., (2013) have refined a protocol for the generation of induced astrocytes (iAstrocytes) within 26 days from induced neural progenitor cells (iNPCs), thus bypassing the glial progenitor stage. Collaboration with Laura Ferrauiolo from the Sheffield Institute of Translational Neuroscience at the University of Sheffield has provided the opportunity to investigate the morphological characteristics of human iAstrocytes. These iAstrocytes have been generated via genetic reprogramming of fibroblasts from skin biopsies (Figure 2). If iAstrocytes can be determined to have many of the same functional properties as mature astrocyte cells *in vitro*, the reprogramming technique will provide an efficient and economic supply of human cells. Furthermore, this technology could act as a replacement technique, replacing the use of primary animal tissue.

6.1.6 Aims

Compartmentalized microfluidics devices offer the opportunity to co-culture astrocytes and neurons *in vitro* with a high degree of experimental control for the investigation of neuron-glial communication and its influence on axon growth and development. Therefore, I aimed to test the feasibility of co-culturing neurons and astrocytes in microfluidic chambers and compare this to co-culture on coverslips in culture plates. Additionally I wanted to investigate whether neurons are viable in the 3D matrigel matrix to determine whether it is a suitable hydrogel for neuron culture. Ultimately the aim was to establish whether a superior *in vitro* model could be created by combining 3D hydrogels with compartmentalized microfluidics devices for the study of astrocyte-neuron interactions.

Traditionally the study of human astrocytes has been hindered by the poor availability of tissue driven by ethical concerns regarding the use of embryonic stem cells and fetal tissue. In this study I aimed to generate preliminary data as part of an initial characterisation of iAstrocyte morphology in 2D and 3D culture conditions (derived from human iNPCs). If iAstrocytes develop a protoplasmic heterogeneous morphology in 2D and 3D *in vitro* culture, similar to primary rat astrocytes, this would be a step towards confirming that iAstrocytes phenotypically represent their intended cell type, and provide the potential to elucidate human astrocyte complexity. In addition to this, a characterisation of iAstrocytes generated from human iNPCs has been conducted to determine how plausible it would be to use such cells to replace the use of primary animal tissue.

6.2 Methods

6.2.1 Generation of Primary Neurons

Primary cortical neurons were cultured to assess the influence of astrocytes on axon growth and development. E18 embryos were collected and placed in 10 ml of chemically defined neurobasal medium (21103049, Invitrogen, Loughborough, UK) and cultures were subsequently generated under sterile conditions at room temperature unless otherwise stated.

Cortices were removed whole from the brain. The meningeal membranes were removed and then cortices were treated with 20 µL DNAse (10 µL/ml, D5025, Sigma-Aldrich) and 200 µL trypsin (100 µl/ml, T1426, Sigma-Aldrich) in a 35 mm petri dish. Cortices were incubated at 37ºC and 5% CO_2 for 30 minutes before 100 µl trypsin inhibitor (50 µl/ml, T9003, Sigma-Aldrich) was added and the cortices were transferred to a falcon tube containing 6 ml neurobasal medium.

Neurobasal medium was removed and replaced to wash the tissue. Next, all medium was removed except for 1.5 ml to which 13 µl/ml DNAse was added. Tissue was dissociated by carefully pipetting up and down approximately 20 times until no clumps were visible and a cloudy suspension was formed. Neurobasal medium was then topped up to 10 ml and the suspension was centrifuged at 250 g for 5 minutes to pellet the cells. Supernatant was removed and the cell pellet was resuspended in 1 ml of neurobasal medium. The final cell suspension was topped up to 5 ml with neuron medium: neurobasal medium with 2% B27 Supplement (17504044, Invitrogen) and 1% Glutamax (35050038, Gibco). The cell suspension was then seeded onto coverslips at a cell density of 1.25 x 10^5 cells per ml, or into matrigel with a cell density of 1 x 10^7 cells per ml.

6.2.2 2D and 3D Cell Culture of Neurons

For 2D culture, neurons were seeded onto PLL coated 22 mm coverslips in 6-well plates at 1.25 x 10^5 cells per ml. Cell culture plates were topped up with 2

ml of neuron medium and cells were cultured for up to 4 weeks *in vitro*. Every 3-4 days wells were topped up with 500 µl of neuron medium.

For 3D culture, neurons were mixed with matrigel and neuron medium to give a final cell density of 10 x 10^6 cells per ml. Matrigel was formed following 30 minutes incubation at 37 °C and 5% CO_2, after which gels were topped up with 400 µL of neuron medium.

6.2.3 Immunofluorescence for Neurons

Coverslips seeded with primary cortical neurons were processed in a similar way to astrocytes for immunofluorescence techniques. Coverslips were first washed with 1 ml PBS and then fixed for 30 minutes with 500 µL of 4% paraformaldehyde (PFA). Next coverslips were washed 3 times with 1 ml PBS containing 10 mM glycine (G8898, Sigma-Aldrich) before being incubated with 500 µl PBS containing 10 mM glycine and 0.2% Triton X-100 for 30 minutes. Coverslips were then washed with 1ml PBS containing 0.1% Triton X-100 and subsequently incubated with 500 µl 3% BSA for 30 minutes at room temperature.

To investigate the growth and development of primary cortical neuron cultures, primary antibodies were selected to visualise axons and the axon growth cone. Primary antibodies include: β-III tubulin at 1:300 (ab18207, rabbit, polyclonal, Abcam) and acetylated tubulin at 1:300 (T7451, mouse, monoclonal, Sigma-Aldrich). Primary antibodies were prepared in 3% BSA and coverslips were treated with 300 µl overnight in a humidified chamber at 4ºC.

After the overnight incubation, coverslips were washed in 1 ml PBS containing 0.1% Triton X-100. Secondary antibodies were also prepared in 3% BSA with a 1:300 dilution, and coverslips were treated with 300 µl for 2 hours at room temperature in a humidified chamber. The secondary antibodies include: Alexa Fluor® 568 goat anti-mouse IgG (A11004, Invitrogen) and Alexa Fluor® 488 goat anti-rabbit IgG (A1008, Invitrogen). Finally, coverslips were washed 3 times with 1 ml PBS containing 0.1% Triton X-100 and once with 1 ml PBS before mounting using 50 µl of Vectashield® with DAPI (H-1500, Vector

Laboratories Inc). Slides were allowed to dry in the dark for 2 hours and then stored in the dark at 4ºC.

6.2.4 Imaging for Neurons in 2D and 3D

Embryonic neurons were generated (see above – section 6.2.1) and either seeded onto 0.1 mg/ml PLL coated 22 mm coverslips, or mixed with 3 mg/ml matrigel and set at 37°C in a 5% CO_2 incubator for 30 minutes before topping up with 400 µl of neuron medium.

An epifluorescent microscope (Nikon Eclipse Ti-E) was used to image fixed and labelled neurons for up to 14 DIV. A confocal microscope (Zeiss 710) was used to image neurons at either 2 or 5 DIV following calcein AM loading for 30 minutes (full parameters shown in appendix, see page 235).

6.2.5 Microfluidics Chambers

For experiments using microfluidics chambers, the protocol from Xona Microfluidics Devices was followed. New chambers (SND150, Xona Microfluidics Devices, New York) were activated with an overnight incubation at room temperature with serum-free medium in a 10 cm petri dish. Devices were then rinsed (feature side up) using 70% industrial methylated spirit (IMS) for 30 seconds and allowed to dry in a sterile environment at room temperature overnight.

PLL was diluted in water (0.1 mg/ml) and 1 ml was applied to the base of nunc dishes so they were totally covered for one hour at room temperature. Nunc dishes were then washed with 2 ml of sterile water twice and allowed to dry. Chambers were assembled on top of the nunc dishes by pressing them down to secure them in place. Following this, 150 µl of media for the relevant cell type was added to the top left well and pipetted gently so it entered the main channel and the same was repeated with the bottom left well. This was repeated for the right side. Chambers were incubated with cell culture media at 37ºC and 5% CO_2 for 1 hour prior to cell seeding.

For neuron only chambers, media was removed from what would become the somal side before neuron addition (with care to prevent creating air bubbles in

the channels) but media was not removed from the axonal side. A neuron suspension of approximately 4 x 10^6 cells was used: 20 µl of suspension was seeded into each somal compartment slowly in order to prevent flow into the channel (otherwise cell attachment was compromised). Next, chambers were put in a 37°C and 5% CO_2 incubator for 30 minutes before topping up somal sides to 100 µl with neuronal medium (axonal compartments contained 80 µl each). After 3-4 DIV, chambers were topped up in a drop-wise manner using 20 µl of neuron conditioned media (media taken from control 6-well plates).

When astrocytes were seeded into chambers, a cell density of 5 x 10^4 cells per ml was used. Astrocytes were seeded into chambers up to 48 hours prior to the addition of neurons – at this point astrocyte medium was removed and replaced with neuronal medium ready for axons to grow into the channel.

Chambers were re-used up to 10-20 times. After each use, chambers were soaked in sterilized water in a beaker for 3 hours and then in 70% ethanol for 30 seconds. Occasionally, five chambers at a time were put into a beaker containing 70% ethanol and then put into the sonicater (Grant Ultrasonic Bath XB2) containing water for no more than ten minutes. Following this, chambers were prepared as normal ready for seeding cells.

To visualise axon growth and astrocyte morphology, the live cell label calcein AM was used. To label neurons that have extended axons to the other side, 1 µM calcein was added to the axonal side. This was done when axons had crossed the microgrooves which occurs from approximately 5 DIV. Adding calcein to the cell body side will label all of the cells.

1 µM calcein AM (20 µl) was added into neuron conditioned media from control 6-well plates (where cells were plated at the same density) and then the media from these plates was added to neurons in the microfluidic chambers on either the axon or soma side for 30 minutes (after removing the medium). To prevent axon loss resulting from media replacement, chambers were imaged immediately post calcein AM treatment. 1 µM calcein AM was also added into the astrocyte side for 30 minutes.

6.2.6 Induced Neural Progenitor Cells

6.2.6.1 Conversion and Maintenance of Induced Neural Progenitor Cells

The method was adapted from (Meyer *et al.*, 2013) and an original cell line was provided by Dr Laura Ferrauiolo from the University of Sheffield. The investigations in this study have been conducted using the same cell line derived from an individual patient who consented to the use of their fibroblasts post biopsy. The patient was a 65 year old Caucasian male. Dr Alex Rathbone provided technical support for iNPC maintenance and iAstrocyte differentiation.

In brief, the Stegment® Reprogramming Lentivirus Set Human OSLN (Sigma Life Science) was used to generate iNPCs. It includes hOct 4, hSox2, hLin28 and hNanog as prepackaged lentivirus particles for reprogramming fibroblast cells - these have been shown to direct a variety of differentiated cells into pluripotent stem cells with embryonic stem cell-like properties.

Dissociation of skin biopsies (2 cm^3) and culture expansion of the fibroblasts was initiated within 30 minutes post sampling under sterile conditions. Skin samples were washed twice in PBS and half a centimetre strips were cut and incubated with 25 ml of 0.05% trypsin/EDTA (Invitrogen) in a 50 ml conical tube at 37°C for 45 minutes. Next, 20 ml of DMEM media containing 10% FBS was added and cells were centrifuged at 350 g for 4 minutes. Medium was aspirated and replaced with fresh DMEM containing 10% FBS before plating in a 6-well plate.

One day post seeding, a mixture consisting of the retroviral vectors Oct3/4, Sox2, Klf4, and c-Myc was applied and cells were incubated overnight in a final volume of 700 µl medium/viral vector. The following day cells were washed twice with PBS and then regular fibroblast medium (DMEM plus 10% FBS) was applied for 3 days. After this recovery time, the cells were washed with PBS once before 2 ml of NPC conversion medium consisting of DMEM/F12, 1% N2, 1% B27, 20 ng/ml FGF2, 20 ng/ml LEGF, and 5 µg/ml

heparin (Sigma-Aldrich) was added to the cells. The medium was then changed every day.

6.2.6.2 Maintenance of Induced Neural Progenitor Cells

To culture iNPCs, fibronectin (FC010-5MG, Sigma-Aldrich) coated plates were prepared: 6 ml of 5 µg/ml fibronectin coating solution was placed on each 10 cm tissue culture plate (1 mg/ml of human fibronectin was added to PBS in a 1:200 ratio at room temperature). The 10 cm tissue culture plates (150350, Thermo Fisher Scientific) were incubated for 5 minutes at room temperature. Next human iNPC proliferation media was removed from iNPCs and the cells were washed in 5 ml of PBS. PBS was removed and 1 ml of accutase (11599686, Gibco Life Sciences) was added to the iNPCs which were incubated with the solution for 4 minutes in a 37°C and 5% CO_2 incubator. Plates were gently taped to dislodge the cells from the plate completely and then 5 ml of PBS was added to lift the iNPCs and mix and transfer them to a 20 ml tube. iNPCs were centrifuged at 200 g for 4 minutes at room temperature after which the supernatant was pipetted off and the iNPC pellet was re-suspended in an appropriate amount of human iNPC proliferation media.

The composition of human iNPC proliferation media is as follows: 500 ml DMEM/F-12, Glutamax (11524436, Fisher Scientific) with 1% N-2 (11520536, Fisher Scientific), 1% B-27 (11530536, Fisher Scientific) and 0.01% 4 mg/ml FGF (AF-100-18b, Peprotech, London, UK). Once the fibronectin coating solution was removed from tissue culture plates, 12 ml of warm human iNPC proliferation media was added before an appropriate volume of the re-suspended iNPC solution was added.

iNPC proliferation plates were kept in a 37 °C and 5% CO_2 incubator for up to 4 days (or until the iNPCs reach 80% confluency) and then were split again according to the protocol described here. Culture media was replaced every 2 days. Since FGF loses activity within a week the media needs to be replenished with fresh FGF weekly.

6.2.6.3 Induced Astrocyte Generation from Induced Neural Progenitor Cells

iNPCs were cultured for up to 21 DIV before they were induced to become astrocytes. After a suspension of iNPCs had been generated, cells were seeded into the relevant formats to begin the process of iAstrocyte induction. iNPCs were seeded onto 0.1 mg/ml PLL coated coverslips, 0.1 mg/ml PLL coated 24-well plates, within 3 mg/ml matrigel or within 5 mg/ml hyaluronic acid gels.

iNPCs were treated with the following media composition to derive human induced astrocytes (iAstrocytes): Dulbecco's Modified Eagles Medium (DMEM, D5796, Sigma-Aldrich), 0.2% N-2 (11520536, Fisher Scientific), 10% FBS (10500064, Gibco Life Sciences) and 0.5% penicillin/streptomycin (P0781, Sigma-Aldrich). Culture medium was replaced every 3 days and iAstrocytes were used experimentally after 5 DIV.

6.2.7 Induced Astrocytes

6.2.7.1 Calcein AM Loading

iAstrocytes were treated with 1µM calcein AM for 30 minutes at 37°C and 5% CO_2 for investigations into cell viability and morphology. iAstrocyte differentiation media containing calcein AM was removed and replaced with imaging buffer to maintain cell viability during imaging (see section 2.3.1 for buffer composition).

6.2.7.2 Immunofluorescence

iAstrocytes were fixed and treated according to the immunofluorescence protocol previously described for primary astrocytes (see section 2.3.2). GFAP was used to distinguish differences between control and forskolin (FSK) treated astrocyte morphology.

6.2.7.3 Inducing Stellation

10 µM forskolin (FSK) (0.4% in DMSO vehicle) was added directly to the bathing medium for astrocytes in both 2D and 3D culture formats for 3 hours

at 37ºC and 5% CO_2 to induce iAstrocytes stellation. FSK was removed by washing with either astrocyte medium or imaging buffer (see section 2.3.1 for buffer composition).

6.2.7.4 Imaging

Live or fixed fluorescence microscopy was carried out with micromanager software and the 10x magnification lens on an Olympus IX70. Coverslips had a 100 ms exposure time to the LED source (470nm peak, 10% intensity). Live imaging was also conducted with Zen software and either the 10x or 40x magnification lenses on a Zeiss 710 confocal. Imaging parameters for different culture formats using different objectives are described in the appendix.

6.2.7.5 Analysis

Confocal images for iAstrocytes cultured on PLL coated 24-well plates, within 3 mg/ml matrigel or within 5 mg/ml hyaluronic acid were subjected to post imaging processing. Z scales were altered using Zen software according to previous calculations with 4 micron fluorescent beads in primary astrocyte preparations (see section 5.3.2.1). Images were analysed with Volocity software: box ROI were drawn around iAstrocytes to measure volume, surface area, shape factor and longest axis based on fluorescence intensity. A total of 33 cells were analysed for iAstrocytes cultured in 3 mg/ml matrigel, 46 cells cultured in 5 mg/ml hyaluronic acid, and 21 cells in 2D, from a minimum of two separate iAstrocyte induction procedures.

6.2.8 Statistics

Graph Pad Prism (Windows Version 7.01) was used to determine significant differences in morphological parameters measured for iAstrocytes cultured in the three different culture conditions (2D, 3D matrigel and 3D hyaluronic acid). Data with normal distributions (shape factor and longest axis) were analysed with an ordinary one-way ANOVA with Tukey's multiple comparisons test. Morphological parameters which were not normally distributed (volume and surface area) were analysed using a Kruskal Wallis One Way ANOVA test with Dunn's correction for multiple comparisons. Outliers from data sets were

discovered using Grubb's test and excluded from the analysis appropriately (0.05 significance level).

6.3 Results

6.3.1 Primary Neuron Development *In Vitro*

To investigate normal neuronal development *in vitro*, neurons cultured on poly-l-lysine (PLL) coated coverslips were fixed at different time points to compare axon length. Cells were labelled for acetylated tubulin in neurons fixed after 2, 5 and 12 DIV (Figure 3). Neurons showed the development of dendrites at 2 DIV and axons were polarised by this stage (but not in all neurons) (Figure 3A). Neurons developed clearly defined axons and numerous dendrites extending from cell bodies at 5 DIV (Figure 3B). At 12 DIV the neuronal network was extremely dense with processes from lots of neurons, thus it was not possible to identify individual cells (Figure 3C).

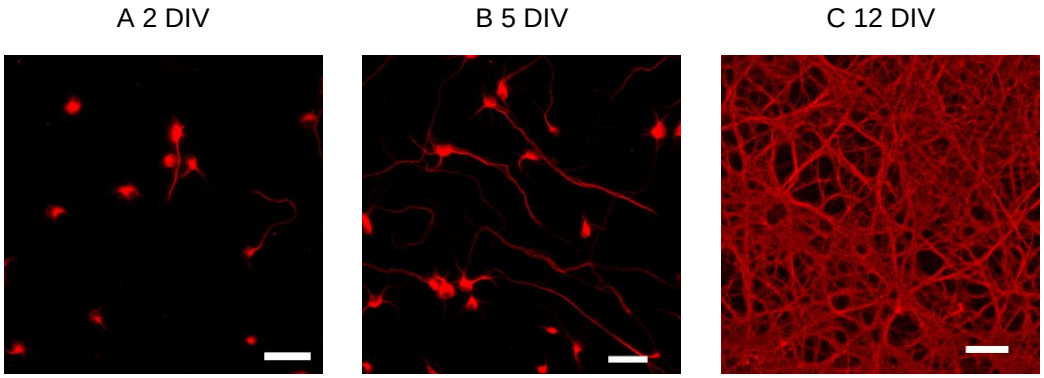


Figure 3. Cortical neuron development *in vitro*. Neurons were fixed after 2 DIV (A), 5 DIV (B) and 12 DIV (C) and labelled with acetylated tubulin (red). Representative images are shown where N = 3 biological replicates, equivalent to three separate neuron preparations from 3 different sets of embryos. Scale bars = 50 µm.

Neurons were also labelled for β-III tubulin to confirm results found with acetylated tubulin (Figure 4). At 2 DIV, neuron cell bodies and dendrites are distinguishable (Figure 4A). By 5 DIV, axon outgrowth and development was clear (Figure 4B). By 12 DIV, a dense neural network had developed making it extremely challenging to determine individual cells and their processes (Figure 4C).

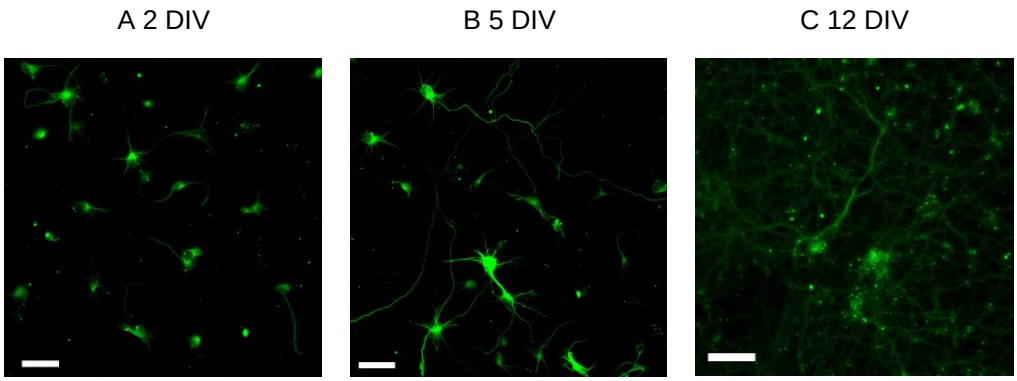


Figure 4. Cortical neuron development *in vitro*. Neurons were fixed after 2 DIV (A), 5 DIV (B) and 12 DIV (C) and labelled with β-III tubulin (green). Representative images are shown where N = 3 biological replicates, equivalent to three separate neuron preparations from 3 different sets of embryos. Scale bars = 50 µm.

6.3.1.1 Axon Length Analysis

To quantify axon growth, acetylated tubulin was used to measure axon length in developing neurons. Neurons fixed after 2 and 5 DIV were analysed by manually tracing from the point of origin of the axon on the cell body to the axonal tip using Image J software (Figure 5). Whilst it was challenging to identify which protrusion from the cell body was the longest at 2 DIV, axons were quite clearly defined for cells at 5 DIV (see Figures 3 & 4). Neurons fixed at 12 DIV were not analysed because individual axons were hard to discriminate (see Figures 3 & 4).

Axon length measurements were deduced from a minimum of three preparations where up to 6 embryos where extracted from one pregnant dam in each case to generate a cortical neuron culture. Thus, three separate neuron preparations enabled the analysis of N = 94 neurons traced for cells fixed at 2 DIV, and N = 60 neurons traced for cells fixed at 5 DIV. Mean axon length significantly increased between 2 and 5 DIV, from 33.3 µm to 52.2 µm ($p = 0.0003$) (Figure 5). These results show that it is feasible to accurately measure axonal length in isolated neuronal cultures. The next stage was to apply this method to co-cultures of neurons and astrocytes.

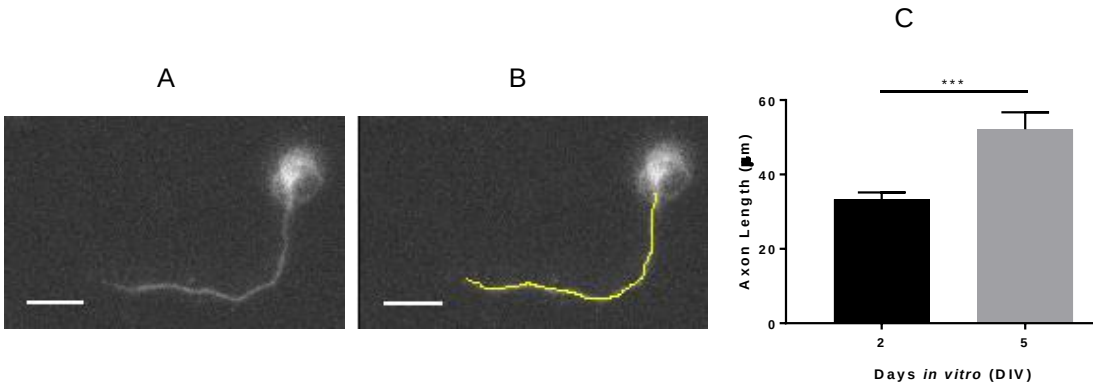


Figure 5. Example of axon tracing for a cortical neuron used to investigate the mean axon length (μm) for neuron cultures fixed at 2 and 5 DIV. A) An example of a clearly polarised neuron fixed after 5 DIV and labelled with acetylated tubulin. B) The corresponding trace drawn for the axon from the point of origin on the cell body to the axonal tip (yellow line). C) Bar chart plot showing the increase in axon length across 2-5 DIV where N = 94 neurons measured at 2 DIV and N = 60 neurons measured at 5 DIV from 3 individual neuron preparations. Mean ± SEM shown. Mann-Whitney t test. Scale bars = 10 μm.

6.3.2 Astrocyte and Neuron Co-Culture

The aim in this study was to compare axon length measurements for neurons cultured alone, neurons cultured on top of a layer of astrocytes and neurons cultured on a layer of forskolin (FSK) treated astrocytes at three time points (2, 5 and 12 DIV) to investigate the effect of neuron-glial interactions on axon development. This has not been possible because acetylated tubulin labelling in co-cultures was more widespread than in cultures of neurons alone (Figure 6). Significant background labelling of astrocytes was evident, suggesting that acetylated tubulin is also present as a component of the astrocyte cytoskeleton (Figure 6E).

To discover if astrocytes were expressing acetylated tubulin, cultures of astrocytes were prepared in the absence of neurons. Control and FSK treated astrocytes were fixed and labelled for acetylated tubulin (Figure 6). Acetylated tubulin labelling was positive for control and FSK treated astrocytes (Figure 6), thus it was necessary to find an alternative and more discriminating axonal marker for axon length analysis for neurons co-cultured with normal or FSK treated astrocytes.

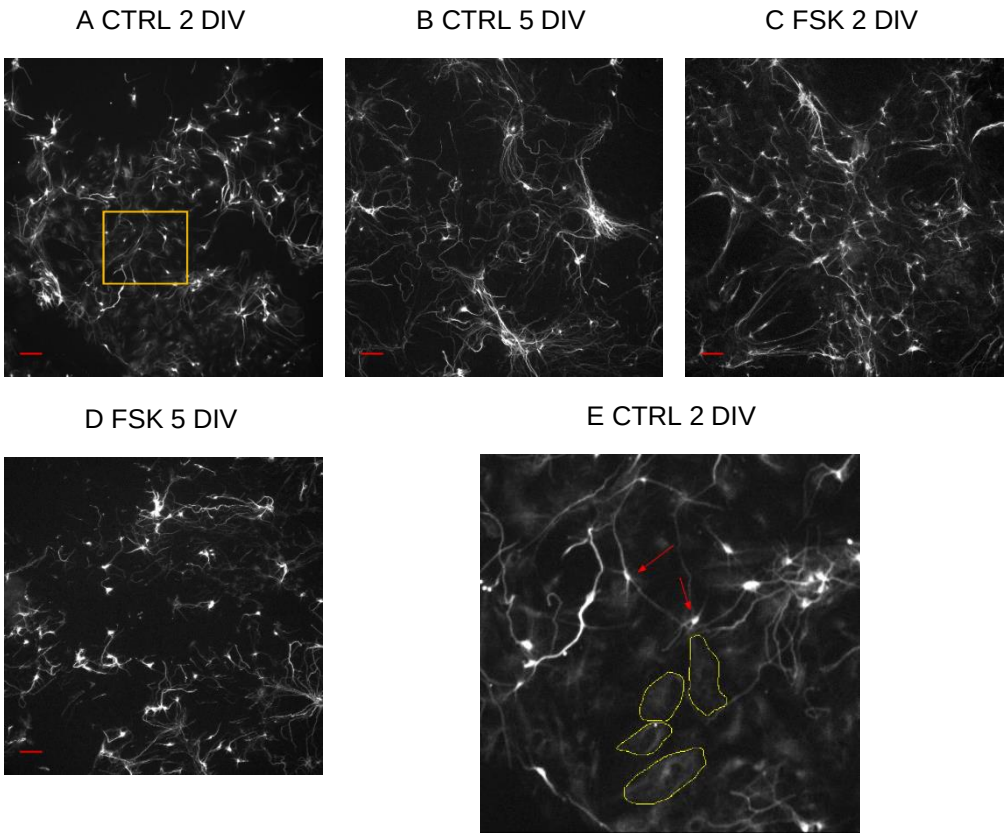


Figure 6. Co-cultures of neurons with control (CTRL) or forskolin (FSK) treated astrocytes fixed after 2 or 5 DIV. Neurons were cultured on a layer of CTRL (A & B) or FSK treated (C & D) astrocytes with neuron medium and fixed at either 2 (A & C) or 5 DIV (B & D). Astrocytes were treated with 10 µm forskolin for 3 hours. E) Cropped yellow square from A to highlight astrocytes (perimeter shown by yellow lines) and neurons (red arrows). Representative images shown where N = 3 biological replicates, equivalent to three separate time-matched astrocyte and neuron preparations. Scale bars = 100 µm.

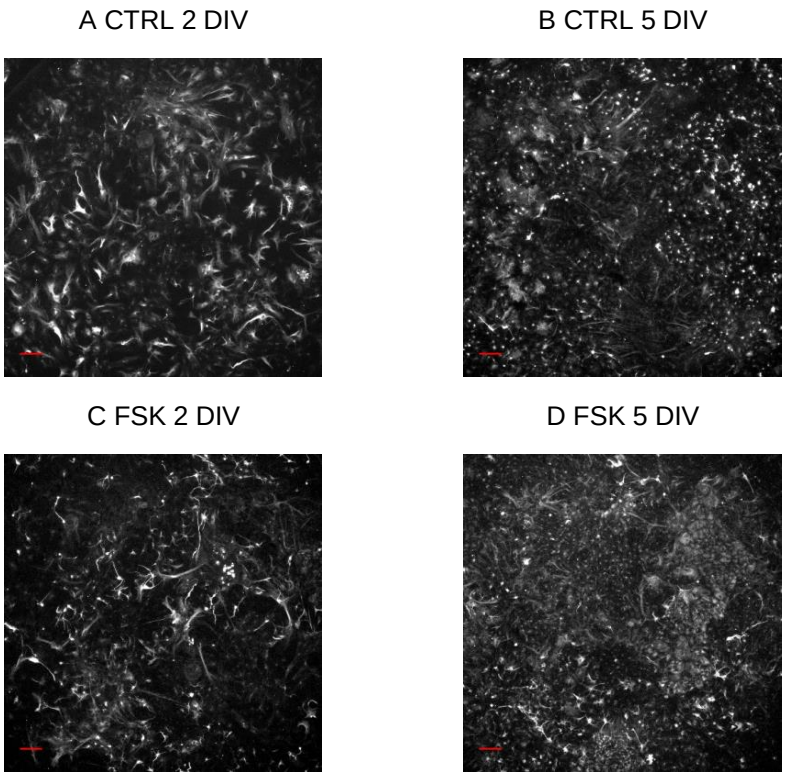


Figure 7. Cortical astrocytes positively label for acetylated tubulin. Astrocytes fixed after 2 (A & C) or 5 DIV (B & D) for control (A & B) or FSK treated (C & D) cells were labelled with acetylated tubulin (1:300 concentration). Astrocytes were treated with 10 µm forskolin for 3 hours. Representative images are shown where N = 3 biological replicates, equivalent to three separate astrocyte preparations. Scale bars = 100 µm.

To determine whether β-III tubulin was a suitable alternative marker to discriminate neurons from astrocytes, cultures of control and FSK treated astrocytes were fixed and labelled for β-III tubulin at 1:300 concentration (Figure 8). β-III tubulin labelling was positive for control and FSK treated astrocytes at this concentration meaning it would not be possible to use this marker to distinguish axons from astrocytic processes (Figure 8).

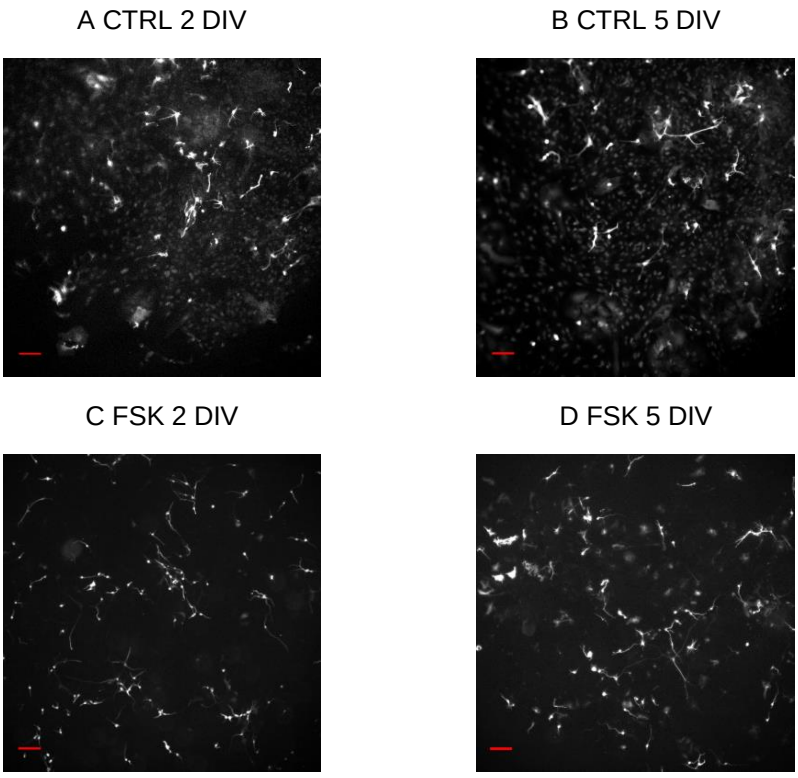


Figure 8. Cortical astrocytes positively label for β-III tubulin. Astrocytes fixed after 2 DIV (A & C) or 5 DIV (B & D) for control (A & B) or FSK treated (C & D) cells were labelled with β-III tubulin (1:300 concentration). Astrocytes were treated with 10 µm forskolin (FSK) for 3 hours. Representative images are shown where N = 3 biological replicates, equivalent to three separate astrocyte preparations. Scale bars = 100 µm.

The failure to establish markers which reliably distinguished axons from astrocytes meant attempts to investigate the influence of astrocytes in mixed cultures did not progress.

6.3.3 Microfluidics Chambers for the Study of Astrocyte-Neuron Interactions

To study the interactions between astrocytes and axons in an alternative culture format, compartmentalized microfluidic devices which provide the ability to study two isolated cell types and analyse their specific interactions have been used. The devices had the potential to overcome the co-labelling issue; axons could grow free of astrocytes which could be seeded into the neuronal cell body side. Calcein AM loading (1µM) and live imaging revealed

that neurons survive in the devices but axons did not reliably cross the microgrooves in neuron-only chambers (Figure 9). Neurons were rounded and appeared to be unhealthy in chambers at 5 DIV (in contrast to neurons growing in control 6-well plates which showed the classic extension of axons) and often neurons did not survive past 5 DIV (Figure 9). There was considerable variation between culture preparations and also variation between chambers.

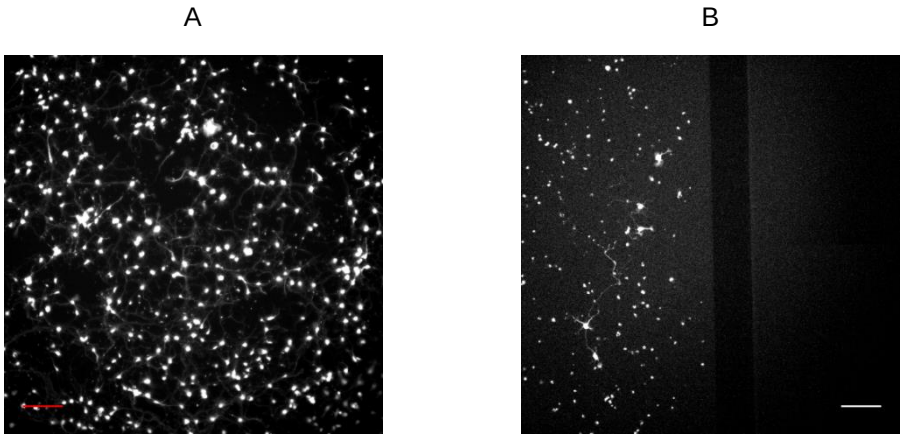


Figure 9. Cortical neuron development in different *in vitro* formats. Neurons were seeded onto either 0.1 mg/ml PLL coated 22 mm coverslips (A) or into compartmentalized microfluidics devices (B) and loaded with 1 µm calcein AM for 30 minutes after 5 DIV. Representative images are shown where N = 9 biological replicates, equivalent to nine separate neuron preparations from nine different sets of embryos. Scale bars = 150 µm.

Neurons that survived more than 5 DIV were unlikely to extend axons across microgrooves and therefore it has not been possible to measure axon length in this *in vitro* format (Figure 10). Estimated 50 µm gaps formed between the channel and microgrooves where no neurons settled and axons did not cross (Figure 10A). Additionally, neurons formed clumps in the channels in some cases which is indicative of a poor *in vitro* culture (Figure 10B).

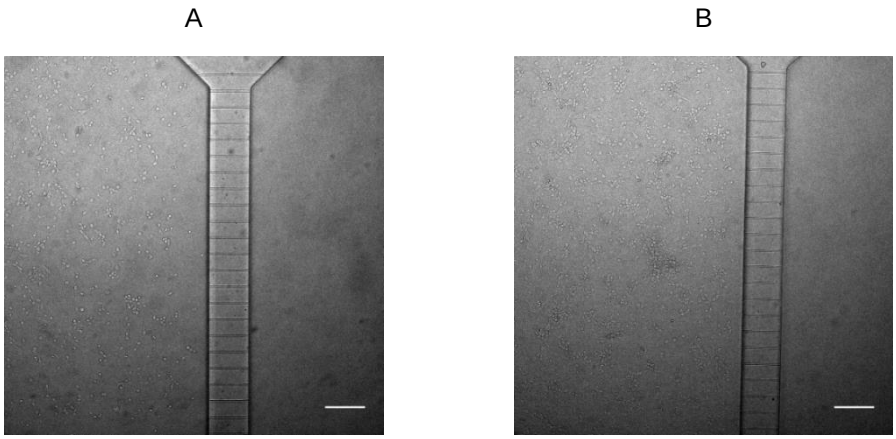


Figure 10. Cortical neuron development in compartmentalized microfluidics devices. Images were taken with bright field after 2 DIV. A) Formation of a gap with no cells occurred between the microgrooves and the channel. B) Cell clumping was observed. Representative images are shown where N = 9 biological replicates, equivalent to nine separate neuron preparations from nine different sets of embryos. Scale bars = 150 µm.

Astrocytes and neurons were co-cultured in microfluidic devices to determine if the presence of astrocytes would influence neuron survival (Figure 11). Neuron survival was improved and cells extended axons across to the astrocyte compartment (Figure 11). However, as with previous exploratory experiments, neurons didn't reliably cross the microgrooves and therefore it has not been possible to measure axon length (Figure 11).

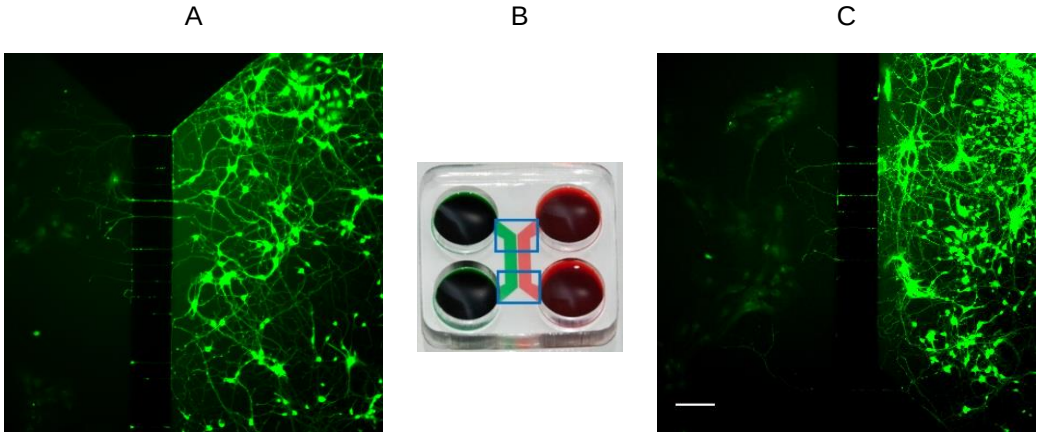


Figure 11. Co-culture of astrocytes and neurons in compartmentalized microfluidics devices. Astrocytes were seeded into the left side (green channel in B) and neurons were seeded into the right side (red channel in B). Astrocytes and neurons were loaded with 1 µm calcein AM for 30 minutes. A) Region represented by the top blue box in B. C) Region represented by the bottom blue box in C. Scale bar = 150 µm.

While the proof of principle of this approach to co-culture has been achieved on occasion, more troubleshooting is required to solve the problems of limited reproducibility.

6.3.4 3D Matrices for Neuron Cell Culture

Neurons encapsulated in 5 mg/ml matrigel were imaged live following calcein AM loading (1 µM) at 2 or 5 DIV. 3D reconstructions of neurons showed that they survived in the hydrogel matrix for up to 5 DIV and it was possible to visualise axon extension from the cell body (Figure 12). This confirms that neuron-astrocyte co-culture in hydrogels would be feasible.

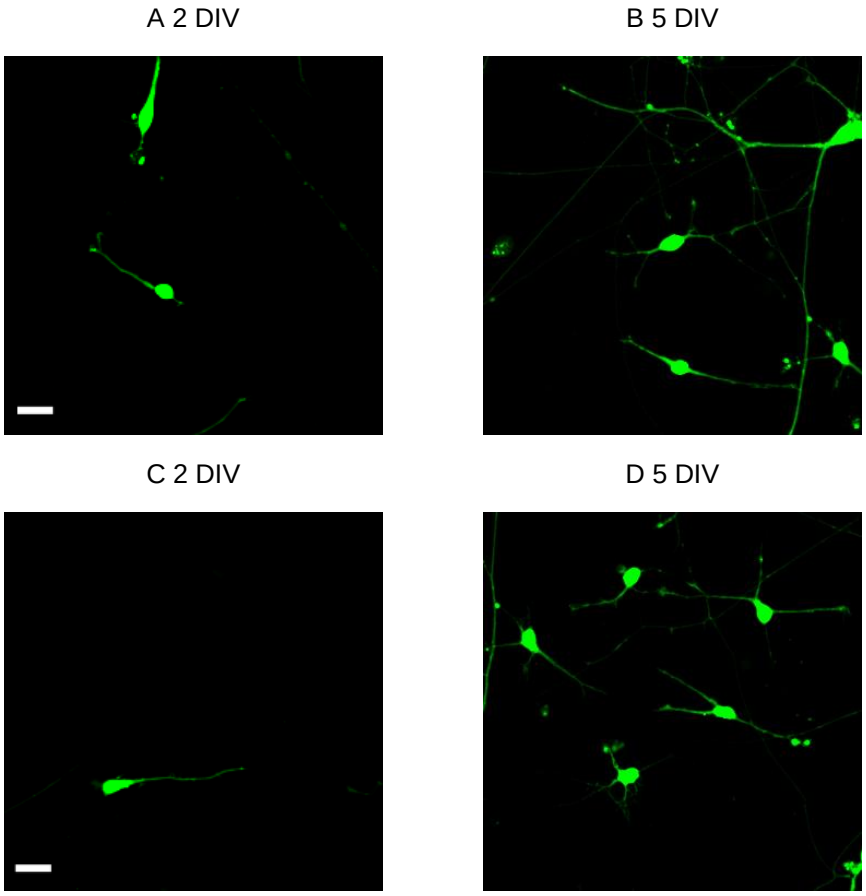


Figure 12. Cortical neuron development in the matrigel matrix. Neurons were cultured in 5 mg/ml matrigel and loaded with 1 µM calcein AM for 30 minutes after 2 DIV (A & C) or 5 DIV (B & D). Representative images are shown where N = 3 biological replicates, equivalent to three separate neuron preparations from three different sets of embryos. Scale bars = 20 µm.

6.3.5 Induced Astrocytes

6.3.5.1 Morphology

To investigate the morphology developed by human iAstrocytes (which were differentiated from iNPCs for 5 DIV) calcein AM loading (1 µM) was carried out for control and FSK treated cells. Both control and FSK treated iAstrocytes were viable (Figure 13). Control iAstrocytes formed a monolayer on the coverslip with fusiform and rounded morphologies (Figure 13A). FSK treated iAstrocytes also had fusiform and polygonal morphologies (Figure 13B), and therefore there were no striking differences between control and FSK treated cell morphology by eye. The usual stellate appearance of primary rat astrocytes treated with FSK was not observed, therefore this suggested that either the iAstrocytes, and/or the neural progenitor cells from which they are derived, may not truly represent this cell type following their derivation from fibroblasts.

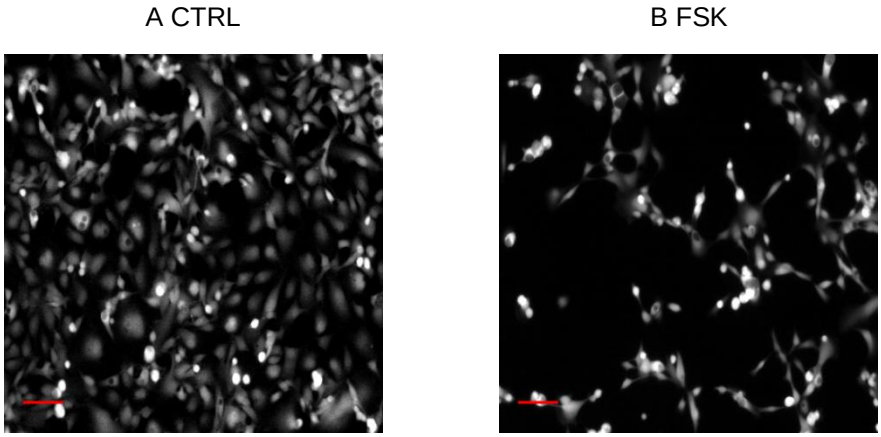


Figure 13. Induced astrocyte (iAstrocyte) viability for control (CTRL) and forskolin (FSK) treated cells. iAstrocytes were loaded with 1 µM calcein AM for 30 minutes and imaged live for control (A) or FSK treated (B) cells. Representative images shown where N = 6 coverslips taken from 2 preparations of the same iNPC cell line. Scale bars = 100 µm.

To determine if FSK treatment reduced cell viability, the number of cells per field of view was counted for control and FSK treated cells. Three fields of view from three coverslips for each condition were analysed and revealed that

FSK treatment significantly reduced the mean number of cells counted (Figure 14). This suggests that FSK treatment interfered with iAstrocyte viability.

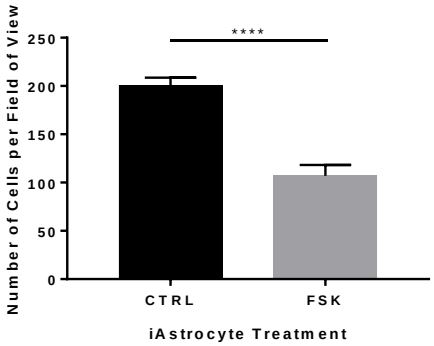


Figure 14. Mean number of cells per field of view for control (CTRL) and forskolin (FSK) treated iAstrocytes. iAstrocytes were cultured on 0.1 mg/ml PLL coated coverslips and loaded with 1 µM calcein AM for 30 minutes prior to imaging. N = 6 coverslips taken from 2 preparations of the same iNPC cell line. Mean ± SEM shown. ****p = <0.0001, Mann Whitney t test.

To discover if iAstrocytes exhibit a similar morphological diversity to primary cells cultured in 2D *in vitro*, cells were fixed and labelled with GFAP after 5 DIV. Due to background fluorescence with GFAP labelled images (Figure 15), it has not been possible to distinguish morphological changes following forskolin addition for control and FSK treated iAstrocytes (Figure 15A & B).

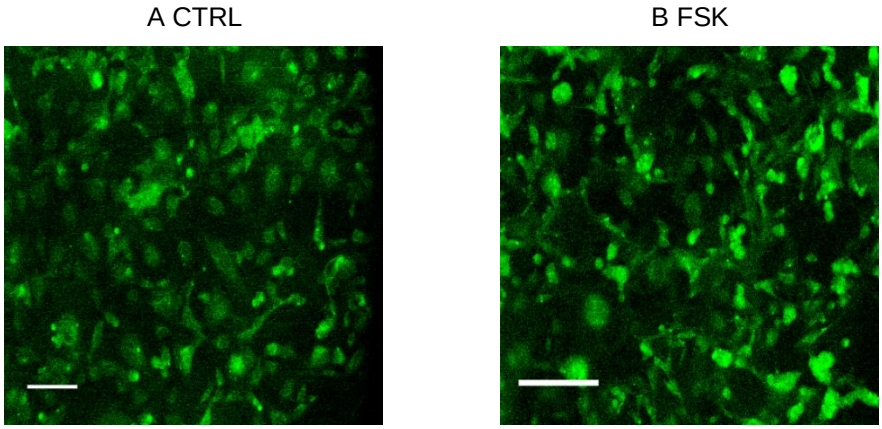


Figure 15. iAstrocyte morphology *in vitro*. Control (A) or FSK treated (B) iAstrocytes were seeded onto 0.1 mg/ml PLL coated 22 mm coverslips and incubated in iAstrocyte differentiation media for 5 days prior to fixing. iAstrocytes were labelled with GFAP primary antibody (green). Representative images are shown where N = 6 coverslips taken from 2 preparations of the same iNPC cell line. Scale bars = 100 µm.

6.3.5.2 Culture in 2D and 3D Environments

Initial morphological characterisations were carried out for iAstrocytes cultured on PLL coated 24-well plates, within 3 mg/ml matrigel and within 5 mg/ml hyaluronic acid. iAstrocytes cultured in all three formats were viable and developed observable heterogeneous morphologies (Figure 16). iAstrocytes cultured in 2D were relatively round with no obvious process extensions from the cell soma (Figure 16A & B). iAstrocytes cultured in 3D matrigel had variable morphologies and developed polygonal cell shapes (Figure 16C & D). iAstrocytes cultured in 3D HA had heterogeneous morphologies (Figure 16E & F). However, the characteristic stellate morphology seen in primary rat astrocytes cultured in hydrogels was not observed for iAstrocytes (see Chapter 5).

6.3.5.3 Detailed Morphology of iAstrocyte Cells Cultured in 2D and 3D

iAstrocyte morphological parameters were analysed from 21 cells in 2D, 33 cells in 3D matrigel and 46 cells in 3D HA generated from one iAstrocyte preparation (equivalent to one donor) (Figures 17 - 19). Volume and surface area distributions showed unimodal right shifted peaks across a similar range for 2D iAstrocytes (Figure 17A & B). Shape factor and longest axis distributions looked to exhibit Gaussian distributions which was confirmed by D'Agostino & Pearson normality tests (Figure 17C & D).

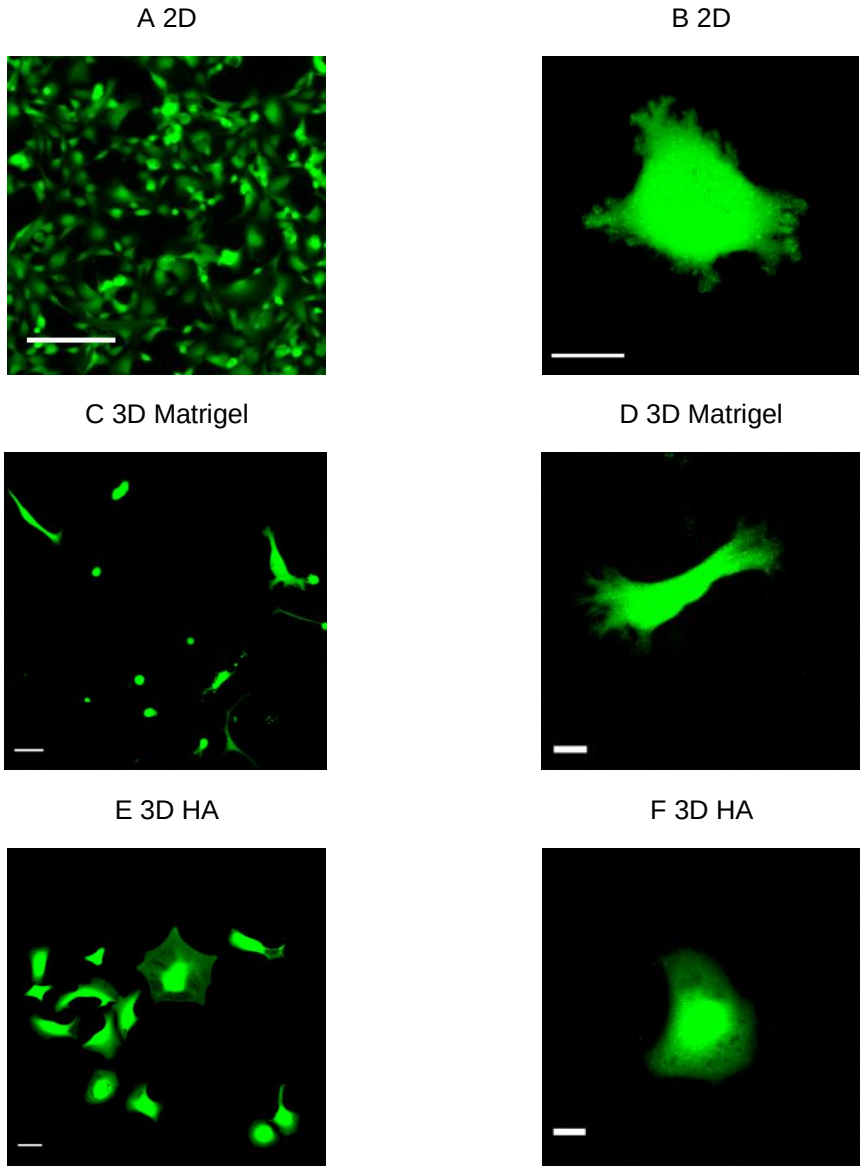


Figure 16. iAstrocyte viability and morphology in different *in vitro* culture formats. iAstrocytes were cultured on 2D poly-l-lysine (PLL) coated 24-well plates (A & B), in 3 mg/ml matrigel (C & D) or in 5 mg/ml hyaluronic acid (HA) (E & F), and were loaded with 1 µM calcein AM for 30 minutes prior to confocal imaging. Representative images are shown where N = 3 preparations of the same iNPC cell line. Scale bars = 50 µm in A, C & F or 20 µm in B, D, & E.

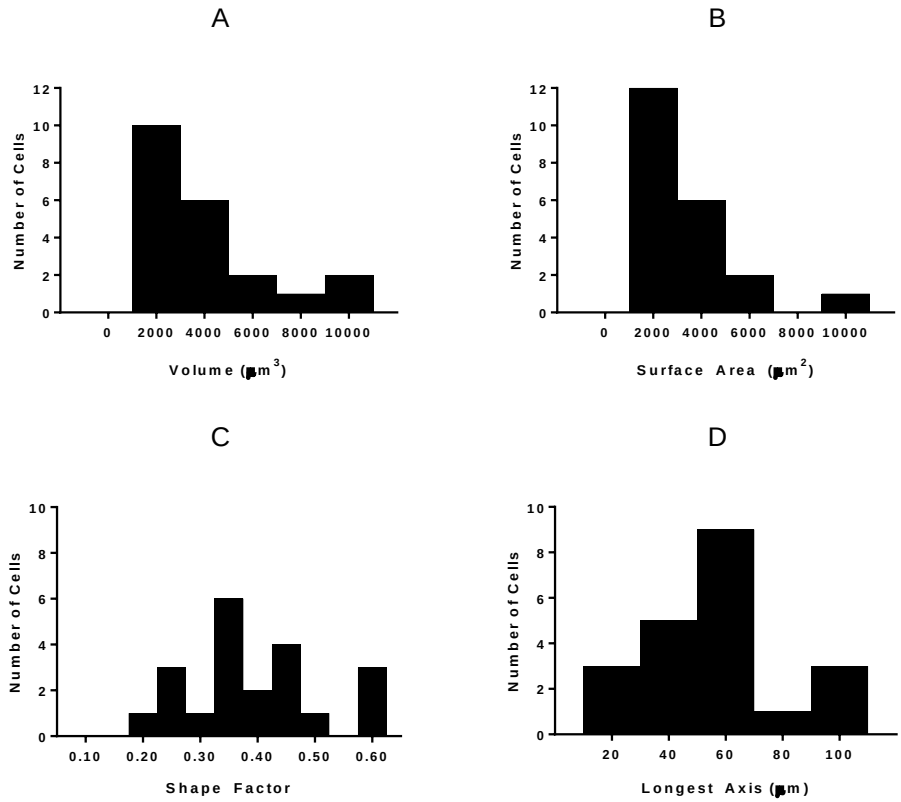


Figure 17. Morphological parameters measured for iAstrocytes cultured on 2D plates. Frequency distribution histograms for iAstrocytes cultured on 0.1 mg/ml PLL coated glass-bottomed 24-well plates. Parameters shown: Volume (μm^3) (A), Surface Area (μm^2) (B), Shape Factor (C) and Longest Axis (µm) (D). N = 21 cells in this initial analysis.

iAstrocytes cultured in 3D matrigel also had unimodal right shifted peaks for cell distribution for volume and surface area parameters, but with a greater range compared to 2D cells (Figure 18A & B). Shape factor and longest axis distributions were Gaussian; whilst shape factor was across a comparable range to 2D, the longest axis for iAstrocytes in 3D matrigel was much greater (Figure 18C & D).

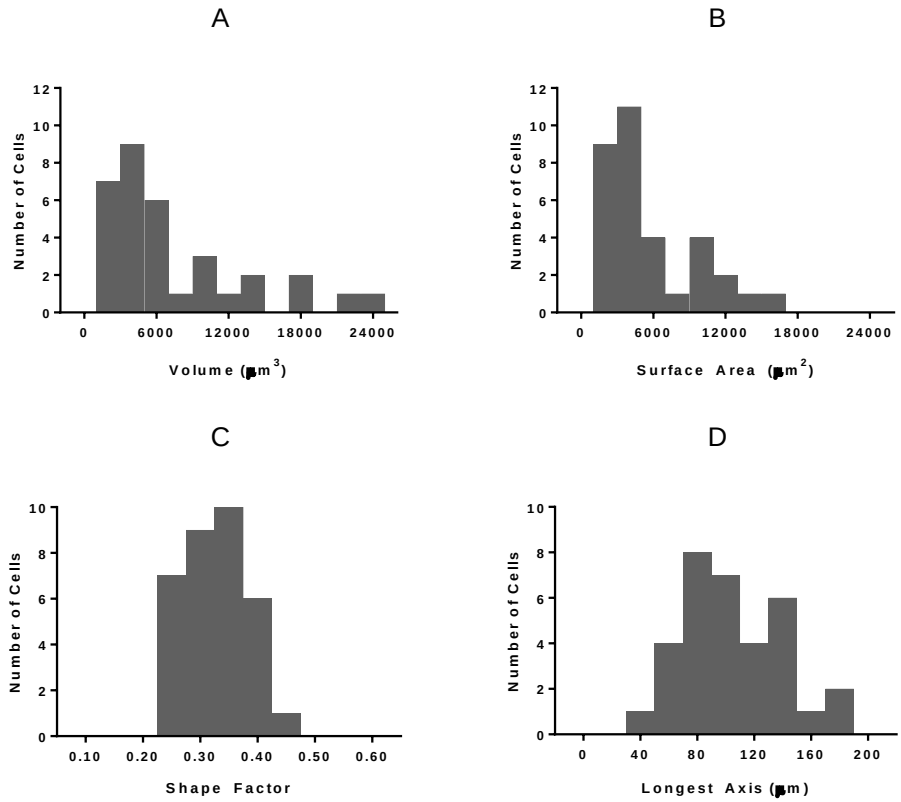


Figure 18. Morphological parameters measured for iAstrocytes cultured in 3 mg/ml matrigel. Frequency distribution histograms for iAstrocytes cultured in 3 mg/ml matrigel. Parameters shown: Volume (μm^3) (A), Surface Area (μm^2) (B), Shape Factor (C) and Longest Axis (µm) (D). N = 33 cells in this initial analysis.

iAstrocytes cultured in hyaluronic acid had right shifted unimodal distributions for volume and surface area measurements which exhibited a greater range than cells in 2D or 3D matrigel (Figure 19A & B). iAstrocyte distributions for shape factor and longest axis were Gaussian and across a similar range to iAstrocytes cultured in matrigel (Figure 19C & D).

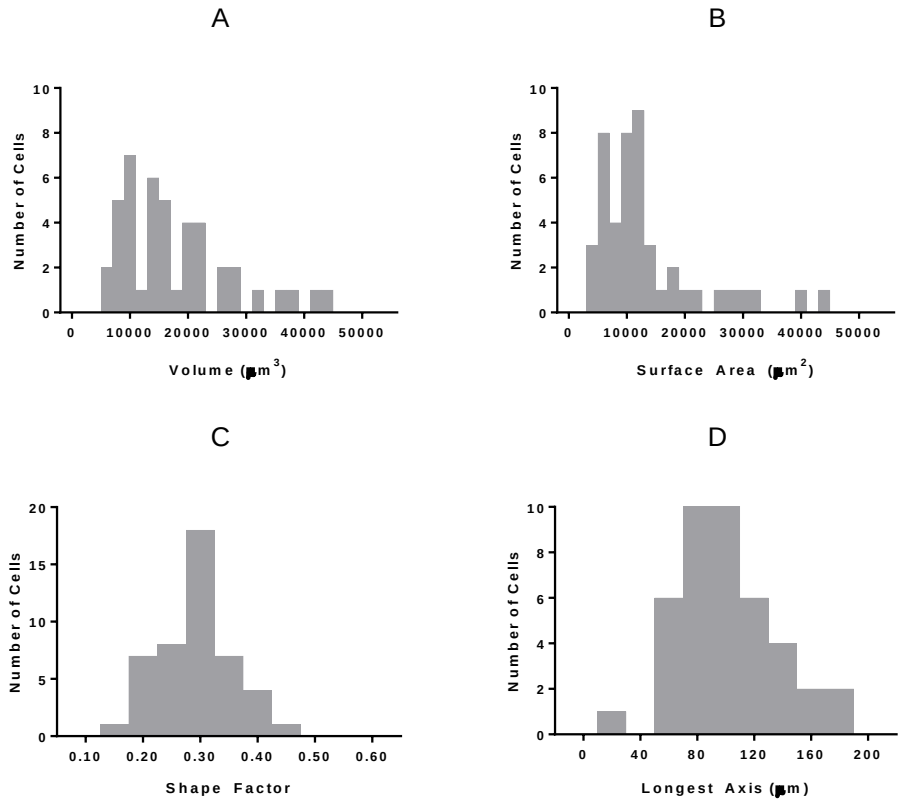


Figure 19. Morphological parameters measured for iAstrocytes cultured in 5 mg/ml HA. Frequency distribution histograms for iAstrocytes cultured in 5 mg/ml hyaluronic acid. Parameters shown: Volume (μm^3) (A), Surface Area (μm^2) (B), Shape Factor (C) and Longest Axis (µm) (D). N = 46 cells in this initial analysis.

6.3.5.4 Statistical Analysis of iAstrocyte Morphologies in Different *In Vitro* Environments

iAstrocyte volume and surface area was significantly greater when cells were cultured in 3D HA compared to 2D and 3D matrigel (p= <0.0001) (Figure 20A & B). iAstrocyte cell volumes and surface areas were approximately three times greater in 3D HA compared to 2D (Figure 20A & B). iAstrocytes cultured in 3D hydrogels had a significantly increased mean for longest axis, which increased from 56 µm in 2D to 105 and 102 µm in matrigel and HA respectively (p= <0.0001) (Figure 20D). Mean shape factor was significantly higher for iAstrocytes cultured in 2D compared to cells in 3D (p = 0.0035 for 2D vs 3D matrigel, p = 0.0294 for 3D matrigel vs 3D HA and p= <0.0001 for 2D vs 3D HA) (Figure 20C).

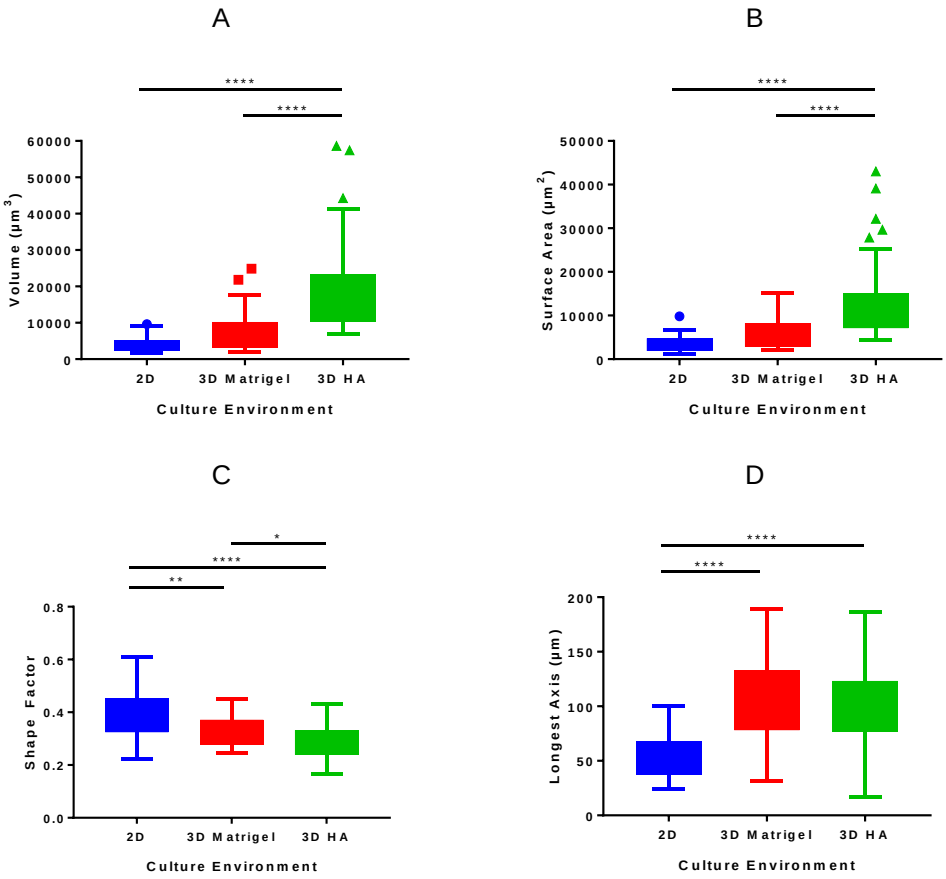


Figure 20. Statistical Analysis of iAstrocyte Morphologies in Different In Vitro Environments. Box and whisker (tukey) plots for iAstrocyte cell volume (A), surface area (B), shape factor (C) and longest axis (D) for cells cultured on either 0.1 mg/ml PLL coated glass-bottomed 24-well plates (2D), within 3 mg/ml matrigel (3D Matrigel) or cells within 5 mg/ml hyaluronic acid (3D HA). N = 21 for 2D cells, 33 for cells in 3D matrigel and 46 for cells in 3D HA. ****p = <0.0001, Kruskal-Wallis ANOVA test with Dunn's correction for multiple comparisons in A and B. Ordinary one-way ANOVA with Tukey's multiple comparisons test in C and D.

Surface area to volume ratios were calculated in order to distinguish geometric differences for iAstrocytes cultured in the different culture environments (Figure 21). Surface area to volume ratio distributions showed unimodal Gaussian distributions across a similar range (confirmed by D'Agostino & Pearson normality tests) for 2D and 3D matrigel culture conditions (Figure 21A & B). In contrast, iAstrocytes cultured in 3D HA showed a right shifted unimodal peak across a smaller range (Figure 21C). Following analysis revealed that the mean surface area to volume ratio for iAstrocytes in HA was significantly smaller compared to cells in matrigel or in

2D (p = 0.0008 for 2D vs 3D HA, and p = <0.0001 for 3D matrigel vs 3D HA) (Figure 21D).

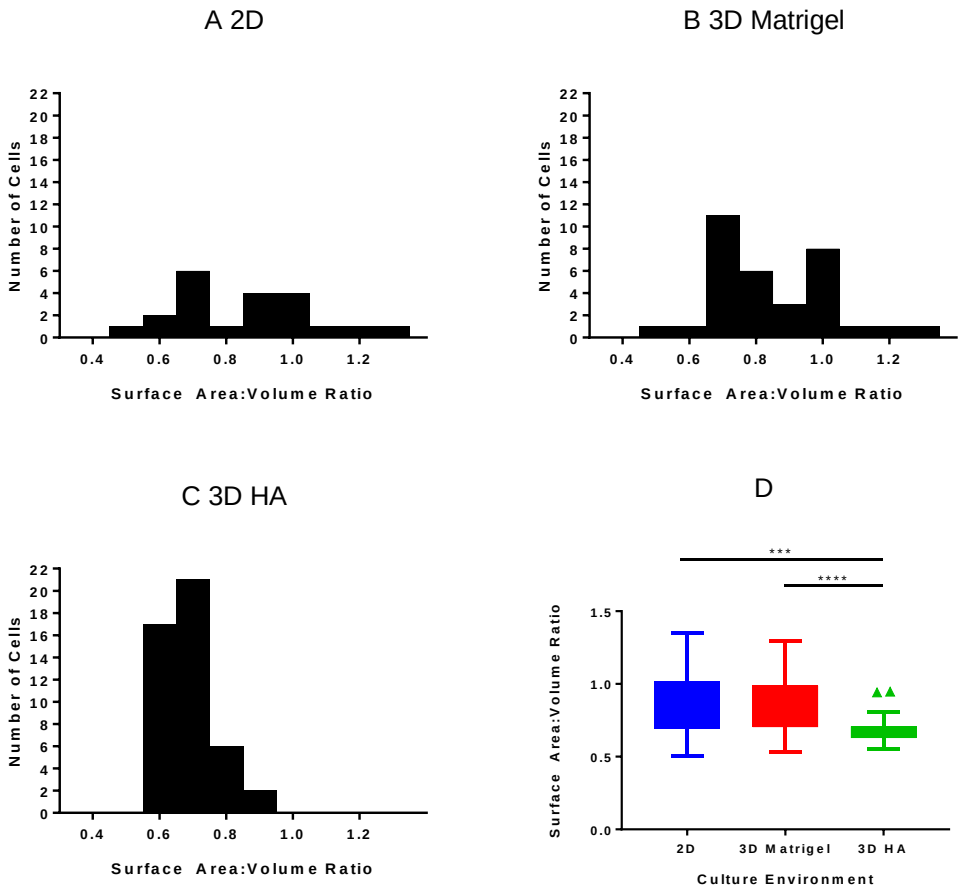


Figure 21. Surface area to volume ratio analysis for of iAstrocytes cultured in different *in vitro* environments. Frequency distribution histograms and a box and whisker (tukey) plot for iAstrocyte surface area to volume ratio for cells cultured on either 0.1 mg/ml PLL coated glass-bottomed 24-well plates (2D), within 3 mg/ml matrigel (3D Matrigel) or cells within 5 mg/ml hyaluronic acid (3D HA). N = 21 for 2D cells, 33 for cells in 3D matrigel and 46 for cells in 3D HA. ****p = < 0.0001, Kruskal-Wallis ANOVA test with Dunn's correction for multiple comparisons in D.

6.3.5.5 Comparison of Primary Rat and Human iAstrocyte Morphology

To discover if iAstrocytes differ in their morphology from primary rat astrocytes, preliminary iAstrocyte data and the complete primary astrocyte data set were compared using relative frequency distributions (Figure 22). iAstrocytes cultured in 2D had smaller volumes and surface areas compared

to primary astrocytes (Figure 22A & B). For iAstrocytes, 86% of cells had a volume of 6,000 μm^3 or less, whereas only 20% of primary astrocytes had a volume of 6,000 μm^3 or less (Figure 22A & B). Whereas 95% of iAstrocytes had a surface area of 6,000 μm^2 or less, only 22% of primary astrocytes had a surface area of 6,000 μm^2 or less (Figure 22A & B). iAstrocytes also had smaller volumes and surface areas, and a reduced range in both instances, compared to primary astrocytes when both cell types were cultured in 3D matrigel (Figure 22C & D). The median volume for iAstrocytes was 5,131 μm^3 which was increased to 16,446 μm^3 with primary astrocytes. Similarly, the median surface area for iAstrocytes was increased from 4,259 μm^2 with iAstrocytes to 17,738 μm^2 in primary astrocytes (Figure 22C & D). In contrast, relative frequency distributions and medians for cell volume and surface area for iAstrocytes and primary astrocytes were closely similar when cultured in 3D HA (Figure 22E & F).

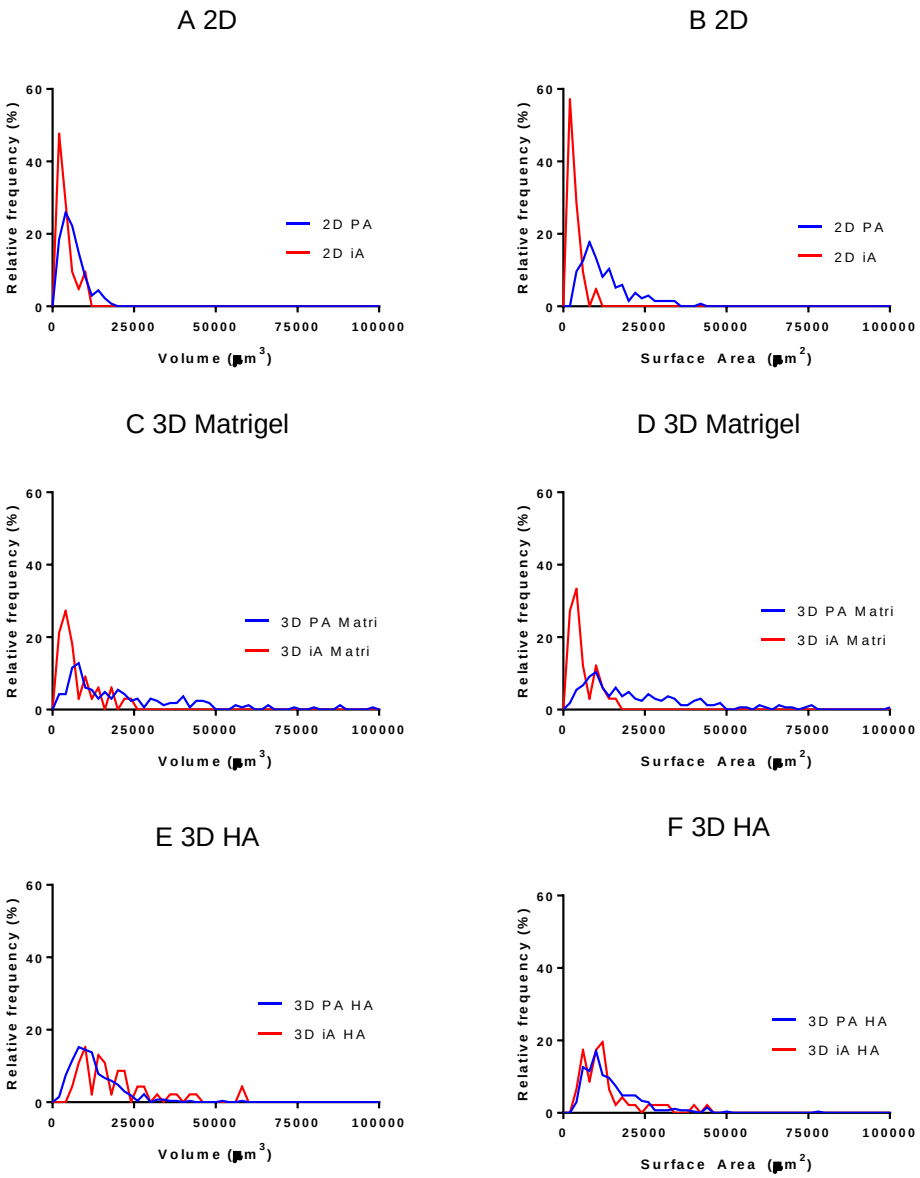


Figure 22. Comparison of Primary Rat and Human iAstrocyte Morphology. Relative frequency distributions for volume (μm^3) and surface area (μm^2) of primary rat astrocytes and iAstrocytes when cultured in 2D (A & B), 3D matrigel (C & D) or 3D HA (E & F). For primary astrocytes: N = 135 for 2D cells, 165 for 3D matrigel & 269 for cells in 3D HA. For iAstrocytes: N = 21 for 2D cells, 33 for cells in 3D matrigel and 46 for cells in 3D HA. PA = Primary Astrocytes, iA = Induced Astrocytes, 2D = Cells cultured in 2D, 3D = Cells cultured within 3D Matrices, Matri = Matrigel, and HA = Hyaluronic Acid.

6.4 Discussion

Successful investigation of neuron-astrocyte interactions *in vitro* requires the development of conditions in which co-cultures can be established, and neurons and astrocytes distinguished. This proved more challenging than anticipated.

6.4.1 2D Culture of Primary Neurons

Primary rat embryonic (E18) cortical neurons were generated to assess their growth and development, and evaluate the influence of astrocytes on axon growth and development. Primary neurons developed neurites by 2 DIV and a clear defined axon by 5 DIV which demonstrates that acetylated tubulin and β-III tubulin images provided useful markers of axon and dendrite development in healthy neurons (Figures 3 & 4). Axon length analysis revealed that mean length significantly increased from 2 to 5 DIV (Figure 5). Axon length analysis was not possible for cells fixed at 12 DIV since a high density of neuronal processes prevented the clear definition of individual neurons and axons (Figures 3C & 4C). Thus an alternative approach to study axon development is necessary: one strategy would be to measure the overall labelling intensity of acetylated tubulin or β-III tubulin, with the assumption that the overall density of fibres would be proportional to the rate of growth of individual axons.

In summary, the growth and development of our cortical neuron cultures was characteristic of *in vitro* cultured cells (Dotti, Sullivan and Banker, 1988; Dajas-Bailador, Jones and Whitmarsh, 2008), however, the study of axon development would benefit from a more sophisticated *in vitro* model.

6.4.2 3D Culture of Primary Neurons

Neuron physiology observed in traditional 2D culture, where there are no cell-cell and cell-matrix interactions in contrast to the *in vivo* environment, may lead to a misinterpretation of neuron function. Primary neuronal cells can be cultured in 3D *in vitro* culture models which have the benefits of more accurately reflecting neural responses *in vivo* (LaPlaca *et al.*, 2010). In this

study I have successfully cultured primary embryonic (E18) cortical neurons in 5 mg/ml matrigel for up to 5 DIV, and observed neurite and axon extension from the cell body (Figure 12). LaPlaca *et al*., (2010) successfully maintained primary neuronal cultures in 3D matrigel for up to 21 DIV and discovered that the viability of cultures was found to be highly influenced by cell density. Neurons developed a typical morphology, but with more elaborate process extension compared to 2D cells (LaPlaca *et al.*, 2010).

Furthermore, matrigel is a suitable 3D matrix for the culture of primary neuronal cultures since these data confirm that neurons are viable and develop characteristic neurite and axon extension (Figure 12). Neurons therefore grow under the same culture conditions suitable for astrocyte culture as established in earlier chapters. Despite this, it must be taken into consideration that the matrigel matrix is not highly representative of the brain microenvironment, and in the future it would be useful to confirm whether neurons are viable in hyaluronic acid since this is a physiologically relevant hydrogel.

6.4.3 Astrocyte and Neuron Co-Culture

Co-culturing cells *in vitro* has long been used to understand more about the interactions of neurons and astrocytes, and the aim of this study was to determine the astrocytic influence on axon growth when seeding neurons on top of a monolayer of astrocytes in 2D culture. Neurons were fixed and labelled following culture with control or FSK treated astrocytes with either acetylated tubulin or β-III tubulin at 2 or 5 DIV. However, it was not possible to discriminate axons and neurites from underlying astrocytic processes (Figure 6). Unexpectedly, this study found that astrocytes were also robustly labelled for these ‘neuron-specific’ markers (Figures 7 & 8). Therefore it has not been possible to measure axon length in response to the presence or absence of astrocytes, and alternative markers are required to achieve this, for example, the use of NeuN or MAP2.

Whilst the expression of tubulin isoforms has been typically well studied in neurons, less attention has been paid to its expression in astrocytes. β-III

tubulin has been found in primary mouse astrocytes: β-III tubulin chains increased between 7 and 12 DIV and remained present for the rest of the culture period which was not changed even following forskolin treatment (Charriere-Bertrand *et al.*, 1989). β-III tubulin expression has also been confirmed in developing GFAP expressing human astrocytes from cerebral hemispheres (Dráberová *et al.*, 2008). Positive expression of both acetylated tubulin and β-III tubulin expression (which highly resembled one another morphologically) has also been found in human cell lines (Knight and Serrano, 2017). Such *in vitro* findings are consistent with findings *in situ* where β-III tubulin has been found to co-localize with GFAP positive immature glial cells in human fetal brain sections (Dráberová *et al.*, 2008).

In summary, while β-III tubulin has long been used as a key neuronal marker, in recent years it has become increasingly recognised for its expression in other cell types, including astrocytes. This confirms the need for other neuron-specific markers that can be used to distinguish astrocytes from neurons in simple co-culture formats.

6.4.4 Microfluidics Chambers

Research to fully comprehend extracellular signals which guide neuronal development and axon growth is still required. Common 2D culture techniques using coverslips are not sophisticated enough to replicate the differing chemical aspects of a neuron's microenvironment *in vivo*, but, microfluidic devices allow the design of specifically tailored microenvironments for different cell compartments and cell types (Millet and Gillette, 2012). Microfluidics devices additionally offer the potential to study neuronal networks *in vitro* by orientating their interactions to reveal neural network properties, helping to elucidate the basic mechanisms of information transmission and its regulation. Gladkov *et al.*, (2017) seeded two sub populations of primary hippocampal neurons in a microfluidic device with asymmetric channels to promote growth in one direction and assessed and compared neurite dynamics, as well as investigating unidirectional spiking pattern and propagation via microelectrode arrays. Morphological and

functional connectivity between the two subpopulations was maintained for up to 25 DIV (Gladkov *et al.*, 2017).

Microfluidics devices also offer great utility for the study of the interactions between neurons and astrocytes: micro-patterned surfaces can guide interactions between the two cell types which are positioned in defined locations. Gao *et al*., (2016) demonstrated the possibility of analysing neuron-astrocyte interactions under physiological and pathological conditions using genetically encoded calcium indicators and the measurement of amplitude and frequency in calcium signalling. It was found that spontaneous and evoked calcium dynamics in astrocytes are modulated by neurons (Gao *et al.*, 2016).

I have successfully co-cultured astrocytes and neurons in compartmentalised microfluidics devices but reproducibility was poor, limiting progress (Figure 11). Cell viability issues with the compartmentalized microfluidic chambers were common, where neurons did not survive past 5 DIV (Figure 9). Cell viability issues are not uncommon in PDMS devices (the material originally used for Xona Microfluidics devices). Millet *et al*., (2007) found that rat primary postnatal hippocampal neuron survival increased from 2 to 7 DIV when PDMS devices underwent serial washes with solvents to remove un-crosslinked oligomers for the improvement of biocompatibility. PDMS has commonly been used for microfluidic devices because it is simple to manufacture, is optically transparent and reversibly adheres to substrates, but the leaching of uncured oligomers from the polymer network into cell culture media may inhibit primary neuron survival (Regehr *et al.*, 2009). Therefore, PDMS devices are not ideal for primary cell culture and it is possible that it influenced the viability of my cortical neuron cultures. I suggest that alternative materials, e.g. silicone, could be used preferentially for microfluidic device designs in the future.

6.4.4.1 Designing Devices for Cellular Compartmentalization in 3D

Coupling compartmentalized microfluidics devices with 3D culture techniques has the potential to develop a sophisticated *in vitro* culture model. It would

allow analysis of cellular interactions in an *in vitro* environment that mimics the brain extracellular matrix more closely than 2D culture techniques.

Huang *et al*., (2009) have previously seeded a metastatic breast cancer cell line in a collagen type I hydrogel, and a macrophage cell line in a matrigel ECM, side by side in a microfluidics chamber. Normal physiological function was observed for macrophage cells which invaded into the neighbouring gel (Huang *et al.*, 2009), suggesting that such *in vitro* culture models are suitable for the study of cellular interactions.

In this study initial investigations into the feasibility of developing a compartmentalized microfluidic device coupled with 3D matrices to study astrocyte-neuron interactions has been conducted. The viability of both neurons and astrocytes has been confirmed when grown for up to 5 DIV in matrigel (Figure 12 & Figure 8 from Chapter 5). Thus, I believe it will be possible to independently mix astrocytes or neurons with matrigel and seed them into the relevant sides of a compartmentalized device.

Rather than separating astrocytes and neurons via a microgroove barrier like in Xona microfluidics devices, it could be replaced with a more physiological entity such as a polycarbonate membrane which is biologically inert. Polycarbonate membranes are barriers offering controlled diffusion of biological agents (Figure 23).

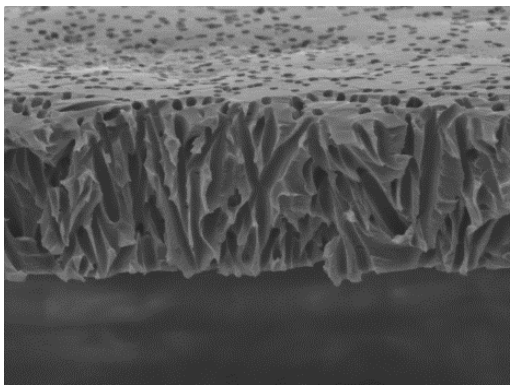


Figure 23. An electron micrograph of a polycarbonate membrane with a series of 5 µm pores throughout the membrane. Image taken from: http://www.atl.semtechsolutions.com/node/18/membrane-filtration-technology.

Polycarbonate membranes can contain up to 5 micron pore sizes meaning that axons could migrate through the barrier, but it is likely to exclude astrocytes processes, thus the influence of astrocytes on axon growth could be measured. Microporous membranes are proven to support the growth of axons into and through micro-channels between 0.8 and 5 microns in diameter (George *et al.*, 2018). The porous membrane can act as a permissive substrate that supports neuronal attachment and growth, as well as a restrictive substrate that limits the interactions between the cultures on either side of the membrane. Furthermore such microporous membranes would facilitate the maintenance of separate neural populations whilst permitting neurite contact between cultures.

6.4.5 Induced Astrocytes

Reprogramming human fibroblasts to induced neural progenitor cells, followed by differentiation into iAstrocytes, provides a new source to study human astrocytes. iNPCs, which had been differentiated for 21 DIV, were then differentiated with human iAstrocyte differentiation medium for 5 DIV to assess control and forskolin treated cell morphology (Figures 13 & 15). FSK treatment didn't result in any striking morphological changes in iAstrocytes following calcein loading (Figure 13) and it has not been possible to discover if FSK treatment causes a dramatic rearrangement to the iAstrocyte cytoskeleton (Figure 15). FSK treatment may evoke iAstrocyte cell death since there was a significant reduction in the number of cells counted per field of view (Figure 14). To determine if forskolin influences adenylyl cyclase activity in iAstrocytes, cAMP levels could be measured to detect if there has been an increase in cAMP.

iAstrocytes cultured on 2D plates, within 3 mg/ml matrigel or within 5 mg/ml hyaluronic acid exhibited a range of rounded, polygonal and fusiform morphologies (Figure 16). Compared to primary rat astrocytes, iAstrocytes cultured in matrigel or HA have few cells with defined process extension from the cell soma (Figure 16 and Figure 8 from Chapter 5). Oberheim *et al.,* (2009) previously discovered that human astrocytes have 10-fold more primary GFAP processes compared to mouse astrocytes, therefore, I believe

that differentiating iNPCs for 5 days is insufficient to generate iAstrocytes. I suggest that iAstrocytes require a longer differentiation period *in vitro* to fully transition to classical astrocyte morphology: I recommend exposing iNPCs to iAstrocyte differentiation media for greater than 7 days, as initial investigations with iNPC differentiation for 7 DIV displayed no clear differences to iNPCs differentiated for 5 DIV.

iAstrocytes cultured in HA were significantly greater in volume and surface area compared to cells cultured in matrigel or in 2D (Figure 20A & B). The longest axis for iAstrocytes cultured in HA was also significantly increased compared to cells in 2D (Figure 20D). This suggests that the culture of iAstrocytes in HA encourages cell growth since cells are larger. Additionally, the significantly decreased surface area to volume ratio for iAstrocytes cultured in HA (Figure 21D) implies that cells cultured in HA are more elongated compared to cells cultured in matrigel or on 2D plates.

iAstrocytes cultured in 2D have a significantly higher shape factor compared to cells in 3D gels (Figure 20C) which implies that cells have more rounded morphologies (as seen in Figure 16A & B). A significantly increased shape factor was also found for primary rat astrocytes cultured in 2D compared to 3D culture (Figures 20E & 12E from Chapter 5) which suggests that the 2D environment inhibits both primary astrocytes and iAstrocytes from developing physiological morphology.

By comparing the relative frequency distributions for volume and surface area for the preliminary iAstrocyte data set with the complete primary astrocyte data set, it can be observed that iAstrocytes are smaller than primary astrocytes when cultured in 2D or 3D matrigel (Figure 22A - D). These findings are in contradiction with those in the literature which state that human astrocytes are larger in diameter than rodent astrocytes (Oberheim *et al.*, 2009). Again, this may result from iAstrocytes not having been differentiated for long enough in culture to develop a typical human astrocyte phenotype.

For iAstrocytes in 2D, the influence of surface coating is undetermined: initial experimentation suggested that fibronectin may support growth and

development more than PLL. If this was determined, this would provide insight into the phenotypic properties of the iAstrocytes when cultured in 2D. Fibronectin promotes complete adhesion of fibroblasts which subsequently develop characteristic morphology (Woods *et al.*, 1986), thus if iAstrocyte growth is better on fibronectin, perhaps iAstrocytes still retain some fibroblast features and are not fully differentiated. This is one possible explanation for the finding that iAstrocytes do not develop a similar morphology to primary rat astrocytes.

A possible alternative surface coating for glass coverslips for the culture of iAstrocytes would include tenascin C. Tenascin C coating has been shown to induce a quiescent phenotype for adult human astrocytes, which showed fewer scar properties, compared to cells cultured on other ECM proteins or PLL in 2D (Holley *et al.*, 2005).

Furthermore, a full characterisation of iAstrocyte phenotype is necessary to confirm whether such cells can be identified as astrocytes and used as a replacement for rodent tissue in *in vitro* studies. Morphological characterisations will facilitate understanding about whether a similar morphological diversity exists in 2D for iAstrocytes and primary cells. Additionally, screening a range of different neurotransmitter receptor classes will determine the expression profile of iAstrocytes and any differences that exist compared to primary cells.

6.4.6 Conclusion

Sophisticated *in vitro* models offer the potential to study astrocyte and neuron interactions with great experimental control and their development is integral to understanding more about neuron-glial communication. It is possible to co-culture astrocytes and neurons in compartmentalized microfluidics devices, and both cell types can survive in matrigel. Additionally, human iAstrocytes can grow in matrigel. Taken together, I hope that these findings will contribute to the possibility of creating a tailored 3D microfluidics system where astrocytes and neurons can be cultured in hydrogel matrices in channels separated by a polycarbonate membrane.

Chapter 7. Discussion

7.1 Aims and Objectives

Throughout the central nervous system (CNS), there are tripartite synapses which comprise of the presynaptic membrane, postsynaptic density and surrounding glial processes, which form a functional unit in the neural network as a result of the close proximity of astrocyte and neuron anatomical domains. This organisation which enables glia to respond to synaptic activity and consequently regulate it, through bidirectional communication mediated by both neurotransmitters and gliotransmitters, was first described in the 1990s (Perea, Navarrete and Arague, 2009). This suggested that glial cells are not merely support cells in the CNS, but have integral roles in information processing; furthermore many researchers now agree that brain function results from coordinated activity in a network of neurons and glia.

Considering that interactions between neurons and glia are at the heart of healthy neurophysiology, breakdown of communication between these cell types is implicated in a wide range of neurodegenerative conditions (Verkhratsky *et al.*, 2014). The numerous roles of astrocytes, and their influences on neurons, still remain to be elucidated and our ultimate goal has been to work towards developing a superior *in vitro* culture model for the study of astrocyte-neuron interactions.

Astrocytes are a heterogeneous cell type exhibiting various morphologies, functions and gene expression profiles when originating from different brain regions (Bayraktar *et al.*, 2015). Considering that astrocytes are highly responsive to their external environment, we have investigated two elements of the *in vitro* culture microenvironment on astrocyte phenotype: cell culture media treatment and the physical substrate of the environment.

Mechanisms of neuron-glial communication have been well studied in the cerebellar cortex where Bergmann glia carry out homeostatic roles to prevent excitotoxicity to Purkinje neurons (Bellamy, 2006). I have investigated vesicle distribution at proposed ectopic sites, prior to and post stimulation protocols

that theoretically deplete this vesicle pool, to understand more about the dynamic changes in glial structure following ectopic transmission.

The study of human astrocytes has revealed their increased complexity compared to primary rodent astrocytes (Oberheim *et al.*, 2009). Thus, studying human astrocytes *in vitro* will determine species-specific properties of astrocytes and generate more translatable clinical findings. A new way to study human astrocytes involves viral reprogramming of skin fibroblasts extracted in biopsies (Meyer *et al.*, 2013). To validate induced astrocytes (iAstrocytes) as a source of human tissue for neuroscience studies, I have started to categorize iAstrocyte morphology and deduce their expression of key astrocytic markers.

7.2 Primary Astrocyte Phenotype *in Vitro*

Astrocyte morphology depends on a number of elements and can change following traumatic insults which induce astrocyte reactivity (Pekny and Nilsson, 2005). For example, nine types of spinal cord astrocytes have been identified in the central nervous system (CNS) (Black, Sontheimer and Waxman, 1993). In this project, studies have been conducted with postnatal (P2) primary rat astrocytes generated from the cortex, thus, the variation in cell morphology observed may reflect that culture generation has occurred from a large area of the brain, containing various types of astrocytes specialized for function.

I have investigated cortical astrocyte morphology and function when cultured on 2D coverslips. The heterogeneous morphology of astrocytes was confirmed via immunofluorescent labelling with the cytoskeletal marker GFAP and the S100β binding protein, as well as calcein AM loading (Figure 1, Chapter 4, page 71). The induction of stellation was confirmed following forskolin treatment, and the dramatic change to astrocyte morphology was observable (Figure 2, Chapter 4, page 72).

Astrocyte function was assessed via calcium signalling since intracellular calcium concentration elevation in astrocytes in response to activity in the neural network is characteristic of primary astrocytes (Agulhon *et al.*, 2008).

High percentages of responding cells to ATP and glutamate were observed, and heterogeneity was found in individual cell responses (Figures 3 & 4, Chapter 4, pages 73 & 75).

Characterising astrocyte phenotype under basal conditions in 2D environments was essential to understand morphological and functional changes to astrocytes in response to different media compositions and different culture environments. This is necessary both to understand the influence of buffer composition on astrocyte physiology, but also to design experiments for the co-culture of neurons and astrocytes, which would separately be cultivated in different media.

For many years the study of astrocytes has involved their extraction from rodent cortical brain tissue, where cells are subsequently cultured on coated 2D surfaces in order to study isolated pure cell populations (Toh *et al.*, 2007). A wealth of knowledge on astrocyte physiology and pathology has been extensively investigated with 2D techniques and confirmed the active roles of astrocytes, however there are undeniable caveats to this common practice (Lange *et al.*, 2012). Firstly, astrocytes are extracted for culture at a developmental time point when they are immature (Cahoy *et al.*, 2008; Foo *et al.*, 2011), and secondly, astrocytes are taken from the 3D brain microenvironment to be cultured on a 2D surface. To counteract experimental practice with immature astrocytes, many researchers use foetal bovine serum (FBS) supplementation in the media (Fang *et al.*, 2017). Whilst this helps to derive mature astrocytes, the influence of serum on the gene expression of developing primary astrocytes is not characterised (Van Der Valk *et al.*, 2004) and thus, such experimental data may not be reliably replicated *in vivo*.

Cell culture studies with both neurons and astrocytes in 3D environments result in cells exhibiting normal function and molecule expression in comparison to culture with 2D substrates (Balasubramanian *et al.*, 2016). Balasubramanian *et al., (*2016) investigated the effects of dimensionality with GFAP-expressing primary postnatal cerebral cortex astrocytes, and found four different morphological groups *in vitro* (round, bipolar, stellate and perivascular) which varied between 2D and 3D populations. When cultured in

a 3D collagen hydrogel the astrocyte population transformed from largely rounded morphologies with some bipolar cells, to a population of stellate and perivascular cells after a few days (Balasubramanian *et al.*, 2016). Astrocytes cultured in this way developed morphologies resembling those frequently found *in vivo* (Balasubramanian *et al.*, 2016). In contrast, astrocytes cultured in 2D were mainly rounded, with few stellate protoplasmic cell morphologies (Balasubramanian *et al.*, 2016). In addition to this, primary astrocytes in 2D cultures are known to be highly reactive limiting the utility of data generated with such *in vitro* methods, and meaning it is difficult to determine further activation in such models (East, Golding and Phillips, 2009). Ultimately, 2D *in vitro* models are poorly representative of the CNS, whereas 3D models can recapitulate the geometry, matrix density, and molecular composition of the extracellular matrix (Lee, Cuddihy and Kotov, 2008).

To address the notion that 2D techniques can't replicate the 3D environment of tissues, researchers in many biological fields are now employing the use of 3D scaffolds and hydrogels to culture various cell types (Mohand-Kaci *et al.*, 2012; Bian *et al.*, 2013; Jiglaire *et al.*, 2014; Worthington, Pochan and Langhans, 2015; Luo *et al.*, 2018). Considering the influence the microenvironment can have on astrocyte function, I have both addressed the impact of culture media, as well as 2D and 3D environments, on astrocyte phenotype.

7.3 Effect of Cell Culture Media on Astrocyte Phenotype

Astrocytes are highly responsive to their environment and I have found that the cell culture media used in 2D *in vitro* techniques can strongly influence astrocyte phenotype. Thus, careful selection of culture media for 2D culture is critical – it is important to reproduce conditions similar to those found in the brain microenvironment in order to generate translatable data.

With the intent to co-culture astrocytes and neurons in compartmentalised microfluidic devices (see section 4.1.4), it was important to determine the

influence of neuronal media on astrocyte phenotype. We investigated both morphological features, and functional responses, of astrocytes cultured with either astrocyte medium (AM), neuronal medium (NM) or neurobasal supplemented with glutamax (NB+G). Astrocytes cultured in NM developed strikingly different morphologies compared to astrocytes cultured in AM (Figures 5 & 6, Chapter 4, pages 77 & 78). We also found that astrocytes cultured with NM had significantly higher percentages of stellate cells from 7 DIV to the end of the time course (Figure 8, Chapter 4, page 80).

Cell shape analysis demonstrated that astrocytes cultured with NB+G had significantly smaller volumes, surface areas and longest axes compared to astrocytes cultured with the other media compositions suggesting that NB+G doesn't support astrocyte growth and development (Figure 7, Chapter 4, page 79). Additionally, we observed that both NM and NB+G media didn't support cell growth across the 14 DIV time course as the number of cells counted per coverslip significantly decreased from 2-14 DIV (Figure 9, Chapter 4, page 82).

Whilst AM and NM media treatments resulted in no change in the percentage of astrocytes responding to ATP following FSK treatment, in contrast, NB+G media treatment with FSK treatment caused a significant increase in the percentage of cells responding (Figure 10, Chapter 4, page 83). Glutamate addition to astrocytes treated with all of the three defined media treatments resulted in a significantly decreased percentage of responding cells following FSK treatment (Figure 11, Chapter 4, page 84).

Determining the phenotype of primary astrocytes in NB+G media was necessary to understand the influence of B27 supplement on primary astrocytes; B27 is frequently added to neuronal cultures to accelerate neurite outgrowth and for long term survival (Brewer, 1995; Kunze *et al.*, 2011). However, it has been found that it can negatively affect synaptic plasticity and neurite integrity, and there is variability in its quality due to the different sources it is obtained from (Chen *et al.*, 2008). My data show that NB+G media treatment for primary astrocytes resulted in a significant increase in the percentage of cells responding to ATP following FSK treatment, compared to

AM media treatment, suggesting that there are alterations to cell-surface receptor expression. Considering that there is now evidence to suggest that serum-free astrocyte conditioned media enables more realistic *in vivo* neuron characteristics, including neuronal outgrowth, network activity, and growth cone shape and size (Pozzi *et al.*, 2017), I believe it will be important to find one cell culture media for both cell types.

In conclusion I have found that astrocyte morphology, function and receptor expression is altered when cultured with neuronal medium or neurobasal supplemented with glutamax. Thus, co-culturing astrocytes and neurons in compartmentalized microfluidics devices will not be straight forward and a medium composition that supports axon growth and development whilst retaining the *in vitro* phenotype of astrocytes is required.

7.3.1 Cell Culture Media Composition

Dulbecco's Modified Eagle's Medium (DMEM) is frequently used as a base cell culture medium to which serum and other supplements are added for the maintenance of specific neural cells. Commonly DMEM is supplemented with FBS to encourage astrocyte maturation (discussed in section 7.2), and glucose is frequently added to culture media if not supplemented in the DMEM.

The concentration of glucose in culture media differs, some researchers use 5 mM but some researchers use as high as 25 mM which I have used in these preparations (Lange *et al.*, 2012). The purpose of working with such high concentrations has been to avoid astrocytes using lactate as a substrate for oxidative metabolism if glucose becomes depleted (Gandhi *et al.*, 2010). At concentrations greater than 15 mM glucose, astrocyte morphology is directly altered *in vitro* resulting in an increase in GFAP and vimentin expression which signals astrocyte reactivity (J. Wang *et al.*, 2012). In terms of astrocyte function, it has been found that high glucose concentrations can alter astrocyte network arrangement via decreased gap junctional communication (Gandhi *et al.*, 2010). It is likely therefore that such unacknowledged

differences to cell culture media can influence astrocyte network activity and therefore calcium responses and function.

We have determined the functional responses of astrocytes when cultured in DMEM alone (with 25 mM glucose) to understand phenotypic alterations in primary astrocytes as a result of components in the cell culture media (Figure 12, Chapter 4, page 85). There were no significant differencse in the percentage of cells responding to ATP or glutamate when cultured with either AM or DMEM, but there was a significant increase in the percentage of FSK treated cells responding to ATP and glutamate when cultured with DMEM compared to AM (Figure 12, Chapter 4, page 85). Furthermore FBS serum in AM influenced astrocyte responses to neurotransmitter following FSK treatment, but because FBS is not a natural component of the extracellular environment, it highlights how such findings must be carefully interpreted since they are not translatable and thus it is important to define an *in vitro* cell culture medium that is highly representative of the extracellular environment.

7.4 Effect of 3D Culture Environment on Astrocyte Phenotype

2D culture methods are repeatedly used for the study of individual astrocyte or neuron populations since they offer a good degree of experimental control and a good proportion of literature exists to compare measured outcomes to (LaPlaca *et al.*, 2010). However, astrocytes cultured on 2D surfaces can exhibit an artificial astrocyte reactivity (East *et al.*, 2010) and cells have more of their surface exposed compared to their *in vivo* environment with unknown phenotypic affects (LaPlaca *et al.*, 2010). Additionally, gene expression and other defining cellular characteristics may not develop due to the lack of cell-cell and cell-matrix interactions (LaPlaca *et al.*, 2010). Thus, analysis of astrocyte phenotype in 3D culture models will be an important step in the field as a way to generate more translatable data, and is hoped to bridge the gap between current *in vitro* models and *in vivo* animal experimentation (Pampaloni, Reynaud and Stelzer, 2007).

I have used 3D culture techniques (e.g. hydrogels such as matrigel and hyaluronic acid) to mimic a more physiological extracellular environment within which astrocytes are known to adopt a non-reactive phenotype. Primary neonatal (P2) cortical astrocytes were successfully cultured in two commercially available hydrogels. Astrocytes cultured within both matrigel and hyaluronic acid developed stellate morphologies where processes extended in all directions from the cell body, a morphology closely resembling that of *in vivo* cells (Figure 8, Chapter 5, page 114) (Khakh and Sofroniew, 2015). In contrast, the engineered polystyrene scaffold alvetex didn't allow the study of astrocyte morphology in 3D (Figures 2 & 3, Chapter 5, pages 106 & 107) and is not a 3D matrix I would recommend since it is a physical scaffold which doesn't replicate the brain extracellular environment.

Characterisation of astrocyte morphology in terms of volume, surface area, shape factor and longest axis has been possible with calcein AM loading and confocal imaging for astrocytes cultured on 2D surfaces or within matrigel or hyaluronic acid gels (Figures 9-14, Chapter 5). We established optimum gel concentrations with matrigel and hyaluronic acid for astrocyte cell culture via calcein AM loading and the calculation of the percentage of viable cells (Figures 4 & 5, Chapter 5, pages 109 & 110). We found that lower concentrations of both hydrogels resulted in a greater percentage of cell survival (Figures 4 & 5, Chapter 5, pages 109 & 110). It was also possible to induce astrocyte stellation in all three culture formats via the addition of forskolin (Figures 9-14, Chapter 5).

Control astrocytes cultured in 3 mg/ml matrigel had a mean volume of 22,029 μm^3, which is in-keeping with findings in the literature (Halassa *et al.*, 2007; Miller and Rothstein, 2016). In contrast to this, control astrocytes in 5 mg/ml hyaluronic acid had a mean volume less than half of this (12,685 μm^3). One possible reason for this difference is the variation in the molecular compositions of the hydrogels: matrigel is rich with growth factors, whereas hyaluronic acid is composed of repeating units of glucuronic acid and N-acetyl-D-glucosamine used for structure in the brain extracellular environment (Wang and Spector, 2009). Therefore these data imply that the culture

microenvironment influences astrocyte development and must be carefully selected.

The calculation of surface area to volume ratio has revealed key differences in population distributions of cells cultured in 2D versus 3D (Figures 15 & 16, Chapter 5, pages 126 & 127). The mean surface area to volume ratio for both control and FSK treated cells was significantly increased for astrocytes cultured in 2D, which indicates that cells are flat with large areas of the cell exposed to cell culture media. The mean surface area to volume ratio was smaller when cells were cultured with 3D hydrogels, which suggests they developed more processes extending out from the cell soma (as seen in Figure 8, Chapter 5, page 114). Furthermore the 3D environment is crucial to enabling astrocytes to develop a more physiologically relevant phenotype when cultured *in vitro*.

7.4.1 3D Matrices for Primary Cell Culture

There are numerous 3D scaffolds and hydrogels that can be used for the culture of astrocyte cells: collagen gels have been used successfully to culture cortical astrocytes which exhibited morphological diversity and underwent maturation (Balasubramanian *et al.*, 2016). In this study, Balasubramanian *et al*., (2016) compared cortical astrocyte morphologies for cells cultured on collagen-coated 2D coverslips or within a 3D matrix of collagen. They found that cortical astrocytes on 2D substrates were predominantly flat and rounded with a large cell body, whereas astrocytes in 3D matrices had smaller cell bodies and more processes extending out from the cell body (Balasubramanian *et al.*, 2016). My results bear many similarities: astrocytes cultured in 2D were flat and protoplasmic, whereas cells cultured in matrigel and HA had more stellate morphologies (Figure 8, Chapter 5, page 114).

Hydrogels can be used for an extensive range of engineering applications, but since their mechanical properties highly influence compatibility with relevant tissues, it is important that gel rheology is characterised prior to their use in tissue engineering strategies (Zuidema *et al.*, 2014). Viscosity of a biomaterial is important because this provides an indication of the sheer stress that will

act on embedded cells (Kane *et al.*, 2018). Kane *et al.*, (2018) carried out rheological measurements to determine the viscosity, shear stress and fluid-flow of matrigel in an experimental set up which mimicked the seeding of a 3D microfluidics device which is an important step towards optimisation of 3D microfluidic cell culture. The experimenters found that temperature changes influenced shear stress experienced by cells.

7.4.1.1 The Brain Extracellular Environment

The brain extracellular environment is essential for structural integrity of tissues and eliciting key roles in transducing cell-cell communication through various signalling pathways (Krishnaswamy *et al.*, 2019). The brain extracellular environment also has essential cell surface receptors which are necessary in proliferation, differentiation and migration. The brain extracellular matrix has a largely unique composition of non-fibrillar components, primarily consisting of proteoglycans, tenascins and hyaluronic acid. Proteoglycans are important and have critical roles in regulating cell adhesion, neurite outgrowth and ECM assembly. Additionally, the brain extracellular matrix also contains matricellular proteins, glycoproteins and enzymes.

Associated with the brain extracellular matrix are a number of neuropeptides, which are endogenous peptides synthesised in large precursor proteins, which act as neurotransmitters when they are co-released with other neurotransmitters (de Wied, 1987). Neuropeptides are catabolized into inactive amino acid fragments by peptidase enzymes which are located on the extracellular surface of the plasma membrane (de Wied, 1987). These neuropeptides are subsequently released into the synaptic cleft in synchronisation with other neurotransmitters and provide greater behavioural flexibility and robustness (Hökfelt, Bartfai and Bloom, 2003; Nusbaum, Blitz and Marder, 2017). Such peptides and their functions are factors not often replicated in 2D or 3D *in vitro* environments, resulting in the derivation of astrocytes and neurons that are not functioning at their *in vivo* capacity.

Working towards a defined 3D hydrogel for *in vitro* astrocyte cell culture, which is highly representative of the *in vivo* brain extracellular environment,

and allows typical experimental procedures to be carried out with ease, is the best hope for reducing the need to replicate *in vitro* findings using animals *in vivo*.

7.4.1.2 Composite Gels

Placone *et al*., (2015) have studied the possibility of culturing human astrocytes in combinatorial hydrogels containing various concentrations of collagen, matrigel and hyaluronic acid. The combinations of collagen, matrigel and HA that they used were selected to provide structural support, endothelial cell compatibility and mimic the brain extracellular environment respectively, since they were working towards a model of the blood-brain barrier (Placone *et al.*, 2015).

The brain extracellular matrix is dominated by hyaluronic acid and tenascin proteins as well as lecticans and proteoglycans, thus it seems appropriate to work with a composite of matrigel and hyaluronic acid: hyaluronic acid is naturally abundant in the brain, and matrigel contains heparan sulphate proteoglycans which also occur naturally in the brain (however collagen does not). Considering that the brain microenvironment exposes astrocytes to an array of signalling molecules, and a unique composition of extracellular matrix, formulating a hydrogel that can replicate as many elements of this as possible would make a great model for *in vitro* cell culture.

Once I had successfully cultured astrocytes in matrigel and HA gels individually, I tried combining 3 mg/ml matrigel with 1.5 mg/ml hyaluronic acid to test if cells would survive in the composite matrix. Gels seeded with cells at normal density (2.5×10^4 cells per ml) were cultured between 2-5 DIV and imaged following 1 µM calcein AM loading for 30 minutes. Astrocytes survived in this composite matrix but they did not appear to be as abundant as cells cultured in 3 mg/ml matrigel or 5 mg/ml HA alone. This suggests that mixing matrigel and HA gels generated an environment which was interfering with cell viability – although considering the success of Placone *et al.,* (2015), gel formation may be the problematic factor.

7.4.1.3 Peptide Gels

In recent years, 3D cell culture matrices have moved towards the use of self-assembling peptide hydrogels (SAPHs) which consist of alternating hydrophobic and hydrophilic amino acids (Ayerst, Merry and Day, 2017). Such peptide hydrogels spontaneously form nanofiber scaffolds and have the advantages of traditional hydrogels. There is also the possibility of adding components to the gel to precisely tailor the 3D cell environment, including serum.

SAPHs from small molecular building blocks provide highly tuneable materials which have been posited to lead the next generation of bio-materials (Thornton *et al.*, 2009). It is preferable that such self-forming customizable hydrogels will do so under physiological conditions, including formation at 37°C and at a pH of 7-7.5 (Thornton *et al.*, 2009). In the last 10 years a number of ways in which this self-forming capability can be triggered have been identified: environmental changes (such as pH) or the application of a stimulus (such as light or enzymes).

Different types of SAPHs have been investigated for their biocompatibility and tailorable properties, with the ever-increasing knowledge that mechanical properties can be optimised to match the stiffness of the native extracellular matrix the hydrogel is intended to replicate (Wan *et al.*, 2016). Wan *et al.,* (2016) discovered that the FEFEFKFK peptide can be successfully used as both a cell culture scaffold and as a method of drug delivery. Specifically, Wan *et al*., (2016) cultured bovine chondrocytes within the FEFEFKFK SAPH and found that the cells developed a rounded morphology, were able to proliferate and even produced collagen type II (cartilage ECM component), suggesting that cells were able to adopt their *in vivo* phenotype (Wan *et al.*, 2016).

SAPHs have also been proven to enhance the potential for regeneration in neural tissues following brain injury via the encapsulation of neural stem cells (NSCs). Cheng *et al.*, (2013) linked a laminin-derived motif on the C-terminal to enrich self-assembling peptide RADA16 as a functional peptide-based scaffold which subsequently developed a mechanical stiffness similar to brain

tissue. This formulation augmented the survival of NSCs encapsulated in the hydrogels and reduced the proportion differentiating to form newly proliferated astrocytes (Cheng *et al.*, 2013). This method was found to improve the state of regeneration in brain tissue for up to 6 weeks post transplantation. In summary, the emergence of matrices such as SAPHs is exciting because blank matrices give researchers full control over the molecules to add into the matrix for specific primary cells types.

7.4.1.4 Polysaccharide Gels

One major drawback to working with synthetic hydrogels is the issue of toxicity arising from their chemical cross-linking. One driving factor for the discovery of biologically compatible hydrogels, is the biomedical applications including using them as biomaterials for implants into the brain microenvironment following trauma.

Polysaccharides synthesised from bacteria have emerged as a new source of hydrogel. For example, cellulose exopolysaccharide (CEC), produced from sugarcane molasses, is of low cost and suitable for 3D astrocyte and neuron primary cultures (Gonçalves-pimentel *et al.*, 2018). Investigators of this CEC tested cell viability, growth and cell function via calcium imaging and used a polystyrene scaffold and matrigel as comparative controls (Gonçalves-pimentel *et al.*, 2018)**.** The biocompatible CEC was appropriate for the differentiation of cortical astrocytes or neurons in single cell culture or co-culture (Gonçalves-pimentel *et al.*, 2018). Such gels demonstrate the therapeutic potential of different materials obtained from renewable sources.

7.4.1.5 Summary

Establishing optimal hydrogels for *in vitro* cell culture is no easy task; gels must be permeable to allow diffusion (nutrient uptake and waste removal), allow cell migration, and be stable to withstand external changes. Thus, customisable and self-arranging peptide gels may be a worthwhile up and coming avenue, and so too may polysaccharide gels if they can be confirmed for their biocompatibility and low toxicity. Since astrocytes are extremely

sensitive to their external environment, culture format should be carefully considered in order to study astrocytes in a physiologically relevant manner.

7.5 Primary Neuron Development *in Vitro*

7.5.1 2D Culture

In vitro cell culture approaches have been significant in the discovery of the mechanisms that underpin neuronal polarity; the growth of primary cortical neurons on coated coverslips in tissue culture plates is well classified. Neurons have been found to develop immature neurites by 2 DIV, and by 5 DIV neurons have dendrites and an axon (Dotti, Sullivan and Banker, 1988). My primary neuron cultures have developed in this way, with numerous dendrites and axons clearly visible at 5 DIV (Figures 3 & 4, Chapter 6, pages 160 & 161). Axon length increased significantly from 2-5 DIV showing that neurons were viable and developed in a characteristic manner in 2D culture (Figure 5, Chapter 6, page 182).

A goal of this project was to characterise the growth of axons in response to the absence or presence of astrocytes, and with astrocytes that had been forskolin treated, to infer more about neuron-glial communication. Due to a lack of neuron-specific markers (Figures 6 - 8, Chapter 6), it was not possible to decipher the influence of a monolayer of astrocytes on the development of neurons. Since it was not possible to distinguish astrocytic processes from neurites and axons (Figure 6, Chapter 6, page 163), an alternative strategy was required for the assessment of astrocyte influence on neuron growth and development.

7.5.2 3D Culture

Primary embryonic cortical neurons were viable when cultured within matrigel: axons were clearly identifiable at 2 and 5 DIV representing neuron growth and survival (Figure 12, Chapter 6, page 168). Reliably culturing primary neurons with such 3D *in vitro* techniques is of high importance since it has been proposed that 3D environments will allow neurites to extend in all directions as neurons grow in a similar manner to *in vivo* (Tarus *et al.*, 2016). I

hypothesize that, if it is possible to combine this hydrogel with 3D microfluidics devices, it would be possible to successfully co-culture astrocytes and neurons in a sophisticated *in vitro* culture model that replicates elements of the *in vivo* microenvironment.

7.6 Astrocyte-Neuron Interactions

7.6.1 Ectopic Transmission in the Cerebellar Cortex

Astrocyte and neuron communication is integral to normal brain function and in recent years ectopic neuron-glial transmission has been discovered as a new mechanism of communication between the two cell types. I have attempted to work with an *in vitro* environment for investigating neuron-astrocyte interactions that is more physiologically relevant, but ultimately this needs to be compared to the same process in situ. Thus this project has investigated the morphology and anatomical interaction of astroglial processes and synapses in the cerebellum.

Cerebellar slices generated by Dr Katharine Dobson from the Bellamy lab, where the stimulation protocol was known to induce long term depression from neurons to glia following repetitive stimulation in the 0.1-1 Hz range have been analysed. The aim was to firstly identify the ectopic vesicle pool using a 1 Hz stimulation frequency protocol that would deplete the pool to identify where any activity was taking place, and, secondly, determine the effect of ectopic transmission on Bergmann glial cells, including potential influences to their morphology via changes to synaptic coverage.

There were no major changes to the distribution of the vesicles located at glial-facing regions of the presynaptic terminal following the stimulation protocol (Figure 5 & Table 1, Chapter 3, pages 53 & 54), thus it has not been possible to confirm this population as the ectopic vesicle pool. The stimulation in this study did not influence the number of vesicles at the active zone or their spatial distribution relative to the glial facing membrane (Figures 4 & 5, Chapter 3, pages 52 & 53). However there was a small but significant increase in the mean distance at the midpoint for the 1Hz stimulation population meaning there was a detectable change in the synapse coverage

by Bergmann glia (Figure 6, Chapter 3, page 56), which suggests that there can be astrocyte rearrangement within a 10 minute time frame (the period of excitation), but further experimentation is necessary to discover this mechanism. Considering that glia have dynamic and motile processes that respond to synaptic signalling, the hope for this study was to discover how dynamically morphological changes occur in response to changes in synaptic transmission.

7.6.2 Compartmentalized Microfluidics Devices

The use of compartmentalized microfluidics chambers would be one way to overcome the labelling issue encountered when co-culturing astrocytes and neurons on 2D coverslips. Neuronal cell culture will benefit from sophisticated 2D *in vitro* culture formats because neurons grown on coverslips can form random synaptic connections which makes it difficult to distinguish axons from dendrites morphologically. The use of compartmentalised microfluidics chambers is one way to achieve anatomical separation of neuron domains which can prevent this problem. Thus, the hope was that culturing neurons in one side of a compartmentalized microfluidics device, either alone or with astrocytes on the other side, would reveal the association of the two cell types in axon outgrowth.

Whilst it has been possible to co-culture astrocytes and neurons using compartmentalized microfluidics devices, this success was not reliable enough to measure axon length when axons crossed microgrooves into the astrocyte compartment (Figure 11, Chapter 6, page 167). Issues of cell viability and lack of axon extension across microgrooves were encountered frequently (Figures 9 & 10, Chapter 6, pages 166 & 167), thus it was challenging to culture primary cells in these devices.

7.7 Induced Astrocytes

Human astrocytes are not in abundant supply, thus, new technologies to reprogramme other cell types into induced astrocytes have the capacity to provide an efficient supply of human tissue. Induced neural precursor cells (iNPCs) were treated with iAstrocyte differentiation media for 5 DIV and live-

cell loading with calcein AM revealed that cells were viable and exhibited heterogeneous morphology (Figure 13, Chapter 6, page 169). Morphological assessment following FSK treatment suggested that iAstrocytes didn't undergo stellation (Figure 13, Chapter 6, page 169). Immunofluorescent GFAP labelling confirmed that the iAstrocyte cytoskeleton undergoes no striking changes following FSK treatment (Figure 15, Chapter 6, page 170). Confocal imaging with iAstrocytes cultured in 2D, 3D matrigel and 3D hyaluronic acid has confirmed cell heterogeneity: iAstrocytes in 3D were more polygonal and showed less process extension from the cell soma than primary astrocytes (Figure 16, Chapter 6, page 172 and Figure 8, Chapter 5, page 114).

In an initial analysis, I have measured the volume, surface area, shape factor and longest axis for iAstrocytes cultured on 2D plates, within 3 mg/ml matrigel or 5 mg/ml hyaluronic acid. Volume and surface area measurements for astrocytes cultured with hyaluronic acid were significantly increased compared to the other culture conditions (Figure 20, Chapter 6, page 176) which indicates that the matrix positively supported cell growth and differentiation. This is supported by surface area to volume ratio data where iAstrocytes cultured in hyaluronic acid had a significantly smaller ratio which implies the extension of astrocytic processes (Figure 21, Chapter 6, page 177). In summary, the preliminary results suggest that iAstrocytes exhibit very different morphologies in comparison to primary astrocytes.

7.8 Conclusion

My personal perspective is that working with base peptide gels, which form when two polymers are added together but allow the addition of growth factors and similar molecules, and developing specific formulations for different cell types in the brain, will be instrumental in progressing the authenticity of 3D culture models *in vitro*. Combining carefully constructed 3D matrices with induced astrocytes from human fibroblasts will facilitate the collection of patient-specific data, which not only has long term implications for disease-specific therapeutics, but will fundamentally allow the study of human astrocytes which are known to exhibit key differences to primary cells.

References

Afridi, R. *et al.* (2020) 'Metabolic Regulation of Glial Phenotypes: Implications in Neuron–Glia Interactions and Neurological Disorders', *Frontiers in Cellular Neuroscience*, 14(February), pp. 1–17. doi: 10.3389/fncel.2020.00020.

Agulhon, C. *et al.* (2008) 'What Is the Role of Astrocyte Calcium in Neurophysiology?', *Neuron*, 59(6), pp. 932–946. doi: 10.1016/j.neuron.2008.09.004.

Agulhon, C., Fiacco, T. A. and McCarthy, K. D. (2010) 'Hippocampal short- and long-term plasticity are not modulated by astrocyte Ca2+ signaling', *Science*, 327(5970), pp. 1250–1254. doi: 10.1126/science.1184821.

Ahmed, E. M. (2015) 'Hydrogel: Preparation, characterization, and applications: A review', *Journal of Advanced Research*. Cairo University, 6(2), pp. 105–121. doi: 10.1016/j.jare.2013.07.006.

Alexandra Adam, S. *et al.* (2012) 'ALDH1A1 is a marker of astrocytic differentiation during brain development and correlates with better survival in glioblastoma patients', *Brain Pathology*, 22(6), pp. 788–797. doi: 10.1111/j.1750-3639.2012.00592.x.

Allen, N. J. (2014) 'Astrocyte Regulation of Synaptic Behavior', *Annual Review of Cell and Developmental Biology*, 30(1), pp. 439–463. doi: 10.1146/annurev-cellbio-100913-013053.

Alliot, F. and Pessac, B. (1984) 'Astrocytic cell clones derived from established cultures of 8-day postnatal mouse cerebella', *Brain Research*, 306(1–2), pp. 283–291. doi: 10.1016/0006-8993(84)90377-9.

Ananthanarayanan, B., Kim, Y. and Kumar, S. (2011) 'Elucidating the mechanobiology of malignant brain tumors using a brain matrix-mimetic hyaluronic acid hydrogel platform', *Biomaterials*. Elsevier Ltd, 32(31), pp. 7913–7923. doi: 10.1016/j.biomaterials.2011.07.005.

Anderson, M. A. *et al.* (2016) 'Astrocyte scar formation aids central nervous system axon regeneration', *Nature*. Nature Publishing Group, 000(1), pp. 1–20. doi: 10.1038/nature17623.

Araque, A. *et al.* (1999) 'Tripartite synapses: Glia, the unacknowledged partner', *Trends in Neurosciences*, 22(5), pp. 208–215. doi: 10.1016/S0166-2236(98)01349-6.

Aurand, E. *et al.* (2012) 'Building Biocompatible Hydrogels for Tissue Engineering of the Brain and Spinal Cord', *Journal of Functional Biomaterials*, 3(4), pp. 839–863. doi: 10.3390/jfb3040839.

Ayerst, B. I., Merry, C. L. R. and Day, A. J. (2017) 'The good the bad and the ugly of

glycosaminoglycans in tissue engineering applications', *Pharmaceuticals*, 10(2). doi: 10.3390/ph10020054.

Baba, K. *et al.* (2018) 'Machinery for Netrin-1-Induced Axon Guidance', *eLIFE*, 7(e34593), pp. 1–35. doi: https://doi.org/10.7554/eLife.34593.

Badiola-Mateos, M. *et al.* (2018) 'Challenges and Future Prospects on 3D in-vitro Modeling of the Neuromuscular Circuit', *Frontiers in Bioengineering and Biotechnology*, 6(December), pp. 1–9. doi: 10.3389/fbioe.2018.00194.

Balakrishnan, S. *et al.* (2011) 'Ectopic release sites lack fast vesicle recycling mechanisms, causing long-term depression of neuron-glial transmission in rat cerebellum', *Glia*, 59(1), pp. 82–93. doi: 10.1002/glia.21078.

Balakrishnan, S. and Bellamy, T. C. (2009) 'Depression of parallel and climbing fiber transmission to Bergmann glia is input specific and correlates with increased precision of synaptic transmission', *Glia*, 57(4), pp. 393–401. doi: 10.1002/glia.20768.

Balasubramanian, S. *et al.* (2016) 'Three-Dimensional Environment Sustains Morphological Heterogeneity and Promotes Phenotypic Progression during Astrocyte Development', *Tissue Engineering - Part A*, 22(11–12), pp. 885–898. doi: 10.1089/ten.tea.2016.0103.

Barateiro, A., Brites, D. and Fernandes, A. (2016) 'Oligodendrocyte Development and Myelination in Neurodevelopment: Molecular Mechanisms in Health and Disease', *Current Pharmaceutical Design*, 22(6), pp. 656–679. Available at: https://doi.org/10.2174/1381612822666151204000636.

Bardy, C. *et al.* (2015) 'Neuronal medium that supports basic synaptic functions and activity of human neurons in vitro', *Proceedings of the National Academy of Sciences of the United States of America*, 112(20), pp. E2725–E2734. doi: 10.1073/pnas.1504393112.

Barnes, A. P. and Polleux, F. (2009) 'Establishment of Axon-Dendrite Polarity in Developing Neurons', *Annual Review of Neuroscience*, 32(1), pp. 347–381. doi: 10.1146/annurev.neuro.31.060407.125536.

Barres, B. A., Chun, L. L. Y. and Corey, D. P. (1989) 'Calcium current in cortical astrocytes: Induction by cAMP and neurotransmitters and permissive effect of serum factors', *Journal of Neuroscience*, 9(9), pp. 3169–3175. doi: 10.1523/jneurosci.09-09-03169.1989.

Barrett, M. J. P. *et al.* (2018) 'Cortical Circuit Activity Evokes Rapid Astrocyte Calcium Signals on a Similar Timescale to Neurons', *Neuron*, 98(4), pp. 726-735.e4. doi: 10.1016/j.neuron.2018.03.050.

Bayraktar, O. A. *et al.* (2015) 'Astrocyte development and heterogeneity', *Cold Spring Harbor*

Perspectives in Biology, 7(1). doi: 10.1101/cshperspect.a020362.

Bazargani, N. and Attwell, D. (2016) 'Astrocyte calcium signaling: The third wave', *Nature Neuroscience*, 19(2), pp. 182–189. doi: 10.1038/nn.4201.

Beavo, J. A. and Brunton, L. L. (2002) 'Cyclic nucleotide research - Still expanding after half a century', *Nature Reviews Molecular Cell Biology*, 3(9), pp. 710–718. doi: 10.1038/nrm911.

Bellamy, T. (2006) 'Interactions between Purkinje neurones and Bergmann glia', *Cerebellum*, 5(2), pp. 116–126. doi: 10.1080/14734220600724569.

Bellamy, T. C. and Ogden, D. (2005) 'Short-term plasticity of Bergmann glial cell extrasynaptic currents during parallel fiber stimulation in rat cerebellum', *Glia*, 52(4), pp. 325–335. doi: 10.1002/glia.20248.

Bellamy, T. C. and Ogden, D. (2006) 'Long-term depression of neuron to glial signalling in rat cerebellar cortex', *European Journal of Neuroscience*, 23(2), pp. 581–586. doi: 10.1111/j.1460-9568.2005.04588.x.

Bellot-Saez, A. *et al.* (2017) 'Astrocytic modulation of neuronal excitability through K+spatial buffering', *Neuroscience and Biobehavioral Reviews*. Elsevier Ltd, 77, pp. 87–97. doi: 10.1016/j.neubiorev.2017.03.002.

Bhattacharjee, N. and Folch, A. (2017) 'Large-scale microfluidic gradient arrays reveal axon guidance behaviors in hippocampal neurons', *Microsystems & Nanoengineering*. Nature Publishing Group, 3(1), pp. 1–14. doi: 10.1038/micronano.2017.3.

Bian, L. *et al.* (2013) 'Hydrogels that mimic developmentally relevant matrix and N-cadherin interactions enhance MSC chondrogenesis', *Proceedings of the National Academy of Sciences of the United States of America*, 110(25), pp. 10117–10122. doi: 10.1073/pnas.1214100110.

Bignami, A. and Dahl, D. (1974) 'Astrocyte- specific protein and neuroglial differentiation. An immunofluorescence study with antibodies to the glial fibrillary acidic protein', *Journal of Comparative Neurology*, 153(1), pp. 27–37. doi: 10.1002/cne.901530104.

Black, J. a, Sontheimer, H. and Waxman, S. G. (1993) 'Spinal cord astrocytes in vitro: phenotypic diversity and sodium channel immunoreactivity.', *Glia*, 7(4), pp. 272–285. doi: 10.1002/glia.440070403.

Blanco-Suárez, E., Caldwell, A. L. M. and Allen, N. J. (2017) 'Role of astrocyte–synapse interactions in CNS disorders', *Journal of Physiology*, 595(6), pp. 1903–1916. doi: 10.1113/JP270988.

Bramanti, V. *et al.* (2007) 'Astroglial-conditioned media and growth factors modulate proliferation and differentiation of astrocytes in primary culture', *Neurochemical Research*, 32(1), pp. 49–56. doi: 10.1007/s11064-006-9224-6.

Brenner, M. (2014) 'Role of GFAP in CNS injuries', *Neuroscience Letters*. Elsevier Ireland Ltd, 565, pp. 7–13. doi: 10.1016/j.neulet.2014.01.055.

Brewer, G. J. (1995) 'Serum- free B27/neurobasal medium supports differentiated growth of neurons from the striatum, substantia nigra, septum, cerebral cortex, cerebellum, and dentate gyrus', *Journal of Neuroscience Research*, 42(5), pp. 674–683. doi: 10.1002/jnr.490420510.

Brown, A. M. and Ransom, B. R. (2007) 'Astrocyte glycogen and brain energy metabolism.', *Glia*, 55(12), pp. 1263–71. doi: 10.1002/glia.20557.

Bryant, S. J. *et al.* (2004) 'Crosslinking density influences the morphology of chondrocytes photoencapsulated in PEG hydrogels during the application of compressive strain', *Journal of Orthopaedic Research*, 22(5), pp. 1143–1149. doi: 10.1016/j.orthres.2004.02.001.

Buffo, A. and Rossi, F. (2013) 'Origin, lineage and function of cerebellar glia', *Progress in Neurobiology*. Elsevier Ltd, 109, pp. 42–63. doi: 10.1016/j.pneurobio.2013.08.001.

Burda, J. E., Bernstein, A. M. and Sofroniew, M. V. (2016) 'Astrocyte roles in traumatic brain injury', *Experimental Neurology*. Elsevier Inc., 275, pp. 305–315. doi: 10.1016/j.expneurol.2015.03.020.

Burda, J. E. and Sofroniew, M. V. (2014) 'Reactive gliosis and the multicellular response to CNS damage and disease', *Neuron*. Elsevier Inc., 81(2), pp. 229–248. doi: 10.1016/j.neuron.2013.12.034.

Bushong, E. A. *et al.* (2018) 'Protoplasmic Astrocytes in CA1 Stratum Radiatum Occupy Separate Anatomical Domains', *The Journal of Neuroscience*, 22(1), pp. 183–192. doi: 10.1523/jneurosci.22-01-00183.2002.

Cahoy, J. D. *et al.* (2008) 'A transcriptome database for astrocytes, neurons, and oligodendrocytes: A new resource for understanding brain development and function', *Journal of Neuroscience*, 28(1), pp. 264–278. doi: 10.1523/JNEUROSCI.4178-07.2008.

Caliari, S. R. and Burdick, J. A. (2016) 'A practical guide to hydrogels for cell culture', *Nature Methods*. Nature Publishing Group, 13(5), pp. 405–414. doi: 10.1038/nmeth.3839.

Campbell, K. and Götz, M. (2002) 'Radial glia: Multi-purpose cells for vertebrate brain development', *Trends in Neurosciences*, 25(5), pp. 235–238. doi: 10.1016/S0166-2236(02)02156-2.

Ceprian, M. and Fulton, D. (2019) 'Glial cell AMPA Receptors in nervous system health, injury and disease', *International Journal of Molecular Sciences*, 20(10), pp. 1–39. doi: 10.3390/ijms20102450.

Chandrasekaran, A. *et al.* (2016) 'Astrocyte differentiation of human pluripotent stem cells: New tools for neurological disorder research', *Frontiers in Cellular Neuroscience*, 10(SEP2016). doi: 10.3389/fncel.2016.00215.

Charriere-Bertrand, C. *et al.* (1989) 'Expression of tubulin, GFAP and of their encoding mRNAs during the proliferation and differentiation of cultured astrocytes', *Neurochemistry International*, 15(2), pp. 215–222. doi: 10.1016/0197-0186(89)90103-4.

Chen, Y. *et al.* (2008) 'NS21: Re-defined and modified supplement B27 for neuronal cultures', *Journal of Neuroscience Methods*, 171(2), pp. 297–247.

Cheng, T. Y. *et al.* (2013) 'Neural stem cells encapsulated in a functionalized self-assembling peptide hydrogel for brain tissue engineering', *Biomaterials*. Elsevier Ltd, 34(8), pp. 2005–2016. doi: 10.1016/j.biomaterials.2012.11.043.

Choi, B. H. and Lapham, L. W. (1978) 'Radial glia in the human fetal cerebrum: A combined golgi, immunofluorescent and electron microscopic study', *Brain Research*, 148(2), pp. 295–311. doi: 10.1016/0006-8993(78)90721-7.

Christopherson, K. S. *et al.* (2005) 'Thrombospondins Are Astrocyte-Secreted Proteins that Promote CNS Synaptogenesis', 120, pp. 421–433. doi: 10.1016/j.cell.2004.12.020.

Clarke, L. E. and Barres, B. A. (2013) 'Emerging roles of astrocytes in neural circuit development', 14(May). doi: 10.1038/nrn3484.

Codeluppi, S. *et al.* (2011) 'Influence of rat substrain and growth conditions on the characteristics of primary cultures of adult rat spinal cord astrocytes', *Journal of Neuroscience Methods*. Elsevier B.V., 197(1), pp. 118–127. doi: 10.1016/j.jneumeth.2011.02.011.

Colombo, J. A. and Reisin, H. D. (2004) 'Interlaminar astroglia of the cerebral cortex: A marker of the primate brain', *Brain Research*, 1006(1), pp. 126–131. doi: 10.1016/j.brainres.2004.02.003.

Colonna, M. and Butovsky, O. (2017) 'Microglia Function in the Central Nervous System During Health and Neurodegeneration', *Annual Review of Immunology*, 35(1), pp. 441–468. doi: 10.1146/annurev-immunol-051116-052358.

Connors, B. W. and Long, M. A. (2004) 'ELECTRICAL SYNAPSES IN THE MAMMALIAN BRAIN', *Annual Review of Neuroscience*, 27(1), pp. 393–418. doi: 10.1146/annurev.neuro.26.041002.131128.

Cornell-bell, A. H. *et al.* (1990) 'Glutamate Induces Calcium Waves in Cultured Astrocytes: Long-Range Glial Signaling ANN', *Science*, 247(24), pp. 2–5.

Cowman, M. *et al.* (2015) 'Viscoelastic Properties of Hyaluronan in Physiological Conditions.', *F1000 Research*, 4(622). doi: 10.12688/f1000research.6885.1.

Croft, W. *et al.* (2015) 'Probabilistic encoding of stimulus strength in astrocyte global calcium signals', *Glia*, pp. 537–552. doi: 10.1002/glia.22947.

D. Jadhav, A., Wei, L. and Shi, P. (2015) 'Compartmentalized Platforms for Neuro-Pharmacological Research', *Current Neuropharmacology*, 14(1), pp. 72–86. doi: 10.2174/1570159x13666150516000957.

Dajas-Bailador, F. *et al.* (2014) 'Regulation of axon growth by the JIP1–AKT axis', *Journal of Cell Science*, pp. 230–239. doi: 10.1242/jcs.137208.

Dajas-Bailador, F., Jones, E. V. and Whitmarsh, A. J. (2008) 'The JIP1 Scaffold Protein Regulates Axonal Development in Cortical Neurons', *Current Biology*. Elsevier Ltd, 18(3), pp. 221–226. doi: 10.1016/j.cub.2008.01.025.

Dani, J. W., Chernjavsky, A. and Smith, S. J. (1992) 'Neuronal Activity Triggers Calcium Waves in Hippocampal Astrocyte Networks', 8, pp. 429–440.

Dehqan Niri, A. *et al.* (2019) 'Tissue engineering scaffolds in the treatment of brain disorders in geriatric patients', *Artificial Organs*, 43(10), pp. 947–960. doi: 10.1111/aor.13485.

Dimos, J. T. *et al.* (2008) 'Induced pluripotent stem cells generated from patients with ALS can be differentiated into motor neurons', *Science*, 321(5893), pp. 1218–1221. doi: 10.1126/science.1158799.

Dobson, K. L., Smith, Z. H. and Bellamy, T. C. (2018) 'Distribution of vesicle pools in cerebellar parallel fibre terminals after depression of ectopic transmission', 13(7), pp. 1–15. doi: 10.1371/journal.pone.0200937.

di Domenico, A. *et al.* (2019) 'Patient-Specific iPSC-Derived Astrocytes Contribute to Non-Cell-Autonomous Neurodegeneration in Parkinson's Disease', *Stem Cell Reports*, 12(2), pp. 213–229. doi: 10.1016/j.stemcr.2018.12.011.

Donato, R. (1999) 'Functional roles of S100 proteins, calcium-binding proteins of the EF-hand type', *Biochimica et Biophysica Acta - Molecular Cell Research*, 1450(3), pp. 191–231. doi: 10.1016/S0167-4889(99)00058-0.

Dotti, C. G., Sullivan, C. a and Banker, G. a (1988) 'The establishment of polarity by hippocampal neurons in culture.', *The Journal of neuroscience : the official journal of the*

Society for Neuroscience, 8(4), pp. 1454–1468. doi: 10.1016/0012-1606(89)90269-8.

Dráberová, E. *et al.* (2008) 'Class III β-tubulin is constitutively coexpressed with glial fibrillary acidic protein and nestin in midgestational human fetal astrocytes: Implications for phenotypic identity', *Journal of Neuropathology and Experimental Neurology*, 67(4), pp. 341–354. doi: 10.1097/NEN.0b013e31816a686d.

Dyck, R. H., Van Eldik, L. J. and Cynader, M. S. (1993) 'Immunohistochemical localization of the S-100β protein in postnatal cat visual cortex: spatial and temporal patterns of expression in cortical and subcortical glia', *Developmental Brain Research*, 72(2), pp. 181–192. doi: 10.1016/0165-3806(93)90183-B.

East, E. *et al.* (2010) 'Alignment of astrocytes increases neuronal growth in three-dimensional collagen gels and is maintained following plastic compression to form a spinal cord repair conduit.', *Tissue engineering. Part A*, 16(10), pp. 3173–84. doi: 10.1089/ten.tea.2010.0017.

East, E., Golding, J. P. and Phillips, J. B. (2009) 'A versatile 3D culture model facilitates monitoring of astrocytes undergoing reactive gliosis', *Journal of tissue engineering and regenerative medicine*, 3, pp. 634–646.

Ebert, A. D., Liang, P. and Wu, J. C. (2012) 'Induced pluripotent stem cells as a disease modeling and drug screening platform', *Journal of Cardiovascular Pharmacology*, 60(4), pp. 408–416. doi: 10.1097/FJC.0b013e318247f642.

Elson, G. N. (2007) 'Specialization of the Neocortical Pyramidal Cell during Primate Evolution', in *Evolution of Nervous Systems*, pp. 191–242.

Even, M. S., Sandusky, C. B. and Barnard, N. D. (2006) 'Serum-free hybridoma culture: Ethical, scientific and safety considerations', *Trends in Biotechnology*, 24(3), pp. 105–108. doi: 10.1016/j.tibtech.2006.01.001.

Fang, C. Y. *et al.* (2017) 'Long-term growth comparison studies of FBS and FBS alternatives in six head and neck cell lines', *PLoS ONE*, 12(6), pp. 1–27. doi: 10.1371/journal.pone.0178960.

Fanò, G. *et al.* (1995) 'The S-100: A protein family in search of a function', *Progress in Neurobiology*, 46(1), pp. 71–82. doi: 10.1016/0301-0082(94)00062-M.

Faulkner, J. R. *et al.* (2004) 'Reactive Astrocytes Protect Tissue and Preserve Function after Spinal Cord Injury', *Journal of Neuroscience*, 24(9), pp. 2143–2155. doi: 10.1523/JNEUROSCI.3547-03.2004.

Fedoroff, S. *et al.* (1987) 'Organization of microfilaments in astrocytes that form in the presence of dibutyryl cyclic AMP in cultures, and which are similar to reactive astrocytes in

vivo', *Neuroscience*, 22(1), pp. 255–266. doi: 10.1016/0306-4522(87)90216-8.

Fendler, J. H. *et al.* (2012) 'Bergmann Glial AMPA Receptors Are Required for Fine Motor Coordination', *Science Magazine*, 336(April), pp. 61–64. doi: 10.1126/science.1206034.

Fendt, S. M. and Verstreken, P. (2017) 'Neurons eat glutamate to stay alive', *Journal of Cell Biology*, 216(4), pp. 863–865. doi: 10.1083/jcb.201702003.

Fernandez-Serra, R. *et al.* (2020) 'Hydrogels for neuroprotection and functional rewiring: a new era for brain engineering.', *Neural Regeneration Research*, 15(5), pp. 783–789.

Fiacco, T. A. *et al.* (2007) 'Selective Stimulation of Astrocyte Calcium In Situ Does Not Affect Neuronal Excitatory Synaptic Activity', *Neuron*, 54(4), pp. 611–626. doi: 10.1016/j.neuron.2007.04.032.

Foa, A. C. O. F. (1893) 'The neuroglia elements in the human brain', *British Medical Journal*, 2(1700), pp. 227–230. doi: 10.1136/bmj.2.1700.227.

Foo, L. C. *et al.* (2011) 'Development of a method for the purification and culture of rodent astrocytes', *Neuron*. Elsevier Inc., 71(5), pp. 799–811. doi: 10.1016/j.neuron.2011.07.022.

Gadea, A., Schinelli, S. and Gallo, V. (2008) 'Endothelin-1 regulates astrocyte proliferation and reactive gliosis via a JNK/c-Jun signaling pathway', *Journal of Neuroscience*, 28(10), pp. 2394–2408. doi: 10.1523/JNEUROSCI.5652-07.2008.

Gandhi, G. K. *et al.* (2010) 'Hyperglycaemia and Diabetes Impair Gap Junctional Communication among Astrocytes', *ASN Neuro*, 2(2), pp. 57–73. doi: 10.1042/an20090048.

Gao, Y. *et al.* (2016) 'Functional imaging of neuron–Astrocyte interactions in a compartmentalized microfluidic device', *Microsystems and Nanoengineering*, 2(August 2015), pp. 1–9. doi: 10.1038/micronano.2015.45.

George, J. H. *et al.* (2018) 'A closer look at neuron interaction with track-etched microporous membranes', *Scientific Reports*. Springer US, 8(1), pp. 1–11. doi: 10.1038/s41598-018-33710-6.

Gladkov, A. *et al.* (2017) 'Design of Cultured Neuron Networks in vitro with Predefined Connectivity Using Asymmetric Microfluidic Channels', *Scientific Reports*. Springer US, 7(1), pp. 1–14. doi: 10.1038/s41598-017-15506-2.

Goldberg, J. L. (2003) 'How does an axon grow?', (650), pp. 941–958. doi: 10.1101/gad.1062303.GENES.

Goldman, J. E. and Abramson, B. (1990) 'Cyclic AMP-induced shape changes of astrocytes

are accompanied by rapid depolymerization of actin', *Brain Research*, 528(2), pp. 189–196. doi: 10.1016/0006-8993(90)91657-3.

Gomes, F. C. A., Paulin, D. and Neto, V. M. (1999) 'Glial fibrillary acidic protein (GFAP): Modulation by growth factors and its implication in astrocyte differentiation', *Brazilian Journal of Medical and Biological Research*, 32(5), pp. 619–631. doi: 10.1590/S0100-879X1999000500016.

Gonçalves-pimentel, C. *et al.* (2018) 'Cellulose exopolysaccharide from sugarcane molasses as a suitable substrate for 2D and 3D neuron and astrocyte primary cultures', *Journal of Materials Science: Materials in Medicine*. Springer US, 29(139), pp. 1–12. doi: 10.1007/s10856-018-6147-0.

Gong, C.-X. *et al.* (2006) 'Impaired Brain Glucose Metabolism Leads to Alzheimer Neurofibrillary Degeneration through a Decrease in Tau O-GlcNAcylation', *Journal of Alzheimer's Disease*, 9(1), pp. 1–12.

Goritz, C., Mauch, D. H. and Pfrieger, F. W. (2005) 'Multiple mechanisms mediate cholesterol-induced synaptogenesis in a CNS neuron', *Molecular and Cellular Neuroscience*, 29(2), pp. 190–201. doi: 10.1016/j.mcn.2005.02.006.

Gottfried, C. *et al.* (2003) 'The influence of the extracellular matrix on the morphology and intracellular pH of cultured astrocytes exposed to media lacking bicarbonate', *Neuroscience*, 121(3), pp. 553–562. doi: 10.1016/S0306-4522(03)00557-8.

Groves, a K. *et al.* (1993) 'The characterization of astrocyte cell lines that display properties of glial scar tissue.', *Developmental biology*, pp. 87–104. doi: 10.1006/dbio.1993.1223.

Guerra-Gomes, S. *et al.* (2018) 'Functional Roles of Astrocyte Calcium Elevations: From Synapses to Behavior', *Frontiers in Cellular Neuroscience*, 11(January), pp. 1–7. doi: 10.3389/fncel.2017.00427.

Guthrie, P. B. *et al.* (1999) 'ATP released from astrocytes mediates glial calcium waves', *Journal of Neuroscience*, 19(2), pp. 520–528.

Halassa, M. M. *et al.* (2007) 'Synaptic Islands Defined by the Territory of a Single Astrocyte', 27(24), pp. 6473–6477. doi: 10.1523/JNEUROSCI.1419-07.2007.

Halldorsson, S. *et al.* (2015) 'Advantages and challenges of microfluidic cell culture in polydimethylsiloxane devices', *Biosensors and Bioelectronics*. Elsevier, 63, pp. 218–231. doi: 10.1016/j.bios.2014.07.029.

Han, X. *et al.* (2013) 'Forebrain engraftment by human glial progenitor cells enhances synaptic plasticity and learning in adult mice', *Cell Stem Cell*. Elsevier Inc., 12(3), pp. 342–

353. doi: 10.1016/j.stem.2012.12.015.

Hartwell, L. H. and Kastan, M. B. (1994) 'Cell cycle control and cancer', *Science*, 266, pp. 1821–28.

Hatanaka, H. and Tsukui, H. (1986) 'Differential effects of nerve-growth factor and glioma-conditioned medium on neurons cultured from various regions of fetal rat central nervous system', *Brain Research*, 395(1), pp. 47–56. doi: 10.1016/S0006-8993(86)80007-5.

Hengst, U. *et al.* (2010) 'Axonal elongation triggered by stimulus-induced local translation of a polarity complex protein', *Nature Cell Bioloyg*, 11(8), pp. 1024–1030. doi: 10.1038/ncb1916.Axonal.

Herculano-Houzel (2010) 'Coordinated scaling of cortical and cerebellar numbers of neurons', *Frontiers in Neuroanatomy*. doi: 10.3389/fnana.2010.00012.

Hermes, M., Eichhoff, G. and Garaschuk, O. (2010) 'Intracellular calcium signalling in Alzheimer's disease', *Journal of Cellular and Molecular Medicine*, 14(1–2), pp. 30–41. doi: 10.1111/j.1582-4934.2009.00976.x.

Hertz, L., Peng, L. and Lai, J. C. K. (1998) 'Functional studies in cultured astrocytes', *Methods: A Companion to Methods in Enzymology*, 16(3), pp. 293–310. doi: 10.1006/meth.1998.0686.

Hirase, H. *et al.* (2004) 'Calcium dynamics of cortical astrocytic networks in vivo', *PLoS Biology*, 2(4), pp. 494–499. doi: 10.1371/journal.pbio.0020096.

Hirrlinger, J., Hülsmann, S. and Kirchhoff, F. (2004) 'Astroglial processes show spontaneous motility at active synaptic terminals in situ', *European Journal of Neuroscience*, 20(8), pp. 2235–2239. doi: 10.1111/j.1460-9568.2004.03689.x.

Hökfelt, T., Bartfai, T. and Bloom, F. (2003) 'Neuropeptides: Opportunities for drug discovery', *Lancet Neurology*, 2(8), pp. 463–472. doi: 10.1016/S1474-4422(03)00482-4.

Hol, E. M. and Pekny, M. (2015) 'Glial fibrillary acidic protein (GFAP) and the astrocyte intermediate filament system in diseases of the central nervous system', *Current Opinion in Cell Biology*. Elsevier Ltd, 32, pp. 121–130. doi: 10.1016/j.ceb.2015.02.004.

Holley, J. E. *et al.* (2005) 'Tenascin C induces a quiescent phenotype in cultured adult human astrocytes', *Glia*, 52(1), pp. 53–58. doi: 10.1002/glia.20231.

Hu, X. *et al.* (2016) 'Heterogeneous astrocytes: Active players in CNS', *Brain Research Bulletin*. Elsevier Inc., 125, pp. 1–18. doi: 10.1016/j.brainresbull.2016.03.017.

Huang, C. P. *et al.* (2009) 'Engineering microscale cellular niches for three-dimensional multicellular co-cultures.', *Lab on a chip*, 9, pp. 1740–1748. doi: 10.1039/b818401a.

Huang, Y. and Thathiah, A. (2015) 'Regulation of neuronal communication by G protein-coupled receptors', *FEBS Letters*. Federation of European Biochemical Societies, 589(14), pp. 1607–1619. doi: 10.1016/j.febslet.2015.05.007.

Hughes, C. S., Postovit, L. M. and Lajoie, G. A. (2010) 'Matrigel: a complex protein mixture required for optimal growth of cell culture.', *Proteomics*, pp. 1886–1890. doi: 10.1002/pmic.200900758.

Iino, M. *et al.* (2001) 'Glia-Synapse Interaction through Ca 2+ -Permeable AMPA Receptors in Bergmann Glia', *Science Magazine*, 292(18), pp. 926–929. doi: 10.1126/science.1058827.

James, L. R. *et al.* (2011) 'High-throughput analysis of calcium signalling kinetics in astrocytes stimulated with different neurotransmitters', *PLoS ONE*, 6(10), pp. 1–13. doi: 10.1371/journal.pone.0026889.

Jeon, N. L. (2008) 'A microfluidic culture platform for CNS axonal injury, regeneration and transport', 2(8), pp. 599–605. doi: https://doi.org/10.1038/nmeth777.

Jiang, H. *et al.* (2005) 'Both the establishment and the maintenance of neuronal polarity require active mechanisms: Critical roles of GSK-3β and its upstream regulators', *Cell*, 120(1), pp. 123–135. doi: 10.1016/j.cell.2004.12.033.

Jiglaire, C. J. *et al.* (2014) 'Ex vivo cultures of glioblastoma in three-dimensional hydrogel maintain the original tumor growth behavior and are suitable for preclinical drug and radiation sensitivity screening', *Experimental Cell Research*, 321(2), pp. 99–108.

Johnston, M. V. *et al.* (1987) 'NGF effects on developing forebrain cholinergic neurons are regionally specific', *Neurochemical Research*, 12(11), pp. 985–994. doi: 10.1007/BF00970927.

La Joie, R. *et al.* (2012) 'Region-specific hierarchy between atrophy, hypometabolism, and 2-amyloid (Aβ) load in Alzheimer's disease dementia', *Journal of Neuroscience*, 32(46), pp. 16265–16273. doi: 10.1523/JNEUROSCI.2170-12.2012.

Jones, V. C. *et al.* (2017) 'Aberrant iPSC-derived human astrocytes in Alzheimer's disease', *Cell Death and Disease*. Nature Publishing Group, 8(3), pp. 1–11. doi: 10.1038/cddis.2017.89.

Kane, K. I. W. *et al.* (2018) 'Determination of the rheological properties of Matrigel for optimum seeding conditions in microfluidic cell cultures', *AIP Advances*, 8(12). doi: 10.1063/1.5067382.

Kanemaru, K. *et al.* (2014) 'In Vivo visualization of subtle, transient, and local activity of astrocytes using an ultrasensitive Ca 2+ indicator', *Cell Reports*. The Authors, 8(1), pp. 311–318. doi: 10.1016/j.celrep.2014.05.056.

Kaur, G. and Dufour, J. M. (2012) 'Cell lines: Valuable tools or useless artifacts.', *Spermatogenesis*, 2(1), pp. 1–5. doi: 10.4161/spmg.19885.

Kettenmann, H. and Verkhratsky, A. (2008) 'Neuroglia: the 150 years after', *Trends in Neurosciences*, 31(12), pp. 653–659. doi: 10.1016/j.tins.2008.09.003.

Khakh, B. S. and Sofroniew, M. V (2015) 'Diversity of astrocyte functions and phenotypes in neural circuits', *Nature Neuroscience*, 18(7), pp. 942–952. doi: 10.1038/nn.4043.

Kimelberg, H. K. (2010) 'Functions of Mature Mammalian Astrocytes: A Current View', *The Neuroscientist*, 16(1), pp. 79–106. doi: 10.1177/1073858409342593.

Kirkley, K. S. *et al.* (2017) 'Microglia amplify inflammatory activation of astrocytes in manganese neurotoxicity', *Journal of Neuroinflammation*. Journal of Neuroinflammation, 14(1), pp. 0–17. doi: 10.1186/s12974-017-0871-0.

Kleinman, H. K. and Martin, G. R. (2005) 'Matrigel: Basement membrane matrix with biological activity', *Seminars in Cancer Biology*, pp. 378–384. doi: 10.1016/j.semcancer.2005.05.004.

Knight, V. Bl. and Serrano, E. E. (2017) 'Post-translational Tubulin Modifications in Human Astrocyte Cultures', *Neurochemical Research*, 42(9), pp. 2566–2576. doi: 10.1016/j.physbeh.2017.03.040.

Krencik, R. *et al.* (2011) 'Specification of transplantable astroglial subtypes from human pluripotent stem cells', *Nature Biotechnology*. Nature Publishing Group, 29(6), pp. 528–534. doi: 10.1038/nbt.1877.

Krishnaswamy, V. R. *et al.* (2019) 'Demystifying the extracellular matrix and its proteolytic remodeling in the brain: structural and functional insights', *Cellular and Molecular Life Sciences*. Springer International Publishing, 76(16), pp. 3229–3248. doi: 10.1007/s00018-019-03182-6.

Kucukdereli, H. *et al.* (2011) 'Control of excitatory CNS synaptogenesis by astrocyte-secreted proteins Hevin and SPARC', *Pnas*, 108(32), pp. 440–449. doi: 10.1073/pnas.1104977108/-/DCSupplemental.www.pnas.org/cgi/doi/10.1073/pnas.1104977108.

Kunze, A. *et al.* (2011) 'Synergistic ngf/b27 gradients position synapses heterogeneously in 3d micropatterned neural cultures', *PLoS ONE*, 6(10). doi: 10.1371/journal.pone.0026187.

Laake, J. H. *et al.* (1995) 'Glutamine from Glial Cells Is Essential for the Maintenance of the Nerve Terminal Pool of Glutamate: Immunogold Evidence from Hippocampal Slice Cultures', *Journal of Neurochemistry*, 65(2), pp. 871–881. doi: 10.1046/j.1471-4159.1995.65020871.x.

Lange, S. C. *et al.* (2012) 'Primary cultures of astrocytes: Their value in understanding astrocytes in health and disease', *Neurochemical Research*, 37(11), pp. 2569–2588. doi: 10.1007/s11064-012-0868-0.Primary.

Langley, R. R. *et al.* (2009) 'Generation of an immortalized astrocyte cell line from H-2K b-tsA58 mice to study the role of astrocytes in brain metastasis', *International Journal of Oncology*, 35(4), pp. 665–672. doi: 10.3892/ijo-00000378.

LaPlaca, M. C. *et al.* (2010) 'Three-Dimensional Neuronal Cultures', *Methods in Bioengineering: 3d Tissue Engineering*, pp. 187–204.

Lau, A. and Tymianski, M. (2010) 'Glutamate receptors, neurotoxicity and neurodegeneration', *Pflugers Archiv European Journal of Physiology*, 460(2), pp. 525–542. doi: 10.1007/s00424-010-0809-1.

Lau, C. L. *et al.* (2014) '3D Electrospun scaffolds promote a cytotrophic phenotype of cultured primary astrocytes', *Journal of Neurochemistry*, 130(2), pp. 215–226. doi: 10.1111/jnc.12702.

De Lázaro, I., Yilmazer, A. and Kostarelos, K. (2014) 'Induced pluripotent stem (iPS) cells: A new source for cell-based therapeutics?', *Journal of Controlled Release*. Elsevier B.V., 185(1), pp. 37–44. doi: 10.1016/j.jconrel.2014.04.011.

Lee, H. Y. *et al.* (2018) 'Enhancement of bio-stability and mechanical properties of hyaluronic acid hydrogels by tannic acid treatment', *Carbohydrate Polymers*. Elsevier, 186(November 2017), pp. 290–298. doi: 10.1016/j.carbpol.2018.01.056.

Lee, J., Cuddihy, M. J. and Kotov, N. A. (2008) 'Three-Dimensional Cell Culture Matrices : State of the Art', *Tissue Engineering: Part B*, 14(1), pp. 61–86. doi: 10.1089/teb.2007.0150.

Lee, Y. *et al.* (2006) 'Astrocyte Heterogeneity Revealed by Expression of a GFAP-LacZ Transgene', *Glia*, 53(1), pp. 677–687. doi: https://doi.org/10.1002/glia.20320.

Levitt, P. and Rakic, P. (1980) 'Immunoperoxidase localization of glial fibrillary acidic protein in radial glial cells and astrocytes of the developing rhesus monkey brain', *Journal of Comparative Neurology*, 193(3), pp. 815–840. doi: 10.1002/cne.901930316.

Levy, A. F. *et al.* (2014) 'Influence of basement membrane proteins and endothelial cell-derived factors on the morphology of human fetal-derived astrocytes in 2D', *PLoS ONE*, 9(3), pp. 1–7. doi: 10.1371/journal.pone.0092165.

Lezi, E. and Swerdlow, R. H. (2016) 'Lactate's effect on human neuroblastoma cell bioenergetic fluxes', *Biochemical Pharmacology*. Elsevier Inc., 99, pp. 88–100. doi: 10.1016/j.bcp.2015.11.002.

Liddelow, S. A. *et al.* (2017) 'Neurotoxic reactive astrocytes are induced by activated microglia', *Nature*. Nature Publishing Group, pp. 1–6. doi: 10.1038/nature21029.

Lieberman, a P. *et al.* (1989) 'Production of tumor necrosis factor and other cytokines by astrocytes stimulated with lipopolysaccharide or a neurotropic virus.', *Proceedings of the National Academy of Sciences of the United States of America*, 86(16), pp. 6348–6352. doi: 10.1073/pnas.86.16.6348.

Lin, C. J. *et al.* (2017) 'Identification of diverse astrocyte populations and their malignant analogs', *Nature Neuroscience*, 20(3), pp. 396–405. doi: 10.1038/nn.4493.Identification.

Linda, K., Fiuza, C. and Nadif Kasri, N. (2018) 'The promise of induced pluripotent stem cells for neurodevelopmental disorders', *Progress in Neuro-Psychopharmacology and Biological Psychiatry*. Elsevier, 84(October 2017), pp. 382–391. doi: 10.1016/j.pnpbp.2017.11.009.

Liu, W., Tang, Y. and Feng, J. (2011) 'Cross talk between activation of microglia and astrocytes in pathological conditions in the central nervous system', *Life Sciences*. Elsevier Inc., 89(5–6), pp. 141–146. doi: 10.1016/j.lfs.2011.05.011.

Loaiza, A., Porras, O. H. and Barros, L. F. (2003) 'Glutamate triggers rapid glucose transport stimulation in astrocytes as evidenced by real-time confocal microscopy', *Journal of Neuroscience*, 23(19), pp. 7337–7342.

Lundin, A. *et al.* (2018) 'Human iPS-Derived Astroglia from a Stable Neural Precursor State Show Improved Functionality Compared with Conventional Astrocytic Models', *Stem Cell Reports*, 10(3). doi: 10.1016/j.stemcr.2018.01.021.

Luo, L. (2002) 'Actin Cytoskeleton Regulation in Neuronal Morphogenesis and Structural Plasticity', *Annual Review of Cell and Developmental Biology*, 18(1), pp. 601–635. doi: 10.1146/annurev.cellbio.18.031802.150501.

Luo, Y. *et al.* (2018) 'Three-dimensional hydrogel culture conditions promote the differentiation of human induced pluripotent stem cells into hepatocytes', *Cytotherapy*, 20(1), pp. 95–1072.

Maclean, F. L. *et al.* (2016) 'A Commentary on the Need for 3D-Biologically Relevant In Vitro Environments to Investigate Astrocytes and Their Role in Central Nervous System Inflammation', *Neurochemical Research*. Springer US, 41(3), pp. 589–592. doi: 10.1007/s11064-015-1697-8.

Marchini, A. *et al.* (2019) 'Multifunctionalized hydrogels foster hNSC maturation in 3D cultures and neural regeneration in spinal cord injuries', *Proceedings of the National Academy of Sciences of the United States of America*, 116(15), pp. 7483–7492. doi: 10.1073/pnas.1818392116.

Martin, N. and Youssef, G. (2018) 'Dynamic properties of hydrogels and fiber-reinforced hydrogels', *Journal of the Mechanical Behavior of Biomedical Materials*. Elsevier Ltd, 85(March), pp. 194–200. doi: 10.1016/j.jmbbm.2018.06.008.

Matsui, K. (2005) 'High-Concentration Rapid Transients of Glutamate Mediate Neural-Glial Communication via Ectopic Release', *Journal of Neuroscience*, 25(33), pp. 7538–7547. doi: 10.1523/JNEUROSCI.1927-05.2005.

Matsui, K. and Jahr, C. E. (2003) 'Ectopic release of synaptic vesicles', *Neuron*, 40(6), pp. 1173–1183. doi: 10.1016/S0896-6273(03)00788-8.

Matsui, K. and Jahr, C. E. (2006) 'Exocytosis unbound.', *Current opinion in neurobiology*, 16(3), pp. 305–11. doi: 10.1016/j.conb.2006.04.001.

Mauch, D. H. *et al.* (2001) 'CNS synaptogenesis promoted by glia-derived cholesterol', *Science*, 294(5545), pp. 1354–1357. doi: 10.1126/science.294.5545.1354.

McComish, S. F. and Caldwell, M. A. (2018) 'Generation of defined neural populations from pluripotent stem cells', *Philosophical Transactions of the Royal Society B: Biological Sciences*, 373(1750), pp. 1–15. doi: 10.1098/rstb.2017.0214.

Meldrum, B. S. (2018) 'Glutamate as a Neurotransmitter in the Brain: Review of Physiology and Pathology', *The Journal of Nutrition*, 130(4), pp. 1007S-1015S. doi: 10.1093/jn/130.4.1007s.

Ménager, C. *et al.* (2004) 'PIP3 is involved in neuronal polarization and axon formation', *Journal of Neurochemistry*, 89(1), pp. 109–118. doi: 10.1046/j.1471-4159.2004.02302.x.

Meyer, K. *et al.* (2013) 'Direct conversion of patient fibroblasts demonstrates non-cell autonomous toxicity of astrocytes to motor neurons in familial and sporadic ALS', *Proceedings of the National Academy of Sciences*, 111(2), pp. 829–832. doi: 10.1073/pnas.1314085111.

Meyer, K. *et al.* (2014) 'Direct conversion of patient fibroblasts demonstrates non-cell autonomous toxicity of astrocytes to motor neurons in familial and sporadic ALS', *Proceedings of the National Academy of Sciences of the United States of America*, 111(2), pp. 829–832. doi: 10.1073/pnas.1314085111.

Middeldorp, J. and Hol, E. M. (2011) 'GFAP in health and disease', *Progress in Neurobiology*.

Elsevier Ltd, 93(3), pp. 421–443. doi: 10.1016/j.pneurobio.2011.01.005.

Miller, R. H. and Szigeti, V. (1991) 'Clonal analysis of astrocyte diversity in neonatal rat spinal cord cultures', *Development*, 113(1), pp. 353–362. doi: https://www.researchgate.net/publication/21390797_Miller_R_H_Szigeti_V_Clonal_analysis_of_astrocyte_diversity_in_neonatal_rat_spinal_cord_cultures_Development_113_353-362?enrichId=rgreq-ef102870fd761da80909b5f6d7d70c6b-XXX&enrichSource=Y292ZXJQYWdlOzIxMzkwNzk3O0FTOjk5MDk5MzE1NTM5OTgxQDE0MDA2Mzg1MjY5NDU%3D&el=1_x_2&_esc=publicationCoverPdf.

Miller, S. J. and Rothstein, J. D. (2016) 'Astroglia in thick tissue with super resolution and cellular reconstruction', *PLoS ONE*, 11(8), pp. 1–11. doi: 10.1371/journal.pone.0160391.

Miller, S., Romano, C. and Cotman, C. W. (1995) 'Growth factor upregulation of a phosphoinositide-coupled metabotropic glutamate receptor in cortical astrocytes', *Journal of Neuroscience*, 15(9), pp. 6103–6109.

Millet, L. J. *et al.* (2007) 'Microfluidic devices for culturing primary mammalian neurons at low densities', *Lab on a Chip*, 7(8), pp. 987–994. doi: 10.1039/b705266a.

Millet, L. J. and Gillette, M. U. (2012) 'New perspectives on neuronal development via microfluidic environments', *Trends in Neurosciences*. Elsevier Ltd, 35(12), pp. 752–761. doi: 10.1016/j.tins.2012.09.001.

Miyazaki, T. *et al.* (2017) 'Glutamate transporter GLAST controls synaptic wrapping by Bergmann glia and ensures proper wiring of Purkinje cells', *Pnas*, 114(28), pp. 7438–7443. doi: 10.1073/pnas.1617330114.

Modo, M. (2019) 'Bioscaffold-Induced Brain Tissue Regeneration', *Frontiers in Neuroscience*, 13(November), pp. 1–26. doi: 10.3389/fnins.2019.01156.

Mohand-Kaci, F. *et al.* (2012) 'Optimized Hyaluronic Acid–Hydrogel Design and Culture Conditions for Preservation of Mesenchymal Stem Cell Properties', *Tissue Eng Part C Methods*, 19(4), pp. 288–298.

Mölders, A. *et al.* (2018) 'Heterogeneity of the astrocytic AMPA-receptor transcriptome', *Glia*, 66(12), pp. 2604–2616. doi: 10.1002/glia.23514.

Moloney, E. B., de Winter, F. and Verhaagen, J. (2014) 'ALS as a distal axonopathy: Molecular mechanisms affecting neuromuscular junction stability in the presymptomatic stages of the disease', *Frontiers in Neuroscience*, 8, pp. 1–18. doi: 10.3389/fnins.2014.00252.

Nakamura, F., Kalb, R. G. and Strittmatter, S. M. (2000) 'Molecular basis of semaphorin-mediated axon guidance', *Journal of Neurobiology*, 44(2), pp. 219–229. doi: 10.1002/1097-

4695(200008)44:2<219::AID-NEU11>3.0.CO;2-W.

Nakayama, R. *et al.* (2016) 'Subcellular calcium dynamics during juvenile development in mouse hippocampal astrocytes', *European Journal of Neuroscience*, 43(7), pp. 923–932. doi: 10.1111/ejn.13188.

Nedegaard, M. (1994) 'Direct Signaling from Astrocytes to Neurons in Cultures of Mammalian Brain Cells', *Science*, 263(March), pp. 1768–1771. doi: https://doi.org/10.1126/science.8134839.

Newman, E. A. (2001) 'Propagation of intercellular calcium waves in retinal astrocytes and Muller cells', *Journal of Neuroscience*, 21(7), pp. 2215–2223.

Newman, E. A. (2003) 'New roles for astrocytes: Regulation of synaptic transmission', *Trends in Neurosciences*, 26(10), pp. 536–542. doi: 10.1016/S0166-2236(03)00237-6.

Nisbet, D. R. *et al.* (2008) 'Neural tissue engineering of the CNS using hydrogels', *Journal of Biomedical Materials Research - Part B Applied Biomaterials*, 87(1), pp. 251–263. doi: 10.1002/jbm.b.31000.

Novak, U. and Kaye, A. H. (2000) 'Extracellular matrix and the brain: Components and function', *Journal of Clinical Neuroscience*, 7(4), pp. 280–290. doi: 10.1054/jocn.1999.0212.

Nowak, L. G. and Bullier, J. (1996) 'Spread of stimulating current in the cortical grey matter of rat visual cortex studied on a new in vitro slice preparation', *Journal of Neuroscience Methods*, 67(2), pp. 237–248. doi: 10.1016/0165-0270(96)00065-9.

Nusbaum, M. P., Blitz, D. M. and Marder, E. (2017) 'Functional consequences of neuropeptide and small-molecule co-transmission', *Nature Reviews Neuroscience*. Nature Publishing Group, 18(7), pp. 389–403. doi: 10.1038/nrn.2017.56.

Oberheim, N. A. *et al.* (2006) 'Astrocytic complexity distinguishes the human brain.', *Trends in neurosciences*. Elsevier, 29(10), pp. 547–53. doi: 10.1016/j.tins.2006.08.004.

Oberheim, N. A. *et al.* (2009) 'Uniquely hominid features of adult human astrocytes', *Journal of Neuroscience*, 29(10), pp. 3276–3287. doi: 10.1523/JNEUROSCI.4707-08.2009.

Oberheim, N. A. *et al.* (2010) 'Uniquely hominid features of adult human astrocytes', *J Neuroscience*, 29(10), pp. 1–23. doi: 10.1523/JNEUROSCI.4707-08.2009.Uniquely.

Ohnuki, M. *et al.* (2014) 'Dynamic regulation of human endogenous retroviruses mediates factor-induced reprogramming and differentiation potential', *Proceedings of the National Academy of Sciences of the United States of America*, 111(34), pp. 12426–12431. doi: 10.1073/pnas.1413299111.

Ohnuki, M. and Takahashi, K. (2015) 'Present and future challenges of induced pluripotent stem cells', *Philosophical Transactions of the Royal Society B: Biological Sciences*, 370(1680). doi: 10.1098/rstb.2014.0367.

Oliveira, J. F. *et al.* (2015) 'Do stars govern our actions? Astrocyte involvement in rodent behavior', *Trends in Neurosciences*, 38(9), pp. 535–549. doi: 10.1016/j.tins.2015.07.006.

Pampaloni, F., Reynaud, E. G. and Stelzer, E. H. K. (2007) 'The third dimension bridges the gap between cell culture and live tissue', *Nature Reviews Molecular Cell Biology*, 8(10), pp. 839–845. doi: 10.1038/nrm2236.

Panatier, A. and Robitaille, R. (2016) 'Astrocytic mGluR5 and the tripartite synapse', *Neuroscience*. IBRO, 323, pp. 29–34. doi: 10.1016/j.neuroscience.2015.03.063.

Park, I. H. *et al.* (2008) 'Disease-Specific Induced Pluripotent Stem Cells', *Cell*, 134(5), pp. 877–886. doi: 10.1016/j.cell.2008.07.041.

Pascual, O. *et al.* (2012) 'Microglia activation triggers astrocyte-mediated modulation of excitatory neurotransmission', *Pnas*, 109(4), pp. 197–205. doi: 10.1073/pnas.1111098109.

Pebworth, M. P., Cismas, S. A. and Asuri, P. (2014) 'A novel 2.5D culture platform to investigate the role of stiffness gradients on adhesion-independent cell migration', *PLoS ONE*, 9(10). doi: 10.1371/journal.pone.0110453.

Pekny, M. and Nilsson, M. (2005) 'Astrocyte activation and reactive gliosis', *Glia*, 50(4), pp. 427–434. doi: 10.1002/glia.20207.

Pekny, M. and Pekna, M. (2019) 'ASTROCYTE REACTIVITY AND REACTIVE ASTROGLIOSIS : COSTS AND BENEFITS STARTING WITH A HEALTHY BRAIN', (Figure 1), pp. 1077–1098. doi: 10.1152/physrev.00041.2013.

Pen, A. E. and Jensen, U. B. (2017) 'Current status of treating neurodegenerative disease with induced pluripotent stem cells', *Acta Neurologica Scandinavica*, 135(1), pp. 57–72. doi: 10.1111/ane.12545.

Perea, G. and Araque, A. (2005) 'Glial calcium signaling and neuron-glia communication', *Cell Calcium*, 38(3-4 SPEC. ISS.), pp. 375–382. doi: 10.1016/j.ceca.2005.06.015.

Perea, G., Navarrete, M. and Arague, A. (2009) 'Tripartite synapses: astrocytes process and control synaptic information', *Trends in Neurosciences*, 32(8), pp. 421–431.

Petravicz, J., Fiacco, T. A. and McCarthy, K. D. (2008) 'Loss of IP3 receptor-dependent Ca2+ increases in hippocampal astrocytes does not affect baseline CA1 pyramidal neuron synaptic activity', *Journal of Neuroscience*, 28(19), pp. 4967–4973. doi: 10.1523/JNEUROSCI.5572-

07.2008.

Pfrieger, F. W. and Barres, B. A. (1997) 'Synaptic Efficacy Enhanced by Glial Cells in Vitro', *Science*, 277, pp. 1684–1687. doi: 10.1126/science.277.5332.1684.

Placone, A. L. *et al.* (2015) 'Human astrocytes develop physiological morphology and remain quiescent in a novel 3D matrix', *Biomaterials*, 42, pp. 134–143. doi: 10.1016/j.biomaterials.2014.11.046.

Polo, J. M. *et al.* (2013) 'A molecular roadmap of cellular reprogramming into iPS cells', *Cell*, 151(7), pp. 1617–1632. doi: 10.1016/j.cell.2012.11.039.A.

Porter, J. T. and McCarthy, K. D. (1997) 'Astrocytic neurotransmitter receptors in situ and in vivo', *Progress in Neurobiology*, 51(4), pp. 439–455. doi: 10.1016/S0301-0082(96)00068-8.

Pozzi, D. *et al.* (2017) 'An improved method for growing neurons: Comparison with standard protocols', *Journal of Neuroscience Methods*. Elsevier B.V., 280, pp. 1–10. doi: 10.1016/j.jneumeth.2017.01.013.

Prah, J. *et al.* (2019) 'A novel serum free primary astrocyte culture method that mimic quiescent astrocyte phenotype', *Journal of Neuroscience Methods*. Elsevier, 320(March), pp. 50–63. doi: 10.1016/j.jneumeth.2019.03.013.

Price, T. N., Burke, J. F. and Mayne, L. V (1999) 'A novel human astrocyte cell line (A735) with astrocyte-specific neurotransmitter function.', *In vitro cellular & developmental biology. Animal*, 35(5), pp. 279–88. doi: 10.1007/s11626-999-0072-y.

Puschmann, T. B. *et al.* (2013) 'Bioactive 3D cell culture system minimizes cellular stress and maintains the in vivo-like morphological complexity of astroglial cells', *Glia*, 61(3), pp. 432–440. doi: 10.1002/glia.22446.

Rastogi, P. and Kandasubramanian, B. (2019) 'Review of alginate-based hydrogel bioprinting for application in tissue engineering', *Biofabrication*. IOP Publishing, 11(4). doi: 10.1088/1758-5090/ab331e.

Regehr, K. J. *et al.* (2009) 'Biological implications of polydimethylsiloxane-based microfluidic cell culture', *Lab on a Chip*, 9(15), pp. 2132–2139. doi: 10.1039/b903043c.

Al Rifai, N. *et al.* (2015) 'Culture of PC12 neuronal cells in GelMA hydrogel for brain tissue engineering', *2015 International Conference on Advances in Biomedical Engineering, ICABME 2015*. IEEE, pp. 254–257. doi: 10.1109/ICABME.2015.7323300.

Rose, C. F., Verkhratsky, A. and Parpura, V. (2013) 'Astrocyte glutamine synthetase: Pivotal in health and disease', *Biochemical Society Transactions*, 41(6), pp. 1518–1524. doi:

10.1042/BST20130237.

Rothermundt, M. *et al.* (2003) 'S100B in brain damage and neurodegeneration.', *Microscopy research and technique*, 60(6), pp. 614–632. doi: 10.1002/jemt.10303.

Rothstein, J. D. *et al.* (1996) 'Knockout of glutamate transporters reveals a major role for astroglial transport in excitotoxicity and clearance of glutamate', *Neuron*, 16(3), pp. 675–686. doi: 10.1016/S0896-6273(00)80086-0.

Rowitch, D. H. and Kriegstein, A. R. (2010) 'Developmental genetics of vertebrate glial-cell specification', *Nature*, 468(7321), pp. 214–222. doi: 10.1038/nature09611.

Roybon, L. *et al.* (2013) 'Human stem cell-derived spinal cord astrocytes with defined mature or reactive phenotypes', *Cell Reports*. The Authors, 4(5), pp. 1035–1048. doi: 10.1016/j.celrep.2013.06.021.

Roybon, L. *et al.* (2014) 'Human stem cell-derived spinal cord astrocytes with defined mature or reactive phenotypes', *Cell Reports*, 4(5), pp. 1035–1048. doi: 10.1016/j.celrep.2013.06.021.Human.

Rungta, R. L. *et al.* (2016) 'Ca2+ transients in astrocyte fine processes occur via Ca2+ influx in the adult mouse hippocampus', *Glia*, 64(12), pp. 2093–2103. doi: 10.1002/glia.23042.

Rusnakova, V. *et al.* (2013) 'Heterogeneity of Astrocytes: From Development to Injury - Single Cell Gene Expression', *PLoS ONE*, 8(8), pp. 1–15. doi: 10.1371/journal.pone.0069734.

Rutecki, P. a. (1992) 'Neuronal Excitability: Voltage Dependent Currents and Synaptic Transmission', *Journal of Clinical Neurophysiology*, 9(2), pp. 195–211. doi: 10.1097/00004691-199204010-00003.

Rutka, J. T. *et al.* (1987) 'Establishment and characterization of five cell lines derived from human malignant gliomas', *Acta Neuropathologica*, 75, pp. 92–103.

Saab, A. *et al.* (2012) 'Bergmann Glial AMPA Receptors Are Required for Fine Motor Coordination', *Science Magazine*, 337(6095), pp. 749–754. doi: 10.1126/science.1221140.

Saab, C. Y. and Willis, W. D. (2003) 'The cerebellum: Organization, functions and its role in nociception', *Brain Research Reviews*, 42(1), pp. 85–95. doi: 10.1016/S0165-0173(03)00151-6.

Santos, R. *et al.* (2017) 'Differentiation of Inflammation-Responsive Astrocytes from Glial Progenitors Generated from Human Induced Pluripotent Stem Cells', *Stem Cell Reports*. ElsevierCompany., 8(6), pp. 1757–1769. doi: 10.1016/j.stemcr.2017.05.011.

Schitine, C. *et al.* (2015) ‘Astrocyte heterogeneity in the brain: from development to disease’, *Frontiers in Cellular Neuroscience*, 9, pp. 1–11. doi: 10.3389/fncel.2015.00076.

Schnitzer, J., Franke, W. W. and Schachner, M. (1981) ‘Immunocytochemical demonstration of vimentin in astrocytes and ependymal cells of developing and adult mouse nervous system’, *Journal of Cell Biology*, 90(2), pp. 435–447. doi: 10.1083/jcb.90.2.435.

Shigetomi, E. *et al.* (2019) ‘Aberrant calcium signals in reactive astrocytes: A key process in neurological disorders’, *International Journal of Molecular Sciences*, 20(4), pp. 1–18. doi: 10.3390/ijms20040996.

Shih, A. Y. *et al.* (2003) ‘Coordinate regulation of glutathione biosynthesis and release by Nrf2-expressing glia potently protects neurons from oxidative stress’, *Journal of Neuroscience*, 23(8), pp. 3394–3406.

Shipley, M. M., Mangold, C. A. and Szpara, M. L. (2016) ‘Differentiation of the SH-SY5Y human neuroblastoma cell line’, *Journal of Visualized Experiments*, 2016(108), pp. 1–11. doi: 10.3791/53193.

Silver, J. and Miller, J. H. (2004) ‘REGENERATION BEYOND THE GLIAL SCAR’, 5(February), pp. 146–156. doi: 10.1038/nrn1326.

Smith, I. *et al.* (2015) ‘Neuronal-glial populations form functional networks in a biocompatible 3D scaffold’, *Neuroscience Letters*. Elsevier Ireland Ltd, 609, pp. 198–202. doi: 10.1016/j.neulet.2015.10.044.

Smithmyer, M. E., Cassel, S. E. and Kloxin, A. M. (2019) ‘Bridging 2D and 3D culture: Probing impact of extracellular environment on fibroblast activation in layered hydrogels’, *AIChE Journal*, 65(12), pp. 1–14. doi: 10.1002/aic.16837.

Sofroniew, M. V. and Vinters, H. V. (2010) ‘Astrocytes: Biology and pathology’, *Acta Neuropathologica*, 119(1), pp. 7–35. doi: 10.1007/s00401-009-0619-8.

Sofroniew, M. V (2009) ‘Molecular dissection of reactive astrogliosis and glial scar formation’, (September), pp. 638–647. doi: 10.1016/j.tins.2009.08.002.

Souza, D. G. *et al.* (2013) ‘Characterization of Adult Rat Astrocyte Cultures’, *PLoS ONE*, 8(3), pp. 1–10. doi: 10.1371/journal.pone.0060282.

Spector, A. A., John, K. and Fletcher, J. E. (1969) ‘Binding of long-chain fatty acids to bovine serum albumin.’, *Journal of Lipid Research*, 10(1), pp. 56–67.

Ståhlberg, A. *et al.* (2011) ‘Defining cell populations with single-cell gene expression profiling: Correlations and identification of astrocyte subpopulations’, *Nucleic Acids Research*, 39(4),

pp. 1–12. doi: 10.1093/nar/gkq1182.

Stansbury, J. W. (2013) ‘Dimethacrylate network formation and polymer property evolution as determined by the selection of monomers and curing conditions’, *Dental Materials*, 28(1), pp. 13–22. doi: 10.1016/j.dental.2011.09.005.Dimethacrylate.

Südhof, T. C. (2012) ‘The presynaptic active zone’, *Neuron*, 75(1), pp. 11–25. doi: 10.1016/j.neuron.2012.06.012.

Tabata, H. (2015) ‘Diverse subtypes of astrocytes and their development during corticogenesis’, *Frontiers in Neuroscience*, 9(APR), pp. 1–7. doi: 10.3389/fnins.2015.00114.

Takahashi, K. *et al.* (2014) ‘Induction of pluripotency in human somatic cells via a transient state resembling primitive streak-like mesendoderm’, *Nature Communications*. Nature Publishing Group, 5(3678), pp. 1–9. doi: 10.1038/ncomms4678.

Tarus, D. *et al.* (2016) ‘Design of Hyaluronic Acid Hydrogels to Promote Neurite Outgrowth in Three Dimensions’, *ACS Applied Materials and Interfaces*, 8(38), pp. 25051–25059. doi: 10.1021/acsami.6b06446.

Tautenhahn, M. *et al.* (2012) ‘Purinergic modulation of the excitatory synaptic input onto rat striatal neurons’, *Neuropharmacology*. Elsevier Ltd, 62(4), pp. 1756–1766. doi: 10.1016/j.neuropharm.2011.12.001.

Taylor, A. *et al.* (2005) ‘A microfluidic culture platform for CNS axonal injury, regeneration and transport.’, *Nature Methods*, 2, pp. 599–605.

Taylor, A. M. *et al.* (2009) ‘Axonal mRNA in uninjured and regenerating cortical mammalian axons’, *Journal of Neuroscience*, 29(15), pp. 4697–4707. doi: 10.1523/JNEUROSCI.6130-08.2009.

Taylor, A. M. *et al.* (2010) ‘Microfluidic Local Perfusion Chambers for the Visualization and Manipulation of Synapses’, *Neuron*. Elsevier Ltd, 66(1), pp. 57–68. doi: 10.1016/j.neuron.2010.03.022.

Taylor, A. M. and Jeon, N. L. (2010) ‘Micro-scale and microfluidic devices for neurobiology’, *Current Opinion in Neurobiology*. Elsevier Ltd, 20(5), pp. 640–647. doi: 10.1016/j.conb.2010.07.011.

Taylor, A. M., Menon, S. and Gupton, S. L. (2015) ‘Passive microfluidic chamber for long-term imaging of axon guidance in response to soluble gradients’, *Lab on a Chip*. Royal Society of Chemistry, 15(13), pp. 2781–2789. doi: 10.1039/c5lc00503e.

Thornton, K. *et al.* (2009) ‘Controlling stiffness in nanostructured hydrogels produced by

enzymatic dephosphorylation', *Biochemical Society Transactions*, 37(4), pp. 660–664. doi: 10.1042/bst0370660.

Toda, M. *et al.* (2002) 'Cell Growth Suppression of Astrocytoma C6 Cells by Glial Fibrillary Acidic Protein cDNA Transfection', *Journal of Neurochemistry*, 63(5), pp. 1975–1978. doi: 10.1046/j.1471-4159.1994.63051975.x.

Toh, Y.-C. *et al.* (2007) 'A novel 3D mammalian cell perfusion-culture system in microfluidic channels.', *Lab on a chip*, 7(3), pp. 302–309. doi: 10.1039/b614872g.

Tong, B. C. K. *et al.* (2018) 'Calcium signaling in Alzheimer's disease & therapies', *Biochimica et Biophysica Acta - Molecular Cell Research*. Elsevier, 1865(11), pp. 1745–1760. doi: 10.1016/j.bbamcr.2018.07.018.

Trabelsi, Y. *et al.* (2017) 'The conversion of glutamate by glutamine synthase in neocortical astrocytes from juvenile rat is important to limit glutamate spillover and peri/extrasynaptic activation of NMDA receptors', *Glia*, 65(2), pp. 401–415. doi: 10.1002/glia.23099.

Ugbode, C. I., Hirst, W. D. and Rattray, M. (2016) 'Astrocytes Grown in Alvetex Ò Three Dimensional Scaffolds Retain a Non-reactive Phenotype', *Neurochemical Research*. Springer US, 41(8), pp. 1857–1867. doi: 10.1007/s11064-016-1911-3.

Uggeri, J. *et al.* (2000) 'Calcein-AM is a detector of intracellular oxidative activity', *Histochemistry and Cell Biology*, 122(5), pp. 499–505. doi: 10.1007/s00418-004-0712-y.

Ullian, E. M., Christopherson, K. S. and Barres, B. E. N. A. (2004) 'Role for Glia in Synaptogenesis', 216(April), pp. 209–216. doi: 10.1002/glia.20082.

van der Valk, J. *et al.* (2010) 'Optimization of chemically defined cell culture media - Replacing fetal bovine serum in mammalian in vitro methods', *Toxicology in Vitro*. Elsevier Ltd, 24(4), pp. 1053–1063. doi: 10.1016/j.tiv.2010.03.016.

Van Der Valk, J. *et al.* (2004) 'The humane collection of fetal bovine serum and possibilities for serum-free cell and tissue culture', *Toxicology in Vitro*, 18(1), pp. 1–12. doi: 10.1016/j.tiv.2003.08.009.

Vardjan, N., Kreft, M. and Zorec, R. (2014) 'Dynamics of β-adrenergic/cAMP signaling and morphological changes in cultured astrocytes', *Glia*, 62(4), pp. 566–579. doi: 10.1002/glia.22626.

Vasile, F., Dossi, E. and Rouach, N. (2017) 'Human astrocytes: structure and functions in the healthy brain', *Brain Structure and Function*, pp. 2017–2029. doi: 10.1007/s00429-017-1383-5.

Velasco, I. *et al.* (2003) 'Influence of serum-free medium on the expression of glutamate transporters and the susceptibility to glutamate toxicity in cultured cortical neurons', *Journal of Neuroscience Research*, 71(6), pp. 811–818. doi: 10.1002/jnr.10538.

Verkhratsky, A. *et al.* (2014) 'Glia in the pathogenesis of neurodegenerative diseases.', *Biochemical Society transactions*, 42(5), pp. 1291–301. doi: 10.1042/BST20140107.

Vickerman, V. *et al.* (2008) 'Design, fabrication and implementation of a novel multi-parameter control microfluidic platform for three-dimensional cell culture and real-time imaging', *Lab on a Chip*, 8(9), pp. 1468–1477. doi: Doi 10.1039/B802395f.

Volterra, A., Liaudet, N. and Savtchouk, I. (2014) 'Astrocyte Ca(2+) signalling: an unexpected complexity.', *Nature reviews. Neuroscience*. Nature Publishing Group, 15(5), pp. 327–35. doi: 10.1038/nrn3725.

Wan, S. *et al.* (2016) 'Self-assembling peptide hydrogel for intervertebral disc tissue engineering', *Acta Biomaterialia*, 46, pp. 29–40. doi: 10.1016/j.actbio.2016.09.033.

Wang, F. *et al.* (2012) 'Bergmann glia modulate cerebellar Purkinje cell bistability via Ca 2+-dependent K+ uptake', *Proceedings of the National Academy of Sciences of the United States of America*, 109(20), pp. 7911–7916. doi: 10.1073/pnas.1120380109.

Wang, J. *et al.* (2012) 'High glucose-induced expression of inflammatory cytokines and reactive oxygen species in cultured astrocytes', *Neuroscience*, 202, pp. 58–68. doi: 10.1016/j.neuroscience.2011.11.062.

Wang, T. W. and Spector, M. (2009) 'Development of hyaluronic acid-based scaffolds for brain tissue engineering', *Acta Biomaterialia*. Acta Materialia Inc., 5(7), pp. 2371–2384. doi: 10.1016/j.actbio.2009.03.033.

Wang, X. *et al.* (2006) 'Astrocytic Ca2+ signaling evoked by sensory stimulation in vivo', *Nature Neuroscience*, 9(6), pp. 816–823. doi: 10.1038/nn1703.

Watson, P. M. D. *et al.* (2017) 'The CNS in Three Dimensions', *SAGE*, pp. 1–19. doi: 10.1177/2472555217691450.

de Wied, D. (1987) 'The neuropeptide concept', *Progress in Brain Research*, 72, pp. 93–108.

Won, C. K. and Oh, Y. S. (2000) 'CAMP-induced stellation in primary astrocyte cultures with regional heterogeneity', *Brain Research*, 887(2), pp. 250–258. doi: 10.1016/S0006-8993(00)02922-X.

Wong, A. P. *et al.* (2008) 'Partitioning microfluidic channels with hydrogel to construct tunable 3-D cellular microenvironments', *Biomaterials*, 29(12), pp. 1853–1861. doi:

10.1016/j.biomaterials.2007.12.044.

Woods, A. *et al.* (1986) 'Adhesion and cytoskeletal organisation of fibroblasts in response to fibronectin fragments.', *The EMBO Journal*, 5(4), pp. 665–670. doi: 10.1002/j.1460-2075.1986.tb04265.x.

Worthington, P., Pochan, D. J. and Langhans, S. A. (2015) 'Peptide hydrogels - versatile matrices for 3D cell culture in cancer medicine', *Frontiers in Oncology*, 5(APR), pp. 1–10. doi: 10.3389/fonc.2015.00092.

Xu-Friedman, M. A., Harris, K. M. and Regehr, W. G. (2001) 'Three-Dimensional Comparison of Ultrastructural Characteristics at Depressing and Facilitating Synapses onto Cerebellar Purkinje Cells', *J. Neurosci.*, 21(17), pp. 6666–6672.

Yamaguchi, Y. (2000) 'Lecticans: Organizers of the brain extracellular matrix', *Cellular and Molecular Life Sciences*, 57(2), pp. 276–289. doi: 10.1007/PL00000690.

Yang, I. H. *et al.* (2009) 'Compartmentalized microfluidic culture platform to study mechanism of paclitaxel-induced axonal degeneration', *Experimental Neurology*. Elsevier Inc., 218(1), pp. 124–128. doi: 10.1016/j.expneurol.2009.04.017.

Yeo, L. Y. *et al.* (2011) 'Microfluidic devices for bioapplications', *Small*, 7(1), pp. 12–48. doi: 10.1002/smll.201000946.

Yoshimura, T., Arimura, N. and Kaibuchi, K. (2006) 'Molecular mechanisms of axon specification and neuronal disorders', *Annals of the New York Academy of Sciences*, 1086, pp. 116–125. doi: 10.1196/annals.1377.013.

Yuste, R. (2015) 'From the neuron doctrine to neural networks', *Nature Reviews Neuroscience*. Nature Publishing Group, 16(8), pp. 487–497. doi: 10.1038/nrn3962.

Zamanian, J. L. *et al.* (2012) 'Genomic analysis of reactive astrogliosis', *Journal of Neuroscience*, 32(18), pp. 6391–6410. doi: 10.1523/JNEUROSCI.6221-11.2012.

Zhang, Y. and Barres, B. A. (2010) 'Astrocyte heterogeneity: An underappreciated topic in neurobiology', *Current Opinion in Neurobiology*. Elsevier Ltd, 20(5), pp. 588–594. doi: 10.1016/j.conb.2010.06.005.

Zhao, G. *et al.* (2016) 'Reduced structural complexity of the right cerebellar cortex in male children with autism spectrum disorder', *PLoS ONE*, pp. 1–27. doi: https://doi.org/10.1371/journal.pone.0196964.

Zhao, S. *et al.* (2004) 'Human, mouse, and rat genome large-scale rearrangements: Stability versus speciation', *Genome Research*, 14(10 A), pp. 1851–1860. doi: 10.1101/gr.2663304.

Zhou, Z., Ikegaya, Y. and Koyama, R. (2019) ‘The astrocytic cAMP pathway in health and disease’, *International Journal of Molecular Sciences*, 20(3), pp. 1–27. doi: 10.3390/ijms20030779.

Zipursky SL, et al. L. H. B. A. (2000) ‘The Actin Cytoskeleton - Molecular Cell Biology - 4th edition’, in Darnell, J. E. (ed.) *Molecular Cell Biology 4th Edition*. New York: W. H. Freema, p. Section 21.1 Overview of Neuron Structure and Func. Available at: https://www.ncbi.nlm.nih.gov/books/NBK21535/.

Zuchero, J. B. and Barres, B. A. (2015) ‘Glia in mammalian development and disease’, *Development (Cambridge)*, 142(22), pp. 3805–3809. doi: 10.1242/dev.129304.

Zuidema, J. M. *et al.* (2014) ‘A protocol for rheological characterization of hydrogels for tissue engineering strategies’, *Journal of Biomedical Materials Research - Part B Applied Biomaterials*, 102(5), pp. 1063–1073. doi: 10.1002/jbm.b.33088.

Appendix

Methods

Hyaluronic Acid Hydrogels (Section 5.2.2.3)

I selected the Hystem Hydrogel Kit (Esi-Bio, GS311, 7.5 ml) to generate hyaluronic acid hydrogels for 3D cell culture.

See https://esibio.com/media/wysiwyg/esibio/documents/WEB_Rev._B_GS311_Hystem_7.5_Datasheet.pdf for full manufacturer's instructions.

Overview

The HyStem Hydrogel Kit comprises: Glycosil® (thiol-modified hyaluronic acid), Extralink®-Lite (polyethylene glycol diacrylate - PEGDA), and degassed deionized water (DG Water). Glycosil and Extralink-Lite are packaged as lyophilized solids that are blanketed by nitrogen and under a slight vacuum. A mixed solution of Glycosil and Extralink-Lite forms a transparent hydrogel when mixed.

Storage

Store Glycosil and Extralink-Lite in original vials at -20°C for up to one year. It is recommended to reconstitute each vial in its entirety and reconstituted solutions can be stored at -20°C for up to one month. Use a syringe to add DG Water to Glycosil and remove product from the vials (do not uncap Glycosil vials since material will crosslink in the presence of oxygen).

Preparation

Allow the Glycosil, Extralink-Lite, and DG Water to come to room temperature and under aseptic conditions, using a syringe and needle, add 1 ml of DG Water to the Glycosil vial. Place the vial horizontally on a rocker and leave for 40 minutes for the solids to fully dissolve. Warming up to 37°C and/or gently vortexing will speed dissolution and generate a clear and slightly viscous

solution. Under aseptic conditions, using a syringe and needle, add 0.5 ml of DG Water to the Extralink-Lite vial and invert several times to dissolve.

If encapsulating cells within the hydrogel, resuspend the cell pellet in 1 ml of Glycosil and pipette back and forth to mix. To form the hydrogel, add Extralink-Lite to the Glycosil mix in a 1:4 volume ratio and mix by pipette. When encapsulating cells, allow the solution to react for 10 minutes, then mix again by pipette to ensure even distribution of cells. Gelation will occur within 30 minutes.

Confocal Imaging Parameters for Different 2D and 3D Matrices (Section 2.3.3.1)

Full imaging parameters for 2D 24-well plates (section 2.3.3.1.1) are shown in table 1.

Parameter	Selected Value
Dimensions	1024 x 1024, 16-bit
Zoom	1.0
Objective	C-Apochromat 40x/1.20 Korr M27
Pixel Dwell (µseconds)	1.58
Average	2
Master Gain	700
Digital Gain	1.00
Digital Offset	0.00
Pinhole (µm)	39.6 (1 Area Unit)
Filters	493 – 616
Lasers	488, 2%
Z-Stack Interval (µm)	0.48

Table 1. Final Confocal Imaging Parameters for 2D Plates.

Full imaging parameters for the Alvetex scaffold (section 2.3.3.1.2) are shown in table 2.

Parameter	Selected Value
Dimensions	512 x 512, 16-bit
Zoom	3.0
Objective	C-Apochromat 10x/0.45
Pixel Dwell (µseconds)	6.30
Average	1
Master Gain	Channel 1: ~600 Channel 2: ~1000
Digital Gain	1.00
Digital Offset	0.00
Pinhole (µm)	Channel 1 - 57, Channel 2 - 131
Filters	Channel 1: 410 – 513 Channel 2: 493 – 598
Lasers	405 (2%) & 488 (10%)
Z-Stack Interval (µm)	6.98

Table 2. Confocal Imaging Parameters for Alvetex® scaffold discs.

Full imaging parameters for 3 mg/ml matrigel and 5 mg/ml hyaluronic acid are shown in table 3 (section 2.3.3.1.3).

Parameter	Selected Value
Dimensions	1024 x 1024, 16-bit
Zoom	1.0
Objective	C-Apochromat 10x/0.45
Pixel Dwell (µsecond)	1.58
Average	2
Master Gain	~ 550
Digital Gain	1.00
Digital Offset	0.00
Pinhole (µm)	40
Filters	477 – 554
Lasers	488 nm, 2%
Z-Stack Interval (µm)	1.60

Table 3. Confocal Imaging Parameters for 3 mg/ml Matrigel or 5 mg/ml Hyaluronic Acid.

Full imaging parameters for imaging neurons in 3 mg/ml matrigel are shown in table 5 (section 6.2.4).

Parameter	Selected Value
Dimensions	256 x 256, 16-bit
Zoom	4.0
Objective	C-Apochromat 10x/0.45W
Pixel Dwell (µsecond)	6.30
Average	Line 4
Master Gain	500
Digital Gain	1.00
Digital Offset	0.00
Pinhole (µm)	33
Filters	496 - 603
Lasers	477 nm, 2%

Table 4. Imaging parameters for primary embryonic (E18) cortical neurons in 3 mg/ml matrigel on the Zeiss 710 confocal.

Post Imaging Processing for 3D Z-Stacks (Section 2.3.3.2)

Bead analysis for 2D culture formats is shown in table 5 (see section 2.3.3.2.1).

Length in X (µm)	Length in Y (µm)	Length in Z (µm)
4.36	4.77	5.94
4.77	4.36	4.22
4.36	4.57	3.97
4.57	4.57	3.97
4.15	4.36	4.46
4.57	4.15	4.22
4.36	4.36	5.91

Table 5. Bead lengths in X, Y and Z post Z scale adjustment for beads cultured in 2D formats. Mean length in X = 4.45 µm, mean length in Y = 4.45 µm, mean length in Z = 4.67 µm.

Bead analysis for 3 mg/ml matrigel 3D culture formats is shown in table 6 (see section 2.3.3.2.2).

Length in X (µm)	Length in Y (µm)	Length in Z (µm)
4.15	5.81	5.24
4.98	5.81	4.14
4.98	4.98	5.24
4.98	4.15	4.69
4.98	4.15	4.69
4.98	4.98	4.69
4.98	4.15	5.8
4.98	5.81	5.8
4.98	5.81	5.8
4.98	4.98	4.69
4.15	4.98	5.24
4.98	4.98	5.24
4.98	4.15	5.52
4.98	4.98	5.52
4.15	4.98	4.97
4.98	4.98	4.14
4.15	4.15	4.42
4.98	4.15	5.52
4.15	4.98	5.52
4.98	4.98	6.07
4.98	4.15	5.24

Table 6. Bead lengths in X, Y and Z post Z scale adjustment for beads cultured in 3D matrigel. Mean length in X = 4.78 µm, mean length in Y = 4.86 µm and mean length in Z = 5.15 µm.

Bead analysis for 5 mg/ml hyaluronic acid 3D culture formats is shown in table 7 (see section 2.3.3.2.2).

Length in X (µm)	Length in Y (µm)	Length in Z (µm)
4.98	4.15	4.05
4.98	4.15	4.26
4.15	4.98	4.26
4.15	4.98	4.05
4.98	4.15	4.26
4.15	4.98	4.69
4.98	4.15	4.26
4.98	4.15	4.05
4.98	4.15	4.26
4.98	4.15	4.05
4.98	4.15	4.26
4.98	4.98	4.05
4.98	4.98	4.47
4.15	4.15	4.05
4.15	4.98	4.26
4.15	4.98	4.47
4.15	4.98	4.26

Table 7. Bead lengths in X, Y and Z post Z scale adjustment for beads cultured in 3D hyaluronic acid. Mean length in X = 4.64 µm, mean length in Y = 4.54 µm, mean length in Z = 4.24 µm.